



Diese Dissertation haben begutachtet

Prof. Dr. Ulrich SCHUBERT

Prof. Dr. Nicola HÜSING

## Dissertation

# Titanium/Zirkonium Alkoxides with Bi- and Multidentate Organic Ligands – A Journey from Metallacycles to Titania/Zirconia-based Hybrid Materials

ausgeführt zum Zwecke der Erlangung des akademischen Grades eines  
Doktors der technischen Wissenschaften

unter der Leitung von

o.Univ.Prof. Dr. Ulrich SCHUBERT

E165

Institut für Materialchemie

eingereicht an der Technischen Universität Wien

Fakultät für Technische Chemie

von

Dipl.-Ing. Christian MAURER

Mat.Nr. 0525243

Obere Amtshausgasse 23-25/7

1050 Wien

Wien, am 29.12.2012

Dipl.-Ing. Christian Maurer

*“I did this step very well.  
I hope you do it well.”*

## Acknowledgements

First of all I would like to thank my supervisor Prof. Ulrich Schubert for providing me this interesting and challenging topic for my thesis and for giving me the opportunity to work in his group. He supported me, whenever it was necessary in the last three years and provided me a lot of freedom in my scientific work.

Special thanks to Silvia Pabisch, Johanna Akbarzadeh and Prof. Herwig Peterlik for numerous SAXS measurements. They opened my horizon for this analysis method and answered all stupid questions, a chemist can have. Special thanks to Ernst Pittenauer and Prof. Günter Allmaier, who opened me the chance to apply mass spectrometry on my complexes. Thank you, Ernst, for all your encouragement. It helped a lot.

Many thanks to Michael Puchberger for conducting numerous NMR experiments and answering all my questions about advanced NMR techniques. Additional thanks to Stefan B., Majka and Christine for all their help and support with the single crystal XRD device and the refinement strategies. Thank you Stefan for opening my mind for crystallography.

Thanks to my students Dominik, Paul and Bettina for their encouraged practical work and their interest in my topic.

Very, very big and sincere thanks to my colleagues Aparna, Bernhard, Christine, Elisabeth, Felix, Harald, Hongzhi, Jakob, Johannes, Jingxia, Maïa, Marco, Marina, Melitta, Michael, Miriam, Mohsin, Rupali, Rupert (for repairing everything), Sven (for sweets' support during writing, sharing the passion of coffee and all his knowledge about alkoxides), Stefan E., Stephan R., and Stephan K. for a pleasant working environment and lots of friendship, also outside university.

Special thanks to my former men's office colleagues Christoph, Robert P. (for having surprising action in our hood), Robert L. (for sharing the faith of being the guy with the list and showing me how to handle an overcrowded lab course), Stefan B. (for celebrating the corner time) and Van An. It was a great time with all of you in the "lumber room".

Very big thanks to my recent office colleagues Martin (for being the best IKEA shopping buddy and all concert visits), Matthias (for a lot answered questions about alkoxides, struggling the diploma studies and being a very good friend here at the institute and in real life) and Sarah (for making us laughing about lost prepositions, all her patient software and language support and spending hours of talking to HR guys at career days).

Thanks to Anna, Dominik, Gerald, Ghislain, Julijana, Matthias and Paul, with whom I spent a great time at as well as outside the university and shared the desperate times during the PhD

studies. Thanks for your support and all your visits at my little wine-tasting flat. I enjoyed it very much.

Thanks to all my friends outside university for their understanding and enriching moments. They let me know that chemistry is not all in life. Thanks to all guys in St.Pölten for nice and relaxing Sunday evenings. Thank you Manu for proof reading.

I am greatly indebted to my parents for their perpetual love and their support throughout my studies. They always encouraged me to make my way, in the scientific and the real world. I am deeply grateful to my brother Bernhard for his love and several activities showing me that there are also nice things outside university.

Finally, I want to thank Magdalena for her restless love and support during the last three years of my PhD work. Thanks for giving me a lot of motivation and believing in me.

## Kurzfassung

Organisch modifizierte Titan- und Zirkoniumalkoxide sind weit verbreitete Vorstufen für die Herstellung von Metalloxiden über den Sol-Gel Prozess. Durch die Modifizierung kann einerseits die Reaktivität der Metallalkoxide gegenüber der Hydrolyse herabgesetzt werden und andererseits können weitere funktionelle Gruppen eingeführt werden, welche zur Herstellung von anorganisch-organischen Hybridmaterialien herangezogen werden können.

In der vorliegenden Arbeit wurden Titan- und Zirkoniumalkoxide mit diversen di- und multifunktionalen Liganden modifiziert. Dabei wurde versucht, eine Vorstrukturierung der Metallalkoxide durch gezielte Modifizierung dieser zu erreichen. Diese vorstrukturierten Metallalkoxide sollten im darauffolgenden Sol-Gel Prozess zu strukturierten Metalloxiden führen. Dadurch soll die herkömmliche Verwendung von Tensiden zur Strukturierung vermieden werden.

In einem ersten Ansatz wurden difunktionale bis( $\beta$ -Diketone), bis( $\beta$ -Ketoester), Dioxime und Bis(salicylaldiminate) Liganden zur Vorstrukturierung eingesetzt, um Koordinationspolymer mit Titan oder Zirkonium aufbauen zu können. Die Produkte wurden mittels Einkristallstrukturanalyse untersucht, sofern die Verbindungen kristallin vorlagen. Für die übrigen Substanzen zeigte sich, dass ESI-Massenspektrometrie eine geeignete Analysenmethode zur Bestimmung der chemischen Zusammensetzung darstellte. Die Synthese in unterschiedlichen stöchiometrischen Verhältnissen führte in den meisten Fällen zu dimeren Strukturen  $[\text{ML}(\text{OR})_2]_2$ . In diesen Metallozyklen werden die beiden Metallzentren von zwei difunktionalen Liganden überbrückt. Zwei chelatisierende Gruppen koordinieren zu jedem Metallzentrum. Jeweils zwei Alkoxo-Liganden blieben unsubstituiert am Metallzentrum koordiniert. Mit Ausnahme der Komplexe mit Alkylen-überbrückten Dioximaten waren die Alkoxo-Liganden immer terminal und nicht überbrückend koordiniert. Es konnte gezeigt werden, dass Komplexe mit überbrückenden Alkoxo-Liganden von jenen mit terminalen Alkoxo-Liganden mittels MS/MS Experimenten unterschieden werden konnten. NMR Spektroskopie und DFT Kalkulationen bestätigten die durch ESI-MS gefundenen Strukturen. Es zeigte sich, dass die Metallozyklen vom Typ  $[\text{ML}(\text{OR})_2]_2$  die stabilsten Verbindungen mit diesen Liganden darstellten. Weitere Zugabe von Metallalkoxiden führte zu keiner Änderung der beobachteten Strukturen. Es konnte jedoch gezeigt werden, dass der Einsatz von difunktionalen Liganden keine Bildung von Koordinationspolymeren bedingt.

Der Einsatz von cyclischen Dioximen führte zu schwer löslichen Produkten, welche nur im entsprechenden Alkohol löslich waren und für welche eine polymere Struktur angenommen worden ist. Untersuchungen mittels Festkörper-NMR Spektroskopie bewiesen die Koordination der Dioximate zu den Metallzentren. Weitere Messungen mittels DSC zeigten einen Glasübergang für manche der erhaltenen Verbindungen.

Ein weiterer Weg der Vorstrukturierung wurde durch tri- und tetrafunktionale Liganden bestritten. Dafür wurden Tri- und Tetracarbonsäuren mit Titan- und Zirkoniumalkoxiden umgesetzt. Anschließend partielle Hydrolyse führte zu zwei- und dreidimensional strukturierten Hybridmaterialien, welche allesamt Mikroporosität und spezifischen Oberflächen von bis zu  $350 \text{ m}^2/\text{g}$  auf-

zeigten. IR spektroskopische Untersuchungen bewiesen, dass die Carboxylate auch nach der Hydrolyse am Metallzentrum koordiniert geblieben sind. Die Versuche zeigten keinerlei Einfluss des verwendeten Metallalkoxids, jedoch konnten die Strukturen der verwendeten Liganden in den Strukturen und Eigenschaften der Materialien wiedergefunden werden.

## Abstract

Organically modified metal alkoxides are well known as precursors for sol-gel materials, since partial substitution of the alkoxo groups opens the chance of lowering the reactivity and better controlling of sol-gel processing. To this end, different types of ligands, e.g.  $\beta$ -diketonates,  $\beta$ -ketoesterates, amines and oximates can be used. Sol-gel processing of these metal alkoxo complexes results in unstructured materials. Structuring of the metal oxide materials has to be done by addition of surfactants during sol-gel processing.

In this thesis, pre-organisation of the metal alkoxo precursor was chosen as another approach to obtain structured metal oxide materials. If the pre-organisation retained the hydrolysis reaction, the pre-organisation should be found in the material afterwards. One access for the pre-organisation was through polymeric metal alkoxides, another one could be the formation of MOF-like structures. Concerning the coordination polymers, difunctional, tetradentate ligands were used, which were known for strong coordination to titanium alkoxides to retain the hydrolysis reaction. Therefore, bis( $\beta$ -diketones), bis( $\beta$ -ketoesters), dioximes and bis(salicylaldimine) ligands were reacted with  $\text{Ti}(\text{OR})_4$  and  $\text{Zr}(\text{O}^i\text{Pr})_4 \cdot i\text{PrOH}$ . Single crystal X-Ray diffraction was used for structure determination for all crystalline compounds, whereas ESI mass spectrometry was the analysis method of choice for non-crystalline compounds. Most reactions resulted in the same composition, from which a metallacyclic structure  $[\text{ML}(\text{OR})_2]_2$  were derived, in which both metal centres were bridged by two tetradentate ligands. Two chelating ligand groups and two residual alkoxo groups coordinated to each metal centre. The alkoxo groups were in terminal position, excepting the complexes with dioximates, where two alkoxo ligands bridged the metal centres. Reactions with  $\text{Zr}(\text{O}^i\text{Pr})_4 \cdot i\text{PrOH}$  with alkylene-linked ligands also revealed structures, in which the metal centres were bridged by more than two tetradentate ligands.

Solution NMR investigations and DFT calculations proved the structure elucidated by ESI-MS and XRD. These metallacycles were proved to be the thermodynamically most stable composition. Reactions with higher proportions of metal alkoxides resulted in same metallacycles.

In this contribution, it was proved that only for titanium alkoxo complexes with cyclic dioximates, a polymeric structure could be postulated. Reactions of dioximes with  $\text{Ti}(\text{OR})_4$  resulted in hardly soluble compounds. Solid state NMR spectroscopy proved the coordination of these ligands to the metal alkoxo moiety. Some compounds showed a glass transition, which was typical of polymeric assemblies.

An alternative approach was the use of tri- and tetracarboxylic acids with rigid linkers. Reactions of  $\text{Ti}(\text{OR})_4$  with these ligands resulted in insoluble network-like structure, which were non-porous and unstructured. Therefore, additional partial hydrolysis was applied. The obtained materials were microporous with microporous surface areas up to  $340 \text{ m}^2/\text{g}$ . The investigations proved that the structure could be influenced by the used ligand and the applied  $\text{Ti}:\text{H}_2\text{O}$  ratio. 2D layered and 3D structures were observed. Experiments with trifunctional ligands with other functionalities showed, that these structural features were only observed with carboxylates.

## Parts of this work have been published

“Cyclic bis(b-diketonate)- and bis(b-ketoesterate)-bridged titanium and zirconium alkoxide derivatives”; C. Maurer, E. Pittenauer, Van An Du, G. Allmaier, U. Schubert, *Dalton Transactions* **2012**, *41*, 2346 - 2353.

“Dioximate and Bis(salicylaldimate)-bridged Titanium and Zirconium Alkoxides”; C. Maurer, E. Pittenauer, M. Puchberger, G. Allmaier, U. Schubert, *Eur. J. Inorg. Chem.*, submitted.



## Abbreviations

acac	acetylacetonate
acac-H	acetylacetone
ATR	attenuated total reflection
BET	Brunauer, Emmett, Teller
<sup>n</sup> Bu	n-butyl
<sup>t</sup> Bu	tert-butyl
COSY	correlation spectroscopy
Cp	cyclopentadien
CP	cross polarization
DFT	density functional theory
DLS	dynamic light scattering
DMF	dimethylformamide
DMSO	dimethylsulfoxide
DSC	differential scanning calorimetry
ESI	electrospray ionization
Et	ethyl
<i>F</i>	structure factor
GOF	goodness of fit
HK	Horvath-Kawazoe
HMBC	heteronuclear multiple-bond correlation
HSQC	heteronuclear single quantum correlation
<i>I</i>	intensity
IR	infrared
L	ligand
$\lambda$	wavelength
MAS	magic angle spinning
Me	methyl
MOF	metal organic framework
MS	mass spectroscopy
$\mu$	absorption coefficient
NMR	nuclear magnetic resonance
OMc	methacrylate
<i>p/p</i> <sub>0</sub>	relative pressure
<sup>i</sup> Pr	isopropyl
<i>q</i>	scattering vector
SALEN	salicylidene
SAXS	small angle X-ray scattering

SEM	scanning electron microscope
TEM	transmission electron microscope
TGA	thermogravimetric analysis
THF	tetrahydrofuran
tmhd	2,2,6,6-tetramethylheptane-3,5-dionate
TMS	tetramethylsilan
TOCSY	total correlation spectroscopy
XRD	X-ray diffraction
<b>Z</b>	number of formula units per unit cell

#### NMR Abbreviations

$\delta$	chemical shift
s	singlet
d	doublet
t	triplet
q	quartett
m	multiplet

# Table of contents

1	Introduction	1
1.1	Sol-gel chemistry	1
1.2	Modification of transition metal alkoxides	4
1.3	Ligands	11
1.3.1	Bis-( $\beta$ -diketones), triketones, tetraketones and bis-( $\beta$ -ketoesters)	11
1.3.2	Dioximes	14
1.3.3	Bis(salicylaldiminates)	15
1.3.4	Tri- and tetra-carboxylic acids	17
1.4	Structured and porous titanium oxides	19
2	Research goals	21
3	Modification of group(IV) metal alkoxides with bifunctional ligands	22
3.1	Modification of titanium alkoxides with bis( $\beta$ -diketones)	22
3.1.1	Reaction of titanium alkoxides with arylene-bridged bis( $\beta$ -diketones)	22
3.1.2	Reaction of titanium alkoxide with alkylene-bridged bis( $\beta$ -diketones)	27
3.2	Modification of zirconium isopropoxide with bis( $\beta$ -diketones)	31
3.3	Modification of titanium isopropoxide with 1,1,2,2-tetraacetyethane (taet-H)	36
3.4	Modification of titanium alkoxides with bis( $\beta$ -ketoesters)	38
3.5	Modification of zirconium isopropoxide with bis( $\beta$ -ketoesters)	42
3.6	Modification of titanium isopropoxide with butanoic acid-3-oxo-3-(triethoxysilyl) propyl ester	45
3.7	Modification of titanium isopropoxide with 1,5-diphenyl-pentane-1,3,5-trione	46
3.8	Modification of titanium ethoxide with 1,6-diphenyl-hexane-1,3,4,6-tetraone	49
3.9	Modification of titanium ethoxide with 1,5-pentanedial-1,5-dioxime	51
3.10	Modification of titanium alkoxides with 2,5-hexanedione-2,5-dioxime	54
3.11	Modification of titanium alkoxides with cyclic-linked dioximes	60
3.11.1	Modification of titanium alkoxides with cyclohexylene-linked dioxime	61
3.11.2	Modification of titanium alkoxides with arylene-linked dioximes	63
3.12	Modification of titanium ethoxide with 1,4-bis-[(2-hydroxy-ethylimino)-methyl]-benzene	66
		XI

3.13	Modification of titanium alkoxides with bis(salicylaldimate)-ligands	67
3.14	Modification of zirconium isopropoxide with bis(salicylaldimate) ligands	71
3.15	Conclusions	73
4	Modification of group(IV) metal alkoxides with tri- and tetrafunctional ligands	75
4.1	Modification of $\text{Ti}(\text{O}^i\text{Pr})_4$ with benzenetribenzoic acid	75
4.1.1	Structural investigation of benzenetribenzoate-based titanium alkoxo materials	75
4.1.2	Structural investigation of benzenetribenzoate-based titania materials	78
4.2	Modification of $\text{Ti}(\text{O}^i\text{Pr})_4$ with 1,3,5-tricarboxybenzene	85
4.3	Modification of $\text{Ti}(\text{O}^i\text{Pr})_4$ with 1,3,5-tris(4-carboxy-biphenyl)benzene	88
4.4	Modification of $\text{Zr}(\text{O}^i\text{Pr})_4 \cdot ^i\text{PrOH}$ with benzenetribenzoic acid	91
4.5	Modification of $\text{Ti}(\text{O}^i\text{Pr})_4$ with benzenetetra benzoic acid	96
4.6	Modification of $\text{Ti}(\text{O}^i\text{Pr})_4$ with tetrakis(4-carboxyphenyl)silane	100
4.7	Modification of $\text{Ti}(\text{OEt})_4$ with adamantyl tetracarboxylic acid	103
4.8	Modification of $\text{Ti}(\text{O}^i\text{Pr})_4$ with tri(4-acetylphenyl-4-oxime)amine	105
4.9	Conclusions	109
5	Summary	111
6	Experimental Section	115
6.1	General methods and materials	115
6.2	Analytical techniques	115
6.2.1	Single crystal X-ray diffraction	115
6.2.2	Nuclear magnetic resonance spectroscopy	116
6.2.3	Mass spectrometry	116
6.2.4	Infrared spectroscopy	117
6.2.5	Gas sorption measurement	117
6.2.6	Small angle X-ray scattering	117
6.2.7	X-ray powder diffraction	117
6.2.8	Dynamic light scattering	118
6.2.9	Density functional calculations	118
6.3	Synthesis of the ligands	118
6.3.1	Synthesis of arylene-bridged bis( $\beta$ -diketones)	118
6.3.2	Synthesis of alkylene-bridged bis( $\beta$ -diketones)	118

6.3.3	Synthesis of 1,1,2,2-tetraacetyethane (taet)	119
6.3.4	Synthesis of bis( $\beta$ -ketoester)	119
6.3.5	Synthesis of butanoic acid-3-oxo-3-(triethoxysilyl)propyl ester { $\beta$ -ketoester 5}	120
6.3.6	Synthesis of 1,5-diphenyl-pentane-1,3,5-trione	120
6.3.7	Synthesis of 1,6-diphenyl-hexane-1,3,4,6-tetraone	121
6.3.8	Synthesis of dioximes	121
6.3.9	Synthesis of 1,3-bis-[(2-hydroxy-ethylimino)-methyl]-benzene	124
6.3.10	Synthesis of bis(salicylaldiminate) ligands	125
6.3.11	Synthesis of Benzenetribenzoate (BTB-3)	125
6.3.12	Synthesis of 1,3,5-tri(4-acetylphenyl-4-oxime)benzene (TAPOB-3)	126
6.3.13	Synthesis of Benzenetetrabenzoate (BTB-4)	127
6.3.14	Synthesis of tetrakis(4-carboxyphenyl)silane (TCPS)	127
6.3.15	Synthesis of 1,3,5-tris(4-carboxybiphenyl)benzene (TCBB)	128
6.4	Synthesis of complexes	129
6.4.1	Synthesis of $\{\text{Ti}[\text{bis}(\beta\text{-diketonate})](\text{O}^i\text{Pr})_2\}_n$	129
6.4.2	Synthesis of $\text{Zr}_2[\text{bis}(\beta\text{-diketonate})]_{4-x}(\text{O}^i\text{Pr})_x$	131
6.4.3	Synthesis of $[\text{Ti}(\text{taet})(\text{O}^i\text{Pr})_2]_2$ (10)	132
6.4.4	Synthesis of $\{\text{Ti}[\text{bis}(\beta\text{-ketoesterate})](\text{O}^i\text{Pr})_2\}_2$ , $\{\text{Zr}[\text{bis}(\beta\text{-ketoesterate})](\text{O}^i\text{Pr})_2\}_2$ and $\text{ZrTi}[\text{bis}(\beta\text{-ketoesterate})]_2(\text{O}^i\text{Pr})_4$	132
6.4.5	Synthesis of $[\text{Ti}(\beta\text{-ketoesterate 5})(\text{O}^i\text{Pr})_2]_2$ (18)	134
6.4.6	Synthesis of $[\text{Ti}_2\text{O}(\text{O}^i\text{Pr})_4(1,5\text{-diphenyl-pentane-1,3,5-trionate})]_2$ (19)	135
6.4.7	Synthesis of $\text{Ti}_2(1,6\text{-diphenyl-hexane-1,3,4,6-tetraonate})(\text{OEt})_6$ (20)	135
6.4.8	Synthesis of $[\text{Ti}(1,5\text{-pentanedial-1,5-dioximate})_2(\text{OEt})_2]_2$ (21)	135
6.4.9	Synthesis of $[\text{Ti}(2,5\text{-hexanedione-2,5-dioximate})_2(\text{OR})_2]_2$	135
6.4.10	Synthesis of $[\text{Ti}(\text{aryl-dioximate})(\text{OR})]_x$ and $[\text{Ti}(\text{cyclohexyl-dioximate})(\text{OR})]_x$	136
6.4.11	Synthesis of $\text{Ti}_2\{1,4\text{-bis-}[(2\text{-hydroxy-ethylimino)-methyl}]\text{-benzene}\}_2(\text{OEt})_4$ (29)	137
6.4.12	Synthesis of $\{\text{Ti}[\text{bis}(\text{salicylaldiminate})](\text{OR})_2\}_2$ and $\{\text{Zr}[\text{bis}(\text{salicylaldiminate})](\text{O}^i\text{Pr})_2\}_2$	137
6.5	Synthesis of titanium/zirconium hybrid materials	140
6.5.1	Ti_BT B-3	140
6.5.2	TiO_BT B-3	140

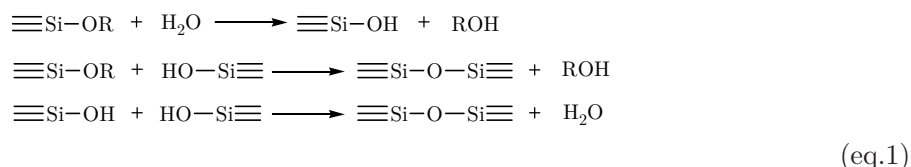
6.5.3	TiO_TCB	141
6.5.4	TiO_TCBB	141
6.5.5	ZrO_BTBB-3	142
6.5.6	TiO_BTBB-4	142
6.5.7	TiO_TCPS	143
6.5.8	TiO_ATC-4	143
6.5.9	TiO_TAPOA-3	144
6.6	Crystallographic data	145
7	References	147
8	Curriculum Vitae	155

# 1 Introduction

## 1.1 Sol-gel chemistry

Sol-gel chemistry allows creating an oxide network by the reaction of molecular precursors at ambient temperature. The synthesis is a stepwise process: First, a sol is built in the reaction medium, while in a second step gelation of the sol forms the network structure. Finally, removal of the solvent yields the oxide material. Depending on the synthesis parameters, as well as drying and evaporation methods, different structures and types of materials (aerogels, xerogels, *etc.*) are achieved. Various preparation methods permit wide-spread applications like coatings, catalyst supports, ceramic fibers and electroceramic powders.<sup>1</sup>

Silica gels belong to the best investigated materials in sol-gel chemistry. Two reactions can be observed during sol-gel processing. First, the hydrolysis of the alkoxy silane occurs, while in a second step condensation forms siloxane Si-O-Si bonds. A maximum of siloxane bonds has to be reached for gel formation. The sol-gel process is influenced by steric parameters, Si/H<sub>2</sub>O ratio, solvent, temperature and the used catalyst (pH value) and precursor. All reactions are summarized in equation 1.<sup>1</sup>



The most common precursors are silicon alkoxides and sodium silicates. Reactions are carried out in water or organic solvents (e.g. alcohols) depending on the precursor used. It is quite important to control the pH of the reaction mixture, as it influences the morphology of the resulted material. The point of zero charge for Si-OH species is between pH 1.5 and 4.5. Under strong acidic conditions, positively charged groups are obtained. These protonated substituents provide a proper leaving group (water or alcohol) and a higher electrophilicity of the silicon centre. A nucleophilic attack of water (hydrolysis) or other silanols (condensation) becomes easier. A five membered transition state is formed. Cleavage of alcohol results in an inversion of the silicon tetrahedron with one siloxane group. The hydrolysis rate under acidic conditions depends on the electron providing substituents of the silicon centre. The higher the +I effect, the better the positive charge on the transition state can be stabilized.<sup>1,2</sup>

Strongly basic conditions cause a higher nucleophilicity of the silicon atom that promotes attacks of <sup>-</sup>OH or additional Si-O<sup>-</sup> groups and permits the formation of a negatively charged transition state. In case of basic conditions, hydrolysis occurs by a S<sub>N</sub>2 mechanism. This reaction is an equilibrium, and a reaction of <sup>-</sup>OH and Si-O-Si is not excluded under certain reaction conditions.<sup>1,2</sup>

During the whole gelation process, a competition is going on between hydrolysis and condensation reactions. The ratio of hydrolysis to condensation reaction rates is responsible for the resulted

properties of the material. Acids and bases are often used as catalysts in silicon based sol-gel processing. As discussed above, different reaction types are possible at varying pH-values. The hydrolysis rate reaches a minimum at pH=7, while highest condensation rates are observed at pH = 4.5. Under acidic conditions, the rate-limiting step is the condensation reaction, whereas the the hydrolysis reaction limits the total reaction rate under basic condition.<sup>1</sup>

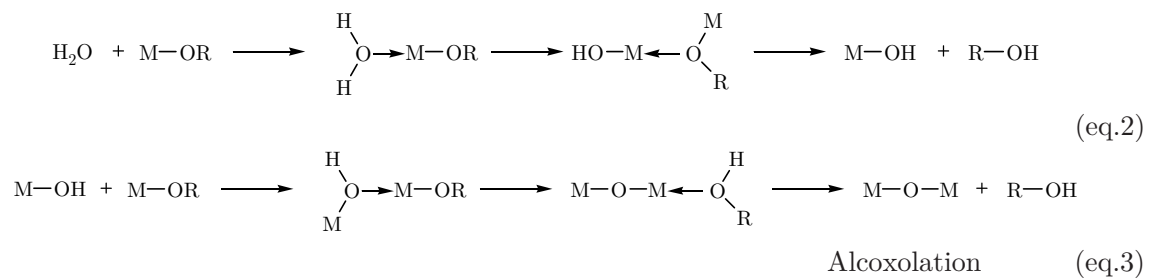
The first step of the sol-gel process builds small particle with silanol groups. These particles can then grow to larger size or agglomerate. If the particles agglomerate and condense, a gel can be formed under certain conditions. The time, which is necessary to obtain a gel starting from the beginning of the hydrolysis, is characteristically defined as the gel time. It depends on the used experimental setup and can be decreased by parameters that influence the condensation rate. At the gel point (after gel time) the reaction mixture turns from viscous liquid to an elastic gel body. The remaining solvent is then caught in the gel.<sup>1</sup>

The sol-gel process is not stopped at this gel point; furthermore, reactions are going on as condensable sol species remain in the gel's pores and structural changes are possible depending on the experimental parameters. Neighbouring Si-OR or Si-OH groups can get in touch with each other due to the high flexibility of the gel and condense to additional siloxane bridges. The gel thus becomes stiffer. This process is called aging.<sup>1</sup>

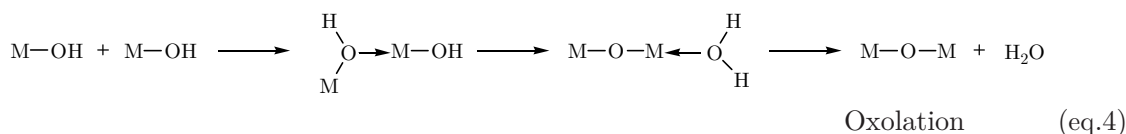
When the aged gels are dried by standard methods, a tremendous shrinking can be observed. The gel volume decrease is nearly similar to the volume, which has been occupied by the solvent. Shrinking of the gel enables additional siloxane group formations. Additional drying leads to a collapse and cracking of the network, so called xerogels are obtained. In the widespread use of sol-gel materials in the field of coatings and films, the shrinkage problem can be disregarded. Special methods have been developed for drying without shrinking. There the solvent/sol is replaced by a gas. Supercritical drying is one access to yield non-shrinking gels (aerogels).<sup>1</sup>

Besides silicon alkoxides, transition metal alkoxides belong to a group of well investigated sol-gel precursors. Their Lewis acidic character promotes nucleophilic attacks (e.g. OH<sup>-</sup>) that cause an additional risen hydrolysis rate. Reaction rates of titanium alkoxides are too high to form gels; in fact a precipitation is formed after direct hydrolysis.<sup>1</sup>

Hydrolysis and condensation of coordinatively saturated metal alkoxide follow a nucleophilic substitution mechanism involving an addition step, proton transfer step and an elimination step (see equation 2-4).<sup>2</sup>

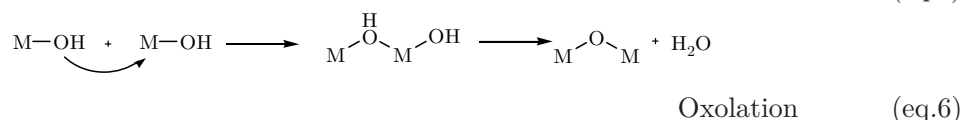
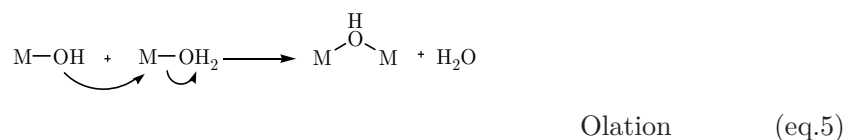






In the first step, hydrolysis causes formation of very reactive metal centres with hydroxo groups. This reaction is promoted by an increase of the charge density on the transition metal centre. It becomes slower, the more hydroxo groups are coordinated on the centre atom. The exact composition of the hydrolysed metal alkoxide is influenced by charge, electronegativity and coordination number of the metal centre and the pH of the corresponding solution. Depending on these parameters, equilibrium of three domains  $[\text{M}-(\text{OH})_2, \text{M}-\text{OH}, \text{M}=\text{O}]$  can be observed.

These unstable metal hydroxides condense either with another metal hydroxide or a metal alkoxide under the cleavage of alcohol or water. Two different types of condensation reactions of transition metal precursors are distinguished. Both only vary in nature of the bridging unit between the metal centres.<sup>1,2</sup>



Olation is widely observed in metal precursors that are coordinatively unsaturated. Solvents (e.g. water) are coordinated for additional saturation of the coordination sphere. In this case, a hydroxy group is formed as the bridging unit. (see eq.5) Kinetics of olation depends on the lability of the aquo ligand and is raised by a larger size and a smaller charge of the metal ion. Several different structural motives for hydroxo bridged metal centres are possible. The kinetics of olation is known to be fast, as no proton transfer in the associated transition state is necessary.<sup>2,3</sup>

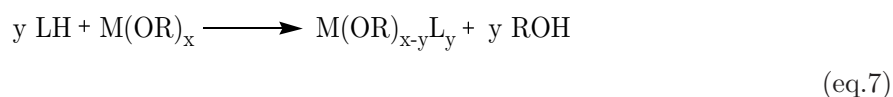
However, in case of coordinatively saturated metals, oxolation is a two step addition/elimination process with the initial formation of an unstable hydroxo bridge, followed by the proton transfer and the elimination of water/alcohol and formation of an M-O-M oxo bridge. (see eq.6)

The thermodynamic behaviour of all three reactions is mainly influenced by the nucleophilic character of the entering group and the electrophilicity of the metal centre. In case of metal alkoxides, the degree of oligomerization is another parameter affecting sol-gel chemistry. The oligomeric character of most transition metal alkoxides influences the solubility as well as the reaction kinetics. The higher the oligomerization, the lower the hydrolysis rates. As oligomerization is controllable by the solvent used, kinetics of the hydrolysis can also be regulated by the solvent chosen. The size and the electron-withdrawing effect of the alkoxo groups also affect the reaction rates. The hydrolysis kinetics slows down by increasing the alkyl chain length. Herein, the steric hindrance is increased and Lewis acidity of the metal centre fallen.<sup>1,2,3</sup>

## 1.2 Modification of transition metal alkoxides

Metal alkoxide precursors are widely used as molecular precursors for material synthesis like sol-gel processing. Especially  $d^0$ -metal alkoxides (Ti, Zr) are established in the field of ceramic coatings or glass applications. In comparison to silicon alkoxides, the alkoxy groups of titanium/zirconium promote the strong Lewis acidic character of the metal centre. The positive partial charge on Ti/Zr is twice the value of that of silicon alkoxides. This high Lewis acidity allows them to be used as an acidic catalyst in organic chemistry. All other structural and chemical properties can be attributed to this high Lewis acidity. In fact, this high electrophilicity tends to raise their coordination sphere by the formation of oligomeric structures with bridging alkoxides.<sup>4</sup> Therefore, the increased Lewis acidity is responsible for the much higher reactivity towards hydrolysis. For example, the reaction of titanium alkoxides with water yields no longer a gel but instead  $\text{TiO}_2$  precipitation.<sup>1,5</sup>

Modification of the transition metal alkoxides with suitable organic molecules is the most proper way to lower the reaction rate. Either one or more alkoxo groups are substituted by an anionic ligand or a neutral Lewis base ligand is additionally coordinated. First substitution reaction follows a  $\text{S}_\text{N}$  type pathway (eq.7).<sup>2</sup>



The reaction may be seen as a simple proton exchange reaction. The tendency for substitution rises proportional to the nucleophilicity of the ligand. The introduced ligand blocks additional coordination sites on the metal centres and decreases the electrophilicity of the centre atom. Less unsaturated coordination sites lower the tendency of oligomerization, which is important concerning to the question of solubility. The higher the electronegativity of the coordinating group is, the slower the ligands are removed during the hydrolysis and condensation process. Furthermore, the substitution lowers the connectivity of the metal alkoxide. This promotes gel formation instead of crystalline precipitation.<sup>1,4</sup>

The M-C bond is not stable towards hydrolysis for most metal alkoxide precursors used, and ligands bearing hetero atoms such as oxygen, sulphur or nitrogen must be introduced. The range of possible ligands is widely open; the use of  $\beta$ -diketones, carboxylic acids, amines, oximes, amino alcohols and also alcohols has to be considered.<sup>2</sup>

One way of lowering the Lewis acidity is the coordination of Lewis basic solvents like alcohols or amines. The stability of the solvent adducts depends on the Lewis basicity of the solvent and Lewis acidity of the metal centre. Coordination of alcohols results in octahedrally coordinated titanium centres. (Figure 1.1) One solvent molecule (alcohol/amine) coordinates to each titanium centre, which are bridged by two  $\mu_2$ -OR groups. The proton of the coordinated alcohol additionally interacts with a neighbouring alkoxo group by hydrogen bonding. The solvent adduct is assumed to be an intermediate in an alkoxo exchange.<sup>5</sup>

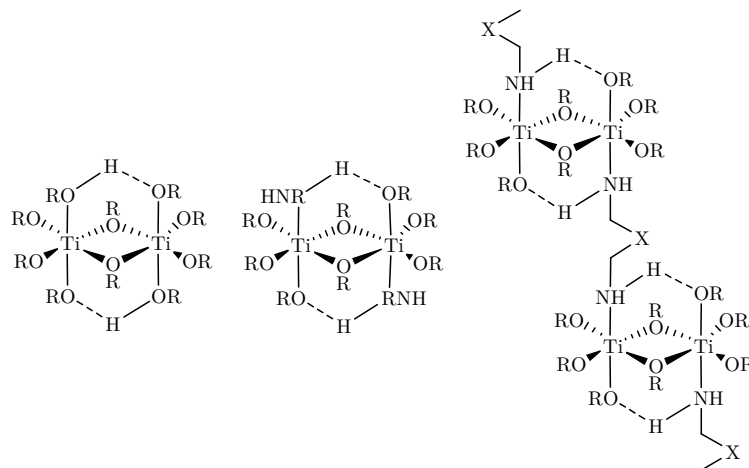


Figure 1.1: Titanium alkoxides modified with Lewis bases

The amine adducts show a similar structure as discussed for the alcohol adducts. They are known for 1-aminopropane, benzylamine, 1-butylamine, cyclohexylamine, 3-aminopropyltriethoxysilane and several other amines.<sup>6,7</sup> Using diamines instead of mono-amines leads to polymeric arrangements. In these complexes, the titanium centre is octahedrally coordinated, and each titanium alkoxide dimer is connected by one diamino ligand.<sup>7-9</sup> (Figure 1.1) Unfortunately, the coordination strength of the coordinated alcohols and amines is too less to retain hydrolysis.

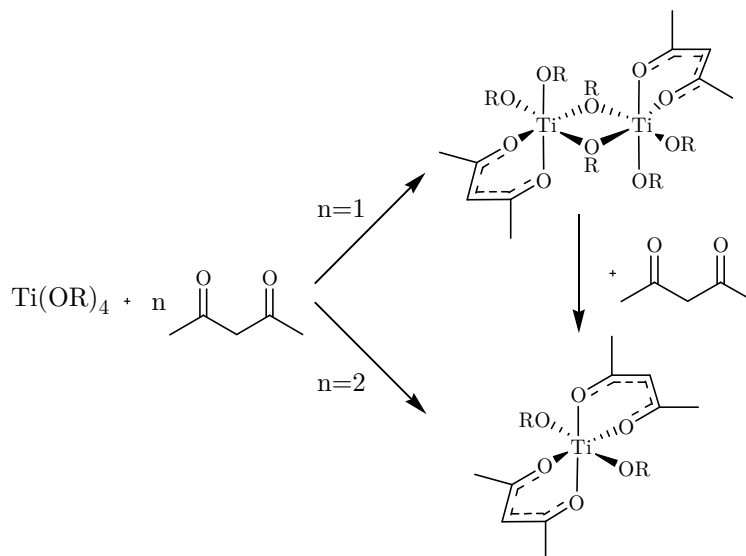
Bi- and tridentate ligands are focused to block more than one coordination site on the metal centre.  $\beta$ -Diketonates and carboxylates, which are the most commonly used ligands, act as a chelating or bridging ligands with a stronger bonding to the metal centre than the replaced alkoxo group and/or other mono-dentate ligands. The alkoxo group/ligand exchange reaction is an equilibrium reaction, which is thus shifted to the product side. This equilibrium causes a partially cleavage of the ligand-metal bonding, also with multidentate as well as chelating ligands, during sol-gel processing. Furthermore, multidentate ligands permit stereochemically selective hydrolysis, as reactivity of the *trans*-position to the ligand differs significantly from the *cis*-position.<sup>1,4,5</sup>

Additional functionalities might be introduced by the modification of the metal alkoxides. Coordination of ligands with polymerizable groups permits formation of inorganic-organic hybrid materials after sol-gel processing and polymerisation with co-monomers. The advantages of these materials can be seen in the covalent connections between the inorganic and the organic material.<sup>1</sup> Furthermore, metal alkoxides are known modified by ligands with trialkoxysilanyl groups, which are precursors for mixed metal/silicon oxide materials.<sup>10</sup>

Organically modified titanium alkoxides belong to the best investigated transition metal alkoxide systems. Compared to other metal alkoxides, group IV metal alkoxides have a quite simple coordination and structural chemistry. The most frequently observed coordination number is six, compounds with coordination numbers between seven or eight are rarely known.<sup>5</sup>

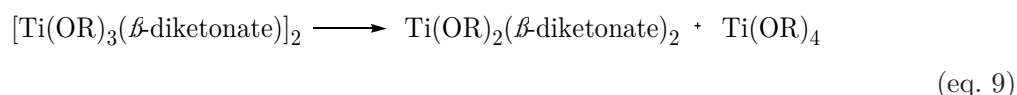
$\beta$ -Diketones are often applied in the modification of titanium alkoxides. When acetylacetone is allowed to react with titanium alkoxides, it forms two types of complexes  $[\text{Ti}(\text{acac})\text{OR}_3]_2$  and

$\text{Ti}(\text{acac})_2(\text{OR})_2$ . Depending on the ratio of titanium alkoxide to acetylacetone, the dimeric (1:1) or the monomeric (1:2) complex is formed.<sup>11</sup> (see Scheme 1.1)



**Scheme 1.1: Possible products from reaction of  $\text{Ti}(\text{OR})_4$  and  $\beta$ -diketones**

Both complexes are in equilibrium. Addition of acetylacetone to the dimeric compound yields  $\text{Ti}(\text{acac})_2(\text{OR})_2$ . Both metal alkoxo complexes show an octahedral coordination sphere. In contrary to the solid state structure of these complexes, the structure of  $\text{Ti}(\text{acac})_x\text{OR}_{4-x}$  is quite complex in solution. The dimeric complex is in equilibrium with the monomeric, disubstituted titanium alkoxo complex and the unsubstituted metal alkoxide. (see eq.9)



The degree of disproportionation depends on the kind of the alkyl group. The bulkier the alkoxo ligand is, the more the equilibrium is shifted to the monomeric complex and the titanium alkoxide.<sup>12</sup> Concerning the disubstituted titanium alkoxide  $\text{Ti}(\beta\text{-diketonate})_2(\text{OR})_2$ , a complete disubstitution is only observed in acetylacetone, while larger  $\beta$ -diketones result in complexation ratios up to 1.5. Addition of acetylacetone does not result in the formation of  $\text{Ti}(\text{acac})_4$  as observed for zirconium alkoxides.<sup>13,14</sup> Titanium alkoxides are only known for the substitution of two OR groups; the coordination number of six is favoured. A substitution of the  $\beta$ -diketone unit in 3-position decreases the Lewis basicity and yields a smaller coordination ratio.<sup>14</sup> Reaction of  $\text{Zr}(\text{O}^i\text{Pr})_4 \cdot ^i\text{PrOH}$  and  $\beta$ -diketones results in similarly substituted complexes as described for titanium.

Similar observations are made with modified  $\beta$ -diketones and  $\beta$ -ketoesters. Several titanium alkoxo  $\beta$ -diketonates are known, where the ligand is modified to act as a precursor for inorganic organic hybrid materials. Much work has been done in the investigation of titanium alkoxides

substituted with 3-(propyltrimethoxysilyl)acetylacetone. Both complexes, mono- and di-substituted titanium isopropoxides, are observed. Homogenous titania-silica materials may be prepared with this ligand.<sup>10</sup> One drawback of this single-source precursor is hydrodeacylation, which is a titanium alkoxide-catalyzed cleavage of the  $\beta$ -diketonate unit. This side reaction is only observed in  $\beta$ -diketones substituted in the 3-position and is promoted by the +I effect of the alkyl group.<sup>15</sup>

$\beta$ -Ketoesters permit introduction of functionalities with the ester group more easily. Although side reactions such as transesterification are known, they are as commonly used as  $\beta$ -diketones.<sup>16</sup> Allyl-acetoacetate and methacryloxyethylacetoacetate are two possible ligands with polymerizable groups.<sup>14</sup> Also hydrolysable trialkoxysilanyl groups can be introduced in the  $\beta$ -ketoester.<sup>17</sup>

Carboxylates are the second prominent group of ligands for titanium alkoxide modification. As expected from the above discussed titanium alkoxo ( $\beta$ -diketonates), only few examples of dimeric, mono-substituted titanium carboxylate complexes are known.<sup>18,19</sup> Furthermore, reactions of group(IV) metal alkoxides with an excess of carboxylic acids (1:4 to 1:8) yield metal oxo clusters  $M_wO_x(OH/OR)_y(RCOO)_z$ . Hereby, a substitution reaction, as observed with other Lewis bases, occurs. The presence of  $Ti(OR)_3(RCOO)$  units are observed by spectroscopic methods. Hereby, a dimeric complex is obtained, in which the carboxylate acts as a bridging ligand. (Figure 1.2)

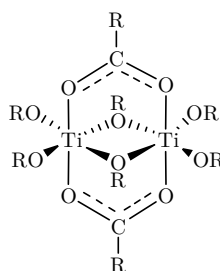
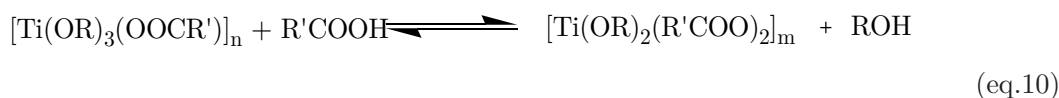


**Figure 1.2: Schematic structure of mono-substituted titanium carboxylate**

In contrary to this, the structure of  $Ti_2(O^iPr)_6(\mu_2-OOC-CMe_3)(\mu_1-OOC-CMe_3)(^iPrOH)$  shows a bridging as well as mono-dentate carboxylate. Similar behaviour is observed in the structure obtained from the reaction of titanium alkoxides with phthalic anhydride.<sup>18,20</sup> Disubstituted complexes similar to  $Ti(acac)_2(O^iPr)_2$  have never been observed because the second carboxylate is bonded much weaker.<sup>5</sup> Equilibrium between the mono-substituted complex/ free carboxylic acid and the disubstituted titanium alkoxide/ free alcohol is present. (see eq.10) This equilibrium is on the educt side.



The free carboxylic acid may permit an esterification reaction with the released alcohol. Ester formations are catalyzed by Lewis acids, so this side reaction is promoted. Water is produced very

slowly in the reaction mixture, and this leads to a partial hydrolysis of the metal alkoxides. Group(IV) metal oxo cluster can be formed quite precisely.<sup>21,22</sup> If a large excess of carboxylic acids is added, the cluster formation is promoted. Enough acid is left for water formation. The different types of clusters can be distinguished by the Ti:O ratio and the complexation ratio.<sup>22</sup>

No systematic investigations have been done on the influence of defined parameters on the cluster formation. One parameter is the titanium alkoxide used.  $\text{Ti}(\text{OEt})_4$  and  $\text{Ti}(\text{OPr})_4$  lead to clusters with lower complexation ratios as the reaction performed with  $\text{Ti}(\text{O}^i\text{Pr})_4$ . The different size of the alkoxo ligands or the various degree of aggregation is a possible explanation for these observations.<sup>23,24</sup>

A second influence is given by the  $\text{RCOOH}:\text{Ti}$  ratio. If a too small proportion of carboxylic acid is used, all carboxylate groups coordinate to the titanium centre and only less acid is left for ester formation. Thus, less water is produced. Therefore, clusters with high Ti:O and low complexation ratios are formed with many remaining alkoxo groups. These clusters show a low degree of condensation. Large excess of acid promotes the water formation and results in clusters with a high complexation ratio. The excess of carboxylates blocks additional coordination sites, which are necessary for a higher degree of condensation. Therefore, a medium  $\text{RCOOH}:\text{Ti}$  ratio is best to reach clusters with the highest degree of condensation.<sup>5</sup>

Additional influence is given by acid itself. It is assumed that different bonding strength, acidity and steric hindrance impact the formed cluster. Detailed and systematic investigations have never been done in this field.<sup>5</sup>

In most common titanium oxo carboxylate clusters, similar structural motives can be observed. First, the coordination number of titanium is mostly six. Second, the carboxylate ligands act as bridging ligands in contrary to  $\beta$ -diketonates or  $\beta$ -ketoesterates. Third, in most cases the oxo groups show  $\mu_3$ -coordination. Although much research has already been done in this field, it is not clear, which type of cluster is built at a defined titanium alkoxide/ carboxylic acid ratio.<sup>5</sup>

Several clusters are possible, where carboxylate ligands bear another functionality. As covered for titanium alkoxo ( $\beta$ -ketoesterates), polymerizable group such as in methacrylate or p-vinylbenzoate groups can be introduced. After gel formation, they react in a free-radical polymerization with additional monomers under the formation of organic-inorganic hybrid materials, where the inorganic and organic moieties are connected by strong covalent interactions.<sup>5,25</sup> Another way is the direct polymerization of these clusters with additional monomers without previous gelation step. Hereby, the synthesis yields a cluster-reinforced polymer. Mechanic and thermal properties can be influenced on a molecular scale.<sup>5,26,27</sup>

Substituted carboxylic acids with OH and  $\text{NH}_2$ -groups in  $\alpha$ -position are favoured in the coordination to group IV metals due to the possibility to form a five membered chelate ring if the carboxylic group and the amine/hydroxy group are coordinated together to the metal centre. Observations of alanine and other amino acids reveal different coordination motives as discussed above for unsubstituted carboxylates. No bridging carboxylate units are present; the structural geometry of the dimeric structures shows similarities with the later discussed titanium amino alcoholates. The

carboxylate is no longer coordinated in a chelating manner; only one oxygen atom of the COOH group is involved in the coordination.<sup>28-31</sup> (Figure 1.3) This five-membered ring blocks the ester formation, and therefore only molecular metal alkoxo complexes are achievable. The structural chemistry of hydroxy carboxylate ligands is very versatile because of the possible dianionic character of the used ligand.

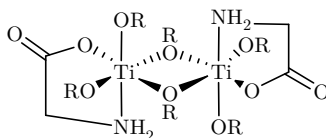


Figure 1.3: Schematic structure of lysinate modified titanium alkoxide

Some clusters are known, in which phosphonic acids are used instead of the carboxylic ones. In comparison to the carboxylate clusters, ester formation is not as easy with phosphonic acids. Clusters without oxo groups are very likely. In contrary to carboxylates, the phosphonate groups  $\text{RPO}_3^{2-}$  are dianionic and tridentate ligands. Clusters such as  $[\text{Ti}(\text{OR})_2(\text{O}_3\text{P}^t\text{Bu})]_4$ ,  $\{\text{Ti}(\text{C}_5\text{Me}_4\text{Et})[\mu\text{-O}_2\text{P}(\text{OH})\text{Me}][\mu\text{-O}_2\text{P}(\text{O})\text{Me}]\}_2$  and  $[\text{Ti}(\text{O}^i\text{Pr})_3(\mu\text{-O})_2\text{P}(^t\text{Bu})(\text{OSiMe}_3)]_2$  are possible by the reaction of titanium alkoxides with the phosphonic acids or their monoesters. These clusters show only phosphonate and terminal alkoxo ligands. Addition of stoichiometric proportions of water results in titanium oxo phosphonate clusters such as  $[\text{Ti}_4(\mu_3\text{-O})(\text{O}^i\text{Pr})_2(\text{O}^i\text{Pr})_3(\mu\text{-O}^i\text{Pr})_3(\text{O}_3\text{PR})_3]_3$  ( $\text{R} = \text{Ph}, \text{Me}, ^t\text{Bu}, 4\text{-CNPh}$ ), in which not each titanium atom is connected with each other by a  $\mu_3$ -oxo bridge. (Figure 1.4) Herein, the fourth metal ion is only connected by bridging phosphonate.<sup>32-36</sup>

In contrary to phosphonates, the corresponding phosphinates are bidentate, anionic ligands, which show similar coordination behaviour as carboxylates. Reaction of  $\text{Ph}_2\text{PO}(\text{OH})$  with  $\text{Ti}(\text{O}^i\text{Pr})_4$  yields  $[\text{Ti}(\mu_3\text{-O})(\text{O}^i\text{Pr})(\text{Ph}_2\text{PO}_2)]_4$  with a  $\text{Ti}_4\text{O}_4$  core, which is identical to known carboxylate clusters.<sup>33</sup> Analogous to the above described dimeric complexes with phosphonate ligands  $[\text{Ti}(\text{OR})_3(\mu\text{-O})_2\text{PRR}']_2$  ( $\text{R} = \text{OSiMe}_3$ ), similar structures are possible with phosphinates.<sup>37</sup> (Figure 1.4)

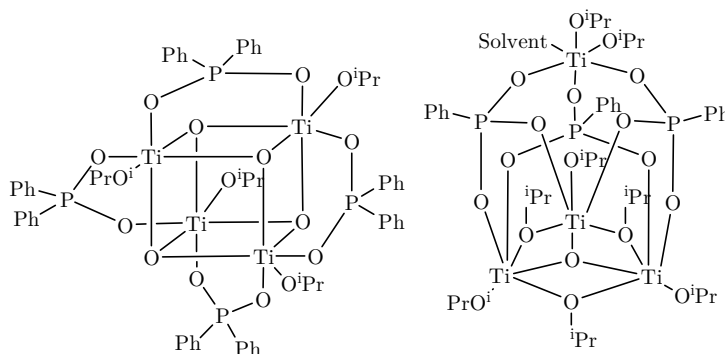


Figure 1.4: Schematic structure of known titanium phosphinate and phosphonate oxo clusters

Amino alcohols are another prominent group of ligands used in modification of titanium alkoxides. They belong to the group of bidentate ligands bearing one hydroxy and one neutral coordinative group, similar to hydroxyether (e.g. 2-methoxyethanol). Mono- to tetra-substituted complexes are possible with 2-amino ethanol and other derivatives.<sup>38-40</sup> NMR experiments prove the equilibrium between monomeric and dimeric complexes for the monosubstituted titanium alkoxide in solution.<sup>41,42</sup> The solid state structure of the dimeric product can be derived from the structure of the unsubstituted titanium alkoxide  $\text{Ti}_2(\text{OR})_8(\text{LH})_2$  ( $\text{LH} = \text{ROH}, \text{RNH}_2$ ). Herein, LH is the amino group of the ligand. Similar to unsubstituted titanium alkoxide, the protons of the amine interact with the coordinated oxygen of one alkoxide by hydrogen bonding. Both metal centres are octahedrally coordinated, the amino group coordinates axial to the titanium alkoxo plane. (Figure 1.5) Similar structures are also possible with hydroxyethers.<sup>5</sup>

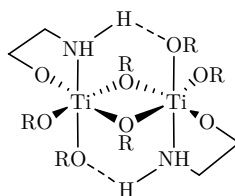


Figure 1.5: Schematic structure of titanium alkoxo ethanolamino

The disubstituted titanium alkoxo derivatives have a monomeric structure with an octahedrally coordinated titanium atom. In contrary to the mono- and disubstituted titanium alkoxo derivatives, the structure of tri- and tetra-substituted compounds have not been clarified. A bidentate coordination of two ligands and a monodentate bonding of two additional ligands is assumed.<sup>41</sup> In the whole group of amino alcohol derivatives, no polymeric structures are possible in contrary to adducts of diamines with titanium alkoxides.<sup>8</sup>

Oximes are also commonly used ligands in modifying titanium alkoxides.  $[\text{Ti}(\text{ON}=\text{C}_6\text{H}_{10})_2(\text{O}^i\text{Pr})_2]_2$  and  $[\text{Ti}(\text{ON}=\text{C}_6\text{H}_{10})(\text{O}^i\text{Pr})_3]_2$  are obtained by the reaction of oximes with titanium alkoxides with different titanium alkoxide/oxime ratios.<sup>43</sup> In both complexes, a side-on coordination of the oximate group is observed. While the mono-substituted complex has a 6-fold coordinated titanium centre, the disubstituted titanium alkoxides belong to the rare examples of 7-fold coordinated titanium complexes. (Figure 1.6). The disubstituted titanium complex seems to be preferred and is also achieved with Ti:oxime ratios of 1:1, while the mono-substituted titanium alkoxide is only possible with selected oximes.<sup>43-45</sup>

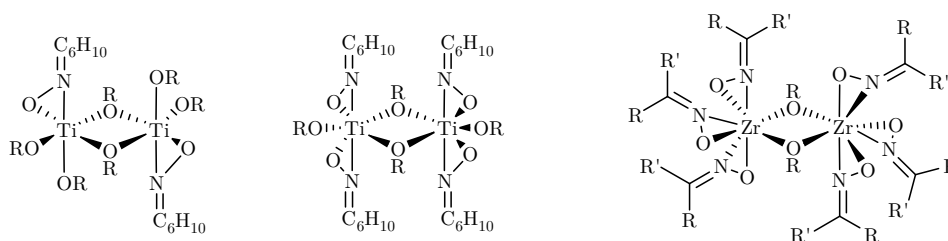


Figure 1.6: Oximate derivatives of titanium and zirconium alkoxides with oximes



In contrary to the tetra-substituted titanium(amino alcoholate) complex, the corresponding oximate complex is possible at elevated temperature, and the structure has already been determined.  $\text{Ti}(\text{p-anisaldoximate})_4$  has an 8-fold coordinated metal centre with an anti-prismatic coordination geometry.<sup>44</sup> Latest results show tri- and tetra-substituted titanium alkoxo complexes with cyclohexanone oximate and acetone oximate with monomeric arrangement.<sup>45</sup>

Reactions of zirconium alkoxide with various oximes yield different structural motives. Experiments with acetone oxime result in mono-substituted zirconium butoxide complexes.<sup>46</sup> In contrary to the titanium alkoxide, most of their zirconium analogues prefer 8-fold coordinated metal centres with three coordinated oximates and two  $\mu_2$ -OR groups. Only dimeric complexes are possible. (Figure 1.6) There are no hints that tetra-substituted compounds such as  $\text{Ti}(\text{p-anisaldoximate})_4$  can be obtained.<sup>47</sup>

## 1.3 Ligands

### 1.3.1 Bis-( $\beta$ -diketones), triketones, tetraketones and bis-( $\beta$ -ketoesters)

Overviews about organometallic complexes with bis( $\beta$ -diketonate), triketonate and tetraketonate ligands are given by the review articles of Aromi *et al.* and Vigato *et al.*<sup>48,49</sup> The following part only deals with the coordination chemistry of later used ligands and their derivatives.

First results have achieved for complexes of  $\text{CuCl}_2$ ,  $\text{FeCl}_3$  and  $\text{GaCl}_3$  with 1,1'-(1,4-phenylene)bisbutane-1,3-dione. Trimeric and tetrameric metallacycles are prepared with this ligand. In  $\text{Cu}_3\text{L}_3$ , each metal centre is disubstituted, two  $\beta$ -diketonates are coordinated to each copper cation, and each ligand bridges two metal centres (Figure 1.7 left).<sup>50</sup> The synthesis of these cyclic complexes can be extended to other late transition metal cations such as  $\text{Ni}(\text{II})$ ,  $\text{Zn}(\text{II})$  or  $\text{Co}(\text{II})$ .

1,1'-(1,3-Phenylene)bisbutane-1,3-dione permit the formation of dimeric metallacycles (Figure 1.7 right). In case of the above discussed metal cations, additional neutral ligands (pyridine, ethylpyridine, bipyridine, *etc.*) are necessary to stabilize the complexes. Although they differ from metal to metal, the principle structure, metallacycle with bridging bis( $\beta$ -diketonates), can be observed for all compounds. Most of the complexes are characterized by single crystal XRD and FTIR spectroscopy. NMR spectroscopy is no method of choice due to the paramagnetism of the metal cations used. Most metallacycles are synthesised by simple ligand exchange reactions with the ligand and metal chlorides in presence of an inorganic base to catch the released  $\text{HCl}$ .<sup>51-56</sup>

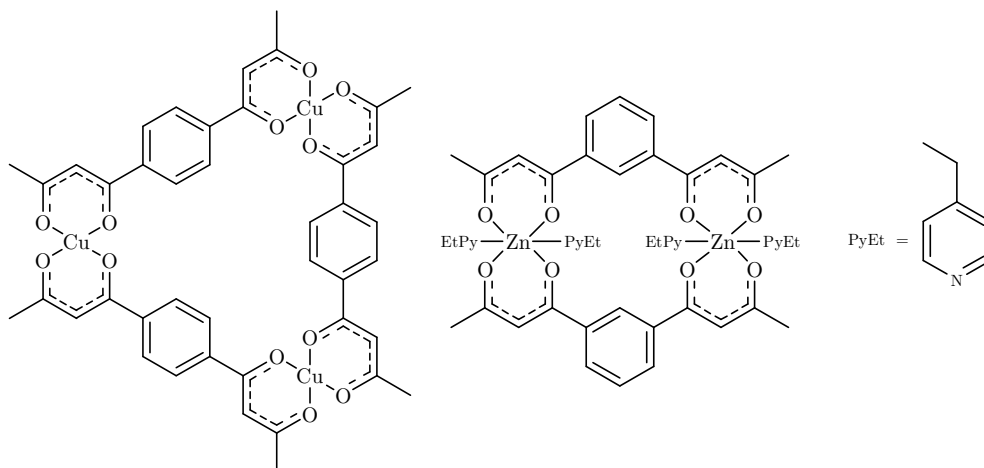


Figure 1.7: Schematic structure of trimeric and dimeric metallacycles

In contrary to the commonly observed metallacycles, zinc acetate dihydrate and 1,1'-(1,4-phenylene)bis-(3-phenylpropane-1,3-dione) form an 1D-coordination polymer in presence of pyridine. Each metal centre is octahedrally coordinated by two  $\beta$ -diketonate units and two pyridines.<sup>57</sup>

First investigations on alkylene-linked bis( $\beta$ -diketones) were done by Bassetti *et al.* UV/VIS and IR spectroscopic investigations proved a composition of  $[\text{CuL}]_n$ , an equilibrium between monomeric, cyclic oligomeric and polymeric compounds was assumed first.<sup>49,58</sup>

Bis( $\beta$ -diketones) linked in the 3-position also form metallacycles. For example, reaction of [1,3-phenylenebis(methylen)]-bis(2,4-pentanedione) with Cu(II) yields two different metallacycles  $\text{Cu}_2\text{L}_2$  and  $\text{Cu}_4\text{L}_4$  (Figure 1.8). In both compounds, each copper cation is coordinated by two  $\beta$ -diketonates, each ligand bridges two metal cations. Other dimeric metallacycles are possible by the use of substituted derivatives of these ligands.<sup>59-62</sup> One example of an early transition metal is the reaction of  $\text{VX}_3(\text{thf})_3$  ( $\text{X} = \text{Cl}$  or  $\text{Br}$ ) with the sodium salt of [1,3-phenylenebis(methylen)]-bis(2,4-pentanedione). It yields the same dimeric metallacycles as with late transition metals.<sup>63</sup>

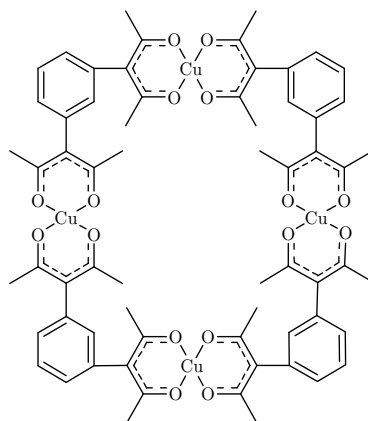
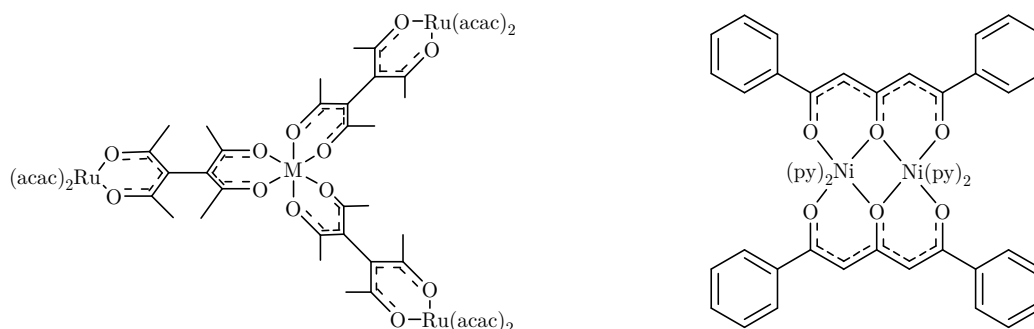


Figure 1.8: Schematic structure of a Cu(II)-metallacycle with [1,3-phenylenebis(methylen)]-bis(2,4-pentanedionate)

1,1,2,2-Tetraacetyethane (taet-H) is the bis( $\beta$ -diketone) with the shortest possible linker in 3-position. A couple of complexes with Co(II), Ru(III), Pd(II) and Cu(II) are known. While Co(II) is forming the known metallacycle, the ruthenium and copper complexes have a dimeric arrangement with only one bridging taet ligand. The remaining coordination sites are saturated by additional acac ligands.<sup>64-68</sup> Furthermore, taet may bridge two different metal ions. Reaction of  $\text{Ru}(\text{acac})_2(\text{taet})$  with other metal ions yields star-like structures with the composition  $\{[\text{Ru}(\text{acac})_2(\text{taet})]_3\text{M}\}$  ( $\text{M}=\text{Al}$  or  $\text{Fe}$ ). Mass spectrometry and powder XRD as well as DFT calculations confirm the proposed structure (Figure 1.9 left).<sup>69</sup>

Reactions of 1,5-diphenyl-1,3,5-pentane-1,3,5-trione, a triketone, with late transition metals yield complexes of composition  $\text{M}_2\text{L}_2$ . Molecular structures of these complexes are known for Co(II) and Ni(II) (Figure 1.9 right). Each ligand bridges two metal centres, the centre oxygen of the triketonate is coordinated to both metal centres. In both cases, a second neutral Lewis base is coordinated to the metal centre.<sup>70,71</sup> Additional complexes with Ni(II), Co(II) and Cu(II) are known with 1,1,1-trifluoro-2,4,6-heptanetrione and 1,1,1,7,7,7-hexafluoro-2,4,6-heptanetrione. The composition and molecular structure is similar to the complexes discussed above.<sup>72</sup>



**Figure 1.9: Schematic structure of  $\{[\text{Ru}(\text{acac})_2(\text{taet})]_3\text{M}\}$  ( $\text{M} = \text{Al}$  or  $\text{Fe}$ ) and  $\text{Ni}_2\text{L}_2(\text{py})_4$**

Reactions of 1,7-diphenyl-1,3,5,7-heptanetetron, a tetraketone, with Cu(II), Ni(II) or Co(II) results in chelate complexes, the structure of which has not been determined yet. IR spectroscopy shows a full coordination of all keto groups; several possible structures have been postulated.<sup>73</sup> Reaction of the ligand with a mixture of uranyl acetate and another metal acetate ( $\text{M} = \text{Fe}$ ,  $\text{Co}$ ,  $\text{Mn}$ ,  $\text{Ni}$ ) of pyridine yields trinuclear complexes of the composition  $(\text{UO}_2)_2\text{ML}_2\text{py}_4 \cdot 2\text{py}$  in the presence (Figure 1.10). Structural investigations show that the guest metal is coordinated in the central position of the tetraketonate, while the uranyl units are in the outer, terminal position. The central oxygen atoms bridge two different metals.<sup>49,74</sup> Furthermore, reactions of 1,7-diphenyl-1,3,4,5,7-heptanepentaone with Co(II) result in binuclear complexes, in which two keto groups are coordinated to each metal centre.<sup>75</sup>

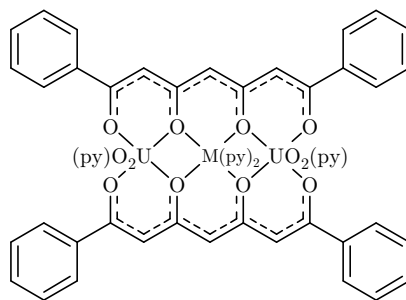


**Figure 1.10: Schematic structure of  $(\text{UO}_2)_2\text{ML}_2\text{py}_4 \cdot 2\text{py}$  ( $\text{M} = \text{Fe}, \text{Co}, \text{Mn}, \text{Ni}$ )**

Only few examples with this group of ligands have been reported with titanium, zirconium or metal alkoxides. Ugrinova *et al.* employed bis( $\beta$ -diketones) linked by 2,2'-biphenyldiyl, 2,2'-tolandiyl or 2,2'-bis(methylene)biphenyl moieties in the reaction with  $\text{Ti}(\text{O}^i\text{Pr})_4$  and obtained monomeric complexes  $\text{Ti}(\text{O}^i\text{Pr})_2[\text{bis}(\beta\text{-diketonate})]$ .<sup>76</sup> Similar results with 2,2'-biphenyl-bis(4-ferrocenyl-2,4-butanedione) have also been reported by Dulatas *et al.*, of which a crystal structure is obtained with metal alkoxides with larger OR groups.<sup>77</sup> A dimeric complex  $\text{Ti}_2\text{L}_3$ , the first titanium-containing metallacycle, is obtained with  $\text{TiCl}_3(\text{THF})_3$  and 1,3-bis(3-phenyl-3-oxopropanoyl)benzene. Similar to the structures discussed above, all bis( $\beta$ -diketonates) bridge both titanium centres.<sup>78</sup>

Only few examples of bis( $\beta$ -ketoesterate) complexes have been reported. First investigations with tetramethylene bis-acetoacetate were done with beryllium sulfate. Kluiber *et al.* postulated an equilibrium between dimeric cyclic structures, known from structural investigations of metal bis( $\beta$ -diketonate) complexes, and polymeric moieties. A glass transition temperature, typical for polymeric species, is measured for these species, and IR spectroscopy proves the complete coordination of the ligand.<sup>79</sup> Mehrotra *et al.* has conducted experiments with different alkylene-linked bis( $\beta$ -ketoesters) and titanium/zirconium alkoxides. They result in compounds of different solubility. Observing different substitution degrees for varying equivalents of titanium/zirconium alkoxides, dimeric and/or polymeric structures are assumed.<sup>80-83</sup>

### 1.3.2 Dioximes

Experiments with titanocene dichloride and various dioximes were done by Carraher *et al.* to synthesise titanium polyoximates. Molecular masses, starting from 8000 g/mol, are detected for all dioximes in the mass spectra, and IR spectroscopic experiments proved a complete coordination of dioximates. A polymeric structure is postulated for these compounds.<sup>84</sup> Single crystal X-ray diffraction find a dimeric structure  $[\text{TiCp}_2(\text{dioximate})\text{TiCp}_2]\text{X}_2$  ( $\text{X} = \text{Cl}^-, \text{Br}^-$  or  $\text{NO}_3^-$ ) with only one side-on coordinated oximate group per titanium centre.<sup>85</sup> Studies of the reaction of titanium tetrachloride and benzildioxime show no polymeric species but mono- and disubstituted titanium complexes. Although no molecular structure is determined by single crystal X-ray diffraction, NMR spectroscopy proves the side-on coordination of all oximate groups.<sup>86</sup> Comparable observations are made with di(pentafluorophenyl)glyoxime and Fe(II) resulting in monomeric

complexes, in which two mono-deprotonated dioximates coordinate to the octahedrally coordinated metal centre.<sup>87</sup> Similar results with 1,2-dioxime derivatives have been observed by Varhelyi *et al.* with platinum and Masuda *et al.* and Dutta *et al.* with cobalt (Figure 1.11).<sup>88-90</sup>

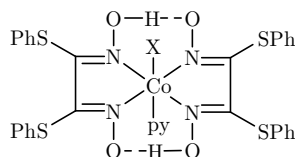


**Figure 1.11: Schematic structure of  $\text{CoCl}(\text{dSPHgH})_2\text{py}$**

Concerning the reactions of metal alkoxides with dioximes, Baumann *et al.* reported a cyclic tetrameric structure, which was isolated from the reaction of  $\text{Ti}(\text{O}^i\text{Pr})_4$  and 2,4-pentanedione dioxime. In these compounds, two dimeric titanium units are bridged by dioximates. Each dimer contains two titanium atoms bridged by two alkoxo and one dioximate ligands (Figure 1.12).<sup>43</sup>

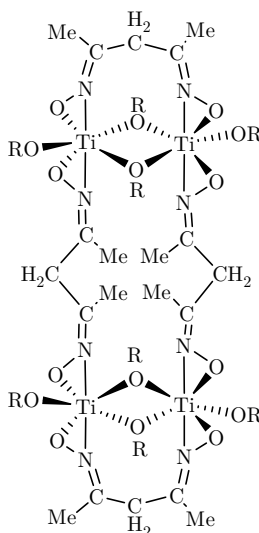


**Figure 1.12: Schematic structure of  $\text{Ti}_4(\text{O}^i\text{Pr})_8(\text{ON}=\text{CMe}-\text{CH}_2-\text{CMe}=\text{NO})_4$**

### 1.3.3 Bis(salicylaldiminates)

Reactions of  $\text{Cu}(\text{II})$  with bis(salicylaldimate) ligands with various length of the alkylene spacer yield two different types of structures. Ligands with ethylene, propylene or butylene spacers result in monomeric complexes  $\text{CuL}$ , whereas dimeric complexes  $[\text{CuL}]_2$  are achieved with 1,5-bis(salicylideneamino)pentane or 1,6-bis(salicylideneamino)hexane. These dimeric structures are comparable to the metallacycles discussed in chapter 1.3.1. All postulated structures are confirmed by single crystal X-ray diffraction experiments.<sup>91</sup> Similar structural motives are observed in various complexes of bis(salicylaldiminates) with  $\text{Pt}(\text{II})$ ,  $\text{Cu}(\text{II})$ , and  $\text{Pd}(\text{II})$  (Figure 1.13). Single crystal X-ray diffraction shows syn- and anti-coordinated dimeric complexes.<sup>92,93</sup> Compounds with

a bridging bis(salicylaldiminate) ligand are obtained for Mn(III). Only one ligand bridges both metal centres, the coordination sphere of the metal is saturated with monodentate ligands.<sup>94</sup>

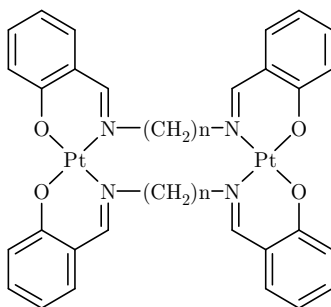


Figure 1.13: Schematic structure of  $\{\text{Pt}[\text{bis}(\text{salicylaldiminate})]\}_2$

Monomeric compounds are observed in Ni(II) or Co(II) and bis(salicylideneamino)alkanes and with Pd(II) and 1,4-bis(salicylideneamino)benzene.<sup>95-97</sup>

Titanium bis(salicylaldiminate) complexes are hardly known. Tsuchimoto *et al.* published two different structures, which were determined from crystals obtained by the reaction of  $\text{TiO}(\text{acac})_2$  and 1,2-bis(salicylideneamino)ethane. A dimeric structure with bridging oxo groups and one coordinated bis(salicylaldiminate) ligand per titanium is reported, whereas also one-dimensional polymer chains with  $[\text{LTi}=\text{O} \cdots \text{LTi}=\text{O} \cdots \text{LTi}=\text{O}]_n$  are observed.<sup>98</sup> Comparable structures have been reported by Choudhary *et al.*<sup>99</sup> Experiments with several modified 1,2-bis(salicylideneamino)ethane derivatives and  $\text{TiCl}_4$  prove the monomeric character of the obtained complexes (Figure 1.14).<sup>99-101</sup> Tetramers are obtained with ligands bearing two bis(salicylaldiminate) units. Each ligand coordinates to two titanium atoms. Both  $\text{LTi}_2$  units are connected by additional Ti-O-Ti bridges.<sup>102</sup>

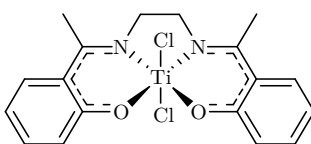


Figure 1.14: Schematic structure of  $\text{Ti}[\text{bis}(\text{salicylaldiminate})]\text{Cl}_2$

Balsells *et al.* and Quiroz-Guzman *et al.* reported several structures of monomeric titanium isopropoxide complexes with different SALAN ligands. Each titanium atom centre is octahedrally coordinated; the two isopropoxide ligands are in *cis*-position to each other (Figure 1.15).<sup>103,104</sup> Similar monomeric complexes are obtained from the reaction of  $\text{Ti}(\text{OEt})_4$  and a hybrid SALAN/SALEN tetradentate ligand.<sup>105</sup> Additional monomeric complexes with titanium aryloxo ligands and several 1,4-bis(salicylideneamino)benzene derivatives have been reported by Tzuber *et al.* In these complexes both aryloxo ligands are in *trans*-position to each other, while the bis(salicylaldiminate) ligand coordinates in the equatorial positions. If both aryloxo ligands are substituted by 1,2-dihydroxybenzene, the alkoxo ligands coordinate in *cis/cis*.<sup>106,107</sup>

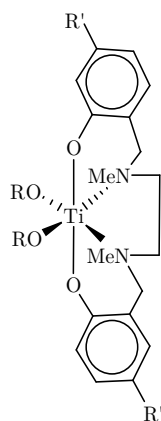


Figure 1.15 Schematic structure of  $\text{Ti}(\text{SALAN})(\text{O}^i\text{Pr})_2$

### 1.3.4 Tri- and tetra-carboxylic acids

Benzenetribenzoate (BTB-3), benzenetetrabenzoate (BTB-4), tetrakis(4-carboxyphenyl)silane (TCPS) and adamantyl tetracarboxylate (ATC) are commonly used building blocks for metal-organic frameworks.

$\text{Co}(\text{II})$  forms a MOF with BTB-3. The metal building blocks are no longer single metal cations, but instead  $\text{Co}_3(\text{COO})_6$  units. The central  $\text{Co}(\text{II})$  is octahedrally coordinated by six carboxylate oxygen atoms. The  $\text{Co}(\text{II})$  cations are bridged by four carboxylate groups, and they form a linear arrangement. Two residual solvent molecules are coordinated to each terminal cobalt atom. Each  $\text{Co}_3$ -complex is connected through six BTB-3 ligands with the neighbouring trimeric complexes (Figure 1.16 left).<sup>108</sup> Other  $\text{Co}(\text{II})$ -MOFs with trimeric building blocks are known, in which three cobalt atoms are coordinated to one central  $\mu_3\text{-OH}$  group. Another bridging carboxylates connect the Co atoms with each other and link the building blocks with other clusters in all directions.<sup>109</sup> MOFs with similar structures are postulated for  $\text{Al}(\text{III})$ -MOFs with BTB-3. In these compounds, chains of  $\text{Al}(\text{III})$  are built; each  $\text{Al}(\text{III})$  is octahedrally coordinated and bridged by three carboxylate groups to the next  $\text{Al}(\text{III})$  (Figure 1.16 right). Due to the absence of single crystals, the structure is calculated by theoretical methods and compared with powder XRD and spectroscopic measurements.<sup>110</sup>

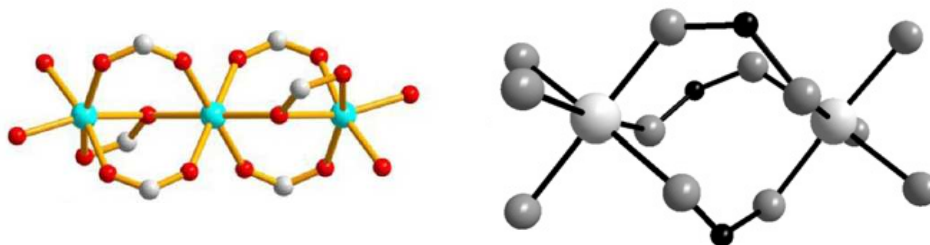


Figure 1.16: Schematic structure of the MOF building blocks of  $\text{Co}(\text{II})$ -BTB-3-MOF<sup>108</sup> (left) and  $\text{Al}(\text{III})$ -BTB-3-MOF<sup>110</sup> (right)

Pillared paddle wheel MOFs with BTB-4 and Zn have been reported by Gadzikwa *et al.*, in which BTB-4 is coordinated to four independent Zn moieties. Two tetrameric assemblies are connected by four diamino ligands (Figure 1.17).<sup>111-113</sup> Similar structural motives are also achieved using diamino functionalized Mn(II)(bis(salicylaldiminate)) complexes as a linker between the tetrameric assembly.<sup>114</sup> Independent of the pillared paddle wheel structures, other Zn-MOFs are achievable with BTB-4. In  $\text{Zn}_2(\text{BTB-4}) \cdot 3 \text{H}_2\text{O}$  each zinc atom is coordinated to four bridging carboxylate ligands, connecting them to the next metal centre. Dimeric units of  $\text{Zn}_2(\text{COO})_2$  are formed, which build zigzag chains of Zn-carboxylates, which are connected by BTB-4 in each direction.<sup>115</sup>

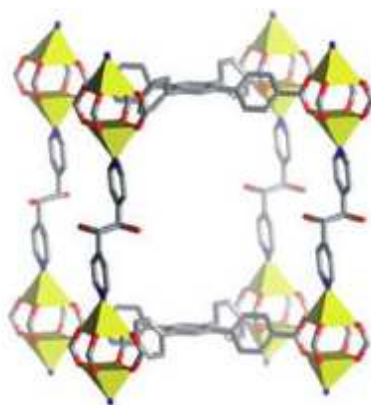
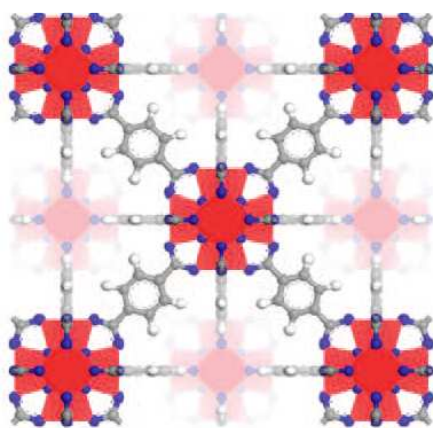


Figure 1.17: Model of pillared paddle wheel Zn-BTB-4-MOF<sup>113</sup>

Cu-MOFs with TCPS contain dimeric  $\text{Cu}_2(\text{COO})_4$  complexes; one TCPS ligand bridges four Cu building blocks. In Zn(II), Mn(II) and Cd(II)-MOFs with TCPS, two metal atoms are bridged by at least two or three carboxylates. The metal carboxylate chains formed are connected by TCPS ligands.<sup>116</sup> Another Zn carboxylate MOFs with TCPS are also reported by Lambert *et al.*, in which the zinc atoms are bridged by two carboxylates.<sup>117</sup>

MOFs of these ligands and titanium, zirconium or any metal alkoxides have not been reported. Nevertheless, structural investigations have been published about MOFs containing Zr(IV) and terephthalic acid (UiO-66). In these structures, the metal core is a zirconium oxo cluster instead of a single metal ion. These structures are synthesised by solvothermal synthesis of  $\text{ZrCl}_4$  and terephthalic acid. Six dicarboxylic acids connect the cluster in each direction. Comparable structures are determined for biphenyl-dicarboxylate and terphenyl-dicarboxylate (Figure 1.18).<sup>118</sup> Guillerm *et al.* has proved that this cluster can also be synthesised by ligand exchange reactions between  $\text{Zr}_6\text{O}_4(\text{OH})_4(\text{OMc})_{12}$  and terephthalic acid. X-ray powder diffraction confirms that the obtained MOF architecture is identical to the above discussed UiO-66, synthesised with  $\text{ZrCl}_4$ . Furthermore, UiO-66-like clusters with *trans,trans*-muconic acid are possible with this procedure.<sup>119</sup>





**Figure 1.18: Molecular structure of UiO-66<sup>118</sup>**

Ferey *et al.* have reported a titanium dicarboxylate compound with MOF architecture (MIL-125). Solvothermal synthesis is done with  $\text{Ti}(\text{O}^i\text{Pr})_4$  and terephthalic acid in DMF. Single crystal X-ray diffraction and additionally theoretical calculations determine a structure, which is built by  $\text{Ti}_8\text{O}_8(\text{OH})_4$  cluster cores. Comparable to UiO-66, six dicarboxylate ligands connect the building units.<sup>120</sup>

## 1.4 Structured and porous titanium oxides

Titanium oxide materials are used in applications, where their electrochemical properties, photocatalytic activity, chemical stability and non-toxic behaviour play an important role. Especially porous and structured anatase is investigated in the fields of thin film coatings, photocatalysis and catalytic supports. The main route to synthesise titanium oxide materials is sol-gel processing. Controlled hydrolysis of organically modified titanium alkoxides or chlorides results in amorphous and (meso)porous materials with a high surface area. Crystalline materials are obtained by an annealing step at 300 °C, during this treatment the porous architecture collapses.<sup>121</sup>

The use of structure-directing agents (templates) is a common way to synthesise structured titanium oxide materials. These templates (for example, block copolymers, ionic tensides, *etc.*) are amphiphilic. They form supramolecular arrays such as spherical micelles. Structuring is mainly based on hydrophobic/hydrophilic interactions. The properties of these arrays depend especially on the surfactant concentration. Increasing the template proportion leads to micellar phases and liquid crystals. Structural motives and pore size can be defined by choosing a suitable template. The removal of the template can be conducted by extraction and/or calcination steps. The structure remains even after elimination of the template after sol-gel processing.<sup>1,122</sup>

Pioneering work has been done by Antonelli *et al.*, who have reported a modified sol-gel route of acetylacetonate modified titanium alkoxides to obtain mesoporous  $\text{TiO}_2$ .<sup>123</sup> Yang *et al.* have first reported the use of amphiphilic poly(alkylene oxide) block copolymers to introduce mesoporosity to titanium and other metal oxides.<sup>124,125</sup> Soler-Illia *et al.* have summarized and broadened investigations in different templating techniques with a couple of varying block copolymers, with which

meso-structured materials are possible.<sup>126</sup> Using different templates also allows the preparation of materials with hierarchical pore structure, in which different kinds of porosity are present in one material.

A special technique to introduce mesoporosity via templating in thin films is evaporation-induced self-assembly (EISA). Structured assemblies result by slow evaporation of the solvent in presence of a surfactant. This method has been developed for silicon-based sol-gel processing,<sup>127</sup> but proves to work well also for the preparation of mesoporous transition metal oxides.<sup>128,129</sup>

## 2 Research goals

Many group (IV) metal oxide materials with defined structure and porosity are used in numerous applications. Chapter 1.4 covers several methods for the preparation of these materials. In most syntheses, structure-directing agents are used to obtain a defined architecture of the material and large porosity. Only few examples have been reported until now, in which no surfactant is used to achieve these properties.

The main goal of this work is the synthesis of pre-organized/pre-structured precursors for the preparation of porous and structured group (IV) metal oxides. The structure and design of the precursor should determine the later structure of the oxide material. Various structural motives of metal alkoxides are considered. Coordination polymers are a promising access to introduce any kind of pre-organisation. In these polymeric assemblies the ligands should block as many coordination sites as possible to render hydrolysis and coordination only possible in defined directions. Some examples of such polymeric structures are known with diamines.<sup>7,8</sup> Herein, the Ti-N bond is hydrolytically unstable, however the pre-organisation does not sustain sol-gel processing. Oligomeric structures are also known with dioximate ligands.<sup>43</sup> Oximate groups are known for their stronger interaction with the metal alkoxide, and the pre-structuring should be retained.

Therefore, using difunctional, tetradentate chelating ligands might allow the formation of coordination polymers, in which pre-organisation is retained in the final material. In a first attempt, bis( $\beta$ -diketones) and bis( $\beta$ -ketoesters) are synthesised, as they are known for strongest coordinative bonding to titanium/zirconium alkoxides. Different linkers, rigid and flexible ones, are introduced to investigate the impact on the structure of the modified metal alkoxides. The ligands will be reacted with various titanium alkoxides to check whether the structure is influenced by the alkoxo groups used. Investigations of the obtained products are done in solution as well as in solid state. The results will be compared to complexes obtained from other tetradentate ligands. Dioximes, especially with cyclic linkers, and various bis-Schiff base are synthesised and used for the modification of titanium alkoxides. Investigations can be extended to other difunctional ligands. All investigations will be extended to zirconium alkoxides, after getting enough information about structure and coordination behaviour of these tetradentate ligands with titanium alkoxide. Furthermore, sol-gel processing should show whether the observed structural assemblies are still present in the final metal oxide material.

Network-like structural motives can be introduced by MOF-like assemblies. Some compounds are reported with zirconium tetrachloride and terephthalic acid (UiO-66), in which the difunctional ligands connect zirconium oxo clusters in three dimensions. This access can be extended to tri- and tetrafunctional ligands. To this end, tri/tetrafunctional carboxylic acids, oximes or  $\beta$ -diketones are synthesised. Different linkers will be introduced to enlarge the linker between the metal moieties. Modifications are carried out with various titanium and zirconium precursors. Different synthetic ways will be tested. Furthermore, the structure and porosity of the materials are compared with them of hydrolyzed materials.

### 3 Modification of group(IV) metal alkoxides with bifunctional ligands

#### 3.1 Modification of titanium alkoxides with bis( $\beta$ -diketones)

##### 3.1.1 Reaction of titanium alkoxides with arylene-bridged bis( $\beta$ -diketones)

Rare examples of titanium bis( $\beta$ -diketonate) complexes were known. Ugrinova et al. applied bis( $\beta$ -diketones) linked by 2,2'-biphenyldiyl, 2,2'-tolandiyl or 2,2'-bis(methylene)biphenyl moieties in the reaction with  $\text{Ti}(\text{O}^i\text{Pr})_4$  and obtained monomeric complexes with the formula  $\text{Ti}(\text{OR})_2[\text{bis}(\beta\text{-diketonate})]$ . The special linkers, in which both functional groups were quite close to each other, preferred coordination of both  $\beta$ -diketonate units to the same metal.<sup>76</sup> No compounds were reported, in which bis( $\beta$ -diketones) were used as ligands for metal alkoxide modification.

Reactions of one molar equivalent of different bis( $\beta$ -diketones) (Figure 3.1) with  $\text{Ti}(\text{O}^i\text{Pr})_4$  resulted in yellowish oils **1**, **2** and **3**. Due to the high flexibility of the spacer groups, the compounds did not crystallise and other methods than single crystal XRD had to be applied to elucidate the composition and structure of the products.

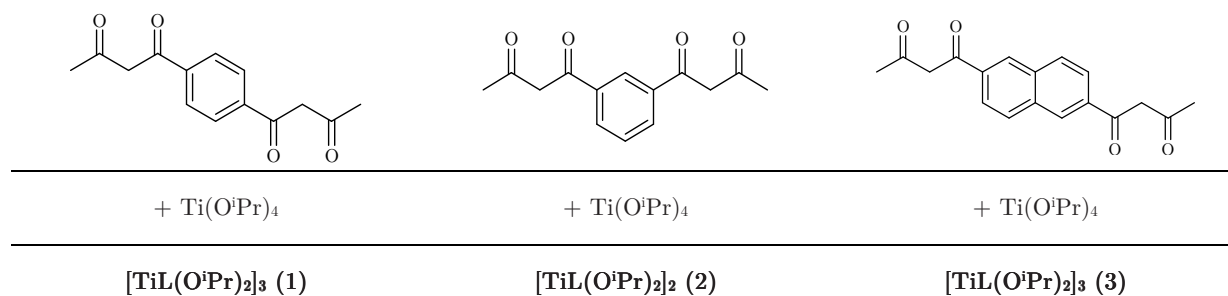


Figure 3.1: Arylene-bridged bis( $\beta$ -diketones) used in this work and the resulting titanium compounds

Electrospray ionization mass spectrometry proved to be a very powerful analysis method. Investigations of **1** resulted in a trimeric structure  $[\text{TiL}(\text{O}^i\text{Pr})_2]_3$ . (Figure 3.1) The compound was detected as the corresponding sodiated complex at  $m/z$  1253.7 (calc. 1253.4). (mass spectrum see Figure 3.2) Another fragment at  $m/z$  1171.6 (calc. 1171.3) was present in the spectrum. It was assigned to  $\text{Ti}_3\text{L}_3(\text{O}^i\text{Pr})_5^+$  and was derived from the same sodiated complex. The most intensive peak at 1311.6 was assigned to the isopropanol adduct of the sodiated complex. The low basicity of the whole compound inhibited the commonly observed protonation of the product. Thus, traces of sodium ions formed the dominating mono-sodiated molecular ion, which was detected in the positive ion ESI mass spectrum.

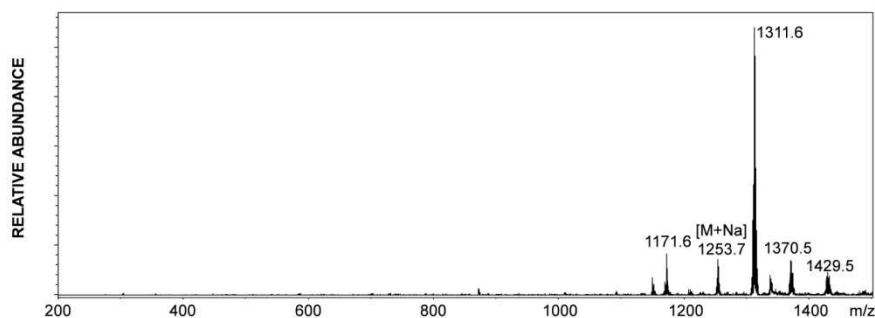


Figure 3.2: Positive ion ESI mass spectrum of  $[\text{TiL}(\text{O}^i\text{Pr})_2]_3$  (**1**)

Considering complexes of Co(II), Ni(II) and Zn (II) with 1,1-(1,4-phenylene)-bis-butane-1,3-dione, a trimeric metallacycle was the most likely structure.<sup>50,52,130</sup> Previous observations had shown that this ligand only built trimeric metallacycles due to its rigid linker.<sup>131</sup> The trimeric structure fitted well with the constitution derived from the mass spectra. In this complex, each titanium atom was coordinated by two terminal isopropoxo and two  $\beta$ -diketonate groups (Figure 3.3). Each bis( $\beta$ -diketonate) connected two  $\text{Ti}(\text{O}^i\text{Pr})_2$  moieties with each other.

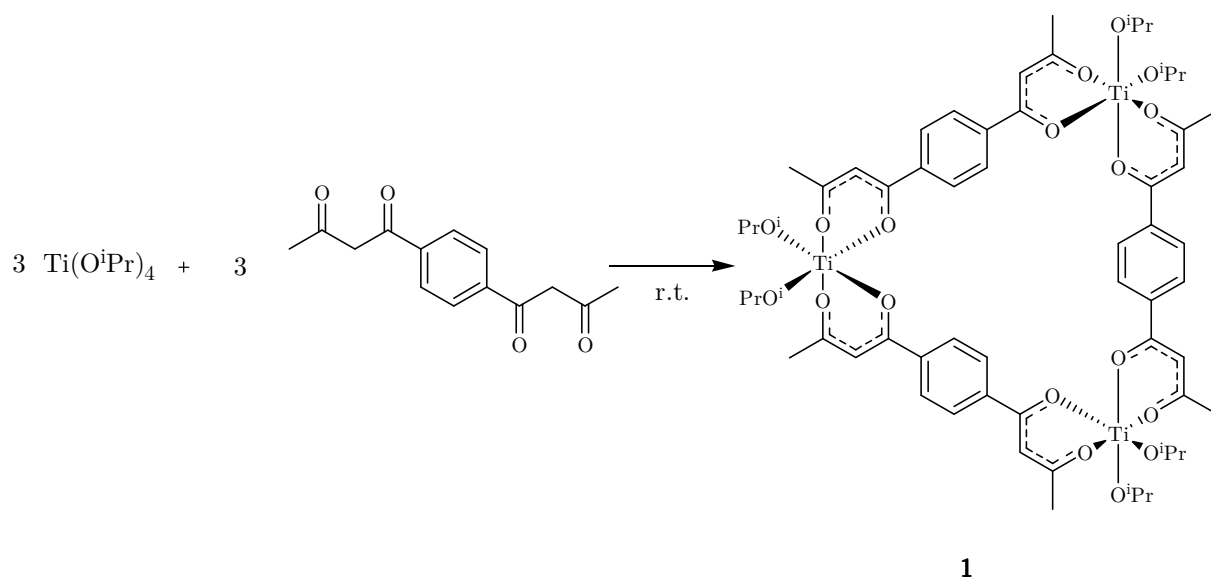


Figure 3.3: Synthesis and suggested structure of **1**

IR and NMR investigations of compound **1** confirmed the assumed structure. IR spectroscopic investigations showed a significant shift of the bands of the characteristic asymmetric C=O stretching frequency from 1602 to 1581, 1517 and 1491  $\text{cm}^{-1}$ . This confirmed a complete coordination of all  $\beta$ -diketonate units to the metal centres. The shift observed for the C=O stretching frequency was in agreement with previous IR investigations of numerous (mostly late transition metal) complexes of type  $\text{ML}$  or  $\text{M}_2\text{L}$  [ $\text{M} = \text{Cu}(\text{II})$ ,  $\text{Ni}(\text{II})$ ,  $\text{Co}(\text{II})$ ,  $\text{VO}(\text{II})$ ,  $\text{Zn}(\text{II})$ ,  $\text{Mn}(\text{II})$ ,  $\text{Mg}(\text{II})$ ,  $\text{Tl}(\text{I})$  or  $\text{Th}(\text{II})$ ;  $\text{L} = 1,1$ -(1,4-phenylene)-bis-butane-1,3-dione].<sup>132</sup>

$^{13}\text{C}$  NMR measurements exhibited four signals between 193.6 and 178.5 ppm assigned to carbonyl groups. Two resonances per  $\text{C}=\text{O}$  group were caused by different positions on the octahedral coordination sphere of titanium, which was only possible with a low symmetry of the substituted titanium moiety. If two equivalent carbonyl carbons of the  $\beta$ -diketonate groups were in *trans*-position to each other, two resonances per  $\text{C}=\text{O}$  group were achieved. Beside the structure in Figure 3.3, a second isomer with lower symmetry exists and probably was the reason for the four  $\text{C}=\text{O}$  resonances. Similar observations were made for  $\text{Ti}(\text{acac})_2(\text{OR})_2$  and  $[\text{Ti}(\text{acac})(\text{OR})_3]_2$ . In  $\text{Ti}(\text{acac})(\text{O}^i\text{Pr})_3$ , two signals at 190.0 and 186.3 ppm were observed.<sup>12</sup>

The HSQC spectra (Figure 3.4) showed a correlation at 6.29/99.0 ppm which was attributed to the  $\text{COCHCO}$  methine proton. Two additional correlation signals at 2.05/27.4 and 2.25/26.5 were observed for the corresponding  $\text{CH}_3\text{CO}$  methyl group, which was in line with coordination to non-equivalent positions on the octahedrally coordinated titanium centre.

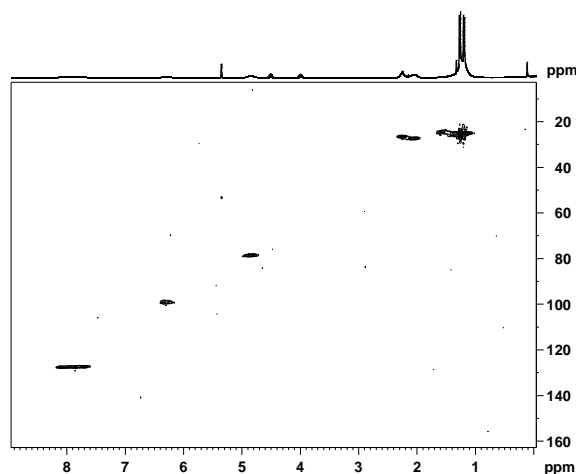


Figure 3.4: HSQC spectra of 1

The  $^{13}\text{C}$  NMR spectrum showed only signals for terminal alkoxo groups at 78.8 and 25.2 ppm. The absence of signals for bridging  $\text{O}^i\text{Pr}$  ligands in the spectra supported the assumed structure. The position of the alkoxo groups to each other could not be determined by both analysis techniques. According to observations of  $\text{Ti}(\text{O}^i\text{Pr})_2(\text{acac})_2$  and other  $\text{Ti}(\beta\text{-diketonate})_x(\text{OR})_{4-x}$ , a *cis* position was quite likely.<sup>12</sup>

Experiments with larger proportions of titanium alkoxide did not result in a different molecular structure. Similar peaks were observed in the mass spectra. Furthermore, a prominent peak at  $m/z$  307.1 (calc. 307.1) was increasing intensity, which was assigned to the  $\text{Ti}(\text{O}^i\text{Pr})_4\text{Na}^+$  ion. Similar observations were made in the corresponding carbon NMR spectra. No changes were observed in the carbonyl group region.

Furthermore, these measurements proved that the trimeric metallacycles with three disubstituted  $\text{Ti}(\text{O}^i\text{Pr})_2$  moieties were the most stable structure. In contrary to investigations of  $\text{Ti}(\text{acac})_x(\text{OR})_{4-x}$ , no equilibrium between the mono- and disubstituted derivate was observed.<sup>12</sup>

A rare example of coordination polymers with an 1,1-(1,4-phenylene)-bis-butane-1,3-dione derivate was reported by Soldatov *et al.* for zinc.<sup>57</sup> Therefore, the ESI-MS experiments were extended to higher molecular masses. The measurements showed no additional signals above  $m/z$  1253.7. Thus, polymeric forms of **1** were excluded.

Moving from 1,1-(1,4-phenylene)-bis-butane-1,3-dione to the corresponding 1,3-arylene linked bis( $\beta$ -diketone) led to a different ESI mass spectrum. A peak at significantly lower mass with  $m/z$  843.5 was the most intensive signal, for which a molecular composition of  $\{[\text{TiL}(\text{O}^i\text{Pr})_2]_2\text{Na}\}^+$  (calc. 843.2) was derived. The above observed peak at  $m/z$  1253.6 was also present in the spectrum but only with very low intensity. (Figure 3.5).

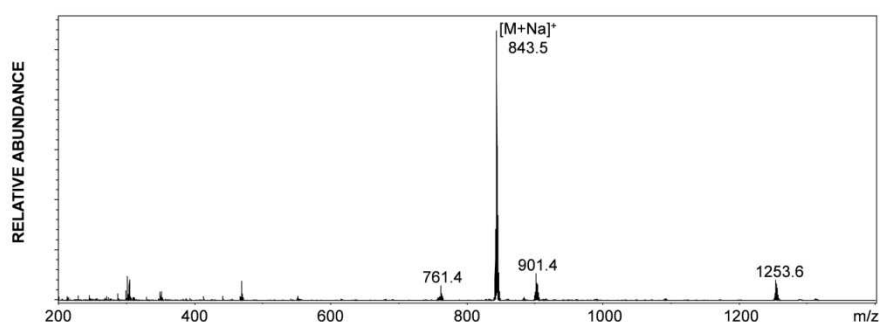


Figure 3.5: Positive ion ESI mass spectrum of **2**

The calculated composition of the sodiated molecule matched well with a dimeric metallacycle, in which each titanium centre was disubstituted and bridged by two ligands with each other. (see Figure 3.6) This would be in line with previous investigations of complexes of 1,1-(1,3-phenylene)-bis-butane-1,3-dione and late transition metal ions. They proved that the smaller angle between both bis( $\beta$ -diketone) units promoted a smaller, only dimeric metallacycle.<sup>51,53,55</sup>

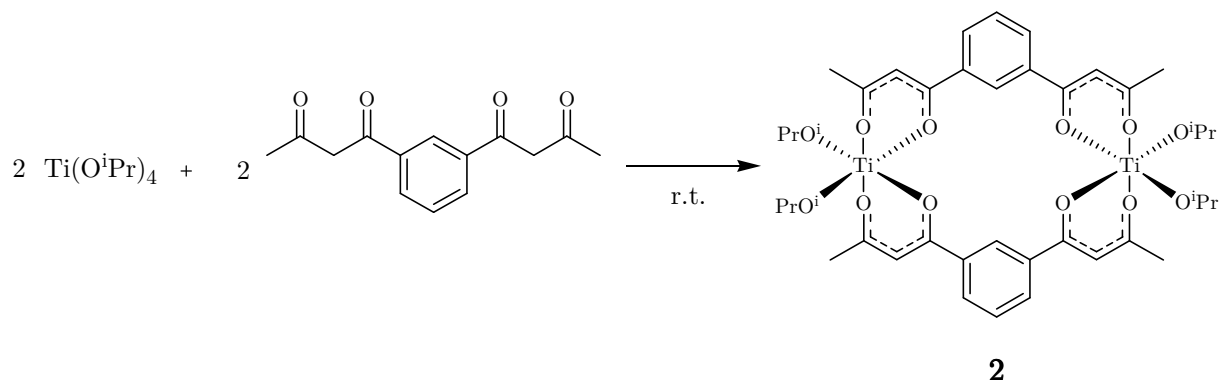


Figure 3.6: Synthesis and proposed structure of **2**

Another peak at  $m/z$  351.0 (calc. 351.1) was present in the mass spectrum, which was attributed to the monomeric complex ion  $[\text{TiL}(\text{O}^i\text{Pr})]^+$ . An equilibrium between a monomeric and a dimeric

complex was theoretically possible. Low energy CID MS/MS measurements of the most prominent peak at  $m/z$  843.5 only resulted in one product ion at  $m/z$  351.0. This experiment proved that the observed monomeric compound was only caused by in-source fragmentation during the ESI-MS measurement and that the compound itself was not present in the solution. Mass spectrometric investigations at higher masses supported the assumed structure, as no polymeric or larger oligomeric species were obtained.

$^{13}\text{C}$  NMR experiments exhibited a significant shift in carbonyl group region. Similar to the spectrum of **1**, four signals were observed. Only one pair of peaks was present for the alkoxo groups in  $^1\text{H}$  and  $^{13}\text{C}$  NMR spectra (Figure 3.7), which excluded bridging units. Both spectra supported the postulated structure. When larger proportions of titanium alkoxide were added, the product composition was not changed; the dimeric titanium alkoxo metallacycle was the preferred arrangement.

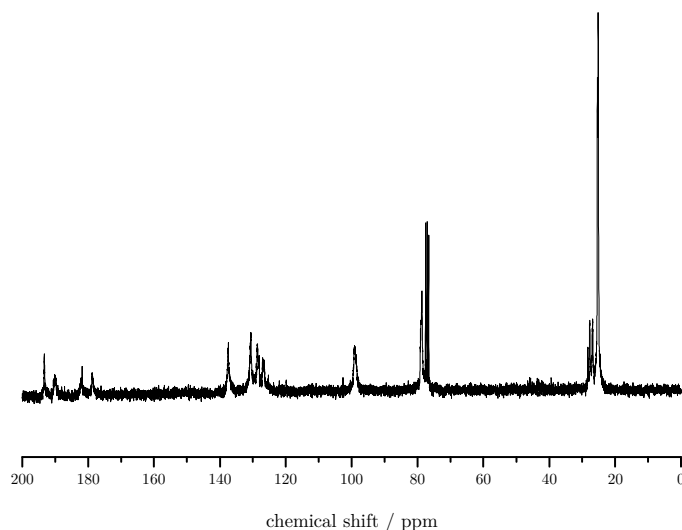
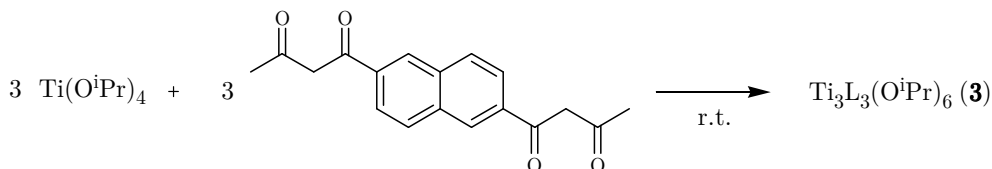


Figure 3.7:  $^{13}\text{C}$  NMR spectrum of **2**

The postulated dimeric metallacycle fitted well with the previously reported dimeric complexes  $\text{Ti}_2\text{L}_3$ . Grillo *et al.* reported the molecular structure of a dimeric complex, in which both Ti(III) centres were bridged by three 1,1-(1,3-phenylene)-bis-butane-1,3-dionate derivates. In comparison to compound **2**, an additional bis( $\beta$ -diketonate) ligand was present, due to the lower oxidation state of titanium in this compound.<sup>78</sup>

The experiments were extended to a bis( $\beta$ -diketone) with a 1,6-naphthylene linker. This ligand was comparable to the above discussed 1,1-(1,4-phenylene)-bis-butane-1,3-dione. Both  $\beta$ -diketones groups were in *para* position to each other. The reaction with  $\text{Ti}(\text{O}^i\text{Pr})_4$  resulted in an oily residue **3**. (Figure 3.8) ESI-MS measurements of compound **3** did not result in any reasonable fragments and was not the method of choice. NMR experiments showed similar spectra, than that obtained from compound **1**.

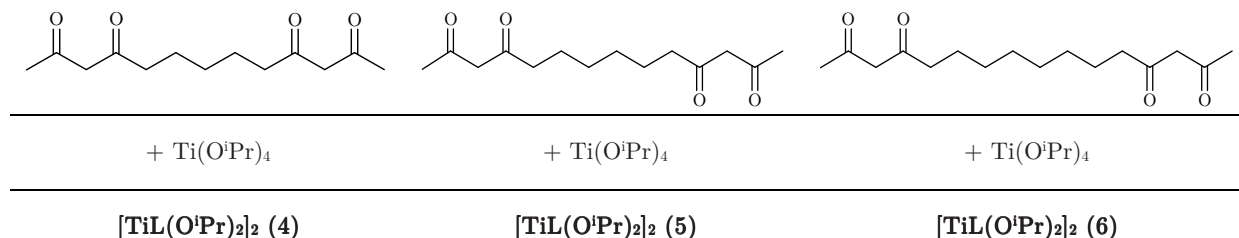


Figure 3.8: Synthesis of compound **3**

The  $^{13}\text{C}$  NMR spectra exhibited four resonances for the carbonyl groups, which were derived from axial/equatorial positioning of each group. Two additional sets of O<sup>i</sup>Pr signals appeared in the  $^1\text{H}$  and  $^{13}\text{C}$  NMR spectra, which were either caused by residual unreacted  $\text{Ti}(\text{O}^i\text{Pr})_4$  or non-equivalent positions (axial/equatorial) of the O<sup>i</sup>Pr units. Previous investigations of Cu(II) complexes with this ligand proved a comparable trimeric, metallacyclic structure similar to the ones known with 1,1'-(1,4-phenylene)-bis-butane-1,3-dione.<sup>50</sup> Therefore, the similar NMR spectroscopic results were good evidence that compound **3** was built up by a trimeric metallacycle.

### 3.1.2 Reaction of titanium alkoxide with alkylene-bridged bis( $\beta$ -diketones)

Reaction of alkylene-bridged bis( $\beta$ -diketones) and  $\text{Ti}(\text{O}^i\text{Pr})_4$  were performed to check whether the rigidity of the linker influenced the structure obtained. Experiments with all bis( $\beta$ -diketones) (Figure 3.9) resulted in oily products **4-6**.

Figure 3.9: Alkylene-bridged bis( $\beta$ -diketones) used in this work and the resulting titanium compounds

Several alternative attempts were done to crystallise one of these compounds and to facilitate structure determination. The experiments failed in a very special way. In some cases, small crystals were isolated after weeks, which were measured by single crystal XRD. Surprisingly, the unit cell matched perfectly with that of the  $\text{Ti}_{11}\text{O}_{13}(\text{O}^i\text{Pr})_{18}$  cluster. The result was independent of the used bis( $\beta$ -diketone) and the titanium alkoxide to ligand ratio. When  $\text{Ti}(\text{O}^i\text{Pr})_4$  was allowed to react with diacetone alcohol or an excess of acetylacetone, clusters of identical constitution were observed by Sanchez *et al.*<sup>133</sup> Hereby, the ketone acted as an oxolation source for cluster formation. This side reaction was caused by a comparable reaction mechanisms, as described in the paper mentioned. This was a good argument, why no solid state structures were determined with such ligands in combination with titanium alkoxides. Therefore, ESI-MS was the method of choice for composition analysis.

All reaction products were investigated in chloroform/2-propanol solutions. No clusters of type  $\text{Ti}_{11}\text{O}_{13}(\text{O}^i\text{Pr})_{18}$  were observed in mass spectra. Each sample was prepared freshly to avoid cluster formation. In each spectrum, one peak for the sodiated complex  $\{[\text{TiL}(\text{O}^i\text{Pr})_2]_2\text{Na}\}^+$  was observed. The same composition was also calculated for the molecular ion of compound **2**. All used alkylene-bridged bis( $\beta$ -diketones) coordinated in the same way, the structure was therefore assumed to be identical to the above proposed dimeric metallacycles. All spectra exhibited signals, which were derived from  $[\text{TiL}(\text{O}^i\text{Pr})]^+$  and  $\{[\text{TiL}(\text{O}^i\text{Pr})_2]\text{Na}\}^+$  (see ESI-mass spectrum and low energy CID MS/MS spectrum of compound **6** in Figure 3.10) These signals were assigned to monomeric species, which were proven by low energy CID MS/MS experiments to be by-products of an in-source fragmentation during the desorption/ionization process.

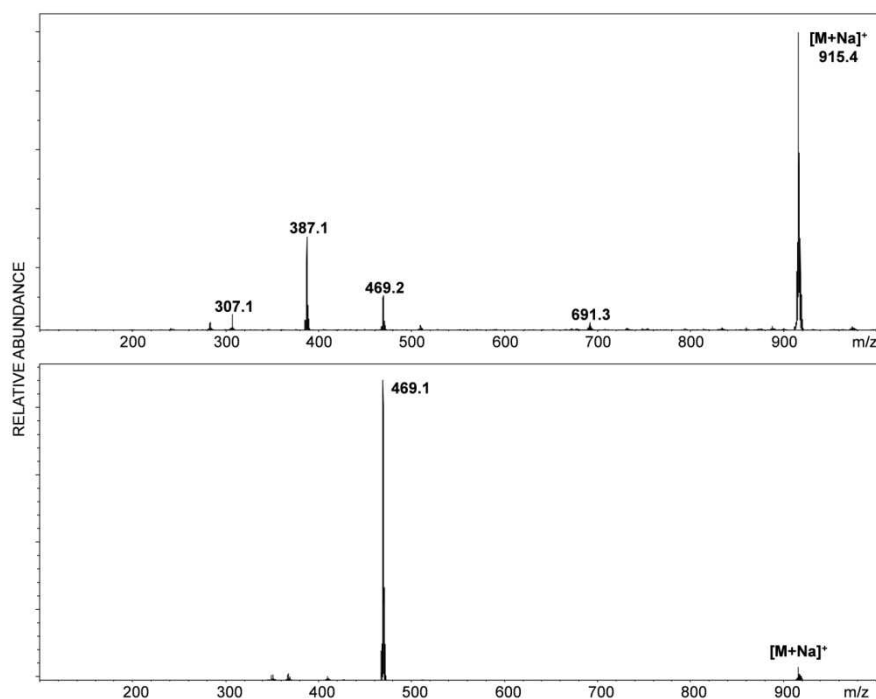


**Figure 3.10: Positive ion ESI mass spectrum and low energy CID MS/MS spectrum of **6****

The existence of bridging alkoxo ligands was excluded by low energy CID MS/MS experiments or NMR investigations. The product ion depended on the nature of the alkoxo groups, which is addressed later on. Starting from a compound  $[\text{TiL}(\text{O}^i\text{Pr})_2]_2$ , two different fragments were observed.  $\text{TiL}_2$  was formed, when O<sup>i</sup>Pr groups were bridging, whereas  $\text{TiL}(\text{O}^i\text{Pr})_2$  was observed, when only terminal alkoxo groups were present. Thus, the formation of  $[\text{TiL}(\text{O}^i\text{Pr})]^+$  and  $\{[\text{TiL}(\text{O}^i\text{Pr})_2]\text{Na}\}^+$  as corresponding product ions proved the proposed structure with only terminal alkoxo groups. The same behaviour in ESI-MS was observed for all compounds **4-6**. Therefore, a dimeric, metal-lacyclic structure, as shown in Figure 3.6, was assumed for compounds **4-6**.

Moreover, NMR investigations supported this assumption. Only one resonance was observed for O<sup>i</sup>Pr groups in the  $^1\text{H}$  and  $^{13}\text{C}$  NMR spectra. Four peaks between 193 and 186 ppm were attributed to both carbonyl groups in the  $^{13}\text{C}$  NMR spectrum. A small shift of the methylene groups

next to the carbonyl units was also present in the  $^{13}\text{C}$  NMR spectrum and was seen as another hint for ligand coordination. (Figure 3.11)

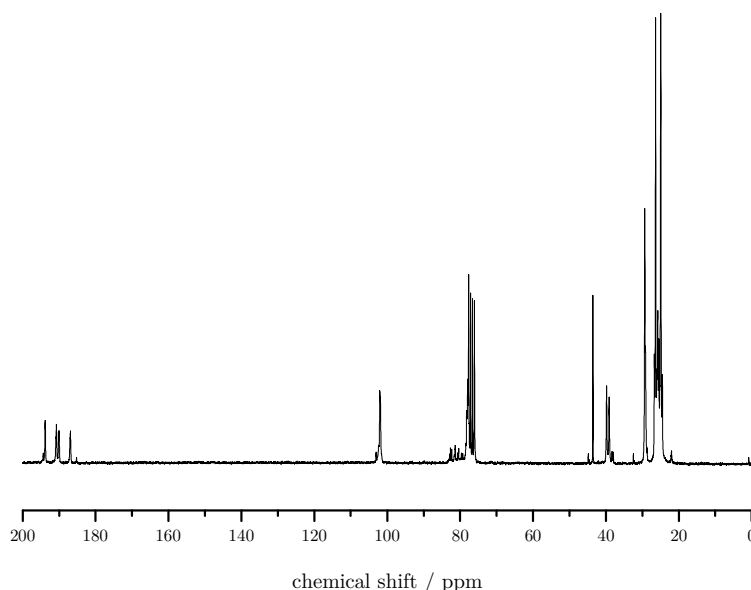


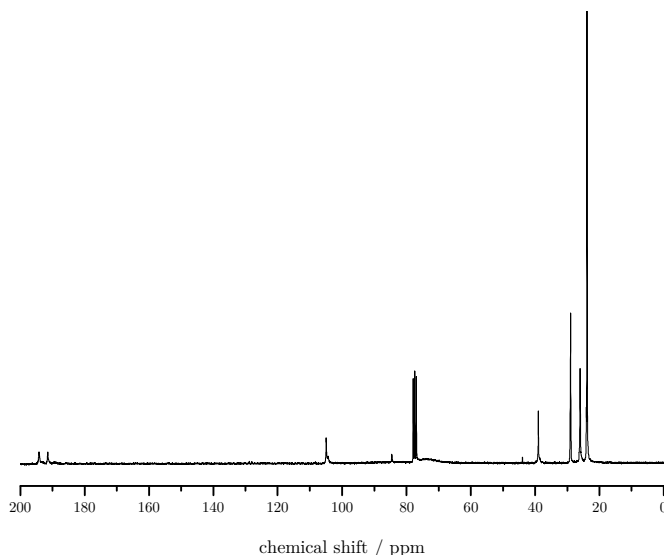
**Figure 3.11:**  $^{13}\text{C}$  NMR spectrum of **6**

The experiments were extended to different titanium alkoxides. Comparable reactions with titanium ethoxide or titanium butoxide resulted in comparable NMR spectra. In each  $^{13}\text{C}$  NMR spectrum, four signals between 195 and 185 ppm were observed for the carbonyl groups, as well as a splitting of the  $\text{COCHCO}$  and the neighbouring  $\text{COCH}_2\text{CH}_2$  proton signals. Thus, the formation of metallacycles was assumed to be independent of the used titanium alkoxide.

2,4,10,12-Tridecanetetrone was reacted with  $\text{TiCl}(\text{O}^i\text{Pr})_3$  in the ratio of 1:1 in presence of triethylamine. The  $^{13}\text{C}$  NMR experiments showed four peaks between 187 and 193 ppm, which were assigned to the carbonyl groups of the bis( $\beta$ -diketonate). The measurement also showed the known  $\text{COCHCO}$  methine resonance at 102 ppm and a split  $\text{COCH}_2\text{CH}_2$  resonance between 38 and 40 ppm. One set of  $\text{O}^i\text{Pr}$  signals was present. The investigations also proved that alternative precursors resulted in the same metallacyclic structure  $[\text{TiL}(\text{O}^i\text{Pr})_2]_2$ .

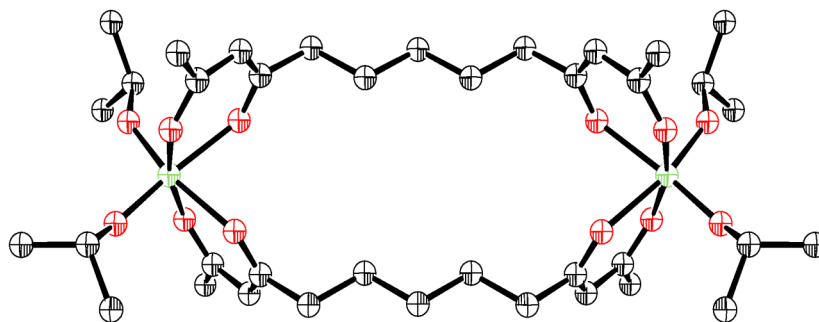
Additional experiments were conducted with  $\text{TiCl}_4$  and the alkylene-bridged bis( $\beta$ -diketone), which yielded immediately a red-coloured precipitate. The reaction products showed a bad solubility in common organic solvents; addition of small portions of 2-propanol improved the solubility tremendously. In contrary to complexes obtained from  $\text{TiCl}(\text{O}^i\text{Pr})_3$  and  $\text{Ti}(\text{O}^i\text{Pr})_4$ , NMR investigations showed only two carbonyl resonances at 191.4 and 194.1 ppm (Figure 3.12), which were in line with previous observations of  $\text{TiCpCl}_2(1,3\text{-diphenyl-1,3-propanedionate})$ . Furthermore, only one  $\text{COCHCO}$  and one  $\text{COCH}_2\text{CH}_2$  signal were present in the  $^{13}\text{C}$  NMR spectrum and fitted well with previous observations.<sup>134</sup> Surprisingly, no  $\text{O}^i\text{Pr}$  signals were observed in the spectra. The NMR results were independent of the used  $\text{TiCl}_4$ /ligand ratio and the used alkylene-bridged bis( $\beta$ -diketone). According to the NMR spectra, a metallacyclic structure was possible, in which the

bis( $\beta$ -diketonates) bridged two  $\text{TiCl}_2$  moieties. Some monomeric complexes of the type  $\text{Ti}(\beta\text{-diketonate})_2\text{Cl}_2$  were known similar to the titanium alkoxo derivatives.<sup>135-137</sup> Therefore, comparable metallacycles were formed.

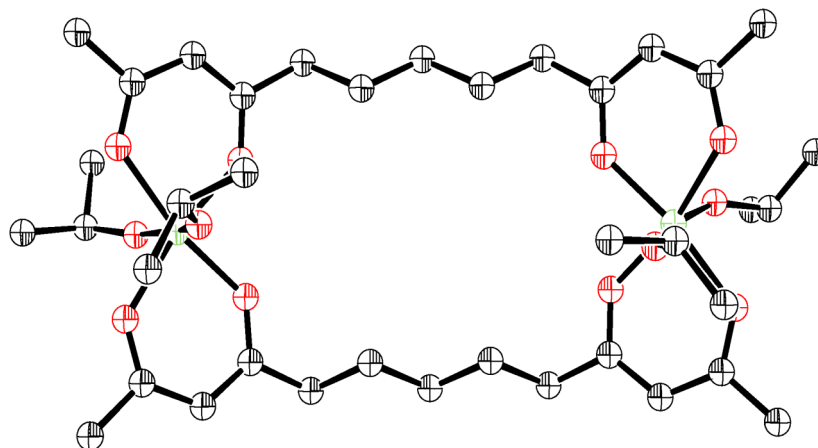


**Figure 3.12:**  $^{13}\text{C}$  NMR spectrum of the reaction of  $\text{TiCl}_4$  with 2,4,11,13-tetradecanetetrone

Both discussed analysis techniques did not provide hints whether both O<sup>i</sup>Pr groups were in *cis/cis* or *trans/trans* position. DFT calculations were carried out to support stereochemical interpretations. Both structures are shown in Figure 3.13 and Figure 3.14. The *cis/cis* arrangement showed a  $C_{2v}$  symmetry, whereas for the *trans/trans* arrangement only a  $C_i$  symmetry was calculated. Moreover, the *cis/cis* configuration was proven to be the thermodynamically more stable isomer. The difference in Gibbs free energy was calculated with 59.5 kJ/mol. The low energy barrier permitted the conversion of both isomers in each other with a small energetic input. The preference for the *cis/cis* positioning was in line with several other  $\text{Ti}(\beta\text{-diketonate})_2(\text{OR})_2$  complexes.



**Figure 3.13:** ORTEP plot of DFT optimized geometries of *cis/cis* 4

Figure 3.14: ORTEP plot of DFT optimized geometries of *trans/trans* 4

After geometry optimization, selected  $^{13}\text{C}$  NMR shifts of both configurations were calculated. (Table 3.1) The calculated data fitted more or less well with the experimental spectra. The calculations proved that two different shifts per carbonyl group were obtained. Moreover, they showed two resonances for the methyl group of  $\beta$ -diketonate and the methylene group neighbouring the  $\beta$ -diketonate unit. Both were caused by two different coordination positions on the titanium atom. A difference in the number of NMR signals was expected because of the different symmetry, but for both configurations the same number of resonances was obtained. The calculated NMR data indicated that there was no clear trend by which the two isomers could be spectroscopically distinguished.

Table 3.1: Comparison of selected calculated (relative to TMS) and measured  $^{13}\text{C}$  NMR shifts (ppm) for 4

	Calculated data cis/cis-isomer	Experimental data	Calculated data trans/trans-isomer
<b>CH<sub>3</sub>COCHCO</b>	27.3 / 26.6	29.3 / 29.2	27.1 / 27.0
CH <sub>3</sub> COCHCO	179.6 / 178.8	189.9 / 187.0	182.3 / 182.7
COCHCO	97.9 / 97.6	101.9 / 101.0	100.1 / 99.2
CHCOCH <sub>2</sub>	186.4 / 185.9	193.7 / 191.0	184.4 / 184.9
CHCOCH <sub>2</sub> CH <sub>2</sub>	44.5 / 44.4	39.7 / 38.9	42.5 / 52.4

### 3.2 Modification of zirconium isopropoxide with bis( $\beta$ -diketones)

The experiments with titanium alkoxides were extended to zirconium alkoxides. They should check whether similar metallacycles were possible. Reactions of  $\text{Zr}(\text{O}^i\text{Pr})_4 \cdot ^i\text{PrOH}$  with different alkylene-bridged bis( $\beta$ -diketones) (Figure 3.15) resulted in colourless residues, which could not be crystallised with different methods. Thus, ESI-MS was the method of choice for composition elucidation of zirconium alkoxo bis( $\beta$ -diketonates).

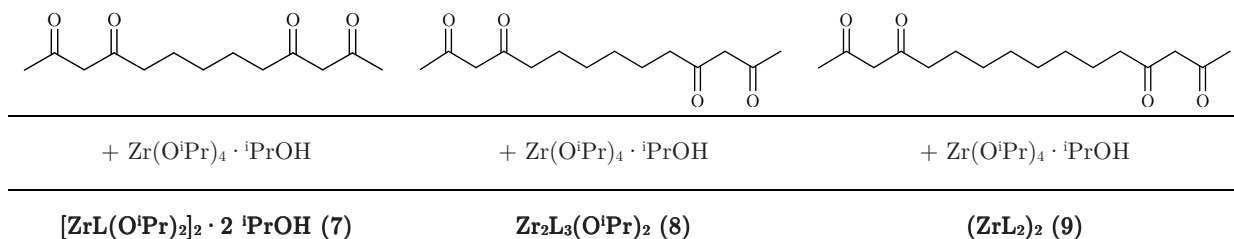


Figure 3.15: Alkylene-bridged bis( $\beta$ -diketones) used in this work and the resulting zirconium compounds

Mass spectra of compound **7** were of comparable composition as the ones observed in compounds **4-6**. One peak was detected at  $m/z$  1035.2 (calc. 1035.4), which was attributed to the sodiated complex  $\{[\text{ZrL}(\text{O}^i\text{Pr})_2]_2(\text{}^i\text{PrOH})_2\text{Na}\}^+$ . Several product ions ( $\{[\text{ZrL}(\text{O}^i\text{Pr})_2]_2(\text{O}^i\text{Pr})(\text{}^i\text{PrOH})_2\}^+$ ,  $\{[\text{ZrL}(\text{O}^i\text{Pr})_2]_2\text{Na}\}^+$  and  $\{[\text{ZrL}(\text{O}^i\text{Pr})_2]_2(\text{O}^i\text{Pr})\}^+$ ) were present in the full-scan spectrum (Figure 3.16).

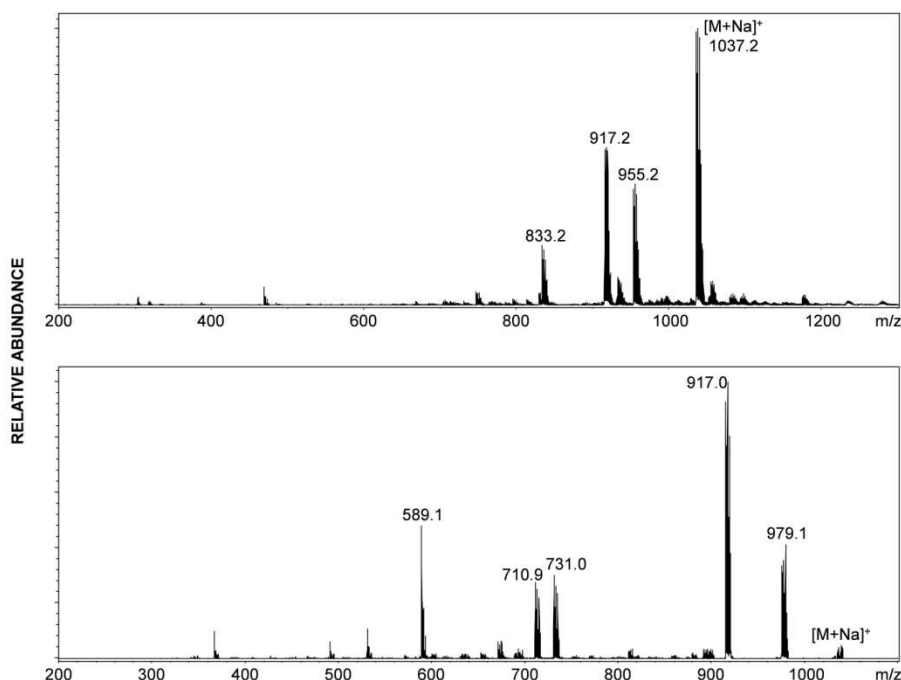


Figure 3.16: Positive ion ESI mass spectrum and low energy CID MS/MS spectrum of  $[\text{ZrL}(\text{O}^i\text{Pr})_2]_2 \cdot 2 \text{}^i\text{PrOH}$  (**7**)

All of them were derived from  $[\text{ZrL}(\text{O}^i\text{Pr})_2]_2(\text{}^i\text{PrOH})_2$ . Low energy CID MS/MS scans of the precursor ion resulted in two product ions at  $m/z$  979.1 and 917.1 assigned to  $\{[\text{ZrL}(\text{O}^i\text{Pr})_2]_2(\text{}^i\text{PrOH})\text{Na}\}^+$  and  $\{[\text{ZrL}(\text{O}^i\text{Pr})_2]_2\text{Na}\}^+$ . Another product ion at  $m/z$  589.1 (calc. 589.1) was assigned to  $(\text{ZrL}_2\text{Na})^+$ . In comparison to the titanium bis( $\beta$ -diketonate) complexes, zirconium favoured the formation of these product ions. It was assumed that the coordinated alcohol promoted the  $\text{Zr}(\text{O}^i\text{Pr})_4$  cleavage.

A dimeric, metallacyclic structure was proposed. Due to the higher coordination numbers of zirconium, an extra 2-propanol was coordinated to each zirconium centre. NMR measurements supported the postulated structure of **7**. (Figure 3.17)

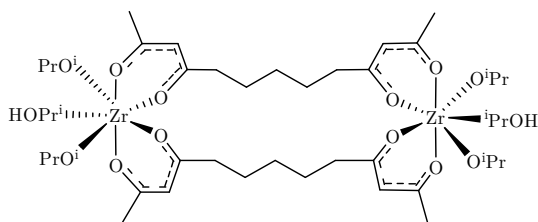


Figure 3.17: Suggested structure of **7**

When the investigations were extended to 2,4,11,13-tetradecanetetron, a completely different mass spectrum (Figure 3.18) was obtained. The sodiated complex **8** was observed at  $m/z$  1077.6 (calc. 1077.3), from which a dimeric zirconium complex  $Zr_2L_3(O^iPr)_2$  was derived.

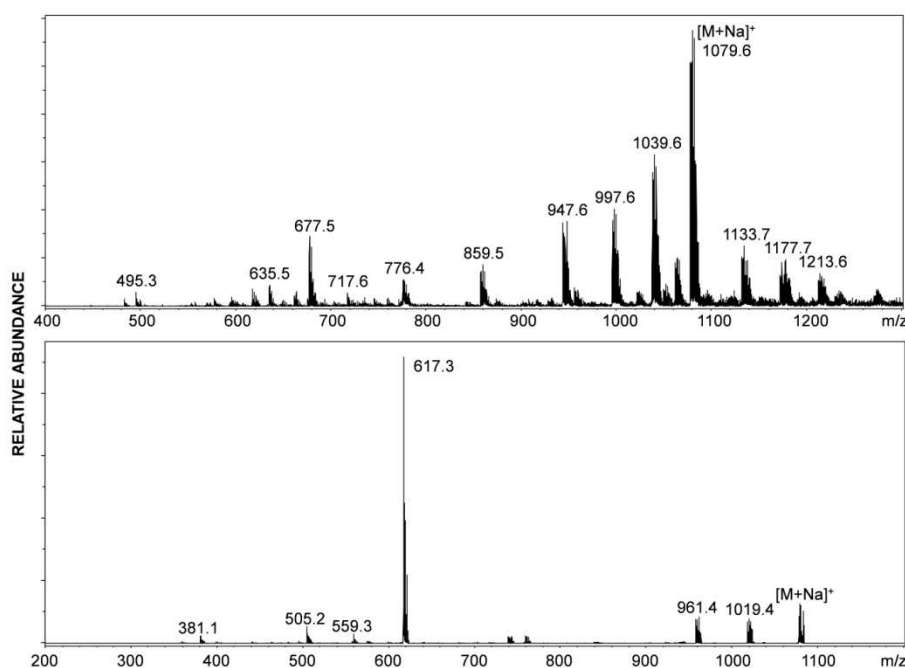
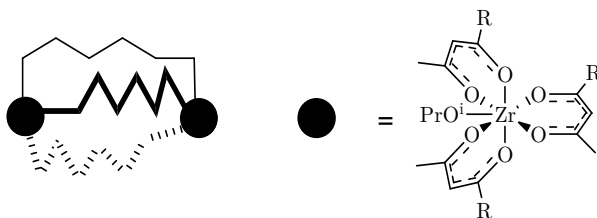


Figure 3.18: Positive ion ESI mass spectrum and low energy CID MS/MS spectrum of  $Zr_2L_3(O^iPr)_2$  (**8**)

In comparison to **7**, three bis( $\beta$ -diketonates) bridged both metal centres and only one terminal alkoxo ligand remained coordinated at the zirconium centre. Thus, zirconium had a coordination number of seven. (Figure 3.19). Next to this peak, additional signals at  $m/z$  995.6 (calc. 995.3) and  $m/z$  677.5 (calc. 677.3) appeared with significantly lower intensity. While the first peak was the fragmentation product  $[Zr_2L_3(O^iPr)]^+$  of the sodiated complex **8**, the second one was caused by a side product of the synthesis and was attributed to a monomeric zirconium complex  $[(ZrL_2)(^iPrOH)]$ . The signals at  $m/z$  1039.6 and 947.6 could not be assigned to a specific fragment of compound **8**.

Low energy CID MS/MS scans of the precursor ion at  $m/z$  1079.6 resulted in one product ion at  $m/z$  617.3 (calc. 617.2), which was assigned to  $[\text{ZrL}_2\text{Na}]^+$ . The three bridging bis( $\beta$ -diketonates) prevented the formation of the product ion  $[\text{ZrL}(\text{O}^i\text{Pr})_2\text{Na}]^+$  known from previous investigations of the corresponding titanium derivatives.

In contrary to all titanium metallacycles previously observed, an increase of the number of bridging bis( $\beta$ -diketonates) was observed.  $\text{Ti}_2[\text{bis}(\beta\text{-diketonate})]_3$  was the only example of group(IV) complexes with three bridging bis( $\beta$ -diketonates). If Ti(III) was used in this compound, the coordination of three bridging ligands was only possible, and the coordination number remained six.<sup>78</sup> Zirconium is known for its larger coordination sphere. Therefore, coordination numbers of seven and eight could also be realized. Compound **8** was one of only few examples of these complexes. Compounds of type  $\text{Zr}_2\text{L}_3(\text{OR})_2$  were only possible with longer linkers. The C5 linker, used with 2,4,10,12-tridecanetetronate, was too short, and the complex would be under steric strain.



**Figure 3.19: Proposed structure of  $\text{Zr}_2\text{L}_3(\text{O}^i\text{Pr})_2$  (**8**)**

NMR investigations of **8** proved the existence of only terminal alkoxo ligands. Resonances for  $\text{O}^i\text{Pr}$  groups were only observed at 72.0 and 26.6 ppm in the  $^{13}\text{C}$  NMR spectrum. All bis( $\beta$ -diketonates) were coordinated in this compound.

Additional experiments were performed with 2,4,13,15-hexadecanetetrone and  $\text{Zr}(\text{O}^i\text{Pr})_4 \cdot {}^i\text{PrOH}$ . The solid residue **9** could not be crystallised with common methods. Investigations with ESI-MS revealed a surprising result. One peak was observed at  $m/z$  1323.7 (calc. 1323.5), which was assigned to the sodiated complex  $[(\text{ZrL}_2)_2\text{Na}]^+$ . Beside this signal, an additional peak of lower intensity appeared at  $m/z$  1079.6 (calc. 1079.4). The second signal was attributed to  $\{[\text{Zr}_2\text{L}_3(\text{O}^i\text{Pr})]\}^+$ , which was derived from  $\text{Zr}_2\text{L}_3(\text{O}^i\text{Pr})_2$ , a side product of the synthesis. The mass spectrum is shown in Figure 3.20.



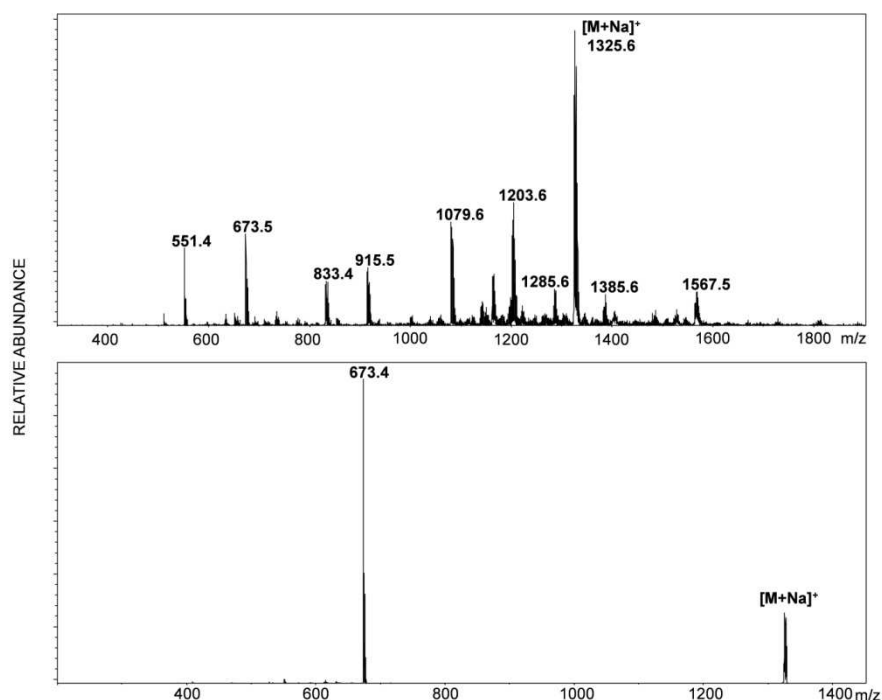


Figure 3.20: Positive ion ESI mass spectrum and low energy CID MS/MS spectrum of  $[\text{ZrL}_2]_2$  (**9**)

The results were surprisingly, with regards to the results of compound **8**. A completely different coordination geometry was caused by the enlargement of the linker by two methylene groups. Instead of three bridging ligands, four bis( $\beta$ -diketonates) bridged both zirconium centres and no  $\text{O}^i\text{Pr}$  groups remained coordinated. The assumed structure is presented in Figure 3.21.

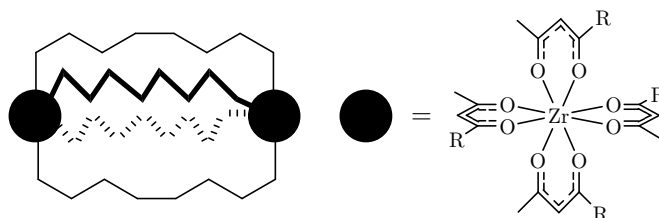


Figure 3.21: Postulated structure of  $[\text{ZrL}_2]_2$  (**9**)

Four  $\beta$ -diketonate units were coordinated to each zirconium centre, resulting in a coordination number of eight. The structure was cryptand-like. The observation is in line with experiments reported by Spijksma *et al.* In contrary to titanium, a  $\text{Zr}(\text{acac})_4$  complex was possible. Compared to this monomeric complex, compound **9** was under risen strain. A bridging coordination of four bis( $\beta$ -diketonates) between two metal centres was not reported before.

Furthermore, the mass spectrum showed that compound **9** was the main product, but several other resonances were present in the spectrum. These additional signals were caused by side products, which were obtained due to the incomplete four-fold substitution of  $\text{Zr}(\text{O}^i\text{Pr})_4 \cdot {}^i\text{PrOH}$ . Hereby,  $\text{Zr}_2\text{L}_3(\text{O}^i\text{Pr})_2$  was the most prominent side product, where only three alkoxo groups were substituted. Similar incomplete substitution was also observed quite often with  $\text{Ti}(\beta$ -

diketonate)<sub>2</sub>(OR)<sub>2</sub>. A maximum degree of substitution was only observed for acac. Complexes with substituted  $\beta$ -diketonates resulted in substitution degree up to 1.5.<sup>5</sup>

The low energy CID MS/MS experiments showed only one fragment at  $m/z$  673.4 (673.2), which was assigned to  $ZrL_2Na^+$ . A homolytic fragmentation occurred. Moreover, this experiment proved that the signal at  $m/z$  673.4 in the full-scan was caused by in-source fragmentation and was no additional side product of the reaction.

<sup>13</sup>C NMR investigations showed four resonances of the carbonyl groups between 194.4 and 188.9 ppm. The COCHCO proton was again shifted to a higher ppm region. Two signals again appeared in the spectrum for the methylene group (COCH<sub>2</sub>CH<sub>2</sub>) neighbouring to the  $\beta$ -diketonate group. Similar to experiments mentioned above, one equivalent of the ligand was used per  $Zr(O^iPr)_4 \cdot ^iPrOH$ . Although no O<sup>i</sup>Pr group was left on the zirconium centres, resonances for O<sup>i</sup>Pr units appeared in the spectrum, which were attributed to the unsubstituted metal alkoxide and additional side products.

### 3.3 Modification of titanium isopropoxide with 1,1,2,2-tetraacetyethane (taet-H)

Numerous examples of late transition metal complexes with taet were reported by different research groups. Dimeric complexes, in which two metal centres were bridged by one taet ligand, are known as well as metallacycles similar to the ones obtained with compounds **1-6**. One example of a tetrameric metallacycle is  $Cu_4(taet)_4(di-2\text{-pyridylamine})_4$ .<sup>64-68</sup> Based on these results, taet-H was used in the modification of group (IV) metal alkoxides. If a mixture of 1,2-dichloroethane/toluene solution was used, the reaction of  $Ti(O^iPr)_4$  with taet-H in the ratio 1:1 (Figure 3.22) resulted in a clear solution. Compound **12** was tried to crystallise in numerous experiments. The product was hardly soluble in alcohols and other commonly used organic solvents. Reactions in other solvents resulted in gel formation or precipitates after several minutes.

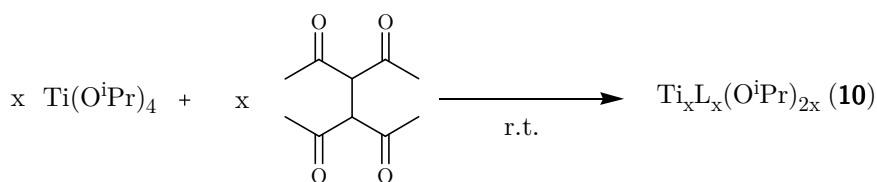


Figure 3.22: Synthesis of compound **10**

The bad solubility in alcohols did not permit investigations by ESI-MS, and therefore NMR spectroscopy was the only access for structure determination. The <sup>13</sup>C NMR spectrum of **10** showed two resonances at 190.7 and 187.7 ppm assigned to different coordinated carbonyl groups (Figure 3.23). This was in line with previous investigations of  $[Ti(acac)(OR)_3]_2$  and  $Ti(acac)_2(OR)_2$ , where also two signals were observed for each acac group because of the coordination of the carbonyl group to non-equivalent coordination sites.<sup>12</sup> Moreover, a <sup>1</sup>H NMR spectrum proved that the

resonance of the C<sup>3</sup>H group at 3.5 ppm (100.2 ppm in the <sup>13</sup>C NMR spectrum) disappeared upon reaction with Ti(O<sup>*i*</sup>Pr)<sub>4</sub>, and a new signal appeared at 112.7 ppm in the <sup>13</sup>C NMR spectrum. Finally, two independent signals were observed for the methyl group of taet in the <sup>1</sup>H and the <sup>13</sup>C NMR spectrum, which was caused by coordination of the β-diketonate groups to non-equivalent coordination sites. This proved the coordination of the ligand. The <sup>13</sup>C NMR spectrum showed one set of O<sup>*i*</sup>Pr signals at 78.7 and 25.0 ppm, which were assigned to terminal alkoxo groups.

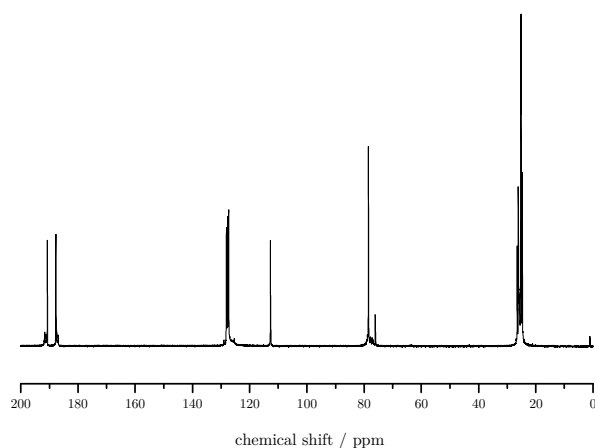


Figure 3.23: <sup>13</sup>C NMR spectrum of 10

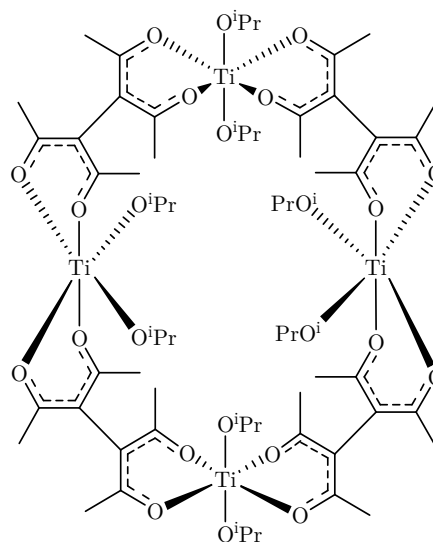


Figure 3.24: Possible schematic structure of 10

Both spectra proved a complete coordination of the ligand to the titanium centre. Due to missing MS information, the postulation of a structure was challenging. According to other reported structures with this ligand and other C<sup>3</sup>-linked bis(β-diketones), a metallacyclic structure was assumed. However, NMR spectroscopy did not permit any assumption whether dimeric, trimeric or tetrameric metallacycles were formed. A dimeric metallacycle should be excluded because of the high steric strain of taet; dimers were only observed for less rigid bis(β-diketones). Therefore, trimeric and tetrameric complexes were more likely (for a schematic structure of tetrameric metallacycle see Figure 3.24).

The experiment was extended to reactions with TiCl<sub>4</sub>. To this end, the TiCl<sub>4</sub>(THF)<sub>2</sub> adduct was reacted with taet-H. Due to the bad solubility of the reaction product, 2-propanol was added, resulting in a clear red-coloured solution. Mass spectrometric investigations were not possible. Therefore, the structure determination was challenging. NMR investigations resulted in spectra, which were comparable to the ones obtained with Ti(O<sup>*i*</sup>Pr)<sub>4</sub>. One resonance for the carbonyl group was observed at 197.2 ppm. The COC(C)CO signal appeared at 123.1 ppm, which proved the coordination. Two methyl signals at 30.4 and 25.4 ppm were observed. This would be in line with non-equivalent coordination sites. One set of O<sup>*i*</sup>Pr signals appeared at 70.8/23.8 ppm in the <sup>13</sup>C NMR spectrum, which fitted with coordinated <sup>*i*</sup>PrOH. Moreover, the NMR investigations proved a complete coordination of taet to TiCl<sub>4</sub>.

### 3.4 Modification of titanium alkoxides with bis( $\beta$ -ketoesters)

In the early 70thies, Mehrotra *et al.* had reported numerous experiments with  $\text{Ti}(\text{OR})_4$  and bis( $\beta$ -ketoesters) in the ratio 2:1. Compounds of composition  $\text{Ti}_2\text{L}(\text{OR})_6$  had been assumed after determination of the released alcohol and the Ti-content/molecular weights. A dimeric structure had been postulated, in which each  $\beta$ -ketoesterate was coordinated to one  $\text{Ti}(\text{OR})_3$  moiety and the residual alkoxo groups were in terminal position. Furthermore, the reactions had been extended to higher  $\beta$ -ketoester/ $\text{Ti}(\text{OR})_4$  ratios, resulting in the complexes  $\text{TiL}(\text{OR})_2$  and  $\text{Ti}_2\text{L}_3(\text{OR})_2$ . The low solubility of some compounds was attributed to polymeric structures. All experiments showed a clear coordination of both  $\beta$ -ketoesterate groups.<sup>80,83</sup>

Starting from these results, reactions of bis( $\beta$ -ketoesters) with group (IV) metal alkoxides should show whether similar metallacycles, as described with bis( $\beta$ -diketones), were possible or polymeric arrangements were observed. Therefore,  $\text{Ti}(\text{O}^i\text{Pr})_4$  was reacted with the  $\beta$ -ketoesters 1-4. All reactions resulted in off-white products **11-14**. (Figure 3.25) Several unsuccessful attempts were done to crystallise the compounds.

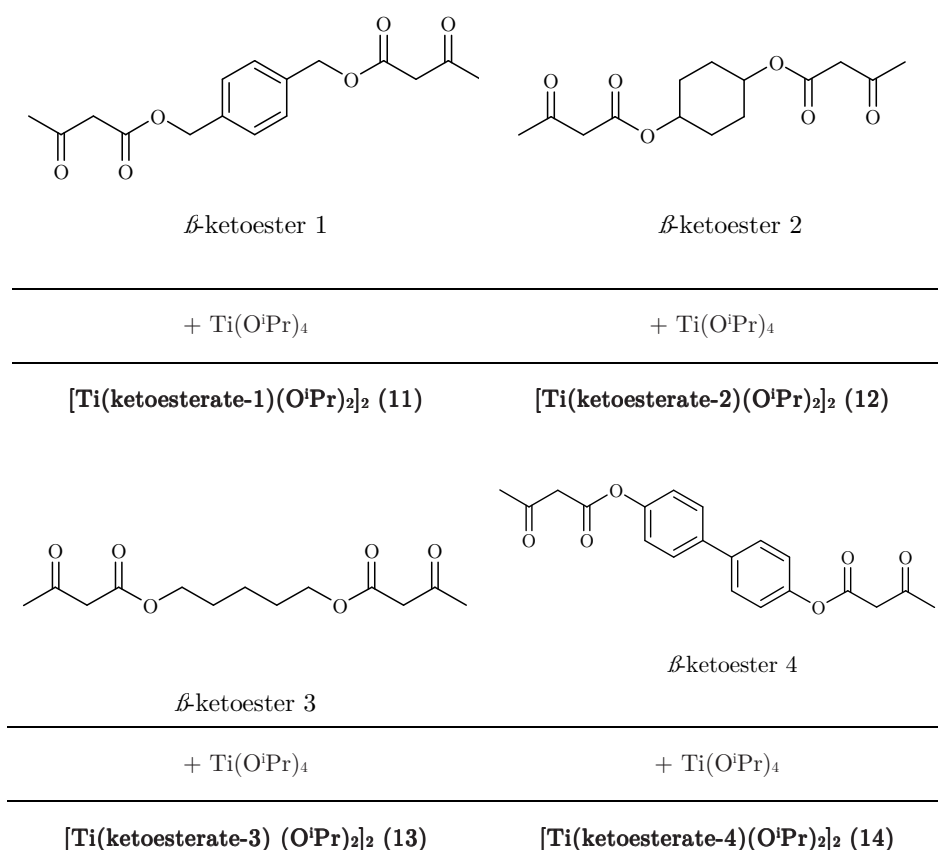


Figure 3.25: Bis( $\beta$ -ketoesters) used in this work and the resulting titanium compounds

The determination of the composition was only done by ESI-MS measurements for compounds **11** and **12** due to solubility reasons. A peak for the sodiated complex was observed for both compounds that was assigned to complexes of composition  $[\text{TiL}(\text{O}^i\text{Pr})_2]_2$ . Additional signals at higher

masses, which were attributed to oligomeric or polymeric species, were excluded. Based on these mass spectra, the same structure as observed for titanium alkoxo bis( $\beta$ -diketonates), was postulated for **11** and **12**. Hereby, a dimeric complex was formed, in which two bis( $\beta$ -ketoesterates) bridged two  $\text{Ti}(\text{O}^i\text{Pr})_2$  moieties. The compounds were of same structure as compounds **2**, **4**, **5** and **6**. This result was slightly unexpected as the  $\beta$ -ketoesters, used for the synthesis of **11** and **12**, were of similar structure compared to 1,1-(1,4-phenylene)-bis-butane-1,3-dione. In both bis( $\beta$ -ketoesters), the functionalities are linked by an 1,4-substituted cyclic spacer, and therefore similar trimeric complexes were expected. However, the additional methylene groups between the linker and the  $\beta$ -ketoester group ( $\beta$ -ketoester 1) and/or the cyclohexylene-spacer ( $\beta$ -ketoester 2) were less rigid to form similar trimeric metallacycles. The structure of the dimeric metallacycle is shown in Figure 3.26.

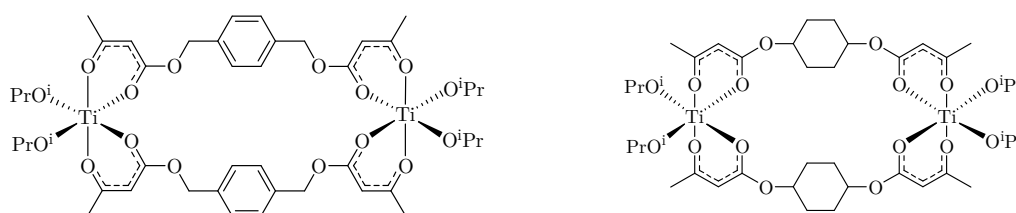


Figure 3.26: Suggested structure of **11** and **12**

Furthermore, low energy CID MS/MS scans were done with compounds **11** and **12** to determine details of the structure (spectrum see Figure 3.27). It was expected that a similar metallacyclic structure would cause a comparable fragmentation pattern, but completely different MS/MS spectra were observed. The typical signals for monomeric product ions  $[\text{TiL}(\text{O}^i\text{Pr})_2\text{Na}]^+$  and  $[\text{TiL}(\text{O}^i\text{Pr})]^+$  did not appear. Moreover, compound **12** was fragmented to three species at  $m/z$  835.3, 751.3 and 667.3. Starting from the precursor ion at  $m/z$  919.3, each peak differed by 84 Da. This special fragmentation pathway was caused by a stepwise cleavage process, in which  $\text{CH}_3\text{COCHCO}$  groups of the coordinated  $\beta$ -ketoesterates were cleaved. All possible products were present in the low energy CID MS/MS spectrum. This fragmentation proved to be typical for all group (IV) metal alkoxo bis( $\beta$ -ketoesterates). Furthermore, the cleavage of  $\text{CH}_3\text{COCHCO}$  groups instead of the complex itself proved the high stability of the dimeric metallacycle.

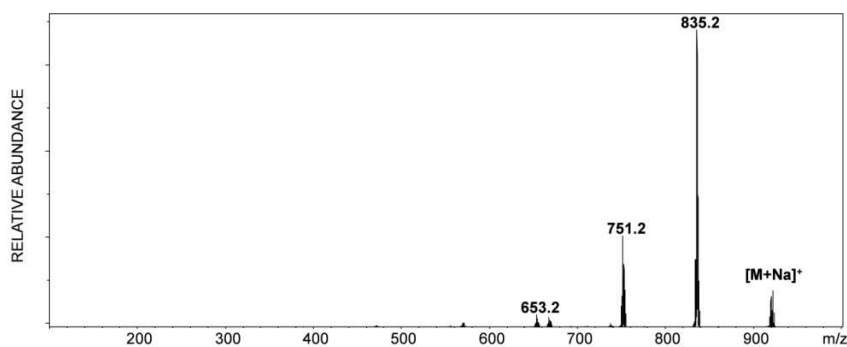


Figure 3.27: Low energy CID MS/MS spectrum of **12**

The investigations were extended to NMR experiments. Herein, the  $^{13}\text{C}$  NMR spectrum proved a complete coordination of the ligand used. Both signals for the uncoordinated bis( $\beta$ -ketoesters) at 166 and 200 ppm disappeared, and two new, more closer signals at 172 and 184 ppm were present in the spectra of the complexes. Such shifted signals were known for coordinated bis( $\beta$ -ketoesterates). Moreover, the signal at 49 ppm, corresponding to the keto form of the  $\beta$ -ketoester, shifted to a new signal at 88 ppm for the enolate form, which was a consequence of the deprotonation and coordination (see  $^{13}\text{C}$  NMR spectrum of **13** as an example in Figure 3.28). A similar shift was also observed in the corresponding  $^1\text{H}$  NMR spectrum. Therein, new signals at 4.80 ppm for  $\text{COCHCOO}$  appeared. The NMR observations were in line with previous investigations of  $\text{Ti}_2(\text{EAA})_2(\text{O}^i\text{Pr})_6$  and  $\text{Ti}(\text{EAA})_2(\text{O}^i\text{Pr})_2$  [EAA = ethyl acetoacetate]. NMR experiments of these complexes also resulted in resonances for coordinated  $\beta$ -ketoesterates at 172.3 and 184.6 ppm and an additional peak at 86.6 ppm for the  $\text{COCHCOO}$  methine group in the  $^{13}\text{C}$  NMR spectrum. Ivanovici *et al.* reported two resonances for the  $\text{CH}_3\text{CO}$  groups in the  $^1\text{H}$  as well as in the  $^{13}\text{C}$  NMR spectrum at 1.81/1.93 and 25.0/25.6 ppm.<sup>17</sup>

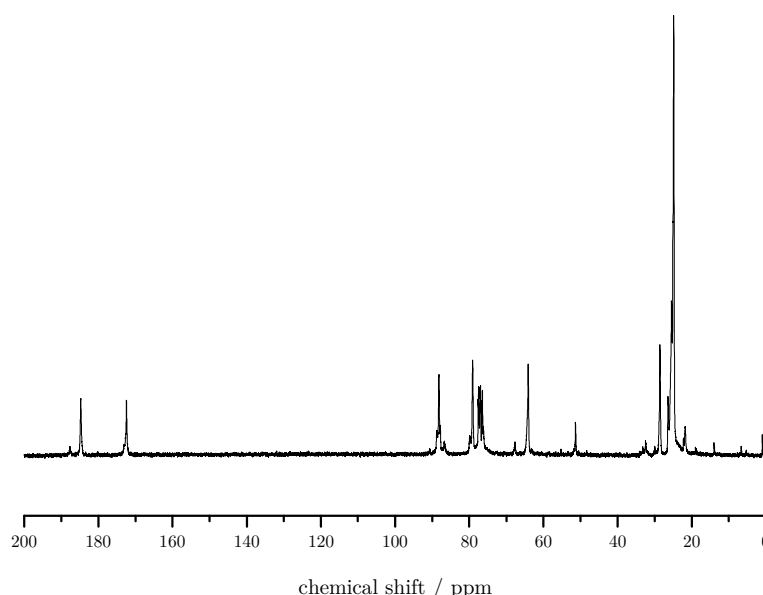


Figure 3.28:  $^{13}\text{C}$  NMR spectrum of  $[\text{Ti}(\beta\text{-ketoesterate } \mathbf{3})(\text{O}^i\text{Pr})_2]_2$  (**13**)

Similar to the metallacycles described above, all products showed only one set of  $\text{O}^i\text{Pr}$  signals at 79/25 ppm in the  $^{13}\text{C}$  NMR spectrum. The HSQC spectrum (Figure 3.29) showed one set of resonances of the  $\text{O}^i\text{Pr}$  methine group at 4.74/79.4 ppm. HSQC spectra showed a correlation resonance at 4.93/87.8 ppm assigned to the  $\text{COCHCOO}$  group and an additional signal at 3.93/64.3 ppm for the  $\text{OCH}_2\text{CH}_2$  methylene group. Similar behaviour was also observed for  $\text{Ti}_2(\text{EAA})_2(\text{O}^i\text{Pr})_6$  and  $\text{Ti}(\text{EAA})_2(\text{O}^i\text{Pr})_2$ .<sup>17</sup> Similar shifts were observed in complexes **11-14**. Therefore, the same structures for all complexes were assumed.

The NMR experiments did not clarify whether the *cis/cis* or *trans/trans* positioning of the isopropoxide groups was preferred. Although no additional DFT calculations were conducted, a simi-

lar result compared to compound **4** was expected. Thus, the *cis/cis* isomer should be the thermodynamically more stable configuration.

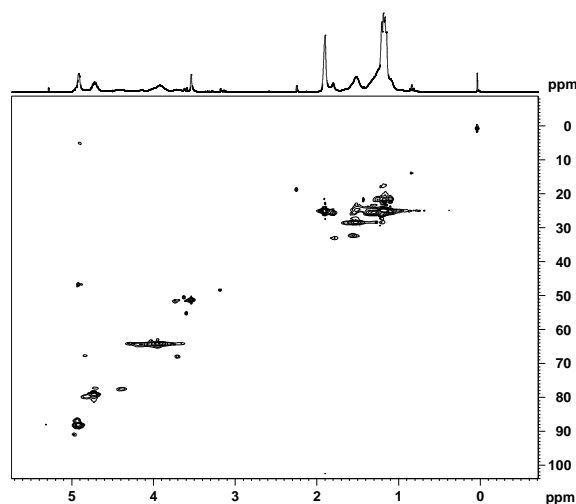


Figure 3.29: HSQC spectra of compound **13**

Reactions of all bis( $\beta$ -ketoesters) with more equivalents of  $\text{Ti}(\text{O}^i\text{Pr})_4$  did not influence the obtained structure. An additional signal at  $m/z$  307.1 (calc. 307.1) appeared in the ESI mass spectrum assigned to the sodiated  $\text{Ti}(\text{O}^i\text{Pr})_4$ . Comparable observations were also made in the NMR experiments. These investigations proved the high stability of the dimeric metallacycles. No equilibrium between mono- and disubstituted titanium alkoxo moieties was observed. If varying equivalents of titanium alkoxides were reacted with bis( $\beta$ -ketoesters), Mehrotra *et al.* had also reported different substitution patterns. In their work, other complexes  $\text{Ti}_2\text{L}(\text{OR})_6$  and  $\text{Ti}_2\text{L}_3(\text{OR})_2$  were postulated. The existence of similar complexes could not be reproduced or proven by the performed NMR and ESI-MS investigations.<sup>83</sup>

The investigations were extended to  $\text{TiCl}_4$ , which was allowed to react with  $\beta$ -ketoesters **1** and **2** in the ratio of 1:1. A slight gas formation was observed. As the pure  $\text{TiCl}_4/\text{bis}(\beta\text{-ketoesterate})$  substitution products were of poor solubility, small proportions of 2-propanol were added. After heating the solution on reflux for 5 min, the reaction mixture became a clear solution and was tried to crystallise it. Additional experiments in presence of non-nucleophilic bases (e.g. triethylamine) resulted in white precipitates of the corresponding hydrochloride, which proved the substitution of the chloride ligands of  $\text{TiCl}_4$ .

The products were only investigated by NMR spectroscopy. All spectra showed broader peaks which indicated exchange reactions. The products of  $\text{TiCl}_4$  with bis( $\beta$ -ketoesters) resulted in comparable spectra as obtained with the metal alkoxides. Both  $^{13}\text{C}$  NMR spectra showed two signals at 174/184 ppm, which were in line with previous observations of  $\text{Ti}(\text{O}^i\text{Pr})_4$  and proved the complete coordination of the ligand. The  $\text{COCH}_2\text{CO}$  methylene signal disappeared and a resonance at around 92 ppm appeared. This proved the coordination to the titanium centre. However, the spectrum did not verify, how many chloride atoms were substituted by 2-propanol. No compara-

ble complexes of type  $\text{TiCl}_{4-x}(\beta\text{-ketoesterate})_x$  are known. Only one example with perchlorate instead of chloride had been reported by Swarts *et al.*,<sup>138</sup> There, a complex  $\text{TiCp}_2(\text{methylacetoacetate})(\text{OCl}_4)$  was obtained. Nevertheless, a metallacyclic structure with the used bis( $\beta$ -ketoesters) was assumed.

### 3.5 Modification of zirconium isopropoxide with bis( $\beta$ -ketoesters)

Bis( $\beta$ -ketoesters) were used to modify zirconium alkoxides. One equivalent of the ligand was allowed to react with one equivalent  $\text{Zr}(\text{O}^i\text{Pr})_4 \cdot ^i\text{PrOH}$ . (Figure 3.30) The resulting solid residues could not be crystallised.

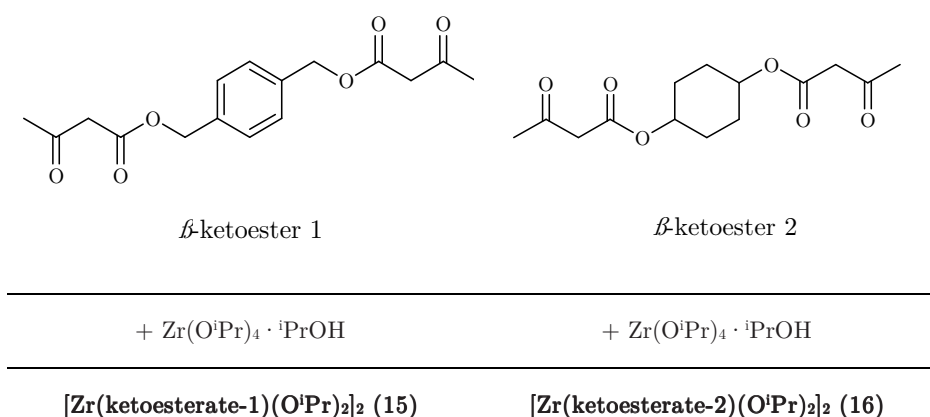


Figure 3.30: Bis( $\beta$ -ketoesters) used in this work and the resulting zirconium compounds

Once more, ESI-MS was the analysis technique of choice to elucidate the composition of the obtained complexes. One peak appeared for both complexes **15** and **16**, which was attributed to the sodiated complex  $[\text{ZrL}(\text{O}^i\text{Pr})_2]_2$ . Thus, a dimeric metallacycle, also observed for the corresponding titanium complexes, was postulated. (Figure 3.31)

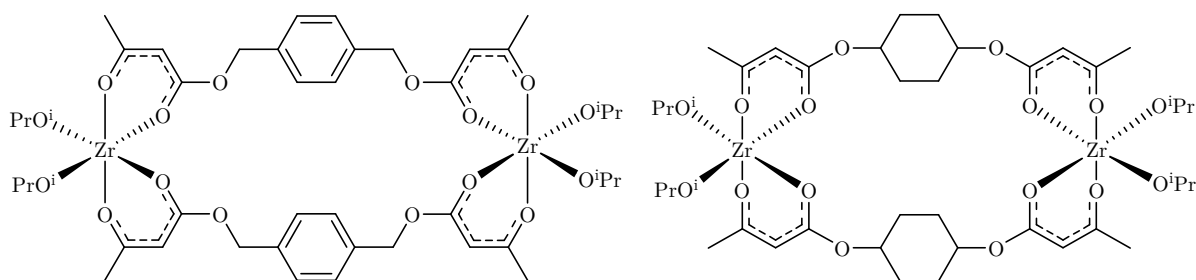


Figure 3.31: Proposed structures of compounds **15** and **16**

No peaks for additionally coordinated 2-propanol appeared in the mass spectrum. The length of the linkers is similar to the bis( $\beta$ -diketones) used before and therefore similar complexes of type  $\text{Zr}_2\text{L}_3(\text{O}^i\text{Pr})_2$  and  $\text{Zr}_2\text{L}_4$  were expected. However, no signals were present, which were derived from zirconium complexes with more than two bridging bis( $\beta$ -ketoesterates). It was assumed that this



coordination behaviour was caused by the bulkier and more rigid linkers in  $\beta$ -ketoester 1 and 2. If more than two bis( $\beta$ -ketoesterates) would bridge both zirconium centres, the steric hindrance would be too big. No hints for trimeric metallacycle, as observed in compound **1**, were present in the spectra.

Low energy CID MS/MS investigations of compound **15** and **16** (Figure 3.32) showed a similar fragmentation pattern as described in Chapter 3.4. Several peaks differed by about 84 Da. This was in line with the stepwise cleavage of  $\text{CH}_3\text{COCHCO}$  groups of the coordinated bis( $\beta$ -ketoesterates). All four fragments were present in the spectrum. Fragmentation of  $[\text{ZrL}(\text{O}^i\text{Pr})_2]_2$  proved that the dimeric metallacycle itself was very stable, and no signals for monomeric species  $\{[\text{ZrL}(\text{O}^i\text{Pr})_2\text{Na}]^+, [\text{ZrL}(\text{O}^i\text{Pr})]^+\}$  appeared in the low energy CID MS/MS scan. Numerous fragments were observed in the EI mass spectra of  $\text{Zr}(\text{O}^i\text{Pr})_2(\text{tert-butylacetoacetate})_2$  and other similar complexes, but no cleavage of the  $\beta$ -ketoesterate was observed there. However, several monomeric fragments were present in the reported spectra.<sup>139</sup> Only parts of the ligand were cleaved but the ring structure itself was retained.

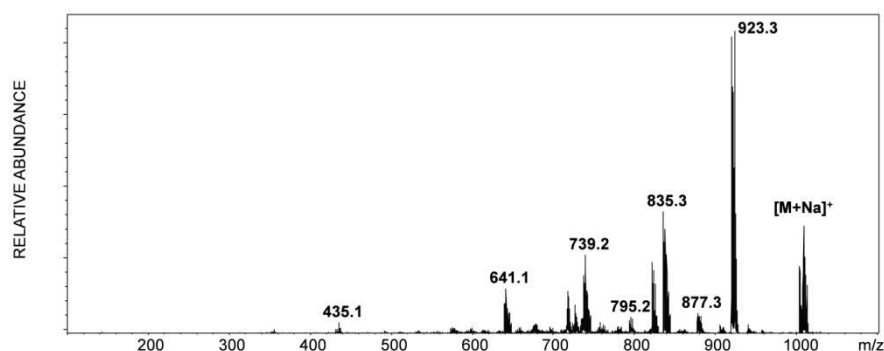


Figure 3.32: Low energy CID MS/MS spectrum of compound **16**

The postulated structure was confirmed by NMR investigations. The  $^{13}\text{C}$  NMR spectrum showed the disappearance of the carbonyl signals of uncoordinated bis( $\beta$ -ketoesters) at 166 and 200 ppm and the more closer resonances of the coordinated bis( $\beta$ -ketoesterates) at 172.7 and 186.3 ppm. This shift is typical of group (IV) metal alkoxo  $\beta$ -ketoesterates and was also observed for  $\text{Zr}(\text{O}^i\text{Pr})_2(\text{tert-butylacetoacetate})_2$ ,  $\text{Zr}_2(\text{O}^i\text{Pr})_6(\text{tert-butylacetoacetate})_2$ , and  $\text{Zr}(\text{allylacetoacetate})_x(\text{O}^n\text{Bu})_{4-x}$ .<sup>14,139</sup> Furthermore, the  $\text{COCHCOO}$  signal at 88 ppm ( $^{13}\text{C}$  NMR) and 5.05-5.32 ppm ( $^1\text{H}$  NMR) appeared. Both shifts proved the complete coordination of the  $\beta$ -ketoesterate groups. NMR experiments only showed one set of signal attributed to  $\text{O}^i\text{Pr}$ . This was in line with the postulated structure with only terminal alkoxo groups coordinated to zirconium. In an additional experiment,  $\beta$ -ketoester 1 was allowed to react with a mixture of titanium and zirconium alkoxides. (Figure 3.34) To this end, both metal alkoxides were mixed in a ratio of 1:1 and ketoester 1 was added afterwards. Compound **17** was isolated by evaporation of the solvent. A solution of **17** was investigated by ESI-MS. (Figure 3.33)

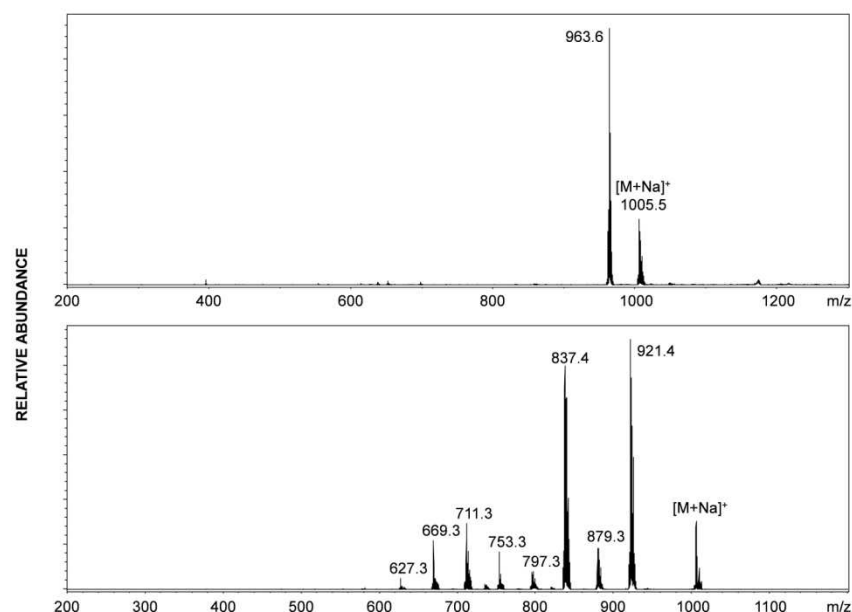


Figure 3.33: Positive ion ESI mass spectrum and low energy CID MS/MS spectrum of 17

The mass spectra showed a very unexpected result. The most intensive peak appeared at  $m/z$  936.6. This was attributed to the complex  $[\text{TiL}(\text{O}^i\text{Pr})_2]_2$  (**11**) known from investigations with  $\text{Ti}(\text{O}^i\text{Pr})_4$  and ketoester **1**, discussed in Chapter 3.4. A second, more unexpected signal appeared at  $m/z$  1005.5 with lower intensity. This was assigned to  $\text{TiZrL}_2(\text{O}^i\text{Pr})_4$ , for which the same metallacyclic structure, as observed for **11** and **15**, was assumed. Both bis( $\beta$ -ketoesterates) bridged the  $\text{Zr}(\text{O}^i\text{Pr})_2$  with the  $\text{Ti}(\text{O}^i\text{Pr})_2$  moiety. (Figure 3.34) This was one of the first metallacycles with mixed metals. Another example was reported previously by Fenton et al. There, the reaction of  $\text{VO}[1,1-(1,4\text{-phenylene})\text{-bis-butane-1,3-dione}]_2$  with copper acetate resulted in the mixed-metal metallacycle  $\text{CuVO}[1,1-(1,4\text{-phenylene})\text{-bis-butane-1,3-dione}]_2$ .<sup>132</sup>

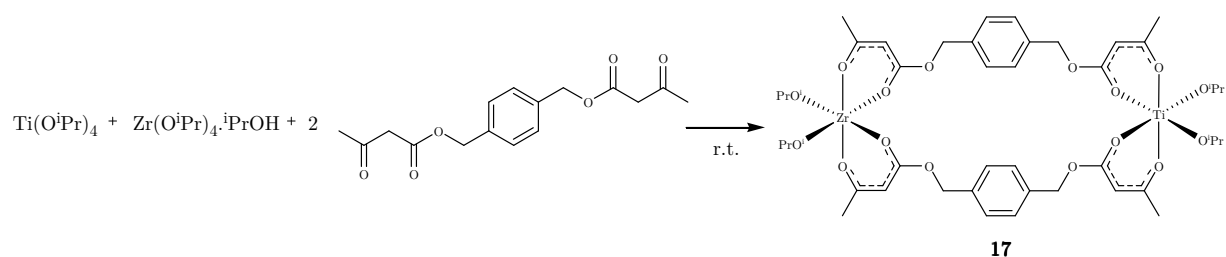


Figure 3.34: Synthesis and postulated structure of 17

Low energy CID MS/MS investigations resulted in a similar fragmentation pathway as observed in the monometallic group(IV) metal alkoxo bis( $\beta$ -ketoesterates). Product ions were obtained at  $m/z$  921.4, 837.4 and 753.3, which differ by 84 Da. This was in line with partial cleavage of  $\text{CH}_3\text{COCHCO}$  groups of the bis( $\beta$ -ketoesterates). The mixed metal core remained stable.

The very intense signal of  $[\text{TiL}(\text{O}^i\text{Pr})_2]_2$  was no longer astonishing. Titanium alkoxides are known for higher reaction rates than zirconium alkoxides. First, most of the  $\beta$ -ketoester **1** coordinated to

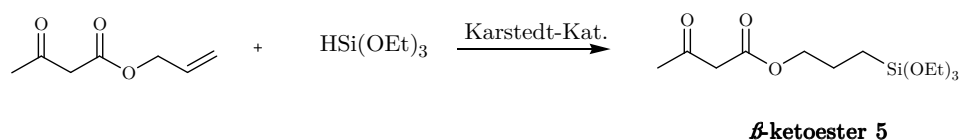
one  $\text{Ti}(\text{O}^i\text{Pr})_x$ . Afterwards, the second uncoordinated  $\beta$ -ketoester group binds to a second  $\text{Ti}(\text{O}^i\text{Pr})_x$  to give complex **11** or a  $\text{Zr}(\text{O}^i\text{Pr})_x$  unit to form complex **17**. Complex **11** was more or less a side product of the reaction, which could not be avoided due to the higher reaction rate.

NMR investigations proved the complete coordination of the bis( $\beta$ -ketoester). The carbonyl signals at 166/200 ppm disappeared and resonances for the coordinated ligand were present at 172.2/185.3 ppm in the  $^{13}\text{C}$  NMR spectrum. Furthermore, signals at 4.84/88.2 ppm appeared, which were derived from the coordinated enolate form of the ligand.  $^{13}\text{C}$  NMR experiments showed two  $\text{O}^i\text{Pr}$  methine resonances at 76.2 and 70.8 ppm, which were attributed to the  $\text{Ti}(\text{O}^i\text{Pr})_2$  and  $\text{Zr}(\text{O}^i\text{Pr})_2$  moieties. Two resonances for the methyl group of the  $\beta$ -ketoesterate unit proved the postulated molecular structure.

### 3.6 Modification of titanium isopropoxide with butanoic acid-3-oxo-3-(triethoxysilyl)propyl ester

Several attempts had already been made to combine titanium alkoxides with alkoxysilane groups to synthesise homogenously dispersed  $\text{TiO}_2/\text{SiO}_2$ . 3-(Propyltrimethoxysilyl)-acetylacetone was reacted with several metal compounds and proven to cleave partially by hydrodeacylation.<sup>10</sup> A second approach was using ethylenediamine-substituted trialkoxysilanes instead.

An alternative access is the use of  $\beta$ -ketoesters. There, the alkoxysilyl unit and the  $\beta$ -ketoester group were easily combined. Hydrosilylation between allylacetoacetate and triethoxysilane with Karstedt catalyst resulted in  $\beta$ -ketoester **5**. (Scheme 3.1)



**Scheme 3.1: Synthesis of  $\beta$ -ketoester 5**

This compound combined the advantages of the two ligands mentioned above. First, the ligand provided a coordinating group that is known for strong coordination to the group (IV) metal alkoxides. Second, the ester bond was a quite stable linker between the coordination group and the alkoxysilyl unit.

Thus, ketoester **5** was used for the modification of titanium alkoxides. The ligand was reacted with  $\text{Ti}(\text{O}^i\text{Pr})_4$  in the ratio of 1:1, and the reaction resulted in an oily residue. Several unsuccessful attempts were made to crystallise compound **18**. The use of different alkoxo groups, ethoxide at Si and isopropoxide at Ti, did not permit the use of alcoholic solutions, although alkoxo exchange reactions could also occur in aprotic solvents. Therefore, ESI-MS experiments were not possible.

Structure determination was only done by IR and NMR investigations. IR spectra resulted in a shift of the asymmetric C=O stretching frequencies from 1717/1650 to 1631/1611  $\text{cm}^{-1}$ , which was evidence for the complete coordination and was in line with observation of  $\text{Ti}(\text{MEAA})_2(\text{O}^i\text{Pr})_2$  and  $\text{Ti}_2(\text{MEAA})_2(\text{O}^i\text{Pr})_6$  [MEAA = (methacryloyloxy) ethyl acetoacetate].<sup>140</sup>

The  $^{13}\text{C}$  NMR spectrum showed two signals at 184.6 and 172.4 ppm, which were in line with previous examples of  $\beta$ -ketoesterate complexes. Both signals at 166 and 200 ppm, assigned to the uncoordinated ligand, were gone. An additional resonance for the COCHCOO group appeared in the  $^1\text{H}$  as well as in the  $^{13}\text{C}$  NMR spectrum. NMR investigations showed two signals of  $\text{O}^i\text{Pr}$  methine protons at 4.73 and 4.21 ppm. This would be in line with a dimeric, alkoxo bridged titanium complex, in which one ligand was coordinated to the titanium centre (see Figure 3.35). Comparable to reactions with acac-H, the reaction of  $\text{Ti}(\text{O}^i\text{Pr})_4$  with  $\beta$ -ketoesters in a ratio of 1:2 resulted in monomeric, disubstituted complexes  $\text{TiL}_2(\text{O}^i\text{Pr})_2$ , whereas reactions in a ratio of 1:1 resulted in dimeric mono-substituted complexes  $[\text{TiL}(\text{O}^i\text{Pr})_3]_2$ ; both species were in equilibrium. Two  $\text{O}^i\text{Pr}$  methine resonances fitted well with reported observations of  $\text{Ti}_2(\text{EAA})_2(\text{O}^i\text{Pr})_6$ .<sup>17</sup> The broad signals indicated ligand exchange reactions in solution. It is also possible that they were caused by partial redistribution of a mono-substituted complex to  $\text{TiL}_2(\text{O}^i\text{Pr})_2$  and  $\text{Ti}(\text{O}^i\text{Pr})_4$ .

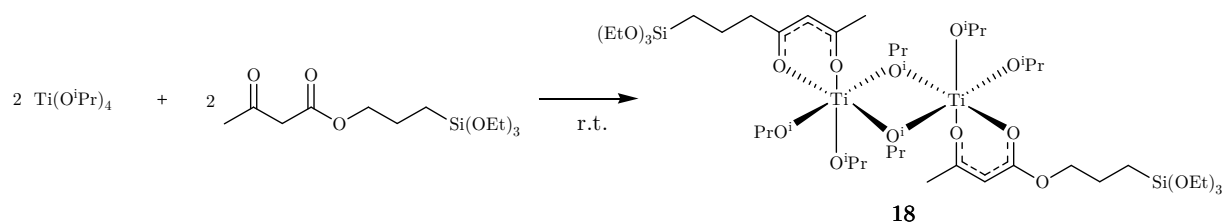


**Figure 3.35: Synthesis and suggested schematic structure of 18**

### 3.7 Modification of titanium isopropoxide with 1,5-diphenyl-pentane-1,3,5-trione

Previous reactions of 1,5-substituted-pentane-1,3,5-trione with late transition metals resulted in dimeric complexes of the type  $\text{M}_2(\text{triketone})_2$  ( $\text{M}=\text{Co}, \text{Cu}, \text{Ni}$ ). There, two triketone ligands bridged both metal ions.<sup>70-72</sup> Based on these results, the triketone was reacted with  $\text{Ti}(\text{O}^i\text{Pr})_4$  in dichloromethane. (Figure 3.36) After one day upon slow diffusion of water, **19**  $\cdot 2\text{CH}_2\text{Cl}_2$  crystallised in solution.

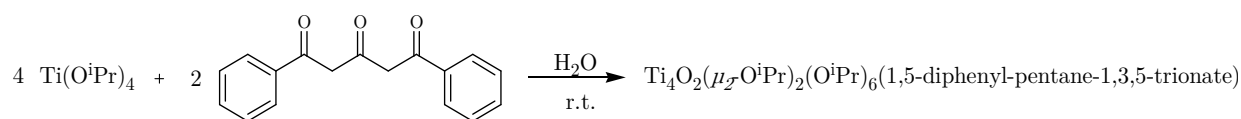


**Figure 3.36: Synthesis of the compound 19**



**Table 3.2: Selected bond distances [pm] and angles [°] of  $19 \cdot \text{CH}_2\text{Cl}_2$  (atoms with an asterisk denote inversion-related atoms)**

Ti(1)-O(1)	197.82(17)	Ti(2)-O(2)	212.01(17)
Ti(1)-O(2)	215.50(16)	Ti(2)-O(3)	197.38(17)
Ti(1)-O(5)	177.17(18)	Ti(2)-O(4)	176.77(16)
Ti(1)-O(6)	182.47(15)	Ti(2)-O(7)	191.05(16)
Ti(1)-O(7)*	218.56(16)	Ti(2)-O(20)	193.20(17)
Ti(1)-O(20)	192.57(16)	Ti(2)-O(20)*	206.29(15)
O(1)-Ti(1)-O(2)	82.47(0)	O(2)-Ti(2)-O(3)	82.37(5)
O(5)-Ti(1)-O(20)	103.67(8)	O(4)-Ti(2)-O(20)	99.29(1)
		O(4)-Ti(2)-O(20)*	176.11(2)
O(6)-Ti(1)-O(7)*	170.11(5)	O(7)-Ti(2)-O(20)	104.05(6)
		O(7)-Ti(2)-O(20)*	79.09(0)
Ti(1)-O(2)-Ti(2)	95.70(2)	Ti(1)-O(20)-Ti(2)	110.50(0)
		Ti(1)-O(20)*-Ti(2)	104.11(5)

Compound **19** was also investigated by NMR experiments. The  $^{13}\text{C}$  NMR spectrum showed two resonances at 182.4 and 176.2 ppm attributed to the carbonyl groups of the coordinated ligand. Both signals of the uncoordinated ligand at 194.1 and 191.0 ppm disappeared. Moreover, the  $\text{COCH}_2\text{CO}$  methylene signal at 50.6 ppm was also gone. Unexpectedly, only one set of  $\text{O}^i\text{Pr}$  signals at 76.0/ 25.4 ppm was present, although bridging alkoxo groups were observed in the solid state structure.

Compound **19** was the only example known, in which a triketone was coordinated to a metal alkoxide. Furthermore, this  $\text{Ti}_4\text{O}_2$  cluster was a rare example of titanium oxo clusters with coordinated  $\beta$ -diketonate groups. While numerous group (IV) metal oxo clusters had been reported with carboxylate ligands (Chapter 1.2), only a few clusters had been published with acac and other  $\beta$ -diketonates.  $\text{Ti}_4\text{O}_2(\text{O}^i\text{Pr})_{10}(\text{acac})_2$ ,  $\text{Ti}_5\text{O}_6\text{cp}_2(1,3\text{-diphenyl-propane-1,3-dione})_6$  and  $\text{Ti}_{18}\text{O}_{22}(\text{OBu})_{26}(\text{acac})_2$  were the only titanium clusters known with  $\beta$ -diketonates and titanium.<sup>142</sup> Moreover, two clusters were known with zirconium,  $[\text{Zr}_4\text{O}(\text{O}^i\text{Pr})_{10}(\text{acac})_4]$  and  $\text{Zr}_{10}\text{O}_6(\text{OH})_4(\text{OPr})_{18}(\text{aaa})_6$ .<sup>133,143</sup>

The formation of a titanium oxo cluster was caused by slow diffusion of water, which was caused either by residual moisture in the ligand or by a leaky closing cap at the flask. These small quantities of water led to partial hydrolysis of the titanium triketonate alkoxo moieties and condense to the  $\text{Ti}_4\text{O}_2$  cluster core. The synthesis was repeated several times, and in each experiment crystals of  $19 \cdot 2 \text{CH}_2\text{Cl}_2$  were obtained. A change of the experimental setup or the use of varying ratios of  $\text{Ti}(\text{O}^i\text{Pr})_4/\text{ligand}$  did not result in compounds of different compositions. Therefore, moisture in the ligands was the more reasonable explanation for the formation of oxo clusters. Moreover, the investigations proved that no polymeric species were possible, in which one triketone combined  $\text{Ti}(\text{O}^i\text{Pr})_x$  moieties.

### 3.8 Modification of titanium ethoxide with 1,6-diphenyl-hexane-1,3,4,6-tetraone

The idea of using polyketones was extended to tetraketones.  $\text{Ti}(\text{OEt})_4$  was reacted with 1,6-diphenyl-hexane-1,3,4,6-tetraone. (Figure 3.38)

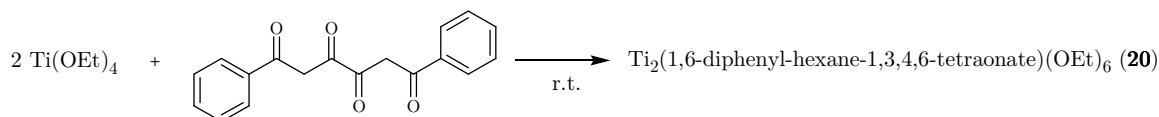


Figure 3.38: Synthesis of compound 20

Numerous crystallisation experiments failed. Thus, ESI-MS was the method of choice to determine the composition of compound 20. The mass spectrometric investigations obtained a peak at  $m/z$  681.2 (calc. 681.2) (Figure 3.39), which can be attributed to the sodiated complex  $\text{Ti}_2\text{L}(\text{OEt})_6$ . Two additional peaks were present at  $m/z$  425.1 and 304.2, which could not be assigned to a certain fragment of compound 20.

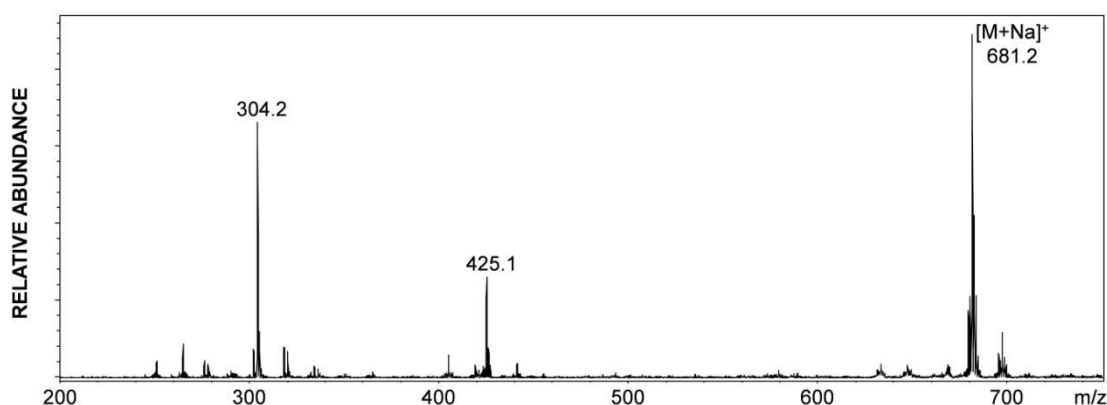


Figure 3.39: Positive ion ESI mass spectrum of 20

Low energy CID MS/MS resulted in several product ions. The most prominent one at  $m/z$  453.0 (calc. 453.1) was assigned to the sodiated complex  $[\text{TiL}(\text{OEt})_2\text{Na}]^+$ . This product ion is caused by  $\text{Ti}(\text{OEt})_4$  cleavage during the fragmentation process. The unknown ion observed before at  $m/z$  425.1 was still present in the MS/MS scans. It is assumed to be caused by an in-source contamination. The product ion at  $m/z$  407.0 and its neighbouring resonance should be attributed to  $[\text{Ti}_2(\text{OEt})_7]^+$ , which was formed due to cleavage of  $\text{Ti}(\text{OEt})_4$ .

Derived from the determined constitution, two structures were theoretically possible. (Figure 3.40) In both cases, the tetradentate ligand bridges the titanium centres. Each titanium atom is coordinated either to three terminal OEt groups or to two terminal and two bridging ethoxides.

Concerning to low energy CID MS/MS scans, the formation of product ions of type  $[\text{TiL}(\text{O}^i\text{Pr})_2\text{Na}]^+$  was only observed if no bridging alkoxo groups are present in the structure. This



would be in line with *isomer 1*. There, the ligand bridges two  $\text{Ti}(\text{OEt})_3$  moieties. This monomeric, structural feature was quite unknown for  $\text{Ti}(\beta\text{-diketonate})(\text{OR})_3$ .<sup>12</sup> Compared to other titanium  $\beta$ -diketonate complexes, mono-substituted titanium alkoxides always showed bridging alkoxo groups.

Although *isomer 2* should be preferred due to the higher coordination number of each titanium centre, it was more or less a hypothetical structure, as the steric strain in the complex was too high, and both titanium centres would be quite near to each other. If each  $\beta$ -diketonate group of the tetraketonate ligand coordinated to different dimeric  $\text{Ti}_2(\text{OR})_6$  moieties, compounds with similar structural features, as observed in *isomer 2*, but less steric strain would be possible. This would result in polymeric assemblies, where mono-substituted, dimeric titanium alkoxo moieties were present as observed for all mono-substituted titanium alkoxo  $\beta$ -diketonates.

The absence of any signals at higher  $m/z$  values attributed to this type of structure was another evidence for the high stability of the structural motive of *isomer 1*, where no bridging alkoxo ligands were present.

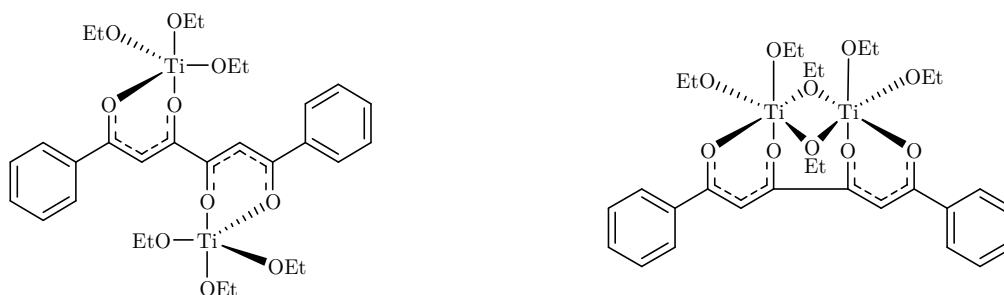


Figure 3.40: Proposed configurations of **20** (isomer 1 [left], isomer 2 [right])

Additional structure elucidation would be easy by NMR spectroscopy, but it was no choice due to the bad solubility of the complex.

*Isomer 1* is supported by previous investigations of Woisetschl ger *et al.* They had used 1,6-bis(ferrocenyl)-hexane-1,3,4,6-tetraone in the reaction with numerous  $\text{PdCl}_2$  and  $\text{IrCl}_2$  complexes. They reported complexes of composition  $\text{M}_2\text{Cl}_2(\text{tetraketonate})\text{L}_2$  ( $\text{L}$ =neutral ligand, e.g.  $\text{PPh}_3$ ), where also one tetraketonate ligand, bridged both metal centres.<sup>144</sup> Mehrotra *et al.* had also postulated structures of type  $\text{TiL}(\text{O}^i\text{Pr})_6$  with bis( $\beta$ -ketoesters).<sup>83</sup> Considering all facts, *isomer 1* was the most likely structure.

In contrary to all complexes with other tetradentate ligands presented in this thesis, only one 1,6-diphenyl-hexane-1,3,4,6-tetraone bridged two titanium centres, although two bridging tetraketones would be possible. Maybe the steric hindrance of the ligand was too high that a coordination of a second ligand was blocked.

However, compound **20** was the first titanium tetraketonate complex known. There were no other complexes reported, where metal alkoxides were used with this group of ligands. But tetraketones also showed no tendency to form polymeric assemblies.



### 3.9 Modification of titanium ethoxide with 1,5-pentanedial-1,5-dioxime

Until present, only few titanium alkoxo complexes were reported with alkylene-linked dioximate ligands. Baumann *et al.* reported a tetrameric complex  $\text{Ti}_4(\text{O}^i\text{Pr})_8\text{L}_4$  ( $\text{L} = 2,4\text{-pentanedioximate}$ ), where the dioximate ligands both bridged dimeric titanium alkoxide units and interconnected two of the dimeric units.<sup>43</sup>

The investigations were extended to dioximes with longer alkylene linkers. Therefore, dioximes were synthesised, in which two or three methylene groups separated the oxime groups. Reaction of  $\text{Ti}(\text{OEt})_4$  with 1,5-pentanedial-1,5-dioxime resulted in colourless prismatic crystals. (Figure 3.41)

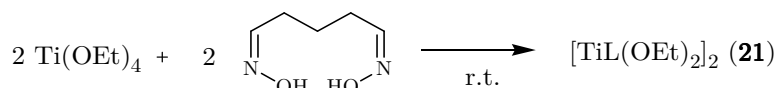


**Figure 3.41: Synthesis of compound 21**

The complex crystallized in the monoclinic space group  $P2_1/c$ . Structural refinement showed two complexes of composition  $\text{Ti}_2(1,5\text{-pentanedial-1,5-dioximate})_2(\text{OEt})_4$ . Both complexes were identical and only differed slightly in the bond distances. The complex was centrosymmetric. (Figure 3.42 [only one complex shown] and Figure 3.43).

Each titanium atom was 7-coordinated by two N and five O atoms. The resulting polyhedrons were edge-sharing. The N-Ti-N axis was slightly bent and showed an angle of  $164.48(7)^\circ$ . Both titanium atoms were bridged by two dioximate ligands and two  $\mu_2\text{-OEt}$  groups. The oximate groups were coordinated side-on. The alkoxo bridges were slightly asymmetric, where the Ti-O distances varied between 202.8 and 204.8 pm. Each titanium atom was coordinated to one  $\mu_1\text{-OEt}$  group. The terminal OEt ligands were out of the  $\text{Ti}_2(\mu_2\text{-OEt})_2$  plane. The titanium centre with two coordinated oximate groups, one terminal and two bridging alkoxo groups, was a structural motive, which was previously observed for other oximate-substituted titanium alkoxides. Baumann *et al.* reported several complexes of comparable structural features.<sup>43,44</sup>

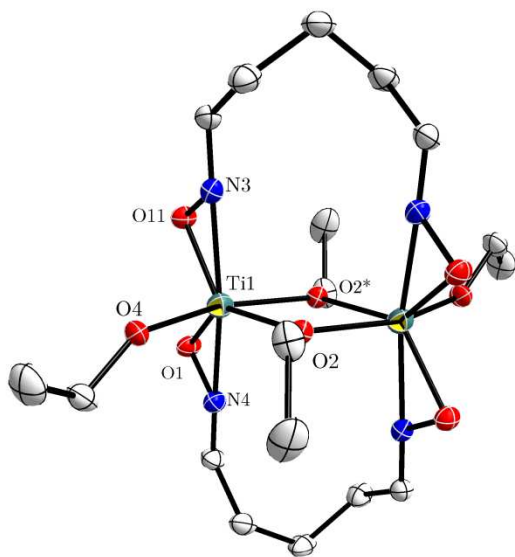


Figure 3.42: Molecular structure of **21** (the ellipsoids are drawn at 50% probability)

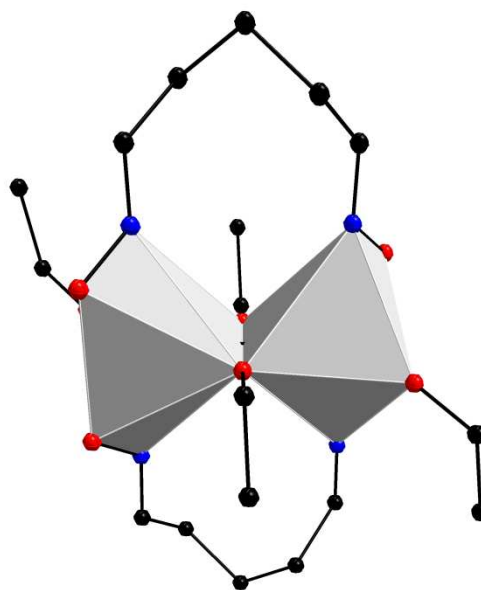


Figure 3.43: Edge-sharing connection of the coordination polyhedral of the Ti atoms

Selected bond length and angles are summarized in Table 3.3. The Ti-O<sub>oximate</sub> and Ti-N<sub>oximate</sub> distances of compound **21** were in good agreement with other literature known, disubstituted titanium oximate alkoxo complexes. The Ti-O<sub>oximate</sub> distances were between 194 and 198 pm, whereas Ti-N<sub>oximate</sub> distances were measured between 205 and 215 pm for previously reported titanium alkoxo oximate complexes.<sup>43-45</sup>

Two isomers were observed in previously investigated titanium alkoxo oximates. Either both N atoms of the oximates are in axial position (*isomer 1*), or the N of one oximate and the O of the second oximate are in axial position (*isomer 2*). (Figure 3.44) Compound **21** was an isomer of type 1. A mixture of isomers was excluded; *isomer 2* would be under considerable steric strain. The examples in literature showed N<sub>oximate</sub>-Ti-N<sub>oximate</sub> angles between 160 and 164° for the obtained configuration, Herein, the N<sub>oximate</sub>-Ti-N<sub>oximate</sub> angle was 164.48(7)°, which was in good agreement with other reported structures. The O<sub>oximate</sub>-Ti-O<sub>oximate</sub> angle of 85.67(7)° also fitted well with complexes of similar configuration.<sup>43-45</sup> Furthermore, comparison of the Ti-O<sub>Et</sub> distances matched well with that of [Ti(cyclohexyl oximate)<sub>2</sub>(OEt)<sub>2</sub>].<sup>43,45,145</sup>

Table 3.3: Selected bond distances [pm] and angles [°] of **21** (atom with an asterisk denote inversion-related atoms)

Ti(1)-O(1)	195.63(14)	O(1)-Ti(1)-O(4)	98.09(6)
Ti(1)-O(2)	204.75(13)	O(1)-Ti(1)-O(11)	85.67(7)
Ti(1)-O(2)*	202.78(13)	O(2)-Ti(1)-O(2)*	71.61(6)
Ti(1)-O(4)	180.68(14)	O(2)-Ti(1)-O(4)	92.07(6)
Ti(1)-O(11)	195.30(14)	O(2)*-Ti(1)-O(4)	162.46(6)
Ti(1)-N(3)	208.97(17)	O(4)-Ti(1)-O(11)	100.09(6)
Ti(1)-N(4)	209.15(18)	N(3)-Ti(1)-N(4)	164.48(7)

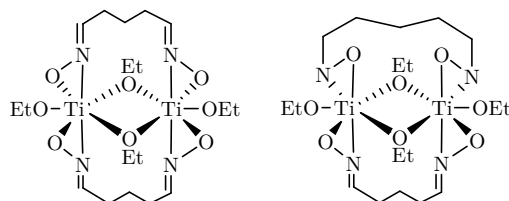


Figure 3.44: Possible isomers of **21** [*isomer 1* (left), *isomer 2* (right)]

In compound **21**, neighbouring oximate moieties at the two titanium atoms were connected through the  $(\text{CH}_2)_n$  spacer. In contrary to  $\text{Ti}_4(\text{O}^i\text{Pr})_8(2,4\text{-pentanedioximate})_4$ , both dioximate ligands bridged the same  $\text{Ti}_2(\text{O}^i\text{Pr})_4$  unit. This difference was caused by less strain of the more flexible 1,5-pentanedial-1,5-dioximate ligand. The complex differed from the metallacycles observed with bis( $\beta$ -diketonate) and bis( $\beta$ -ketoesterate) ligands, in which the ligands bridged two  $\text{Ti}(\text{O}^i\text{Pr})_2$  moieties without alkoxo bridges. Oximate ligands promoted the existence of bridging alkoxo ligands due to their smaller bite angle. Thus, the coordination sphere was less overcrowded.

Compound **21** was investigated by other analysis techniques, which determined the composition of the complex in solution state. ESI-MS resulted in one peak at  $m/z$  555.2 (calc. 555.1), which was attributed to the sodiated complex  $[\text{TiL}(\text{OEt})_2]_2\text{Na}^+$  (Figure 3.45). No protonated ions were detected in the positive-ion mode. The derived composition fitted well with the molecular structure elucidated by the single crystal XRD. Thus, same structure was observed in solid and solution state.

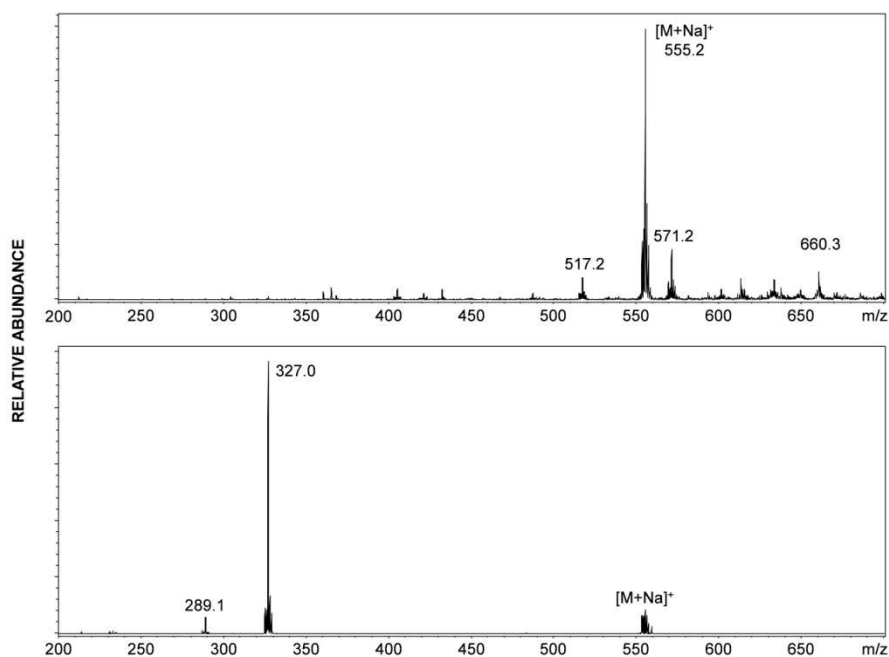


Figure 3.45: Positive ion ESI mass spectrum and low energy CID MS/MS spectrum of **21**

Low energy CID MS/MS measurement resulted in one product ion at  $m/z$  327.0 (calc. 327.1), corresponding to  $[\text{TiL}_2\text{Na}]^+$ , which was in contrast to the fragmentation pathway observed in  $\text{Ti}_2[\text{bis}(\beta\text{-diketonate})_2](\text{O}^i\text{Pr})_4$ . While the metallacycles cleaved in identical fragments  $\text{TiL}(\text{O}^i\text{Pr})_2$ , the bridging alkoxo groups promoted a cleavage of  $\text{Ti}(\text{OEt})_4$  during the fragmentation progress. Therefore, fragments of type  $\text{TiL}_2$  were formed. The different fragmentation pathway of the low energy CID MS/MS experiment thus allowed a clear distinction between alkoxo-bridged and non-bridged titanium complexes.

Additional investigations were done by solution NMR spectroscopy. The  $^{13}\text{C}$  NMR spectrum showed a clear shift of the  $\text{C}=\text{N}$  signal from 150.5 to 139.4 ppm, which was in line with previous investigations of  $[\text{Ti}(\text{oximate})_2(\text{OR})_2]_2$ .<sup>43,44</sup> Moreover, the NMR spectra showed two sets of OEt resonances at 71.7/22.2 and 68.2/18.0 ppm. This matched well with the presence of both, terminal and bridging, alkoxo ligands. This was also proven by  $^1\text{H}$  NMR spectroscopy; two signals appeared at 4.34 and 3.64 ppm.

### 3.10 Modification of titanium alkoxides with 2,5-hexanedione-2,5-dioxime

Titanium alkoxides were also modified with dioximes, where both oximate units were only separated by two methylene groups. 2,5-Hexanedione-2,5-dioxime had a shorter linker than 1,5-pentanedial-1,5-dioxime used in compound **21**. The linker only differed in one additional methylene group from that of 2,4-pentanedioxime, which built oligomeric, cyclic structures.<sup>43</sup> First, 2,5-hexanedione-2,5-dioxime was reacted with  $\text{Ti}(\text{O}^i\text{Pr})_4$  in a ratio of 1:1. (Figure 3.46)

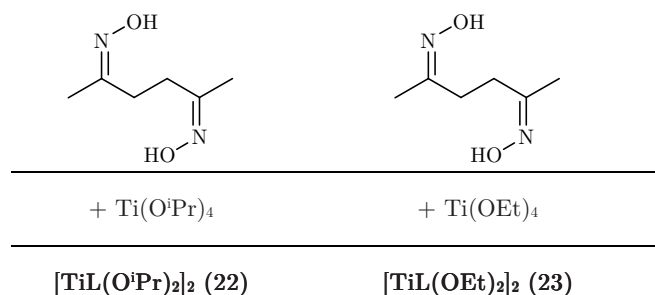


**Figure 3.46:** Dioxime used in this work and the resulting titanium compounds

Crystallisation from 1,2-dichloroethane yielded colourless prismatic crystals of **22**. The complex crystallized in the monoclinic space group  $Cc$ . Structural refinement showed one complex  $[\text{Ti}(2,5\text{-hexanedione-2,5-dioximate})(\text{O}^i\text{Pr})_2]_2$ . The structure was similar to the one of previously described compound **21**. (Figure 3.47).

Each titanium atom was 7-fold coordinated. The  $[\text{TiN}_2\text{O}_5]$  polyhedra were edge-sharing. (Figure 3.48) The titanium atoms were linked by two bridging dioximates and two  $\mu_2\text{-O}^i\text{Pr}$  groups. The oximate groups were nearly coplanar regarding the Ti atoms. The  $\mu_2\text{-O}^i\text{Pr}$  bridges were slightly asymmetric, the Ti-O distances varied between 203 and 204 pm. One  $\mu_2\text{-O}^i\text{Pr}$  remained on each

titanium atom. Both terminal alkoxo groups were nearly in the  $[\text{Ti}\mu_2\text{O}]_2$  plane. The obtained structural motive was comparable to the molecular structure of **21**.

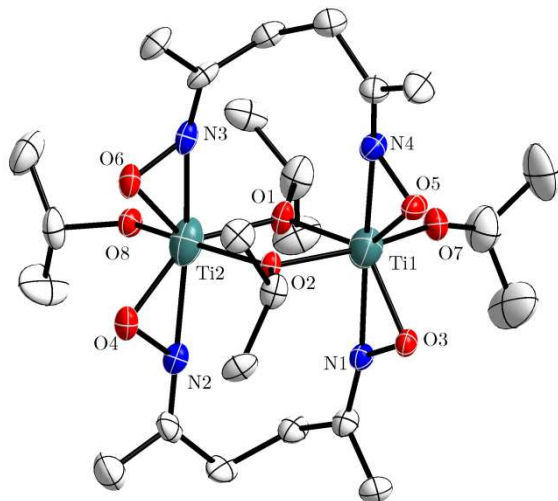


Figure 3.47: Molecular structure of compound **22** (the ellipsoids are drawn at 50% of the probability density function)

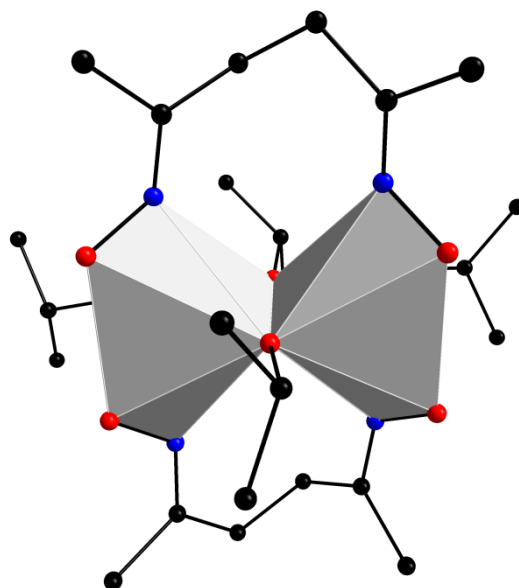


Figure 3.48: Edge-sharing connection of the coordination polyhedral of the Ti atoms

Complex **22** was of same configuration described before for *isomer 1*. Selected bond lengths and angles are listed in Table 3.4. The  $\text{N}_{\text{oximate}}\text{-Ti-N}_{\text{oximate}}$  angles were  $161.23(1)^\circ$  and  $162.89(1)^\circ$ , which was in line with other titanium oximate complexes known in literature.<sup>43,44</sup> The corresponding  $\text{O}_{\text{oximate}}\text{-Ti-O}_{\text{oximate}}$  angles varied between  $85.40(1)^\circ$  and  $86.54(1)^\circ$ . This fitted well with other complexes of type *isomer 1*. The  $\text{Ti-O}_{\text{oximate}}$  distances were in a range of 192.3 and 196.5 pm. Especially, the comparably short distance  $\text{Ti}(2)\text{-O}(4)$  of 192.3 pm evidenced the stronger Ti-oximate interaction compared to other, literature known titanium alkoxo oximates<sup>43,44</sup> and showed the increased steric strain in the complex. In complex **22**, the  $\text{Ti-N}_{\text{oximate}}$  distances were between 203.2 and 216.9 pm and in good agreement with solid state structures of previously in literature reported complexes of type  $[\text{Ti}(\text{oximate})_2(\text{O}^i\text{Pr})_2]_2$ .<sup>43,44</sup> It was unexpected that the Ti-N distance of one oximate of the ligand was significantly shorter than that of the other oximate group. While the  $\text{Ti}(1)\text{-N}(1)$  distance was 203.2 pm, the  $\text{Ti}(1)\text{-N}(4)$  distance was 216.9 pm. The  $\text{Ti}(1)\text{-N}(1)$  distance was very short in comparison to other disubstituted titanium oximate complexes. Similar observations were made with  $\text{Ti}(2)\text{-N}(2)$  and  $\text{Ti}(2)\text{-N}(3)$ , where the  $\text{Ti}(2)\text{-N}(3)$  was significantly shorter. The  $\text{Ti-}\mu_2\text{-O}$  distances were 179.9 and 181.2 pm. They were in comparable range of other dimeric  $[\text{Ti}(\text{oximate})_2(\text{O}^i\text{Pr})_2]_2$  complexes. The  $\text{Ti-}\mu_2\text{-O}$  distances also matched well with the distances measured in comparable complexes.<sup>43,45</sup>

**Table 3.4: Selected bond distances [pm] and angles [°] of **22****

Ti(1)-O(1)	204.64(29)	Ti(2)-O(1)	203.82(32)
Ti(1)-O(2)	202.97(31)	Ti(2)-O(2)	206.19(28)
Ti(1)-O(3)	196.47(32)	Ti(2)-O(4)	192.34(35)
Ti(1)-O(5)	195.37(27)	Ti(2)-O(6)	196.27(28)
Ti(1)-O(7)	179.94(35)	Ti(2)-O(8)	181.19(30)
Ti(1)-N(1)	203.24(38)	Ti(2)-N(2)	214.49(41)
Ti(1)-N(4)	216.89(36)	Ti(2)-N(3)	206.10(37)
O(1)-Ti(1)-O(2)	74.92(1)	O(1)-Ti(2)-O(2)	74.41(1)
O(1)-Ti(1)-O(7)	91.75(1)	O(1)-Ti(2)-O(8)	92.80(1)
O(2)-Ti(1)-O(7)	166.67(1)	O(2)-Ti(2)-O(8)	166.19(2)
O(3)-Ti(1)-O(7)	98.56(1)	O(4)-Ti(2)-O(6)	86.54(1)
O(3)-Ti(1)-O(5)	85.40(1)	O(4)-Ti(2)-O(8)	93.88(1)
O(5)-Ti(1)-O(7)	97.94(2)	O(6)-Ti(2)-O(8)	97.00(1)
N(1)-Ti(1)-N(4)	161.23(1)	N(2)-Ti(2)-N(3)	162.89(1)

Compound **22** was investigated by ESI-MS, but no reasonable spectrum was obtained. It was assumed that this was caused by a lower stability of the complex or the lower solubility in comparison to compound **21**.

Additional structure determination was done by NMR spectroscopy. The  $^{13}\text{C}$  NMR spectrum showed a significant shift of the C=N group from 155.3 to 146 ppm upon coordination, which was in good agreement with earlier observations of titanium acetone oximate and titanium alkoxo cyclohexyl oximates.<sup>45</sup> This clear shift proved the coordination of both oximate groups. Furthermore, the low symmetry of the complex resulted in two methylene signals for the  $\text{CH}_2\text{CH}_2$  chain at 3.12 and 2.12 ppm in the  $^1\text{H}$  NMR spectrum. Two  $\text{CH}_3\text{CN}$  signals at 1.82 and 1.17 ppm were present in the  $^1\text{H}$  NMR spectra as well. Moreover, the  $^{13}\text{C}$  NMR spectrum showed two sets of O<sup>i</sup>Pr signals, which corresponded to the terminal and bridging alkoxo groups.

Compound **22** was also investigated by 2D NMR measurements. The dioximate formed a nine-membered ring with two titanium atoms and one bridging O<sup>i</sup>Pr ligand. (Figure 3.49) Three discrete conformers were possible. They differ by the positioning of the methylene groups of the dioximate. Each conformer led to an independent set of four O<sup>i</sup>Pr signals. Therefore twelve signals were expected for the O<sup>i</sup>Pr groups.

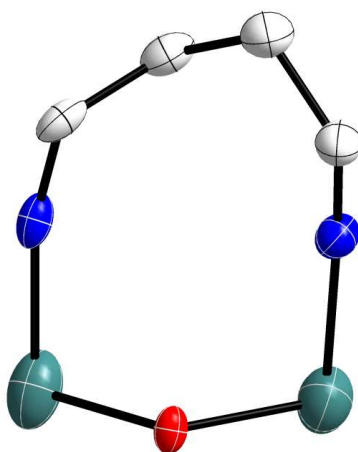


Figure 3.49: Nine-membered building block of 22

Seven different CH signals were observed in the COSY and HSQC spectrum at room temperature (Figure 3.50 and Figure 3.51). The EXSY spectrum at room temperature (Figure 3.52) showed a highly dynamic compound. Two exchange signals at 3.7/4.5 ppm and 4.5/4.85 ppm were observed.

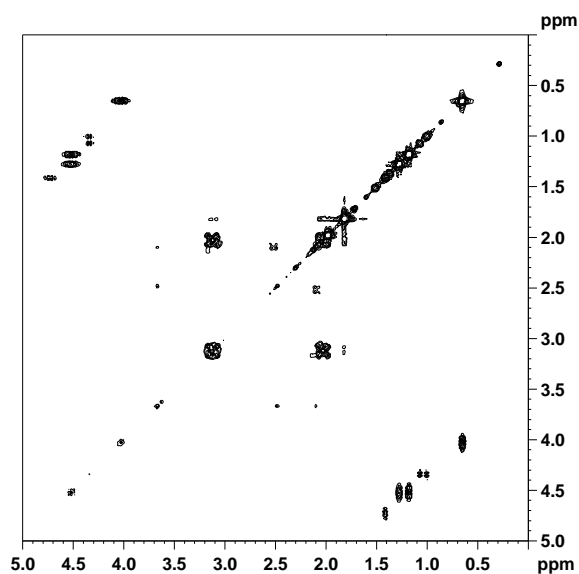


Figure 3.50: COSY spectrum of 22 at room temperature

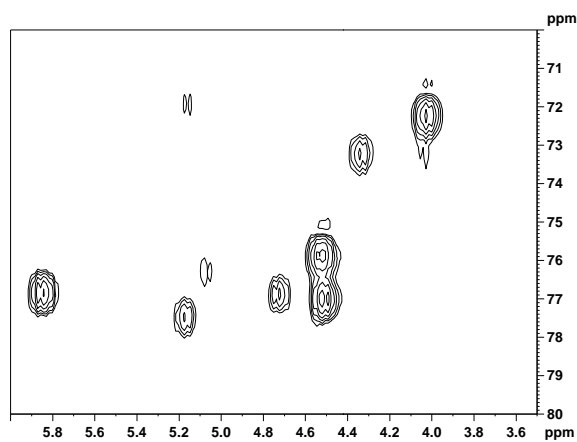


Figure 3.51: HSQC spectrum of 22 at room temperature

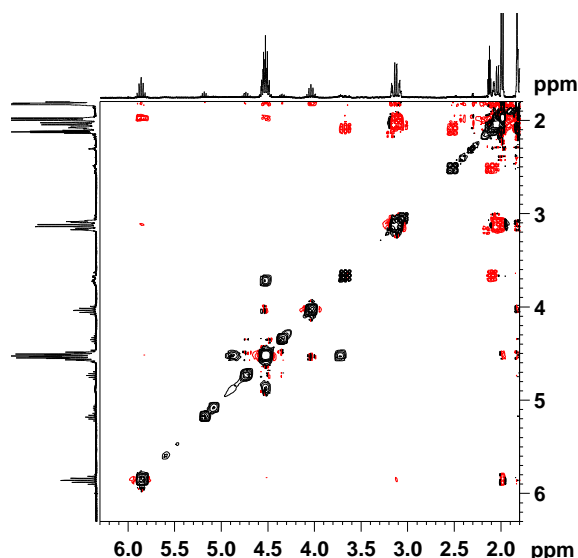


Figure 3.52: EXSY spectrum of compound 22 at room temperature

The resonance at 3.7 ppm was assigned to free 2-propanol; the first set of exchange signals was therefore caused by exchange of residual 2-propanol and a terminal O<sup>i</sup>Pr group. The second exchange signal (4.5/4.85 ppm) was attributed to an exchange between different O<sup>i</sup>Pr groups. Two explanations were possible for this exchange: First, an exchange could occur between terminal and bridging O<sup>i</sup>Pr ligands. Hereby, the O<sup>i</sup>Pr bridges could be cleaved and a dimeric metallacycle without bridging alkoxo groups was formed as a transition state. Twisting of the terminal alkoxo groups and recombination of the bridges resulted in exchanged alkoxo ligands. (Figure 3.53)

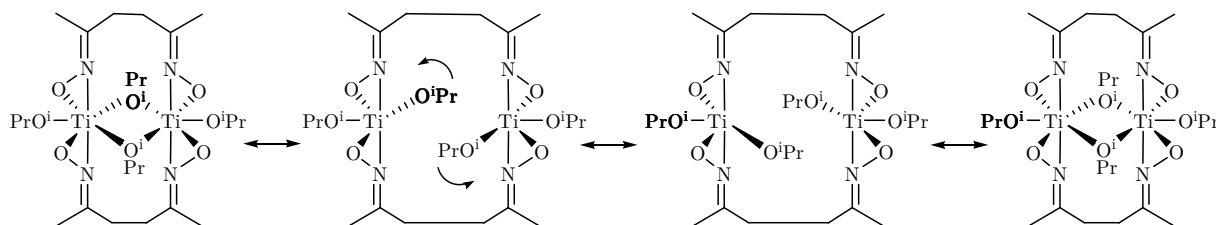


Figure 3.53: Possible exchange reaction observed in EXSY spectrum

Second, a passive exchange could occur. The bridging O<sup>i</sup>Pr groups followed the dynamics of the alkylene chain connecting the oximate groups. If the conformation of the nine-membered ring changed, the bridging O<sup>i</sup>Pr ligands would also be influenced. An exact interpretation of the EXSY spectrum was difficult, as the methylene signals were not split in the HMBC spectrum at room temperature. Two to three signals were only observed, although four signals were expected for this AB system.

Temperature depending <sup>1</sup>H NMR spectroscopy were performed between +20 and -80 °C. Herein, a broadening of the O<sup>i</sup>Pr methine resonance at 4.47 ppm was observed. At -40 °C the signal was split into two independent peaks, which became more and more separated. The CH<sub>2</sub>CH<sub>2</sub> methylene resonance at 2.12 ppm also split into two independent signals at -60 °C.



The COSY spectrum at  $-60\text{ }^{\circ}\text{C}$  (Figure 3.54) revealed eleven to twelve independent CH signals, which proved the existence of at least three different conformers at low temperature. The previously observed exchange signals disappeared in the EXSY spectrum at  $-60\text{ }^{\circ}\text{C}$  (Figure 3.55). The dynamics of both processes was therefore minimized at this temperature.

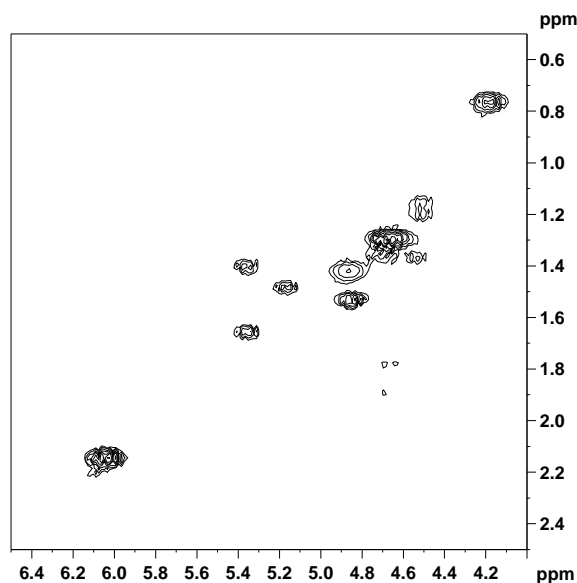


Figure 3.54: COSY spectrum of **22** at  $-60\text{ }^{\circ}\text{C}$

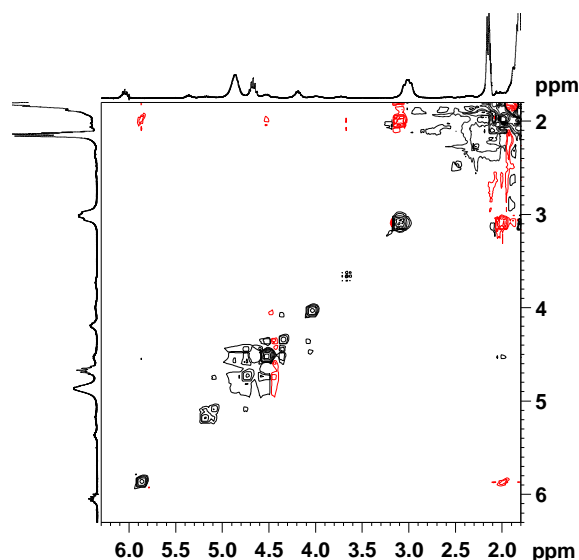


Figure 3.55: EXSY spectrum of **22** at  $-60\text{ }^{\circ}\text{C}$

The investigations were extended to  $\text{Ti}(\text{OEt})_4$ . Several crystallisation attempts with **23** remained unsuccessful. Thus, ESI-MS was performed to check whether a similar complex was formed. Mass spectrometric investigations resulted in one peak at  $m/z$  583.2 (calc. 583.2), which was assigned to the sodiated complex  $\{[\text{TiL}(\text{OEt})_2]_2\text{Na}\}^+$ . (Figure 3.56) A comparable composition was also observed for the isopropoxide derivate **22**. In complex **23**, the titanium atoms were bridged by two 2,5-hexanedione-2,5-dioximate ligands and two  $\mu_2\text{-OEt}$  ligands. Each titanium centre was coordinated to one terminal  $\mu_2\text{-OEt}$  ligand.

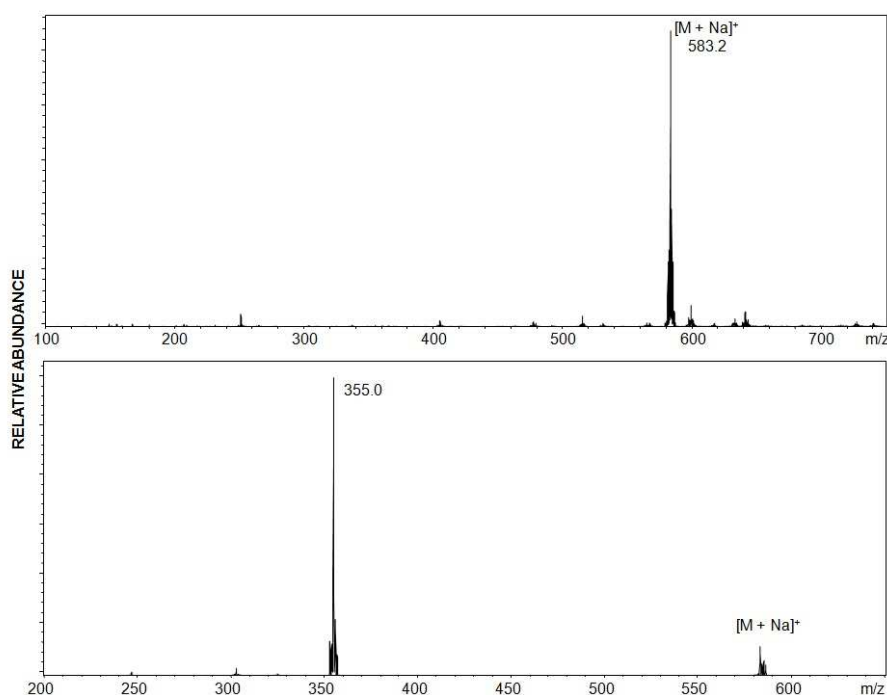


Figure 3.56: Positive ion ESI mass spectrum and low energy CID MS/MS spectrum of  $[\text{TiL}(\text{OEt})_2]_2$  (**23**)

Moreover, low energy CID MS/MS investigations were conducted with compound **23**. Similar to compound **21**, only one product ion of type  $[\text{TiL}_2\text{Na}]^+$  was obtained at  $m/z$  355.0 (calc. 355.1) in the corresponding MS/MS spectrum. Each titanium atom was thus coordinated by two dioximates. This fragmentation was typical for dimeric alkoxo-bridged titanium complexes. The low energy CID MS/MS investigations proved the strong coordination of the dioximate groups, as only  $\text{Ti}(\text{O}^i\text{Pr})_4$  was cleaved during the fragmentation.

Furthermore, NMR investigations confirmed the significant shift of the  $\text{C}=\text{N}$  resonance from 155.3 to 146.0 ppm upon coordination. This was additional evidence for the coordination of the dioximates. The spectrum showed two  $\text{CH}_2\text{CH}_2$  methylene signals at 2.57 and 2.77 ppm, which fitted well with the low symmetry of the complex. The  $^1\text{H}$  and  $^{13}\text{C}$  NMR spectra showed two sets of OEt methylene resonances at 4.35/71.0 and 3.91/70.1 ppm, which were in line with terminal and bridging OEt groups.

Additionally, ESI mass spectrometry and NMR spectroscopy proved that compound **23** was of same structure as observed for **21** and **22**.

### 3.11 Modification of titanium alkoxides with cyclic-linked dioximes

Structural features, comparable to the ones observed in compound **21**, **22** and **23**, are only possible if the linker between both coordinating functionalities was flexible enough to form an alkoxo bridged dimeric  $\text{Ti}_2(\text{O}^i\text{Pr})_4$  unit. The formation of a large ring, as observed in compound **22** (Figure 3.49), was only possible due to the flexible  $\text{CH}_2\text{CH}_2\text{CH}_2$  chain. The longer the chain, the less was the steric strain in the complex. Moreover, it should be possible to avoid these structural

motives by using ligands with stiffer linkers. Cycloalkylene and arylene based linkers should be less flexible linkers between both oxime groups.

### 3.11.1 Modification of titanium alkoxides with cyclohexylene-linked dioxime

Reactions of various metal alkoxides with cyclohexylene-linked dioximes were performed. Reactions of 1,4-cyclohexanedione-1,4-dioxime and 1,3-cyclohexanedione-1,3-dioxime with  $\text{Ti}(\text{OEt})_4$  in different solvents resulted in the hardly soluble compounds **24** and **25**. (Figure 3.57) Both compounds were only soluble in ethanol. If  $\text{Ti}(\text{O}^i\text{Pr})_4$  or  $\text{Ti}(\text{OBu})_4$  were used, similar behaviour was observed. The complexes were only soluble in the corresponding alcohols. Crystallisation experiments with both compounds failed.

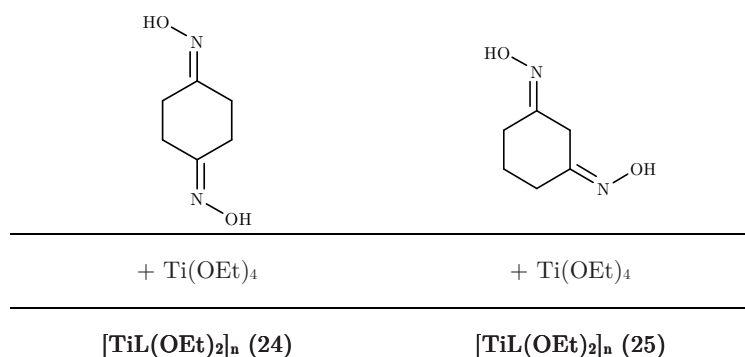


Figure 3.57: Cyclohexylene-bridged dioximes used in this work and the resulting titanium compounds

IR spectroscopy showed a slight shift of the  $\text{C}=\text{N}$  stretching frequency from 1661/1658 to 1652/1640  $\text{cm}^{-1}$  upon reaction. An additional band for the  $\text{C}-\text{O}-\text{Ti}$  stretching frequency appeared. This was in line with previous investigations on oximate-substituted group(IV) metal alkoxo complexes.<sup>47</sup> Additional evidence for the coordination was given by solid state CP-MAS NMR experiments of compound **25**. Herein, the  $\text{C}=\text{N}$  resonance was shifted from 157.8 to 143.0 ppm in the  $^{13}\text{C}$  NMR spectrum. Similar shifts of the  $\text{C}=\text{N}$  peak were also observed in the corresponding NMR spectra of compounds **21** - **23**. The resonance at 143.0 ppm was an explicit proof of the coordination of 1,3-cyclohexanedione-1,3-dioximate. Additional  $^{15}\text{N}$  CP-MAS NMR experiments showed a slightly shifted  $\text{C}=\text{N}-\text{O}$  resonance at 274 ppm. The  $^{15}\text{N}$  NMR shift was in line with CP-MAS NMR investigations of  $\text{Ti}(\text{p-anisalaldoximate})_4$ .<sup>44</sup> The  $^{13}\text{C}$  NMR spectrum also showed one set of OEt resonances at 68.7 and 16.5 ppm.

A lot of effort was done to determine the molecular composition of **24** and **25** by mass spectrometry. ESI- and MALDI-mass spectrometry were used for the determination of the composition, but both techniques failed in the detection of reasonable fragments of both compounds. A variation of the used titanium alkoxide also did not result in more reasonable fragments. However, resonances of pure  $\text{Ti}(\text{OEt})_4$  and 1,3-cyclohexanedione-1,3-dioxime were detected in MALDI-MS. A possible explanation was that the compounds did not dissolve in ethanol but were degraded instead.

The very low solubility of **24** and **25** indicated a polymeric structure. Figure 3.58 shows the differential scanning calorimetry (DSC) curve of compound **25**. The first segment, which was measured with increasing temperature, showed an abrupt decrease of energy at around 80°C. This was attributed to a glass transition. The repetition of the heating segment showed a more intensive decrease and thus proved the reversibility of the process. The glass transition is typical of non-crystalline polymeric arrangement and additionally supported the assumed structure.

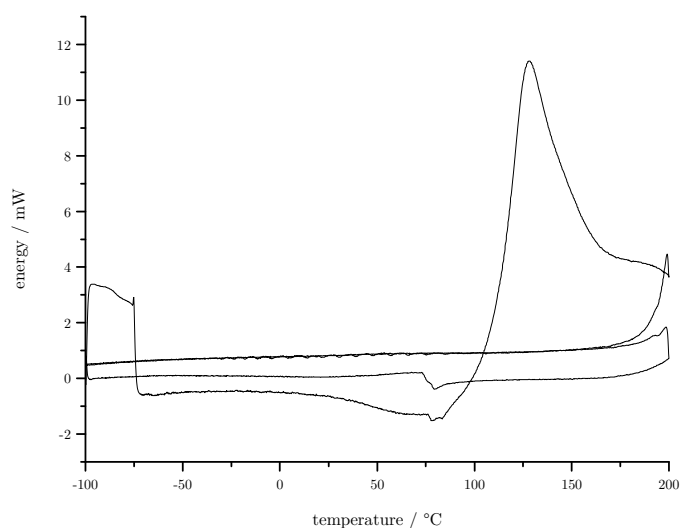


Figure 3.58: DSC curve of compound **25**

No glass transition was observed for **24** and therefore an equilibrium between oligomeric and polymeric structures had to be considered. Polymeric titanium dioximates had been assumed first by Carraher *et al.* They reacted  $\text{TiCl}_2\text{Cp}_2$  with several dioximes (e.g. 1,4-cyclohexanedione-1,4-dioxime) and observed precipitates of a hardly soluble product. Molecular weight determination had resulted in molecular masses up to 8000 g/mol.<sup>84</sup> Afterwards Thewalt *et al.* had isolated single crystals of the corresponding titanium complex and reported a dimeric structure with only one bridging 1,4-cyclohexanedione-1,4-dioximate.<sup>85</sup>

Dimeric complexes can be excluded in the case of **24** and **25**. Three types of polymeric structures were considered for both compounds. (Figure 3.59) Coordination polymers with similar structural features were observed in  $\text{Ti}_4(\text{O}^i\text{Pr})_8\text{L}_4$  ( $\text{L} = 2,4\text{-pentanedioximate}$ ). Both titanium atoms were bridged by two alkoxo groups and one dioximate ligand there. Additional dioximate ligands interconnected the dimeric titanium alkoxo moieties. Comparable structural motives are present in type A.

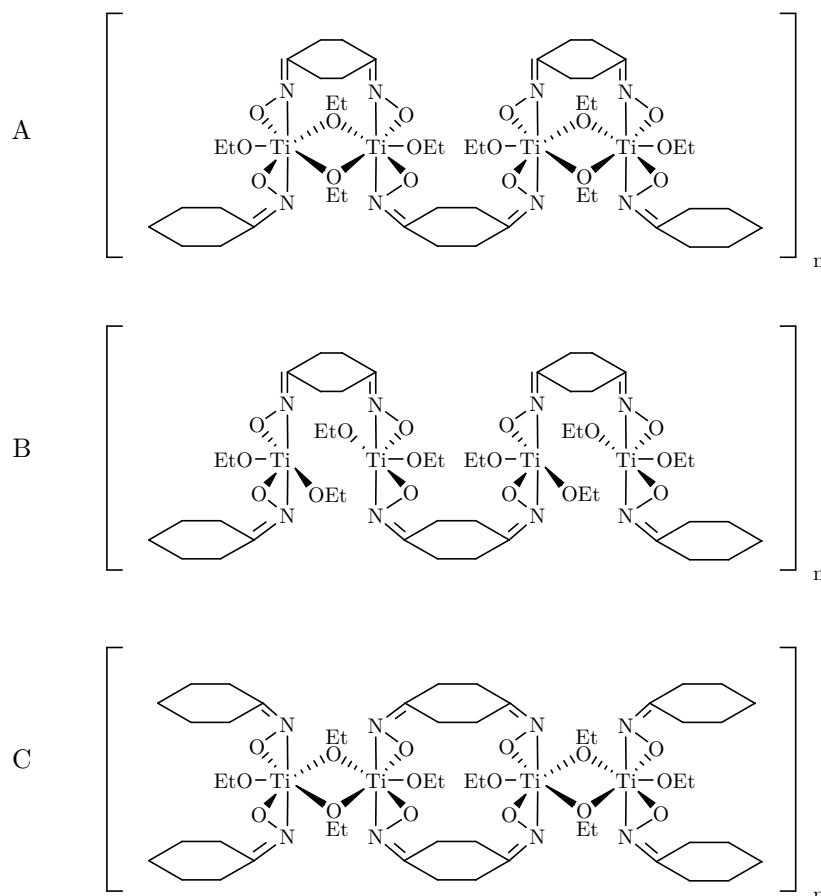


Figure 3.59: Possible structures of polymeric **24**

Experiments were extended to reactions with  $\text{TiCl}_4$  and both dioximes. The reactions were performed with  $\text{TiCl}_4$  or  $\text{TiCl}_4(\text{THF})_2$  adduct. In each case, a hardly soluble product was obtained. Also the use of triethylamine for binding the  $\text{HCl}$  remained unsuccessful.

### 3.11.2 Modification of titanium alkoxides with arylene-linked dioximes

Investigations of titanium alkoxo complexes with cyclohexylene-linked dioximates were limited by the solubility of the compounds. An alternative was the use of arylene-linked dioximes. Thus, experiments with isophthaldialdehyde-1,3-dioxime and terephthaldialdehyde-1,4-dioxime were performed. Reactions with both dioximes and  $\text{Ti}(\text{OEt})_4$  in several solvents resulted in hardly soluble precipitates of **26** and **27**. (Figure 3.60)

Both complexes were only soluble in the corresponding alcohol. Therefore, solution NMR was not possible.

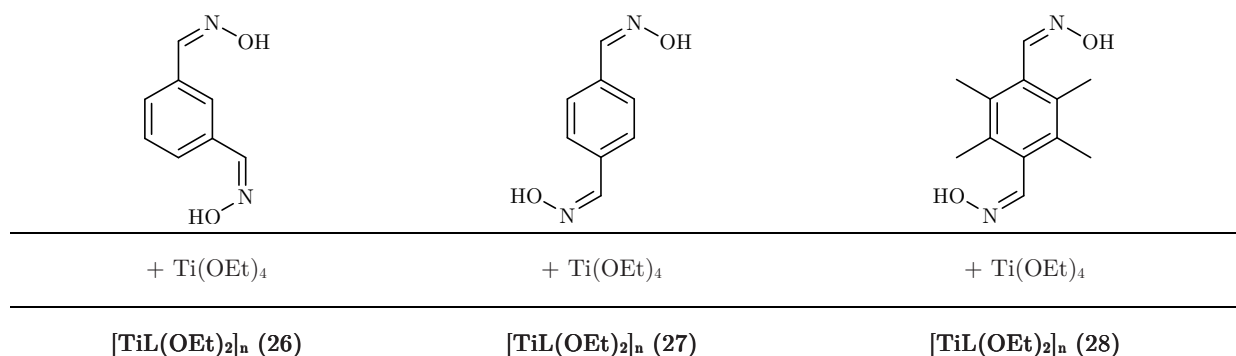
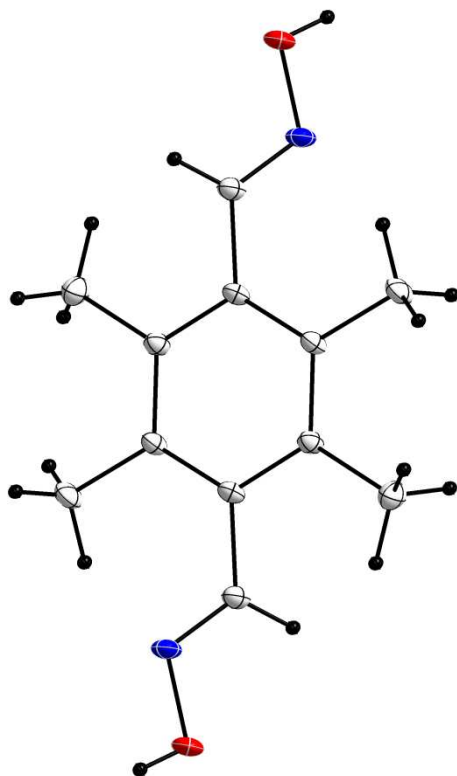


Figure 3.60: Arylene-bridged dioximes used in this work and the resulting titanium compounds

IR spectra of both compounds showed the C-O-Ti stretching frequency at 1376 cm<sup>-1</sup>. Several ESI mass spectra were recorded, which showed no reasonable fragmentation ions. Heating the reaction solution at higher temperature and using other solvents did not change the obtained mass spectra. DSC measurements did not provide any hint for a glass transition. However, oligomeric or polymeric assemblies should not be excluded.

The experiments were extended to reactions with TiCl<sub>4</sub>, which was allowed to react with arylene-linked dioximes or the corresponding sodium or lithium salt. This way was chosen to get more controllability of the reaction, but no remarkable difference of the precipitates obtained was observed.

A further attempt was the use of substituted arylene-linkers. Therefore, 2,3,5,6-tetramethylterephthaldialdehyhde-1,4-dioxime was synthesised and reacted with Ti(OEt)<sub>4</sub>. (Figure 3.60) The thus obtained compound **28** was soluble in large proportions of ethanol over weeks, while it precipitated in other common solvents. Crystallisation experiments from ethanol yielded colourless, prismatic crystals, which were investigated by single crystal XRD. The compound crystallised in a triclinic space group  $P\bar{1}$ . Structure refinement resulted in the uncoordinated ligand 2,3,5,6-tetramethylterephthaldialdehyhde-1,4-dioxime, crystal structure of which was unknown. (Figure 3.61)



**Figure 3.61: Molecular structure of 2,3,5,6-tetramethylterephthaldialdehyde-1,4-dioxime**

The experiments were repeated several times, and each attempt yielded the same crystals. It was assumed that the ligand crystallises much better than the obtained complex. DSC measurements of compounds **28** resulted in curves, which showed no glass transition.

Solubility of the compounds was the main problem in structure determination of these compounds. Therefore, other dioximes with non-polar substituents were synthesised to fall the compounds' polarity and raise the solubility of the corresponding complexes in common organic solvents. A short selection is presented in Figure 3.62.

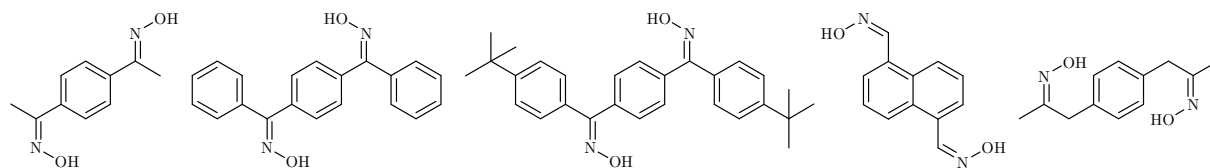


**Figure 3.62: Selection of other dioximes synthesised**

All dioximes were tested in reactions with different titanium alkoxides. All reaction products were of poor solubility. Only the titanium isopropoxo complex of 1,1'-(1,4-phenylene)dipropen-2-on-dioxime was slightly more soluble. An oligomeric or polymeric structure was assumed for all synthesised complexes.

### 3.12 Modification of titanium ethoxide with 1,4-bis-[(2-hydroxy-ethylimino)-methyl]-benzene

The idea of difunctional ligands was extended to tetradentate Schiff bases. Therefore, two simple tetradentate Schiff bases were synthesised by condensation of 2-amino ethanol and isophthal-/terephthaldialdehyde. The resulting 1,4-bis-[(2-hydroxy-ethylimino)-methyl]-benzene was resulted in coordination polymers with  $\text{AgClO}_4$  or  $\text{AgNO}_3$ .<sup>146</sup> The tetradentate Schiff base was allowed to react with titanium alkoxides. Reactions with  $\text{Ti}(\text{O}^i\text{Pr})_4$  in common organic solvents resulted in an insoluble precipitate. Experiments with  $\text{Ti}(\text{OEt})_4$  resulted in the soluble product **29**, which was tried to crystallise from ethanol. First crystals were formed after a week. The compound crystallised in the monoclinic space group  $P2_1/c$ . Structural refinement resulted in the molecular structure of 1,4-bis-[(2-hydroxy-ethylimino)-methyl]-benzene. (Figure 3.63) Comparable to the experiments with compound **28**, the ligand seemed to crystallise much better than the formed complex.

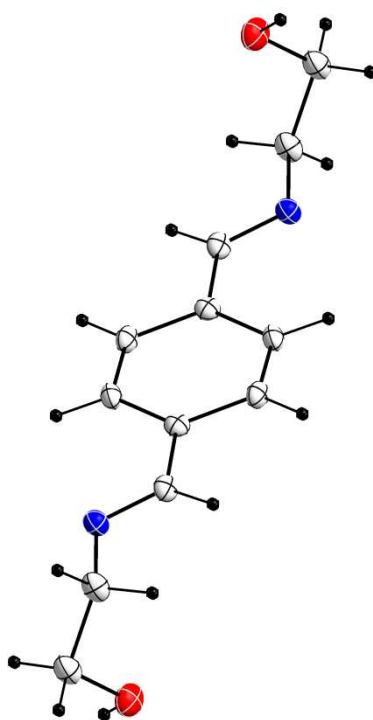


Figure 3.63: Molecular structure of 1,4-bis-[(2-hydroxy-ethylimino)-methyl]-benzene

Due to the bad solubility, ESI-MS experiments remained unsuccessfully with all titanium alkoxides used. Different solvents and varying analysis conditions resulted in mass spectra without any reasonable product ions. Only  $^{13}\text{C}$  NMR experiments were possible for compound **29**. The spectrum showed a slightly shifted  $\text{C}=\text{N}$  resonance at 161.7 ppm. Furthermore, only one set of OEt signals at 70.0 and 19.0 ppm was observed in the NMR experiments.

The metallacyclic assumed structure is presented in Figure 3.64. A possible monomeric complex should be excluded due to the very rigid linker.



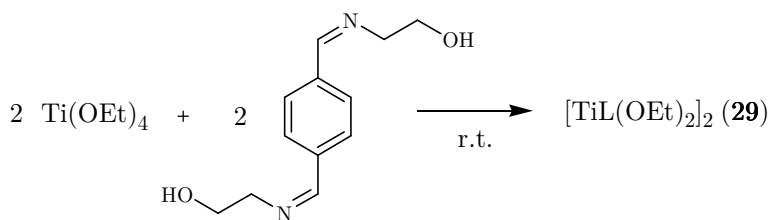


Figure 3.64: Synthesis and proposed structure of compound 29

Herein, two tetradentate Schiff bases bridge two  $\text{Ti}(\text{OEt})_2$  moieties. The alkoxo groups were only in terminal positions. The observations of only one set of OEt resonances in the  $^{13}\text{C}$  NMR spectrum fitted well with the postulated structure.

### 3.13 Modification of titanium alkoxides with bis(salicylaldiminate)-ligands

Bis(salicylaldiminate) ligands were synthesised by condensation of salicylaldehyde and diamines. An overview of the synthesised bis(salicylaldiminate)-ligands and the resulting complexes is presented in Figure 3.65.

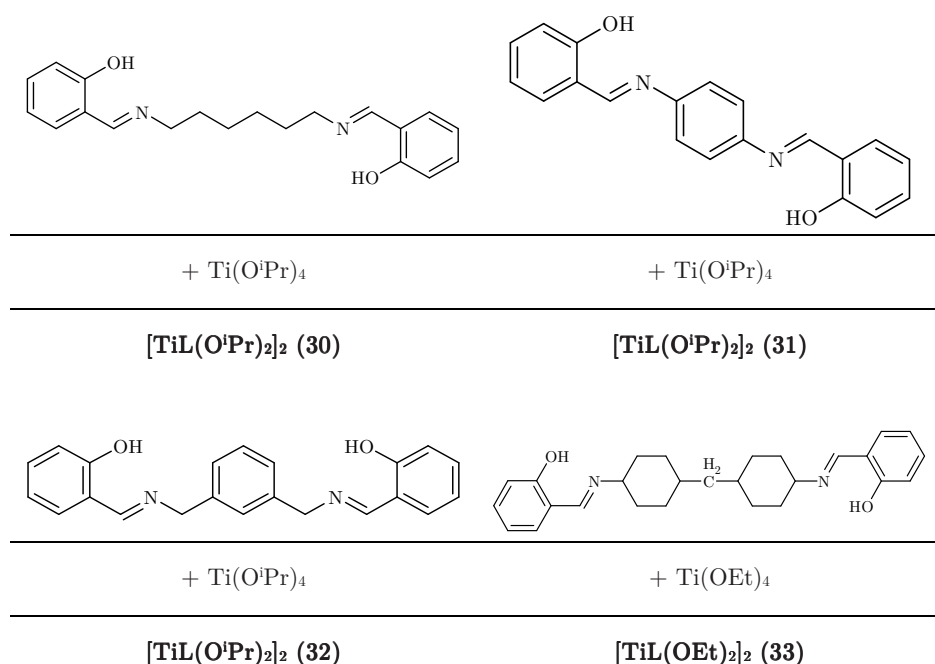


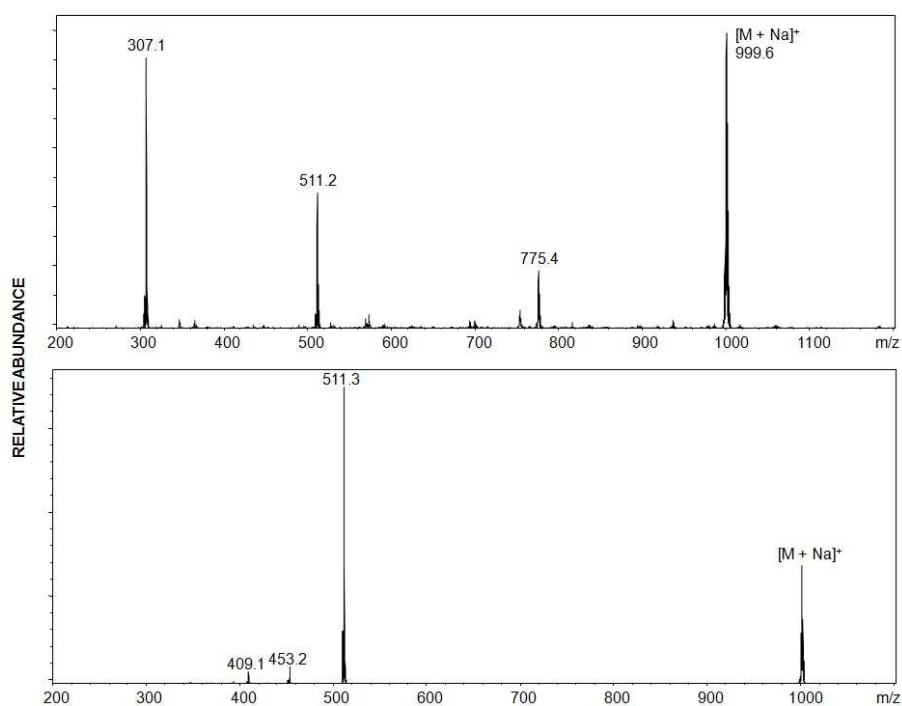
Figure 3.65: Bis(salicylaldiminate)-ligands used in this work and the resulting titanium complexes

Several titanium complexes with tetradentate Schiff bases had been reported. All reported complexes  $\text{TiCl}_2(\text{bis}(\text{salicylideneamino})\text{alkylene})$ ,  $\text{TiCl}_2(\text{bis}(\text{salicylideneamino})\text{arylene})$  and  $\text{Ti}(\text{OArMe}_2)_2[1,4\text{-bis}(\text{salicylideneamino})\text{arylene}]$  showed a monomeric character.<sup>100,101,107</sup> Complexes with late transition metals resulted mostly in complexes of type  $[\text{ML}]_2$ , *e.g.*  $\{\text{Cu}[1,4\text{-bis}(\text{salicylideneamino})\text{p-xylene}]\}_2$ ,  $\{\text{Pd}[1,4\text{-bis}(\text{salicylideneamino})\text{m-phenylene}]\}_2$  and  $\{\text{Pt}[1,4\text{-bis}(\text{salicylideneamino})\text{alkylene}]\}_2$ , which showed a dimeric structure.<sup>92,93</sup> (see Chapter 1.3.3)

When long and flexible linkers were used, a polymeric structure was assumed for  $\{\text{Ni}[1,4\text{-bis(salicylideneamino)alkylene}]\}_n$ .<sup>96</sup> Therefore, this polymeric structure should be transferred to group (IV) metal alkoxides, for which comparable polymers should be obtained.

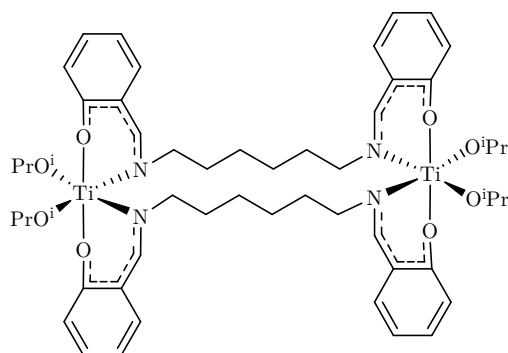
A few bis(salicylaldiminate) ligands were tested in the reaction with  $\text{Ti}(\text{O}^i\text{Pr})_4$  or  $\text{Ti}(\text{OEt})_4$ . All complexes **30-33** were isolated as yellow solids. Crystallisation experiments were conducted unsuccessfully in all cases. ESI mass spectrometry was again the method of choice for the determination of the composition. Mass spectra could only be recorded of compound **30** and **32**. (Figure 3.66) A sodiated complex was obtained for compound **30**, which corresponded to  $[\text{TiL}(\text{O}^i\text{Pr})_2]_2\text{Na}^+$ . The same composition was previously detected for titanium alkoxo complexes of dioximates or bis( $\beta$ -diketonates). The composition corresponded to a dimeric structure with two bridging bis(salicylaldiminate) ligands.

The peak appeared at  $m/z$  775.4 (calc. 775.3) was attributed to  $\{[(\text{TiL}_2)^i\text{PrOH}]\}\text{Na}^+$ , the sodiated monomeric titanium complex with two coordinated bis(salicylaldiminate) ligands. As this signal did not appear in the low energy CID MS/MS spectrum it was no fragmentation product, but instead a by-product of the reaction. Furthermore, low energy CID MS/MS experiments were conducted to answer the question, whether the  $\text{O}^i\text{Pr}$  groups were only terminal or also bridging.

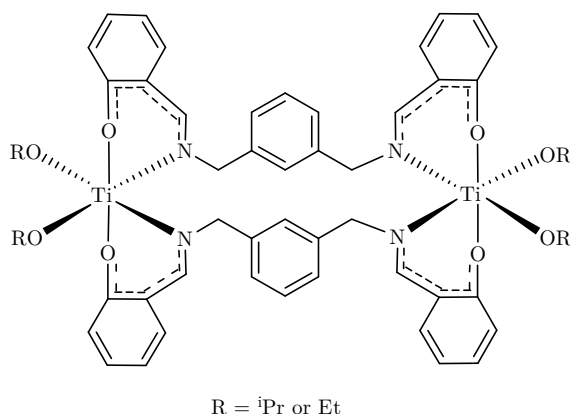


**Figure 3.66: Positive ion ESI mass spectrum and low energy CID MS/MS spectrum of 30**

Fragmentation of **30** only resulted in one product ion, which was detected at  $m/z$  511.3 (calc. 511.2). This peak was attributed to  $[\text{TiL}(\text{O}^i\text{Pr})_2\text{Na}]^+$ . Similar product ions were also obtained for titanium alkoxo bis( $\beta$ -diketonates). These product ions were typical for complexes, in which both  $\text{O}^i\text{Pr}$  groups were in terminal position. Thus, a metallacyclic structure was postulated that is shown in Figure 3.67.

Figure 3.67: Postulated molecular structure of **30**

Comparable results were also achieved from mass spectrometric investigations of **32**. The sodiated complex was observed at  $m/z$  1039.3 (calc. 1039.4), which corresponded to  $\{[\text{TiL}(\text{O}^i\text{Pr})_2]_2\text{Na}\}^+$ . The second peak observed at  $m/z$  957.3 (calc. 957.3) was assigned to  $\text{TiL}(\text{O}^i\text{Pr})_2(\text{O}^i\text{Pr})^+$ , which was only caused by a different mode of ionization. No signals of monomeric side products of type  $\text{TiL}_2$  were observed. Low energy CID MS/MS experiments resulted in the same fragmentation pathway, resulting in one product ion of type  $[\text{TiL}(\text{O}^i\text{Pr})_2\text{Na}]^+$ . Thus, the same structure was assumed for **32**. (Figure 3.68)

Figure 3.68: Suggested structure of **32**

Experiments were extended to reactions with  $\text{Ti}(\text{OEt})_4$ . To this end, 1,3-bis(salicylideneamino)-xylene was reacted with  $\text{Ti}(\text{OEt})_4$  to check, whether variation of the alkoxo groups influenced the metallacyclic structure. The corresponding mass spectrum resulted in a sodiated molecule at  $m/z$  983.4, which was of same composition as observed for the titanium isopropoxo complexes. The fragmentation behaviour was also comparable to the one observed in compounds **30** and **32**. Low energy CID MS/MS of the precursor ion  $\{[\text{TiL}(\text{OEt})_2]_2\text{Na}\}^+$  (Figure 3.69) resulted in two product ions at  $m/z$  503.2 (calc. 503.1) corresponding to  $[\text{TiL}(\text{OEt})_2\text{Na}]^+$  and  $m/z$  755.3 (calc. 755.2) corresponding to  $[\text{TiL}_2\text{Na}]^+$ . Thus, metallacycles were also obtained with  $\text{Ti}(\text{OEt})_4$ , and the metallacyclic structure was independent of the alkoxo groups used. Additional experiments with varying  $\text{Ti}(\text{OR})_4$ : bis(salicylaldiminate) ratio resulted in the same structures.

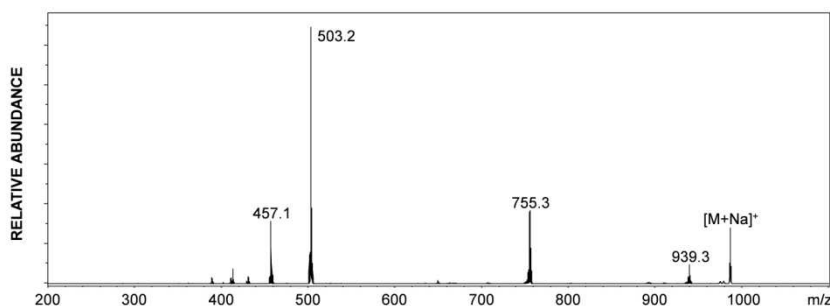
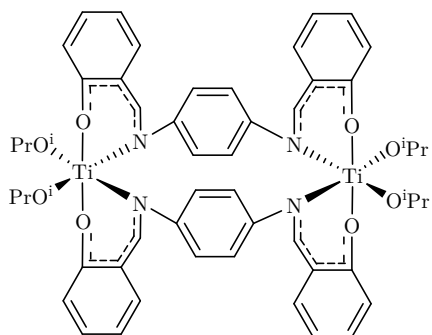
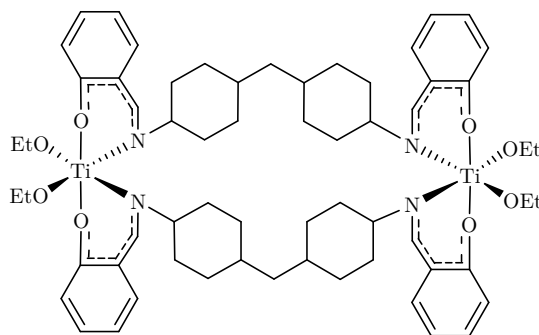


Figure 3.69 Positive ion low energy CID MS/MS spectrum of  $\text{Ti}(1,3\text{-bis(salicylideneamino)-xylene})(\text{OEt})_2$

The used linker did not influence the structural features. Flexible (in **30**) and more rigid linkers (in **32**) resulted in the same metallacyclic structure. Only the solubility was affected by the used linker.

In contrary to previous investigations of Hoyt *et al.* with  $\{\text{Ni}[1,4\text{-bis(salicylideneamino)alkylene}]\}_n$ , a dimeric assembly was formed instead of a polymeric structure.<sup>96</sup> When difunctional ligands were used for modification of metal ions, the possible equilibrium between dimeric and polymeric products had always to be considered. The dimeric species seemed to be the thermodynamically most stable product. Experiments at lower temperature were performed to check, whether a possible kinetic product could be isolated in form of an oligomeric or polymeric assembly. But ESI-MS measurements resulted in the same constitution in each experiment.

Solution structure elucidation of compounds **30-33** was done by NMR experiments. All  $^1\text{H}$  NMR spectra showed a clear shift of the  $\text{CH}=\text{N}$  resonance from 8.33-9.01 ppm to 7.70-8.03 ppm upon reaction. This shift was in line with previous investigations of  $\{\text{Pt}[\text{alkylene-linked bis(salicylaldiminate)}]\}_2$  complexes.<sup>92</sup> Furthermore, a comparable shift was also observed in the  $^{13}\text{C}$  NMR spectra, where the  $\text{C}_{\text{aryl}}\text{-O}$  and  $\text{C}=\text{N}$  resonance differences became smaller, and the chemical shift were observed in the range between 161.9 and 168.4 ppm. In most cases, two sets of  $\text{OEt}/\text{O}^i\text{Pr}$  resonances were observed in the corresponding  $^{13}\text{C}$  NMR spectra. It was assumed that the second  $\text{O}^i\text{Pr}$  resonance was caused by free  $\text{Ti}(\text{O}^i\text{Pr})_4$ , which was also detected in the ESI-MS full scan at  $m/z$  307.1 (calc. 307.1), and which remained unsubstituted in the solution. Especially NMR data of compound **30** matched perfectly with the observation of  $\{\text{Pt}[\text{bis(salicylaldiminate)}]\}_2$ .<sup>92</sup> NMR experiments showed no difference in the spectra of compounds **30-33**. Therefore, a similar metallacyclic structure was assumed also for compounds **31** and **33**. (Figure 3.70 and Figure 3.71)

Figure 3.70: Suggested structure of **31**Figure 3.71: Suggested structure of **33**

However, NMR experiments gave no evidence of the stereochemistry of the complexes. According to DFT calculations with titanium alkoxo bis(*β*-diketonates) (see Chapter 3.1.2), a *cis/cis* arrangement of the O<sup>*i*</sup>Pr groups should be favoured. NMR investigations were also not sufficient to prove which isomer (*trans-syn* or *trans-anti*) was formed.

### 3.14 Modification of zirconium isopropoxide with bis(salicylaldiminate) ligands

Experiments with  $\text{Zr}(\text{O}^i\text{Pr})_4 \cdot i\text{PrOH}$  should prove, whether similar metallacycles were also observed for zirconium.

Three bis(salicylaldiminate) ligands were chosen to modify  $\text{Zr}(\text{O}^i\text{Pr})_4 \cdot i\text{PrOH}$ . The selected ligands and their complexes were shown in Figure 3.72.

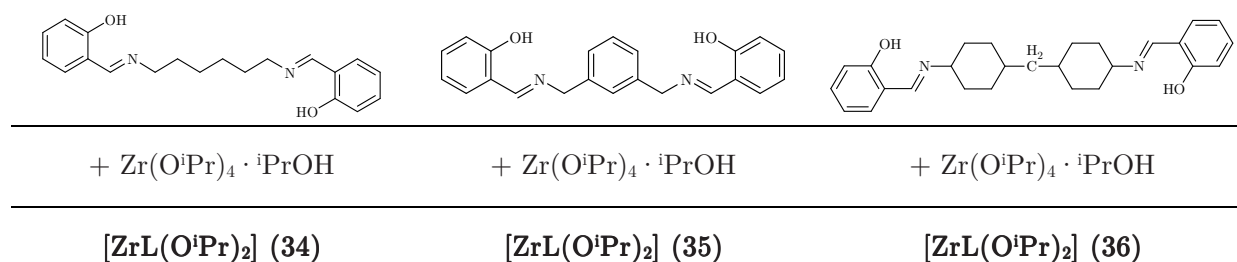


Figure 3.72: Bis(salicylaldiminate) ligands used in this work and the resulting zirconium compounds

Reaction of bis(salicylaldiminate) ligands with  $\text{Zr}(\text{O}^i\text{Pr})_4 \cdot i\text{PrOH}$  resulted in yellow to orange coloured solids. Crystallisation experiments with different solvents/solvent mixtures failed. Thus, the composition of compounds **34** and **35** were determined by ESI mass spectrometry.

Zirconium compound **34** was detected as the chlorinated complex at  $m/z$  1095.3 (calc. 1095.3), which was attributed to  $\{[\text{ZrL}(\text{O}^i\text{Pr})_2]_2\text{Cl}\}^-$ . Furthermore, the positive ion ESI mass spectrum resulted in one peak at  $m/z$  1083.4 (calc. 1083.3), which was assigned to the sodiated complex  $\{[\text{ZrL}(\text{O}^i\text{Pr})_2]_2\text{Na}\}^+$ . The detection of negatively charged group (IV) metal alkoxo complexes was never observed before with other zirconium complexes. From both ions, the same complex  $[\text{ZrL}(\text{O}^i\text{Pr})_2]_2$  was derived. This was in good agreement with ESI-MS experiments of comparable

titanium complexes. In complex **34**, the  $\text{Zr}(\text{O}^i\text{Pr})_2$  moieties were bridged by two bis(salicylaldimate) ligands. The positioning of the  $\text{O}^i\text{Pr}$  groups should be checked by low energy CID MS/MS scans. (Figure 3.73) The positive ion low energy CID MS/MS investigations resulted in one product ion at  $m/z$  553.3 (calc. 553.2), which was assigned to  $[\text{ZrL}(\text{O}^i\text{Pr})_2\text{Na}]^+$ . This fragmentation pathway was well known for metallacycles with only terminal alkoxo groups. The schematic structure of **34** is shown in Figure 3.75.

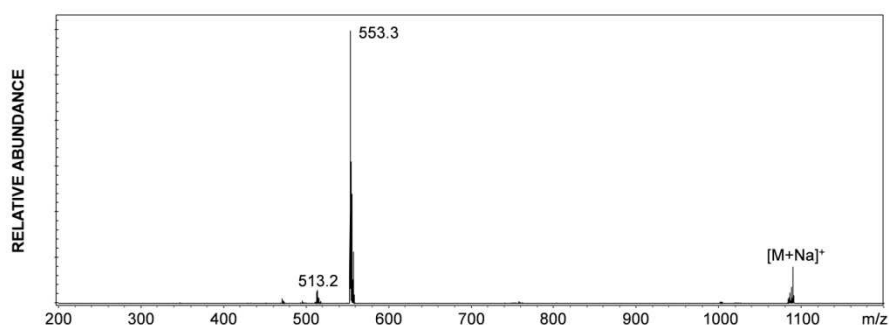


Figure 3.73: Positive ion low energy CID MS/MS spectrum of **34**

ESI-MS experiments of compound **35** (Figure 3.74) resulted in only the chlorinated complex at  $m/z$  1135.2 (calc. 1135.2), which corresponded to the composition  $\{[\text{ZrL}(\text{O}^i\text{Pr})_2]_2\text{Cl}\}^-$ . In contrary to **34**, no positively charged molecule was detected. Similar structural features were derived from this composition. Low energy CID MS/MS investigations resulted in a comparable fragmentation pathway.

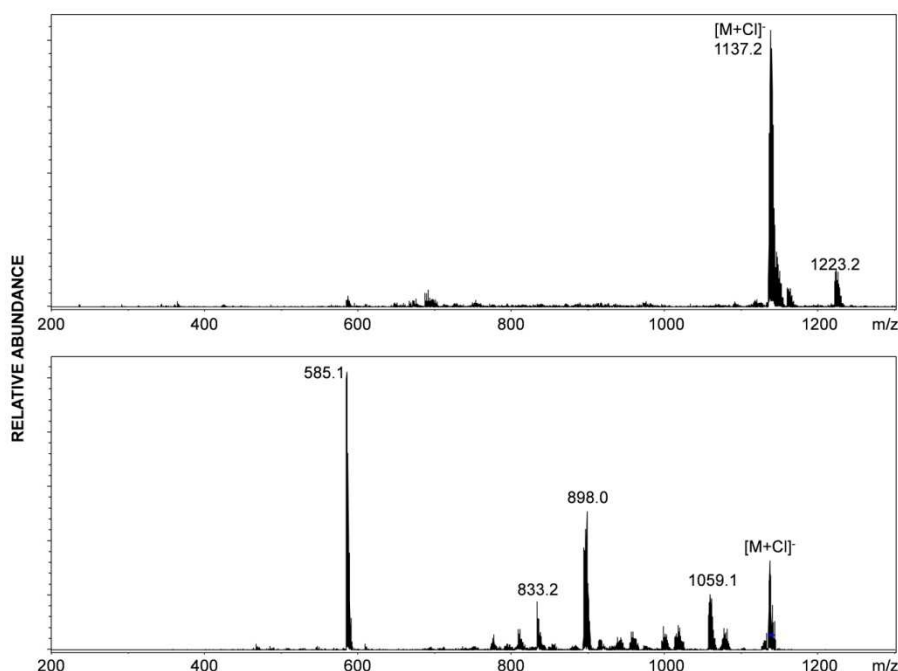


Figure 3.74: Negative ion mass and low energy CID MS/MS spectrum of **35**

Thus, a similar molecular structure was assumed, which is shown in Figure 3.76.

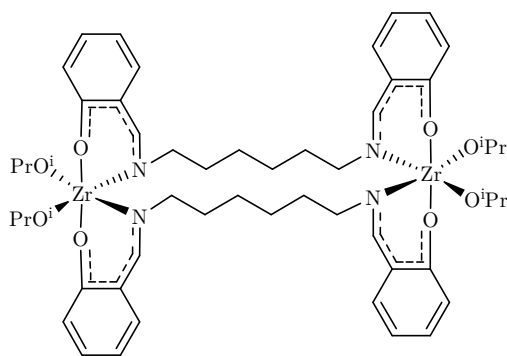


Figure 3.75: Proposed structure of **34**

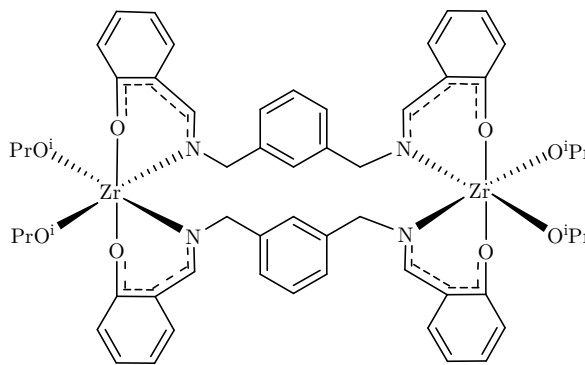


Figure 3.76: Proposed structure of **35**

The obtained metallacyclic structure was similar to the ones observed in zirconium bis( $\beta$ -ketoesterates) (see Chapter 3.5). In contrary to zirconium bis( $\beta$ -diketonate) complexes, no additional 2-propanol was coordinated to the  $\text{Zr}(\text{O}^i\text{Pr})_2$  moieties. No products, in which more than two tetradentate ligands bridge both zirconium centres, were observed in the mass spectrometric investigations. Similar to complexes **15** – **17**, the high steric hindrance of the linkers blocked a third or fourth bridging ligand. Furthermore, the structural feature of the two  $\text{Zr}(\text{O}^i\text{Pr})_2(\text{Schiff base})_2$  moieties was in good agreement with previous observations of zirconium Schiff base complexes.<sup>147</sup>

Solution structure elucidation of **34–36** was done by NMR experiments.  $^1\text{H}$  NMR spectra showed a significant shift of the  $\text{CH}=\text{N}$  resonance from 8.33–8.46 to 7.76–8.08 ppm upon reaction. Small high field shifts were also observed for  $\text{NCH}_2$  peak, while the  $\text{NCH}$  resonance was low field shifted from 3.17 to 4.14 ppm in compound **36**.  $^{13}\text{C}$  NMR spectra showed two resonances for  $\text{C}_{\text{aryl}}\text{O}$  and  $\text{CH}=\text{N}$  between 163.1 and 168.4 ppm. The two shifted signals were caused by the coordination of the ligand. Thus, the resonances were closer to each other. The spectra of **34** and **35** only showed one set of  $\text{O}^i\text{Pr}$  signals at 71.3 ppm, whereas a second  $\text{O}^i\text{Pr}$  resonance appeared in the  $^{13}\text{C}$  NMR spectrum of **36**. This was caused by residual  $\text{Zr}(\text{O}^i\text{Pr})_4 \cdot ^i\text{PrOH}$ . Similar observations of unsubstituted metal alkoxide were made with the titanium complexes. There, the ESI-mass spectra resulted in an additional peak at  $m/z$  307.1 (calc. 307.1) for  $\text{Ti}(\text{O}^i\text{Pr})_4\text{Na}^+$ . It was assumed that the residual, unsubstituted metal alkoxide was caused by an incomplete reaction. As no differences were obtained in the NMR spectrum of **36**, the same metallacyclic structure  $[\text{ZrL}(\text{OR})_2]_2$ , as observed in **34** and **35**, was assumed.

### 3.15 Conclusions

Reactions of titanium alkoxides with difunctional, tetradentate ligands resulted in dimeric metallacyclic structures  $[\text{ML}(\text{OR})_2]_2$ . Herein, two ligands bridged both metal centres. In case of bis( $\beta$ -diketones), bis( $\beta$ -ketoesters) and bis(salicylaldiminate) ligands, the both alkoxo ligands were in terminal positions, whereas the structures with alkylene-linked dioximes showed bridging as well

as terminal alkoxo groups. The difference in the observed structural features was caused by different bite angles and the varying coordination strength of the functional groups. In each structure, the titanium alkoxide was disubstituted. The structure was proven to be independent of the used alkoxo ligands. The obtained structures were rare examples of cyclic titanium alkoxo complexes. Additional DFT calculation of both titanium alkoxo bis( $\beta$ -diketonate) isomers only showed a small difference in the Gibbs free energy between the *cis/cis* and *trans/trans* configuration. Therefore, both arrangements were likely.

However, modification of zirconium alkoxides with the difunctional ligands resulted in slightly different results. The use of ligands with bulkier linkers yielded dimeric complexes of the same composition as that of titanium alkoxides. But in case of ligands with flexible linkers, as used with bis( $\beta$ -diketones), also different structural features were possible. If the linkers got longer, higher substituted zirconium moieties with three or four bridging linkers were observed.

Reaction of a mixture of titanium and zirconium alkoxides proved that mixed metallacycles were also observed, in which the ligands bridged the  $\text{Ti(OR)}_2$  and  $\text{Zr(OR)}_2$  moieties. Unfortunately, this mixed metal complex was not formed exclusively, also the corresponding titanium metallacycle was observed in the ESI mass spectrum.

When the idea of bis( $\beta$ -diketones) was extended to triketones and tetraketones, little differences were observed. The triketone formed tetrameric units, in which one triketonate bridged two titanium atoms, whereas MS investigations of the titanium alkoxo tetraketone only showed dimeric complexes with one bridging ligand.

All difunctional ligands resulted in dimeric, cyclic complexes instead of coordinative polymers. They were thermodynamically more stable. Variation of the reaction parameters also yielded dimeric complexes. However, a polymeric structure was postulated for titanium alkoxo complexes with arylene- or cyclohexylene linked dioximates. Hereby, hardly soluble products were obtained, for which NMR spectroscopic investigations proved the coordination to the metal centres and, for some of them, DSC measurements obtained a glass transition. The low solubility prevented structure elucidation by mass spectrometry and NMR spectroscopy.



## 4 Modification of group(IV) metal alkoxides with tri- and tetrafunctional ligands

### 4.1 Modification of $\text{Ti}(\text{O}^i\text{Pr})_4$ with benzenetribenzoic acid

#### 4.1.1 Structural investigation of benzenetribenzoate-based titanium alkoxo materials

All previously discussed experiments with bifunctional ligands resulted in dimeric complexes, which were the thermodynamically most stable products. Arylene-linked dioximes were the only group of ligands, for which polymeric assemblies were proven. The cyclic oligomers are especially preferred to inorganic compounds and they were also observed for these modified group(IV) metal alkoxides. This led to the conclusion that tetradentate, difunctional ligands were not appropriate ligands to get pre-organised metal alkoxides.

Investigations of Cavka *et al.* on reactions of several dicarboxylates with zirconium tetrachloride led to MOF-like structures, which were highly ordered and porous materials.<sup>118</sup> The idea of these network-like structures was transferred to more versatile ligands with three or more functionalities. Benzenetribenzoate (BTB-3) was chosen as a rigid ligand, which should be tested on the modification of titanium isopropoxide.

In a first attempt, benzenetribenzoic acid (BTB-3) was reacted with titanium isopropoxide in different ratios. (Figure 4.1) The reactions yielded oily to solid residues  $\text{Ti\_BTB-3}$ , which were insoluble in common solvents.

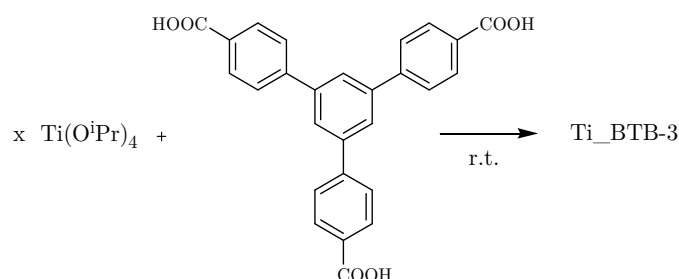


**Figure 4.1: Synthesis of  $\text{Ti\_BTB-3}$**

Therefore, solution NMR or MS investigations were not possible. IR spectroscopy proved the coordination of the tricarboxylate ligand to the titanium centre. (Figure 4.2) The asymmetric  $\text{C}=\text{O}$  stretching frequency was shifted from  $1685/1607 \text{ cm}^{-1}$  to  $1588/1548 \text{ cm}^{-1}$ . The IR spectra showed no  $\text{C}=\text{O}$  stretching frequencies of the tricarboxylic acid or of ester groups, especially for low  $\text{Ti}:\text{COOH}$  ratios. The corresponding IR spectrum is shown in Figure 4.2. The IR spectra were comparable for all applied  $\text{Ti}:\text{COOH}$  ratios. Furthermore, all spectra showed two strong bands at  $1116$  and  $990 \text{ cm}^{-1}$ , which were assigned to  $\text{O}^i\text{Pr}$  groups, and a strong intensive band at  $1404 \text{ cm}^{-1}$ , attributed to symmetric  $\text{C}=\text{O}$  stretching frequency. All spectra were in line with previous IR spectroscopic investigations of titanium oxo carboxylate clusters.<sup>148</sup>

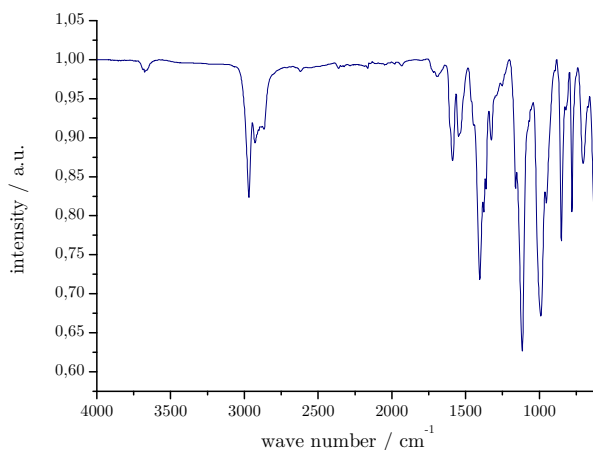


**Figure 4.2: IR spectrum of Ti\_BT B-3 with Ti:COOH=1:1**

The absence of COO ester stretching bands excluded the formation of titanium oxo clusters. Characteristic asymmetric (Ti-O-Ti)( $\mu_3$ -O) stretching bands were also absent in the IR spectra. Thus, a network-like structure was postulated, which was additionally indicated by the insolubility of the obtained products. It was assumed that monomeric or dimeric titanium building blocks were interconnected by the tricarboxylate ligands.

XPS should provide additional insights. Therefore, the dried residue was applied on an indium foil. A small area of the foil was sputtered with gold as a reference material. The resulting spectrum (Figure 4.3) showed a broad band for the O 1s bonding energy, into which two peaks were fitted. The main peak at 530.22 eV was assigned to a Ti-O<sup>i</sup>Pr/TiO<sub>2</sub> bond, whereas the significant smaller peak at 531.22 eV was derived from a Ti-OOC/C=O bond. Both peaks were in good agreement with previous investigations of different carboxylate-based/titania materials.<sup>149-151</sup> Therefore, the XPS spectrum also proved the coordination of the used ligand used. The C 1s signal at 284.3 eV and the Ti 2p<sub>3/2</sub> resonance at 458.8 eV were symmetric signals. The best match was achieved with one fitted peak. The Ti 2p<sub>3/2</sub> and C 1s peaks were in good agreement with previous investigations of carboxylate based titania materials.<sup>150,151</sup> The single Ti 2p<sub>3/2</sub> signal did not provide hints whether different kinds of titanium species were present in the Ti\_BT B-3 material.

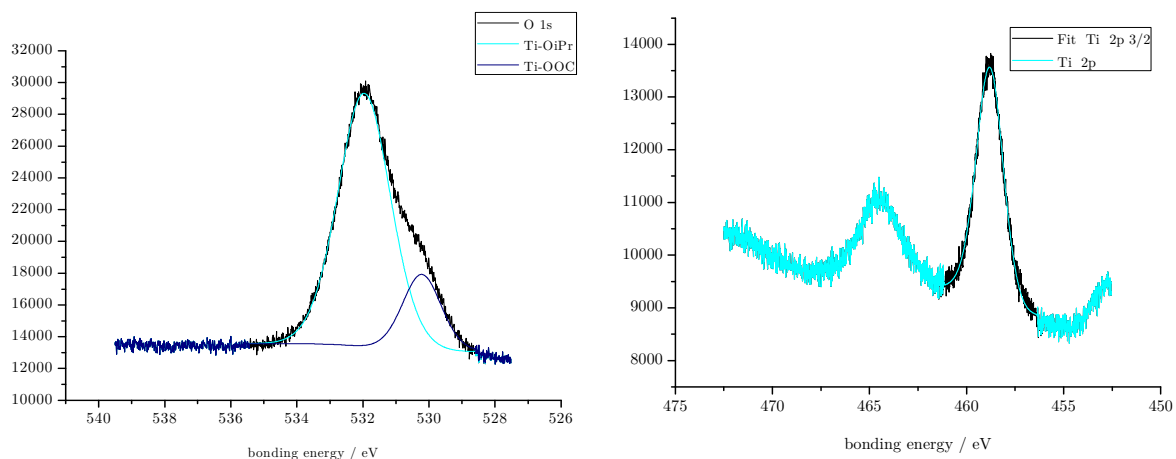


**Figure 4.3: O 1s (left) and Ti 2p (right) XPS spectra of Ti\_BT B-3 and possible fits**

Nitrogen sorption measurements of Ti\_BT B-3 showed a completely non-porous material. Moreover, small angle X-Ray scattering (SAXS) investigations were conducted to get information on structural features of Ti\_BT B-3. The measurements are summarised in Figure 4.4. The SAXS patterns showed a broad scattering maximum around  $5 \text{ nm}^{-1}$  for Ti:COOH ratios up to 1:1 and one around  $7 \text{ nm}^{-1}$  for Ti:COOH ratios of 2:1 and 4:1. The shifted scattering maximum with higher Ti:COOH ratios was caused by a closer distance of the ligand molecules to each other. The higher proportions of  $\text{Zr}(\text{O}^i\text{Pr})_4$  permitted a better connection, which was missing when less metal alkoxide was used. All samples obtained from various Ti:COOH ratios showed a 3D structure, which was derived from the slope (linear part of the SAXS patterns between 0.1 and  $0.3 \text{ nm}^{-1}$ ) in the SAXS patterns scaling with  $q^{-3}$ .

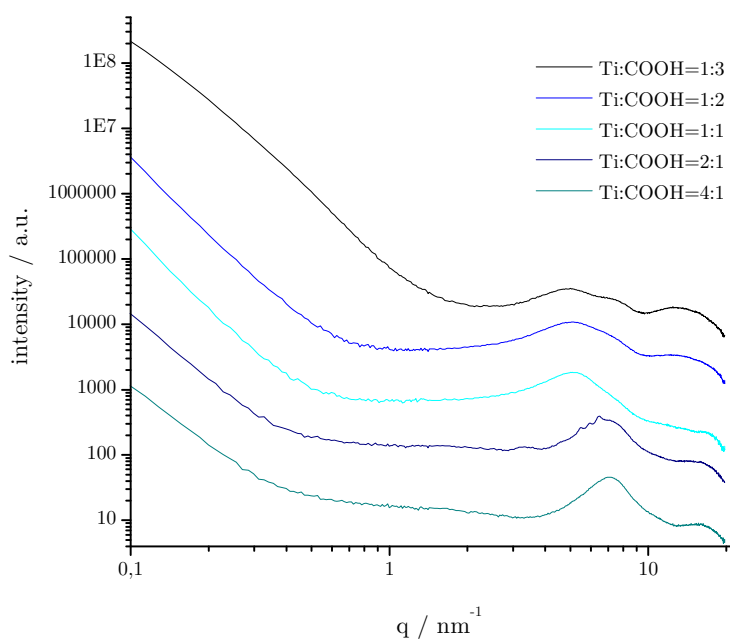


**Figure 4.4: SAXS patterns of Ti\_BT B-3 with varying Ti:COOH ratios (the SAXS patterns are plotted with an offset of 40% on the y axis)**

SAXS proved the network-like structure. It was postulated that each ligand coordinated to a dimeric titanium alkoxo moiety. The tricarboxylates interconnected these building blocks in all directions. The presence of unsubstituted alkoxo groups prevented the formation of a porous network. The postulated structure is presented in Figure 4.5.

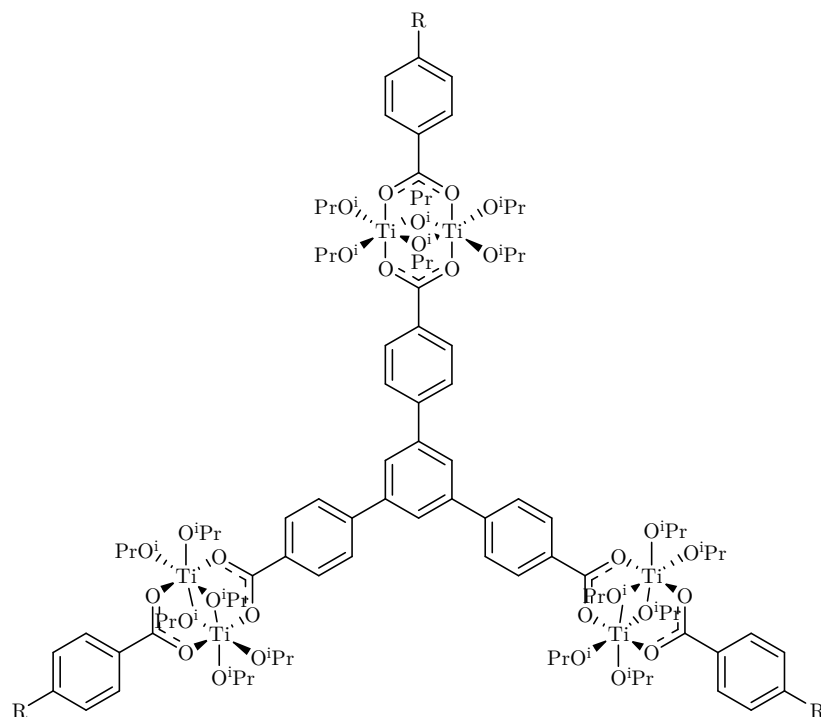


**Figure 4.5: Postulated structure of Ti\_BT B-3**

Therefore, the obtained products were tested for their properties after calcination at 500 °C in air. SAXS investigations showed the absence of the peak around 5 nm<sup>-1</sup>. The intensity fell more strongly, however a 3D structure was assumed again. Calcination of Ti\_BT B-3 had no influence on the porosity of the material, since no increased surface area was observed by the nitrogen sorption measurements.

#### 4.1.2 Structural investigation of benzenetribenzoate-based titania materials

Partial hydrolysis was chosen to get a more rigid connection between the titanium building blocks. The products were synthesised similarly, as described in Chapter 4.1.1. After addition of Ti(O<sup>i</sup>Pr)<sub>4</sub> to the solution of BTB-3, stoichiometric proportions of water were dissolved in THF and added to the Ti\_BT B-3 suspension. (Figure 4.6) The Ti:H<sub>2</sub>O ratio was varied from 4:1 to 1:4 to cover partially and completely hydrolysed materials.

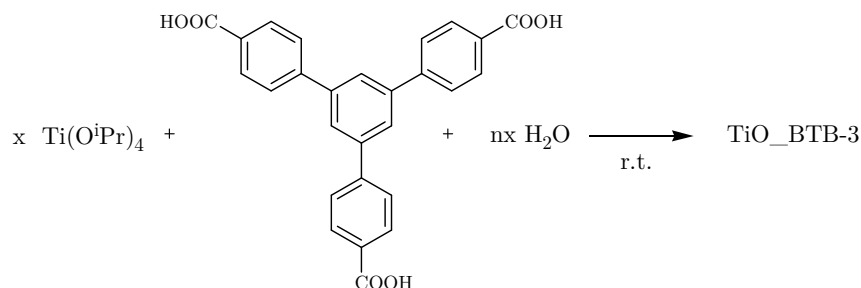


Figure 4.6: Synthesis of TiO\_BTBT-3

IR investigations proved a retained coordination of the tricarboxylate to the titanium centres. Both bands for the C=O stretching vibration were still present in the IR spectra at 1588 and 1548  $\text{cm}^{-1}$ . The lower the Ti:H<sub>2</sub>O ratio, the less intense the C-O frequencies at 1116 and 990  $\text{cm}^{-1}$  were. This was in good agreement with an advanced hydrolysis of the material, where the alkoxo groups were hydrolysed and Ti-O-Ti bonds formed. The IR spectroscopic investigations also showed a more intensive symmetric C=O stretching frequency at 1404  $\text{cm}^{-1}$ , which was in line with the retained coordination of the ligand. No bands for COOR ester groups were present around 1700  $\text{cm}^{-1}$ . Variation of the Ti:COOH ratio did not result in different IR spectra. All spectra were in line with previous IR spectroscopic investigations of titanium oxo clusters.<sup>148,152</sup> Investigations of TiO\_BTBT-3 were conducted with a Ti:COOH=2:1 ratio and varying the varying Ti:H<sub>2</sub>O ratio. The corresponding IR spectra are shown in Figure 4.7.

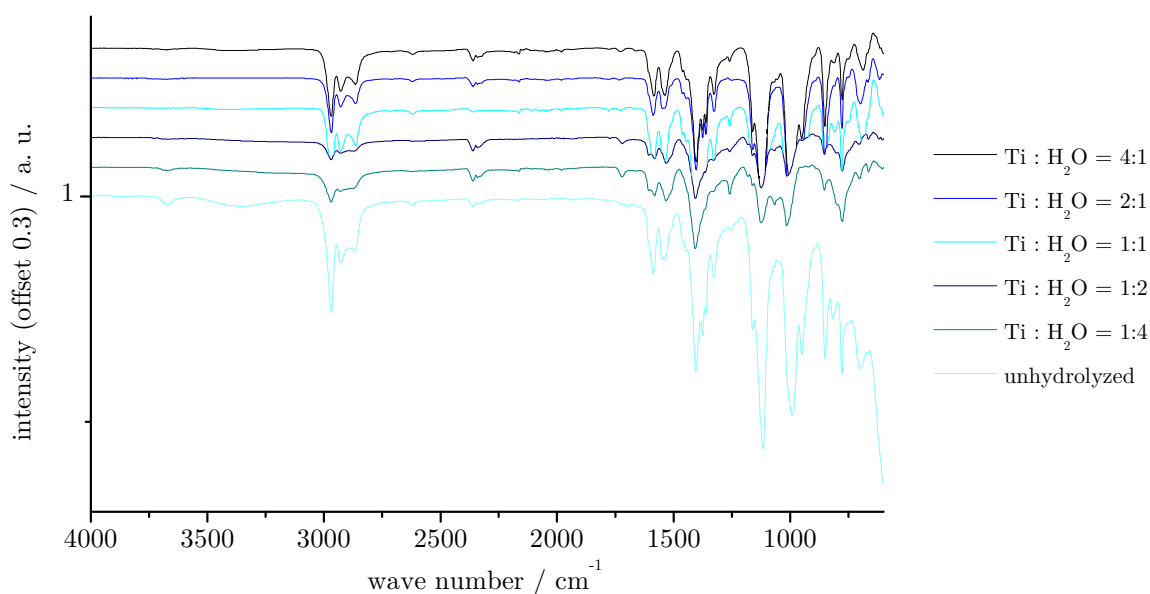
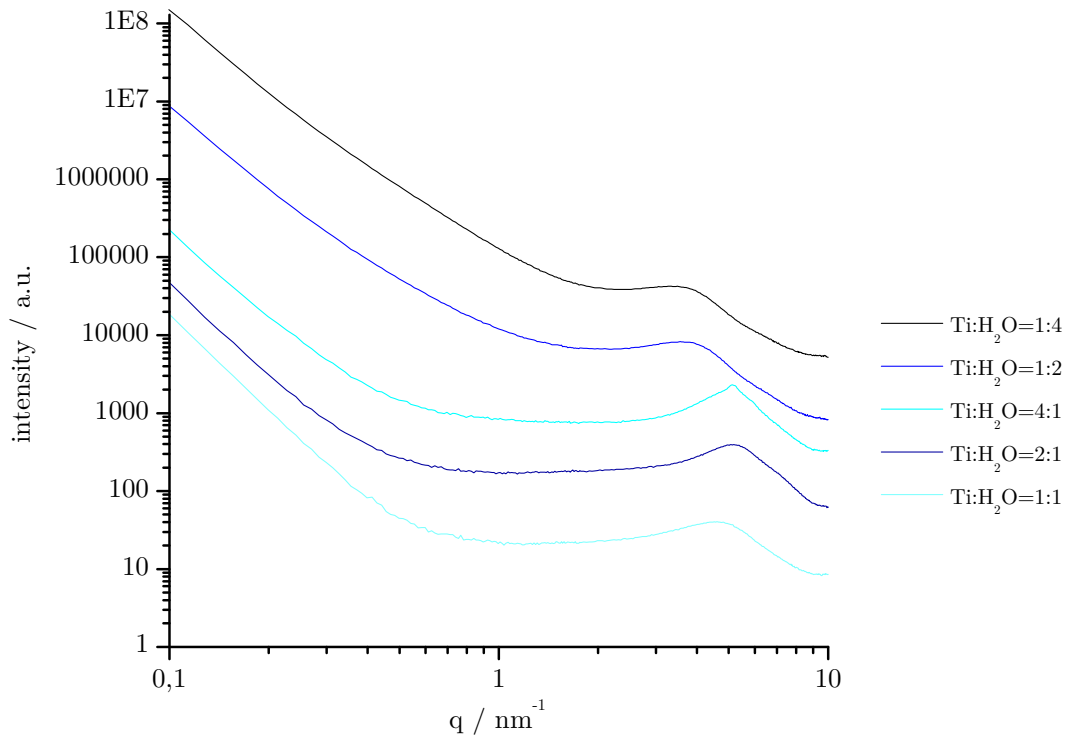


Figure 4.7: IR spectra of Ti:COOH=2:1 with varying water content (the spectra are plotted with an offset of 0.3 on the y axis)

Thus, tricarboxylates were assumed to be suitable ligands, as a possible pre-organisation was retained unchanged during sol-gel processing.

The precipitates were insoluble in all commonly used organic solvents. Therefore, molecular analysis techniques failed in the elucidation of the structural features of TiO\_BTBT-3. TEM and SEM were applied to get more insights in the material's structure. TEM of TiO\_BTBT-3 with Ti:COOH=1:1 and varying Ti:H<sub>2</sub>O ratios failed because the high organic proportions led to a carbon deposit in the area, on which the electron beam was focused. EDX measurements of some regions of the sample resulted in only carbon residues. SEM just showed the morphology of the obtained powder; no new insight was gained.

Therefore, SAXS was applied on these materials. The measurements were carried out at room temperature in vacuum. In a first experiment, TiO\_BTBT-3 with a Ti:COOH ratio of 2:1 and varying Ti:H<sub>2</sub>O ratios were investigated. All SAXS patterns are shown in Figure 4.8.



**Figure 4.8:** SAXS patterns of TiO\_BTBT-3 with Ti:COOH=2:1 and varying Ti:H<sub>2</sub>O ratio (the SAXS patterns are plotted with an offset of 30% on the y axis)

If different Ti:H<sub>2</sub>O ratios were used, the SAXS results differed considerably. While the slope (linear part of the SAXS patterns between 0.1 and 0.4 nm<sup>-1</sup>) of the Ti:H<sub>2</sub>O=1:1 sample was  $q^4$ , samples with higher and lower Ti:H<sub>2</sub>O ratios resulted in significantly lower slopes. From the slope of samples with Ti:H<sub>2</sub>O=1:2 and Ti:H<sub>2</sub>O=1:4, which was  $q^{-2.7}$ , a structure between 2D layered to 3D features was derived. The structure parameters of TiO\_BTBT-3 is summarised in Table 4.1.

**Table 4.1: Parameters of TiO\_BT B-3 with Ti:COOH=2:1 and vary Ti:H<sub>2</sub>O ratios derived from SAXS patterns**

Ti:H <sub>2</sub> O	R <sub>2</sub> /nm	d <sub>2</sub> / nm	$\eta$	Slope q <sup>-n</sup>
1:1	0.49	1.18	0.23	4
1:2	0.62	1.42	0.19	2.7
1:4	0.58	1.58	0.19	2.7
2:1	0.46	1.08	0.25	3
4:1	0.50	1.16	0.29	3

The SAXS measurements showed significant differences to that of Ti\_BT B-3, as the scattering maximum shifted from higher q-values to 3-4 nm<sup>-1</sup>. The shifting of the scattering maximum to lower values was caused by a risen distance between the periodic assemblies. The partial hydrolysis permitted the formation of Ti-O-Ti bridges, which led to a longer connection between the ligand molecules. When the ligand was assumed to be the periodic building block, the enhanced distance between the ligands would be in line with a decreasing q-value. The SAXS measurements showed that the ordering of the structure, derived from the hard-sphere volume fraction  $\eta$ , was decreased proportional to the water proportion. It fell from 0.29 (Ti:H<sub>2</sub>O=4:1) to 0.19 (Ti:H<sub>2</sub>O=1:2/1:4). It was also observed in line with a broadening of the scattering maximum. If a spherical periodic unit was assumed, its radius varied between 0.46 and 0.62 nm. The distance between the periodic units was calculated to be 1.08 to 1.58 nm.

It was unclear whether this feature was caused either by the BT B-3 ligand or a titanium cluster moiety. Experiments with other tricarboxylic acids with different linkers (tris-(biphenyl)benzene or benzene) should provide information about whether the periodic building block was caused by the ligands. The scattering maximum should shift to higher/lower q values with smaller/larger linkers.

Investigations were extended by varying the Ti:COOH ratio. In each case, partial hydrolysis was carried out with varying Ti:H<sub>2</sub>O ratios. Figure 4.10 shows SAXS patterns of compounds prepared with varying Ti:COOH ratio and a Ti:H<sub>2</sub>O ratio of 1:2. In comparison to the SAXS pattern of Figure 4.8, the slope increased to values between q<sup>-3.4</sup> to q<sup>-4.0</sup>. This slope was typical of a 3D structure. All patterns showed a scattering maximum between 3 and 4 nm<sup>-1</sup>. It was assumed that a stable periodic building block was formed. If a cluster was formed like the building block, it was not influenced by an increased titanium alkoxide proportions. The hard sphere volume fraction  $\eta$  decreased proportional to an increasing Ti:COOH and an increasing Ti:H<sub>2</sub>O ratio. The highest hard sphere volume fraction  $\eta$  was observed for a Ti:COOH ratio of 1:4 and was calculated to be 0.42. The decrease of the ordering was caused by building blocks of different size or an additional TiO<sub>2</sub> matrix, which disturbed the ordering of the ligand molecules. A possible structure with low and high proportions of Ti(O<sup>i</sup>Pr)<sub>4</sub> is shown in Figure 4.9.

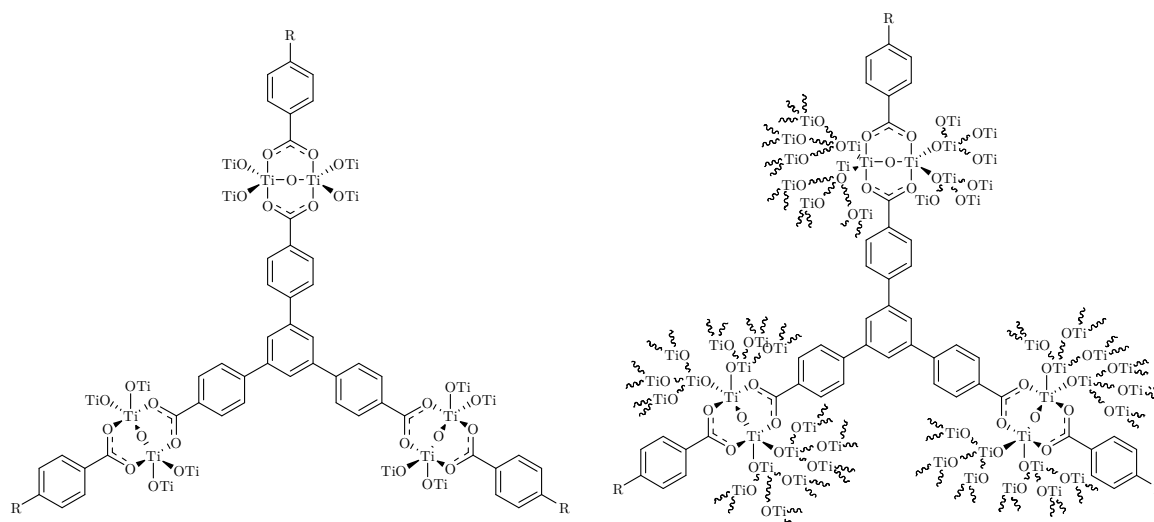


Figure 4.9: Postulated structure of TiO\_BT3 with varying proportions of  $\text{Ti}(\text{O}^i\text{Pr})_4$

An additional scattering maximum of low intensity next to the maximum at  $3\text{--}5\text{ nm}^{-1}$  appeared in samples with Ti:COOH ratios of 1:2 and 1:4. These second scattering maxima were caused by an additional short-range ordering of the ligand, which were only observed in very low Ti:COOH ratios.

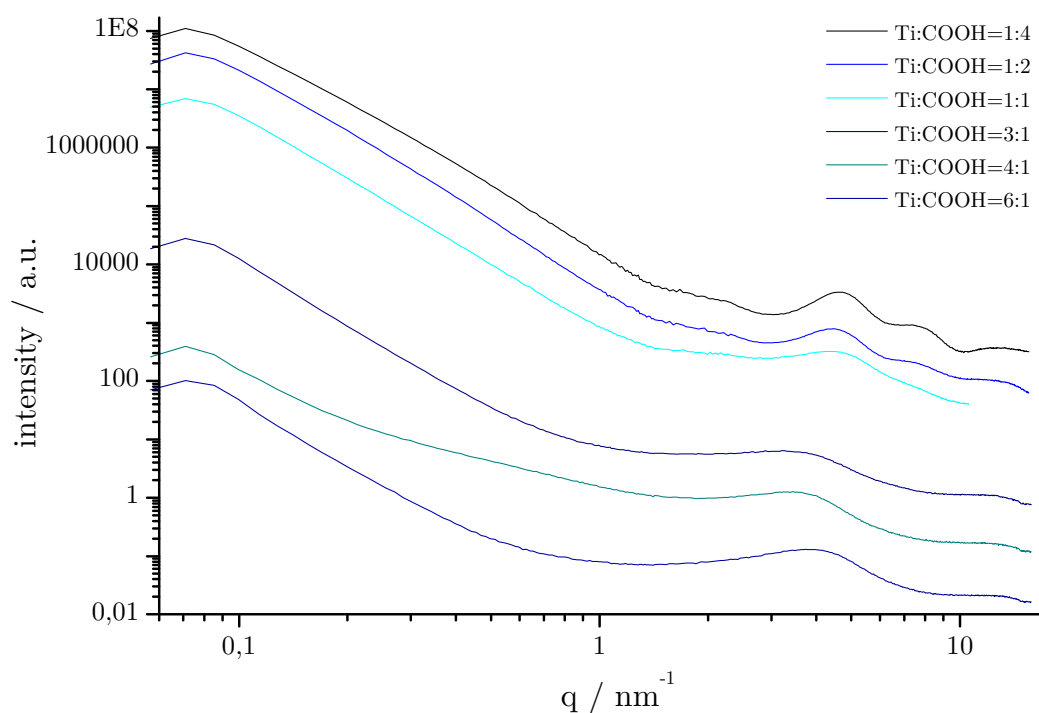


Figure 4.10: SAXS patterns of TiO\_BT3 with  $\text{Ti}:\text{H}_2\text{O}=2:1$  and varying Ti:COOH ratios (the SAXS patterns are plotted with an offset of 30% on the y axis)

A network-like structure was proposed for TiO\_BT3, in which titania-based moieties, dimeric complexes, titanium oxo clusters or titania nanoparticles, were interconnected by the BTB-3



ligands. Addition of water resulted in partial hydrolysis and additional interconnection of the titanium moieties. This was in line with observations of the gas sorption experiments, where porosity was only observed in hydrolysed materials. (Figure 4.12)

The synthesis of TiO\_BT3 was extended to experiments under solvothermal conditions. Therefore, the precipitates of previous syntheses at room temperature were kept under solvothermal conditions to rearrange the structure or the educts were mixed in the autoclave and the whole synthesis was conducted under solvothermal conditions. Both methods did not result in different SAXS patterns. Precipitates were obtained in each case. No crystals were obtained and powder X-ray diffraction only showed a partially crystalline material.

The TiO\_BT3 products were investigated by nitrogen sorption measurements. Figure 4.11 shows the nitrogen sorption isotherms of compounds prepared with different Ti:COOH:H<sub>2</sub>O ratios. The adsorption isotherms revealed a drop at low relative pressure. This was in line with microporous materials. No mesopores, which were often observed in titania-based materials, were found. Both isotherms were of type I with an H4 hysteresis, which corresponds to narrow, slit-like pores. The isotherm with a Ti:COOH ratio of 3:1 also showed the existence of macropores at higher relative pressure. This sorption behaviour was common to all investigated TiO\_BT3 materials.

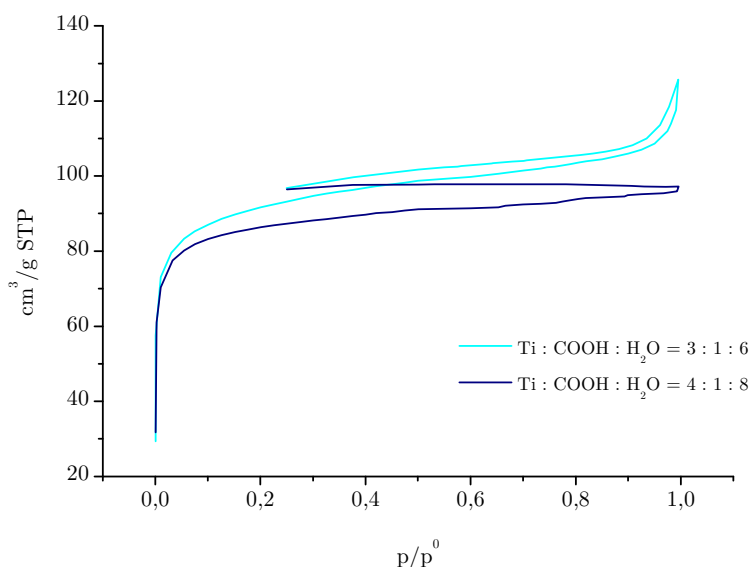


**Figure 4.11: Nitrogen sorption isotherms of two TiO\_BT3 materials with different Ti:COOH:H<sub>2</sub>O ratios**

The microporous surface area was determined by the t-plot method. The total BET surface area was much larger than the calculated microporous surface area. The difference was assigned to the external surface area: This external surface area is known to be caused by the surrounding of particle, agglomerates and surface of wide cracks on these particles.<sup>153</sup> It was more assigned to the morphology of the powder/particles of the materials and gave no additional insights to the structure on a molecular scale.

Figure 4.12 shows the microporous surface areas.

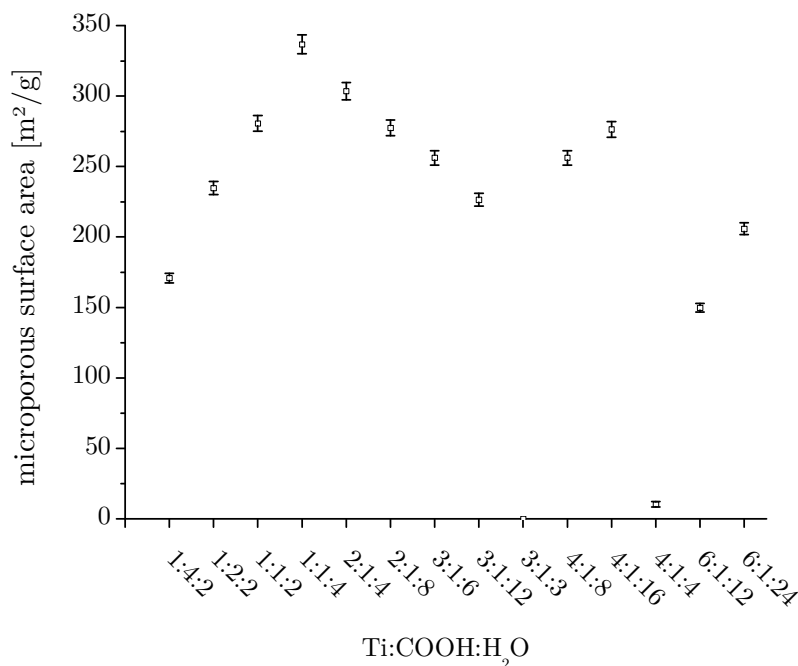


**Figure 4.12: Microporous surface areas of TiO\_BT B-3**

The maximum BET surface area (406 m<sup>2</sup>/g) was determined for materials with a ratio of Ti:COOH:H<sub>2</sub>O=1:1:4. The maximum microporous surface area was 336 m<sup>2</sup>/g. A clear trend was observed for Ti\_BT B-3. Samples with higher and lower Ti:COOH ratios than 1:1 resulted in significant lower surface areas. If the Ti:H<sub>2</sub>O ratio was larger than 1:1, the surface area was independent of the Ti:H<sub>2</sub>O ratio. Samples with a Ti:H<sub>2</sub>O ratio of 1:1 resulted in non-porous materials, as too few alkoxo groups were hydrolysed for the interconnection. The observed trend indicated the highest porosity at a Ti:COOH ratio of 1:1. In case of lower titanium alkoxide proportions, too many carboxylate groups were coordinated. In case of higher Ti:COOH ratios, the structure of the network was surrounded by a TiO<sub>2</sub> matrix, which fallen the porosity.

When the samples were stored for another two months, all porosity was lost. Nitrogen sorption measurements then resulted in no differences whether the samples were stored under inert gas or at air. This loss of porosity was also independent of the used Ti:COOH:H<sub>2</sub>O ratio. This change in porosity was caused by an additional aging of the network, which is observed for all gels.

The samples with highest microporous surface areas were additionally tested in argon sorption experiments. Argon is known for its smaller partial pressure at 77K. Figure 4.13 compares the nitrogen and argon adsorption isotherm of the same TiO\_BT B-3 material.

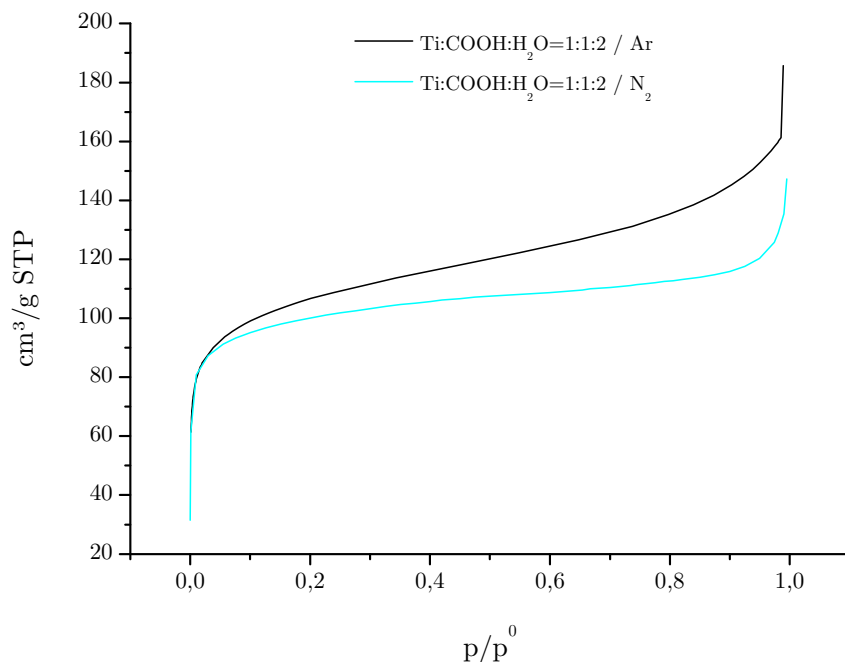


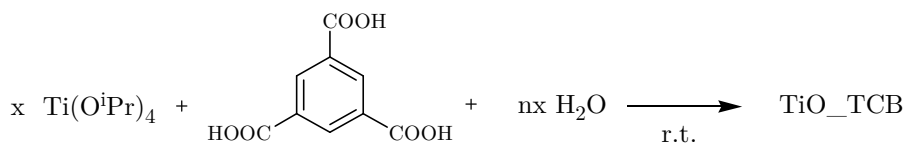
Figure 4.13: N<sub>2</sub> and Ar adsorption isotherms of TiO\_BTBT-3 with defined Ti:COOH:H<sub>2</sub>O ratio

The argon adsorption isotherms showed a similar shape compared to the ones obtained with nitrogen. The calculated BET and microporous surface areas were significantly lower than the ones observed with nitrogen. A maximum microporous surface area was determined with 188 m<sup>2</sup>/g. The use of argon thus enabled the determination of the pore size. The method of Horvath-Kawazoe was used for the calculation, which is suitable for slit-like pores. An average pore width smaller than 0.78 nm was measured for the samples with Ti:COOH=1:1 and varying Ti:H<sub>2</sub>O ratios. The method of Dubinin-Astakhov was chosen as a supplementary model for pore size determination, leading to a calculated mean equivalent pore width of 1.57 nm. This matched well with the distance between periodic assemblies, which was calculated from the SAXS patterns.

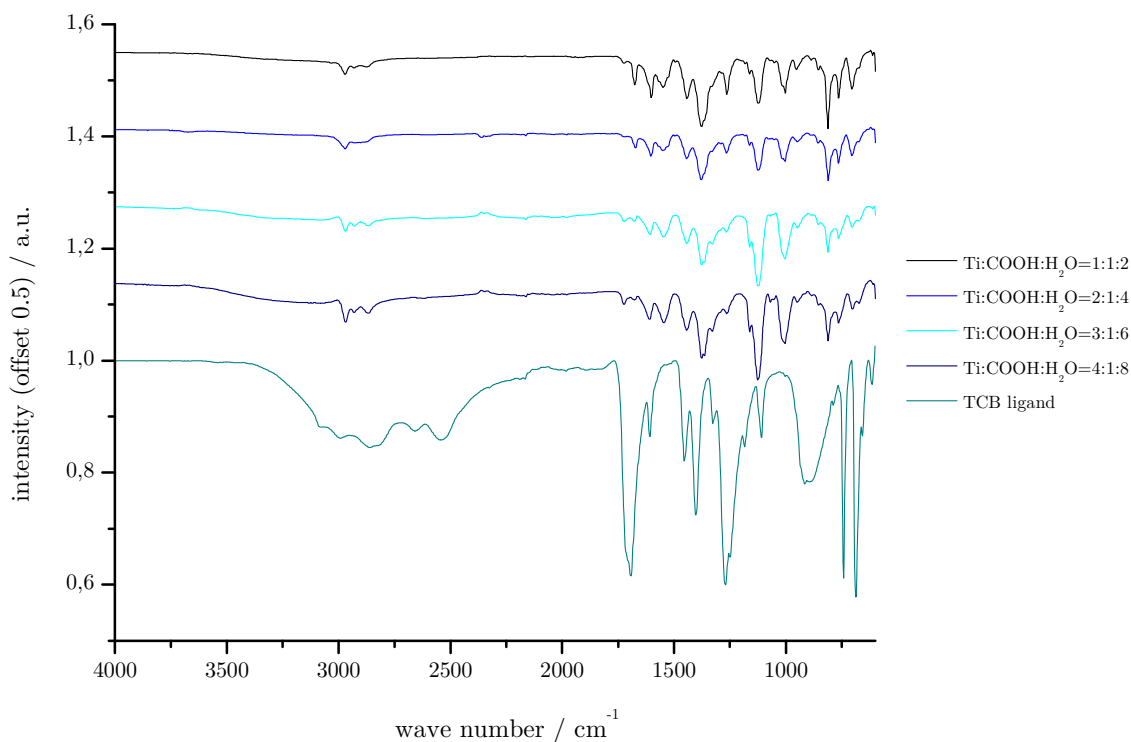
When the TiO\_BTBT-3 samples were calcinated, they were completely dense. The porosity of the material was lost. A collapse of the whole network was caused by the calcination, as the interconnection between the titania-based building blocks were missing. Furthermore, the experiments proved that the ligands and their organisation played an important role for the structure of TiO\_BTBT-3. Powder X-ray diffraction only found crystalline TiO<sub>2</sub>.

## 4.2 Modification of Ti(O<sup>i</sup>Pr)<sub>4</sub> with 1,3,5-tricarboxybenzene

1,3,5-Tricarboxybenzene (TCB) was chosen as a ligand for network-like modification of Ti(O<sup>i</sup>Pr)<sub>4</sub> to investigate the influence of the linker on the obtained structure. Reactions of different proportions of Ti(O<sup>i</sup>Pr)<sub>4</sub> with TCB resulted in white precipitates that were hydrolysed by an addition of stoichiometric amount of water after some minutes. (Figure 4.14)

**Figure 4.14: Synthesis of TiO\_TCB**

The dried residues were investigated by IR spectroscopy. The asymmetric C=O stretching frequency shifted from 1692 to 1676/1602/1550  $\text{cm}^{-1}$  for all materials, which was a clear hint for coordination of the tricarboxylates. It was not clear, whether the signal at 1676  $\text{cm}^{-1}$  was caused by non-coordinated carboxylic groups or ester groups, but it became less intensive the more  $\text{Ti(O}^i\text{Pr)}_4$  was used. The symmetric C=O stretching frequencies shifted from 1453/1401  $\text{cm}^{-1}$  to 1443/1378  $\text{cm}^{-1}$ . Selected spectra are shown in Figure 4.15.

**Figure 4.15: IR spectra of TiO\_TCB with Ti:H<sub>2</sub>O=1:2 and varying Ti:COOH ratios (the spectra are plotted with an offset of 0.5 on the y axis)**

SAXS investigations of all materials showed a 3D structure, which was derived from the slope (linear part of the SAXS patterns between 0.1 and 1  $\text{nm}^{-1}$ ) between  $q^{-3.0}$  and  $q^{-3.6}$  (Figure 4.16). The SAXS patterns showed a scattering maximum above 5  $\text{nm}^{-1}$ . In comparison to TiO-BTB-3, the maxima were shifted to higher  $q$ -values, which was in line with the smaller linker used. The SAXS patterns showed no second scattering maxima at low Ti:COOH ratios, which were observed in BTB-3 and TCBB. This proved that additional phenylene groups had to be present to obtain this short-range ordering.

The material was highly ordered; hard sphere volume fractions above 0.2 were observed for most samples. The distance between periodic assemblies rose with increasing Ti:COOH ratios from 0.82 to 1.26 nm. Similar trends were also observed concerning the size of the periodic assemblies, they rose from 0.52 to 0.96 with increasing Ti:COOH ratios. The increased distance was in good agreement with higher proportions of  $\text{Ti}(\text{O}^i\text{Pr})_4$ , that led to uncoordinated  $\text{TiO}_2$  moieties around the coordination network. The parameters derived from the SAXS patterns are shown in Table 4.4.

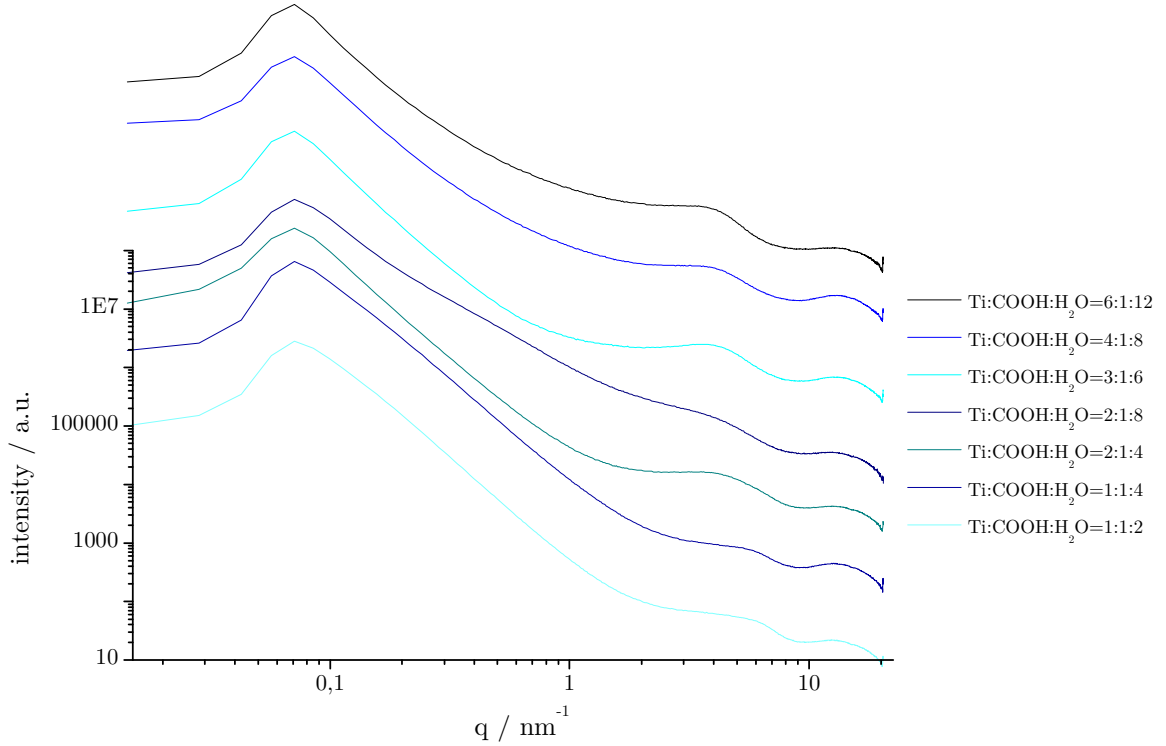


Figure 4.16: SAXS patterns of  $\text{TiO\_TCB}$  (the SAXS patterns are plotted with an offset of 100% on the y axis)

Table 4.2: Parameters of  $\text{TiO\_TCB}$  derived from the SAXS patterns

Ti:COOH:H <sub>2</sub> O	$R_2$ / nm	$d_2$ / nm	$\eta$	Slope $q^{-n}$
1:1:2	0.71	0.94	0.264	3.5
1:1:4	0.52	0.82	0.101	3.5
2:1:4	0.62	1.04	0.158	3.5
3:1:6	0.75	1.18	0.220	3.6
4:1:8	0.79	1.20	0.208	3.0
6:1:12	0.96	1.26	0.267	3.0

The investigations were extended to nitrogen sorption measurements to check whether porosities, similar to  $\text{TiO\_BTB-3}$ , were also observed with  $\text{TiO\_TCB}$  materials. Nitrogen sorption measurements resulted in a microporous material with a microporous surface area up to  $250 \text{ m}^2/\text{g}$ . (Figure 4.17) The microporous surface area rose slightly while  $\text{Ti}(\text{O}^i\text{Pr})_4$  proportions were increasing. The corresponding total BET surface areas varied between  $250$  and  $400 \text{ m}^2/\text{g}$ . Different ex-

ternal surface areas were observed for the TiO\_TCB samples. The microporous surface areas were lower than the surface areas of TiO\_BT-3, which was in agreement with a smaller linker of the ligand. A smaller pore volume and therefore a smaller microporous surface area were caused by the benzene linker. An overview of the observed surface areas is given in Figure 4.17.

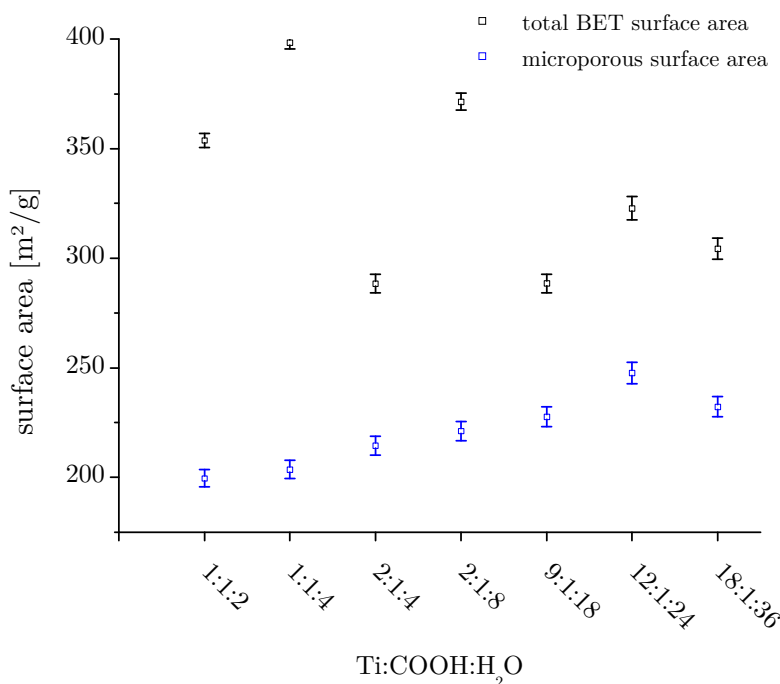


Figure 4.17: BET and microporous surface area of TiO\_TCB

### 4.3 Modification of Ti(O<sup>i</sup>Pr)<sub>4</sub> with 1,3,5-tris(4-carboxy-biphenyl)benzene

1,3,5-Tris(4-carboxy-biphenyl)benzene (TCBB) was chosen to investigate the influence of the linker. TCBB is extended by one phenylene group relative to BTB-3 and two phenylene groups relative to TCB. THF was the only suitable solvent for the material syntheses. (Figure 4.18)

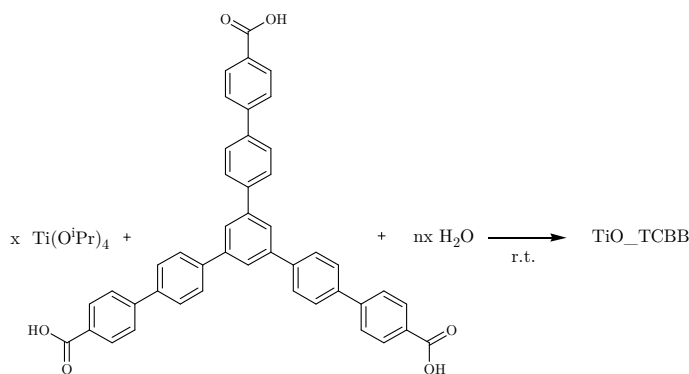
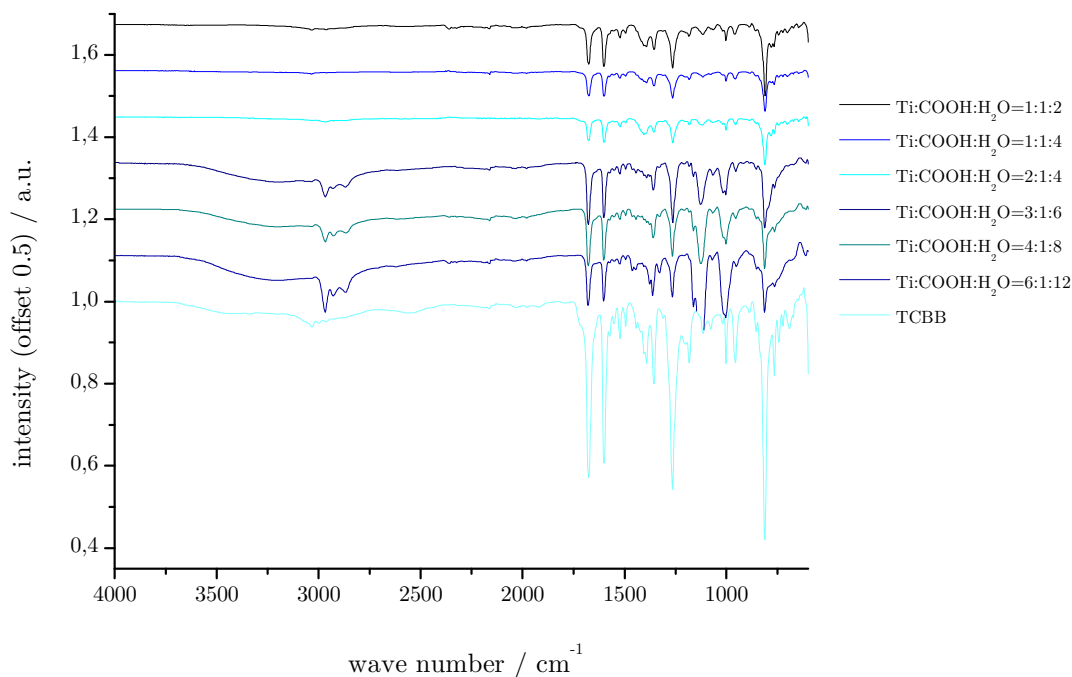


Figure 4.18: synthesis of TiO\_TCBB

The synthesis of TiO\_TCBB was conducted with varying Ti:COOH and Ti:H<sub>2</sub>O ratios. The IR spectra showed no shifts of the asymmetric and symmetric C=O stretching frequency. (Figure 4.19) Two explanations could be taken into consideration: First, due to the bad solubility of the ligand, it did not substitute the alkoxo ligands during the modification process and remained unreacted in the solution. Second, a compound of type Ti\_TCBB could be formed, which was indicated by the precipitate formed after the addition of Ti(O<sup>i</sup>Pr)<sub>4</sub>. After partial hydrolysis, the Ti-COO bond was cleaved and only bands of free TCBB appeared in the IR spectra.



**Figure 4.19:** IR spectra of TiO\_TCBB with varying Ti:COOH:H<sub>2</sub>O ratios (the spectra are plotted with an offset of 0.5 on the y axis)

Additional insight was possible after SAXS investigations. (Figure 4.20) All SAXS patterns showed a slope (linear part of the SAXS patterns between 0.1 and 0.9 nm<sup>-1</sup>) of  $q^{-3.5}$  to  $q^{-3.8}$ , from which a 3D structure was derived. Samples with low Ti:COOH ratios (1:1 and 2:1) resulted in large distances of 2.10 nm between the periodic assemblies, which were of 0.8 nm in size. Higher Ti:COOH ratios showed assemblies of similar size but shorter distances, which were between 1.20 and 1.38 nm. Due to the significantly larger distances than those of TiO\_TCB, an additional hint for influences of the linker on the material was proven. The hard sphere volume fraction was above 0.2 for samples, therefore a material with high ordering was obtained. All materials showed a scattering maximum below 3 nm<sup>-1</sup>. The parameters derived from the SAXS and these patterns are shown in Table 4.3. In contrary to the TiO\_BT3, the scattering maximum was slightly shifted to lower  $q$  values, which was in line with a larger linker. This proved the influence of the linker on the material. Furthermore, the experiments proved that the scattering maximum could

be shifted by varying the linkers. The shift of the scattering maxima was either assigned to varying cluster sizes or to the varying ligand (linker) sizes. The shift of the scattering maxima because of an increased linker size was more reasonable.

The materials with low Ti:COOH ratios showed a second scattering maximum. It was only observed in materials with low Ti:COOH ratios and ligands with at least two connected phenylene linkers. SAXS experiments with the pure ligand in solid state and in solution should prove whether the second scattering maximum was caused by an inter- or intramolecular short-range order of the ligand. An intermolecular ordering could be more likely, as this second scattering maximum was only observed for samples with low Ti:COOH ratios. If less proportions of  $\text{Ti}(\text{O}^i\text{Pr})_4$  were applied and the ligands were quite close to each other, this short-range ordering would only be possible. This is proven by the resulting SAXS patterns. Whereas, an intramolecular short-range ordering should be independent of the Ti:COOH ratio and observed for all samples, which was not the case in these samples.

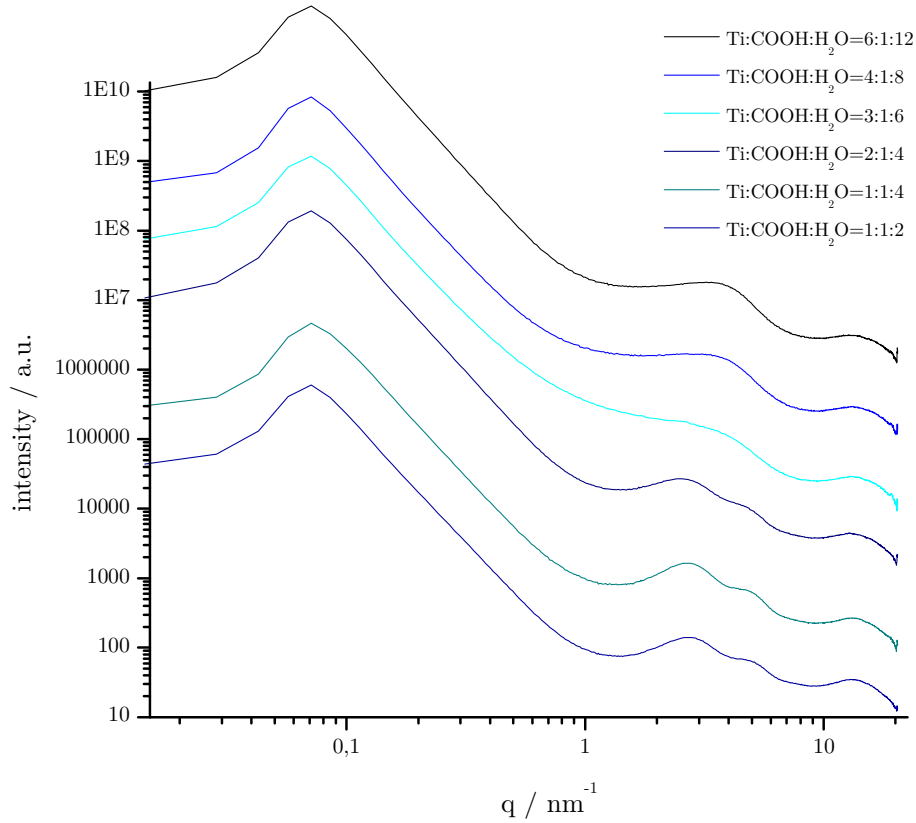


Figure 4.20: SAXS patterns of  $\text{TiO\_TCBB}$  (the SAXS patterns are plotted with an offset of 60% on the y axis)

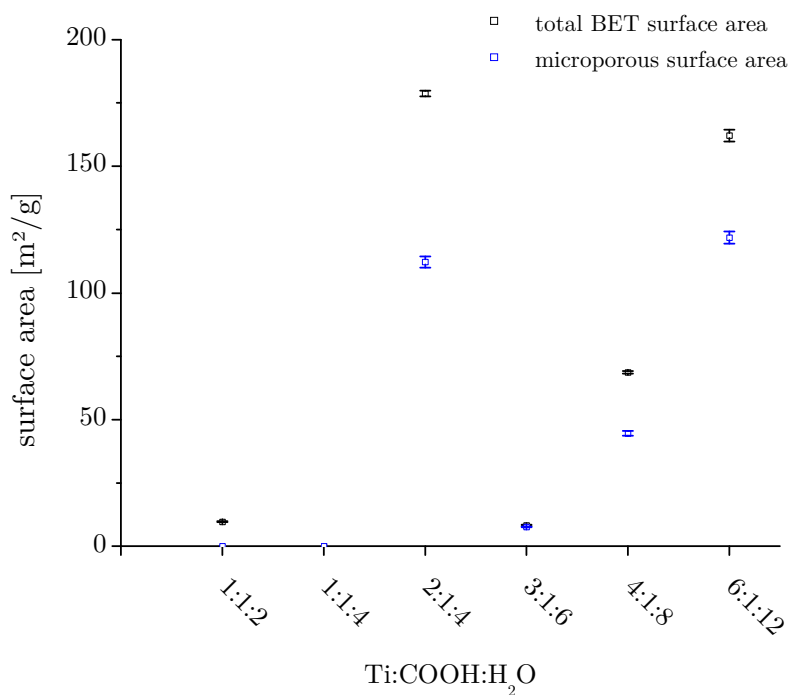


**Table 4.3: Parameters of TiO\_TCBB derived from SAXS patterns**

Ti:COOH:H <sub>2</sub> O	R <sub>2</sub> /nm	d <sub>2</sub> / nm	$\eta$	Slope q <sup>-n</sup>
1:1:2	0.80	2.14	0.263	3.7
1:1:4	0.79	2.14	0.255	3.8
2:1:4	0.82	2.10	0.213	3.8
3:1:6	0.94	1.2	0.208	3.5
4:1:8	0.79	1.32	0.192	3.8
6:1:12	0.75	1.38	0.212	3.8

Additionally, the TiO\_TCBB samples were investigated with nitrogen sorption experiments. (Figure 4.21) The measurements revealed that only few samples were microporous. There was no trend, why some of them showed a microporous surface area of about 110 m<sup>2</sup>/g and others were completely dense.

Furthermore, the measurements of TiO\_TCBB did not prove that a larger linker resulted in an enhanced surface area. It was assumed that the TCBB ligand was too big, and that the titanium building blocks could not sustain these pores. If less metal alkoxide was provided, the pores collapsed


**Figure 4.21: BET and microporous surface area of TiO\_TCBB**

#### 4.4 Modification of Zr(O<sup>i</sup>Pr)<sub>4</sub> · <sup>i</sup>PrOH with benzenetribenzoic acid

Numerous experiments concerning the modification of titanium alkoxides with BTB-3 were performed. Chapter 4.2 and 4.3 proved the influence of the used linker on the observed structural

features. Additional investigations with  $\text{Zr}(\text{O}^i\text{Pr})_4 \cdot {}^i\text{PrOH}$  should prove whether the used metal alkoxide affected the resulted structure. Reactions of  $\text{Zr}(\text{O}^i\text{Pr})_4 \cdot {}^i\text{PrOH}$  with BTB-3 and partial hydrolysis resulted afterwards in off-white precipitates. (Figure 4.22)

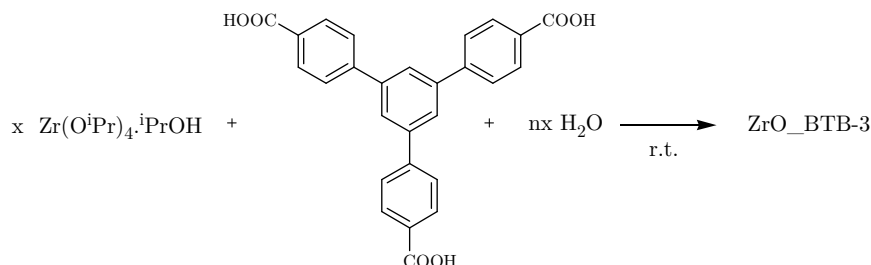


**Figure 4.22: Synthesis of ZrO\_BT B-3**

The spectra (Figure 4.23) showed a significant shift of the asymmetric C=O stretching frequency from 1687/1608  $\text{cm}^{-1}$  to 1585/1535  $\text{cm}^{-1}$ . The symmetric C=O stretching frequency also shifted slightly from 1420 to 1410  $\text{cm}^{-1}$ . Both shifts were observed with all Zr:COOH:H<sub>2</sub>O ratios. The sample with Zr:COOH=1:2 also showed bands for coordinated carboxylate groups. No bands for COOR groups or free carboxylic groups were observed in the spectra. It proved the comparable coordination of the carboxylate groups to zirconium alkoxo moieties as well as the stability of the coordination during partial hydrolysis. The IR spectra were similar to that observed for TiO\_BT B-3.

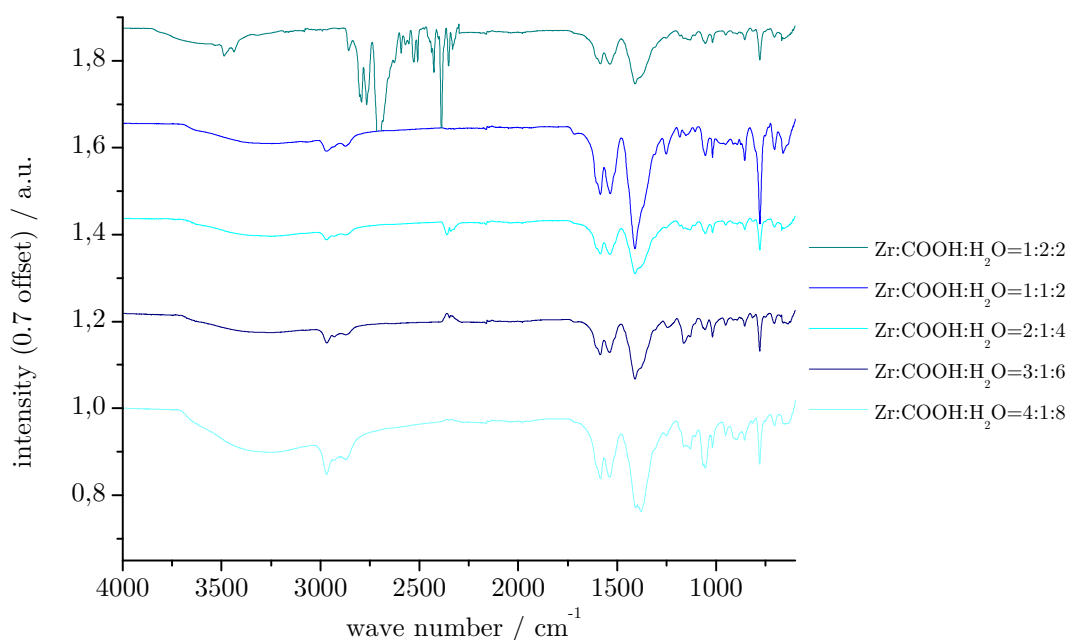


**Figure 4.23: IR spectra of ZrO\_BT B-3 with Ti:H<sub>2</sub>O=1:2 and varying Ti:COOH ratios (the spectra are plotted with an offset of 0.7 on the y axis)**

SAXS measurements of ZrO\_BTBT-3 showed a scattering maximum between 3 and 4 nm<sup>-1</sup> at the same  $q$  value as observed for TiO\_BTBT-3. Figure 4.24 compares the SAXS pattern of M<sup>IV</sup>O\_BTBT-3 prepared from M<sup>IV</sup>:COOH=1:1 and varying M<sup>IV</sup>:H<sub>2</sub>O ratio.

There are two possibilities to explain the observation that the scattering maxima of both scattering patterns were observed at the same  $q$  value. Either the scattering maxima were caused by a periodic arrangement of the ligands, which would be independent of the used metal alkoxide or metal alkoxo/oxo building blocks were of similar size. Concerning the results with TCB and TCBB, the first explanation was more likely. An ordered arrangement of BTBT-3 occurred.

Furthermore, the ZrO\_BTBT-3 samples revealed a second scattering maximum at higher  $q$  values, which were at the similar position as in TiO\_BTBT-3. Thus, this scattering maximum was also independent of the used metal alkoxide and was caused by an additional short-range ordering of the ligand molecules.

Figure 4.24 proves that both samples had a similar slope in the region between 0.1 and 1 nm<sup>-1</sup>. The slope (linear part of the SAXS patterns between 0.1 and 1 nm<sup>-1</sup>) of ZrO\_BTBT-3 (Zr:COOH=1:1) varied between  $q^{-3.1}$  (Ti:H<sub>2</sub>O=1:2) and  $q^{-3.3}$  (Ti:H<sub>2</sub>O=1:4), indicating a 3D structure.

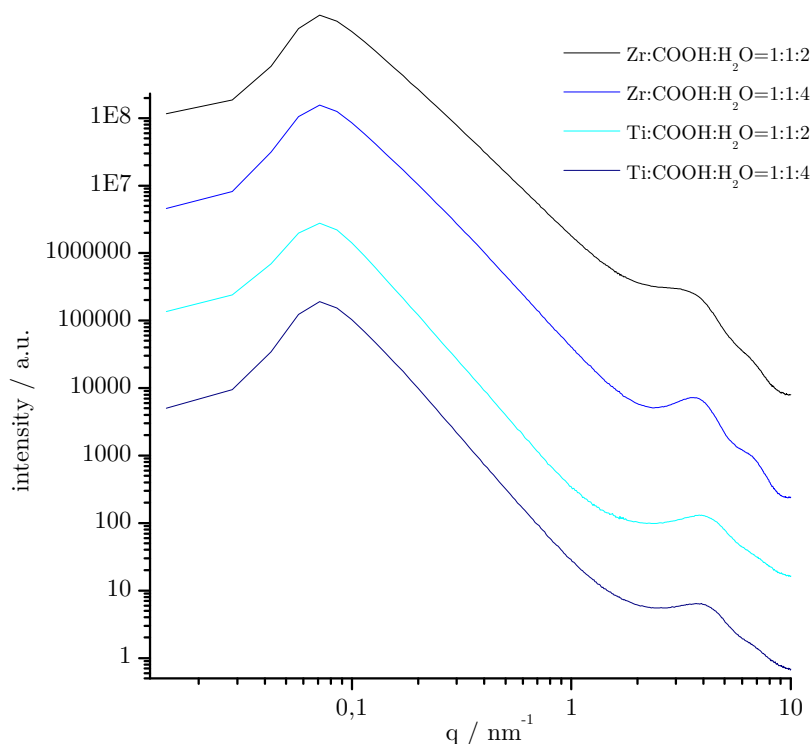


**Figure 4.24:** SAXS pattern comparison of TiO\_BTBT-3 and ZrO\_BTBT-3 with (M:COOH=1:1) (the SAXS patterns are plotted with an offset of 50% on the y axis)

Solvothermal experiments resulted in similar precipitates, for which similar SAXS patterns were observed. The resulting porosity was in same range as for materials synthesised at ambient conditions. This was in agreement with observations of TiO\_BTBT-3 and proved that solvothermal

conditions had no influence on the ordering/structure of the materials. No crystalline MOFs could be isolated.

SAXS investigations were extended to higher Zr:COOH ratios. (Figure 4.25) Among all investigated materials, ZrO\_BT3 with Zr:COOH=1:1 resulted in the highest ordering. The more water and  $\text{Zr}(\text{O}^i\text{Pr})_4 \cdot ^i\text{PrOH}$  were added, the lower the ordering and the less defined the scattering maximum was. The hard-sphere volume fraction  $\eta$  decreased from 0.39 (Zr:COOH:H<sub>2</sub>O=1:1:2) to 0.16 (Zr:COOH:H<sub>2</sub>O=4:1:16). This was in good agreement with an broadening of the scattering maximum with increasing proportions of  $\text{Zr}(\text{O}^i\text{Pr})_4 \cdot ^i\text{PrOH}$  and water, which was caused by zirconia moieties of different and larger size. They disturbed the ordering of the ligand. All fitted parameter are shown in Table 4.4.

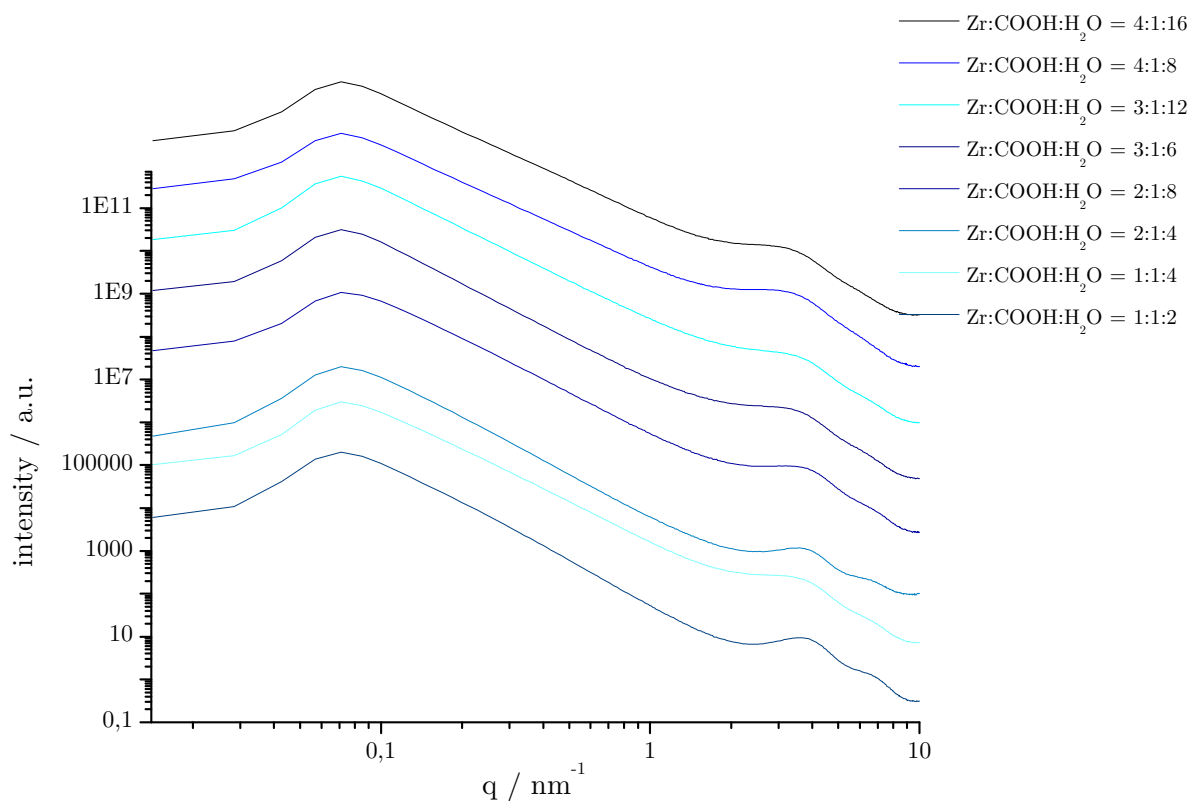


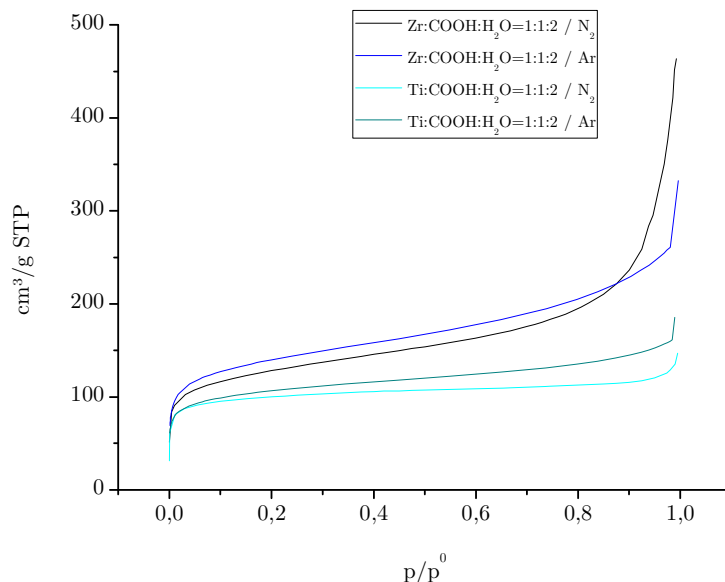
Figure 4.25: SAXS patterns of ZrO\_BT3 with varying Zr:COOH:H<sub>2</sub>O ratios (the SAXS patterns are plotted with an offset of 70% on the y axis)

**Table 4.4: Parameter derived from the SAXS patterns**

Zr:COOH:H <sub>2</sub> O	R <sub>2</sub> / nm	d <sub>2</sub> / nm	$\eta$	Slope q <sup>-n</sup>
1:2:2	0.75	1.54	0.393	3.6
1:1:2	0.77	1.58	0.212	3.1
1:1:4	0.68	1.64	0.300	3.3
2:1:4	0.74	1.56	0.232	3.1
2:1:8	0.75	1.58	0.260	3.3
3:1:6	0.84	1.56	0.183	3.2
3:1:12	0.86	1.48	0.171	3.1
4:1:8	0.77	1.70	0.191	2.9
4:1:16	0.74	1.76	0.166	3.0

The ZrO\_BTBT-3 materials were also investigated by gas sorption measurement. In case of nitrogen as adsorption gas, the isotherms were of same type I as observed with the corresponding titanium compounds. The isotherms indicated a microporous material with the typically big gas uptake at low relative pressures. (Figure 4.26) In contrary to TiO\_BTBT-3, the adsorbed volume did not remain constant when the pressure was raised; the absorbed volume of the ZrO\_BTBT-3 materials rose continuously, which was caused by a higher macroporosity.

Moreover, investigations with argon as adsorption gas showed similar adsorption isotherms. A slightly higher gas uptake was observed with increasing relative pressure. (Figure 4.26)


**Figure 4.26: Comparison of adsorption isotherms of TiO\_BTBT-3 and ZrO\_BTBT-3 with different adsorption gases**

Microporous surface areas above 100 m<sup>2</sup>/g were obtained with nitrogen for all investigated ZrO\_BTBT-3 materials. Similar to TiO\_BTBT-3, a maximum surface area was observed for samples of composition Zr:COOH=1:1. A microporous surface area of 254 m<sup>2</sup>/g was determined there, which was more than 100 m<sup>2</sup>/g smaller than the corresponding microporous surface area of

TiO\_BTBT-3. Furthermore, Figure 4.27 shows three tendencies. First, the lower the Zr:COOH ratio, the higher the microporous surface area was. This was in line with previous investigations of TiO\_BTBT-3. It was assumed that the additional ZrO<sub>2</sub> matrix, which was built because of the excess of Zr(O<sup>i</sup>Pr)<sub>4</sub> · <sup>i</sup>PrOH, filled the obtained pores and therefore decreased the ordering of the structure and the porosity. This was also in line with observations in SAXS. Second, for all measured samples, a similar external surface area of around 200 m<sup>2</sup>/g was determined, which was caused by agglomeration of the material. Third, the total BET surface areas of the ZrO\_BTBT-3 materials were significantly higher than those of TiO\_BTBT-3.

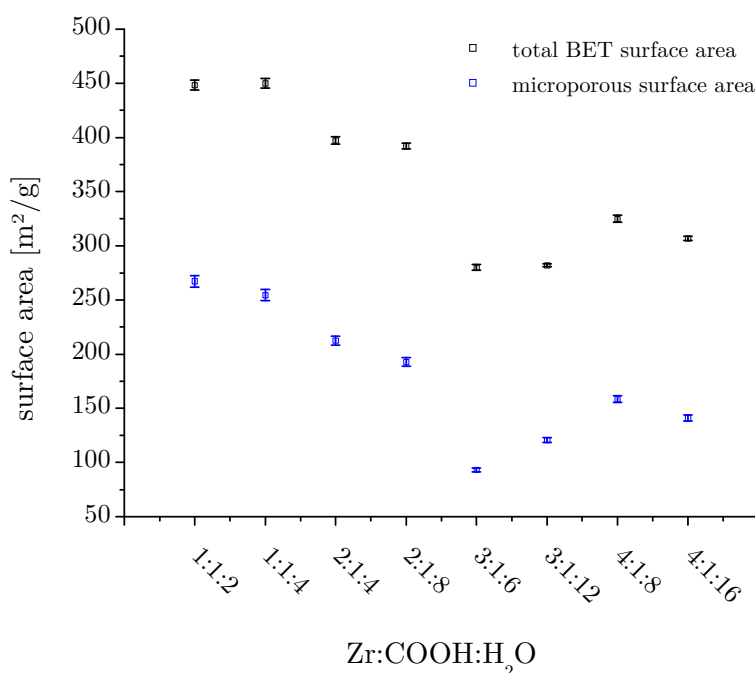


Figure 4.27: BET and microporous surface area of ZrO\_BTBT-3 determined by nitrogen sorption

Gas sorption measurements (Figure 4.26) with argon showed a lower microporous surface area, whereas the external surface area remained comparable. Argon as sorption gas permitted the determination of the pore size of these microporous materials. The method of Horvath-Kawazoe resulted in a median pore width at 0.78 nm, which matched well with previous investigation of TiO\_BTBT-3 with argon. The method of Dubinin-Astakhov resulted in a mean equivalent pore width of 1.67 nm for Zr:COOH=1:1 and 1.86 nm for Zr:COOH=2:1. This mean equivalent pore size was in good agreement with the distance between the periodic assemblies, calculated from the SAXS patterns. This fitted distance should correlate with the pore size.

## 4.5 Modification of Ti(O<sup>i</sup>Pr)<sub>4</sub> with benzenetetra benzoic acid

Investigations with multifunctional ligands were extended to modification with tetracarboxylic acids. These experiments should prove whether the orientation of the carboxylic groups (planar,

tetrahedral, etc.) influenced the obtained materials. The reaction of  $\text{Ti}(\text{O}^i\text{Pr})_4$  with benzenetetracarboxylic acid (BTB-4) resulted in off-white residues. (Figure 4.28)

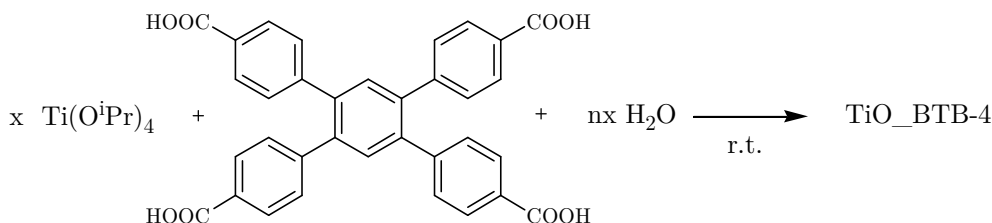


**Figure 4.28: Synthesis of  $\text{TiO\_BTB-4}$**

The dried  $\text{TiO\_BTB-4}$  materials were first investigated by IR spectroscopy. The strong asymmetric  $\text{C}=\text{O}$  stretching frequency at  $1684\text{ cm}^{-1}$  shifted to two intensive bands at  $1607$  and  $1527\text{ cm}^{-1}$ . The symmetric  $\text{C}=\text{O}$  frequency at  $1419\text{ cm}^{-1}$  shifted slightly to  $1407\text{ cm}^{-1}$  and became more intense. Additional bands for the  $\text{C}-\text{O}$  stretching frequencies at  $1123$  and  $1017\text{ cm}^{-1}$  were present in the IR spectra and became more intensive with increasing proportions of  $\text{Ti}(\text{O}^i\text{Pr})_4$ . Figure 4.29 shows a series of IR spectra with  $\text{Ti}:\text{H}_2\text{O}=1:4$  and varying  $\text{Ti}:\text{COOH}$  ratios. No significant difference between each spectrum was observed. Even if the reaction products were hydrolysed, all IR spectra proved the coordination of the carboxylate groups to the titanium centres. It was concluded that the carboxylates retained coordination during the hydrolysis.

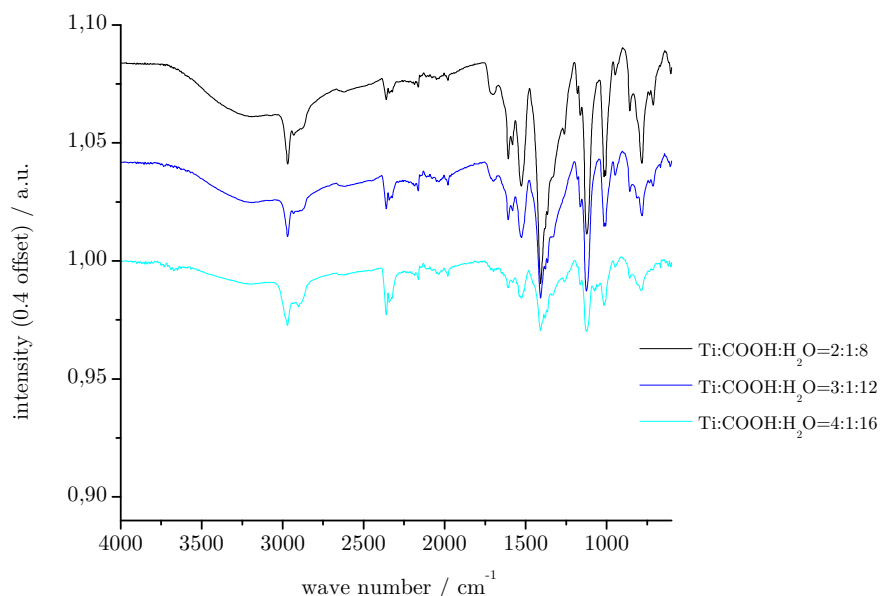


**Figure 4.29: IR spectra of  $\text{TiO\_BTB-4}$  with  $\text{Ti}:\text{H}_2\text{O}=1:4$  and varying  $\text{Ti}:\text{COOH}$  ratios (the spectra are plotted with an offset of 0.4 on the y axis)**

Once more, SAXS investigations were conducted to check whether the additional carboxylate groups compared to BTB-3 influenced the obtained structure. Figure 4.30 summarizes all obtained SAXS patterns for  $\text{TiO\_BTB-4}$  and shows a clear tendency in the structural features. All SAXS patterns had in common that a scattering maximum was observed between  $3$  and  $4\text{ nm}^{-1}$ ,

which was probably again caused by an ordering of the BTB-4 ligand. Although an additional carboxylate group was present in BTB-4 in comparison to BTB-3, the size of the ligand should be in a similar range. Thus, an ordering of the BTB-4 ligands led to scattering maxima of comparable range. The SAXS patterns could be distinguished by the applied Ti:H<sub>2</sub>O ratio. Samples prepared with Ti:H<sub>2</sub>O=1:2 resulted in slopes (linear part of the SAXS patterns between 0.1 and 0.5 nm<sup>-1</sup>) of  $q^{-3.2}$  to  $q^{-3.5}$ . If higher Ti:COOH ratios were applied, the slopes were slight smaller. In case of these less hydrolysed materials, a 3D structure was assumed. The periodic assemblies had a size between 0.60 and 0.68 nm in radius. The distances between these assemblies varied between 1.28 and 1.40 nm. Thus, the periodic assemblies were organised closer to each other compared to TiO\_BT-3, which was in line with lower microporous surface areas observed in the nitrogen sorption measurements and which will be discussed later.

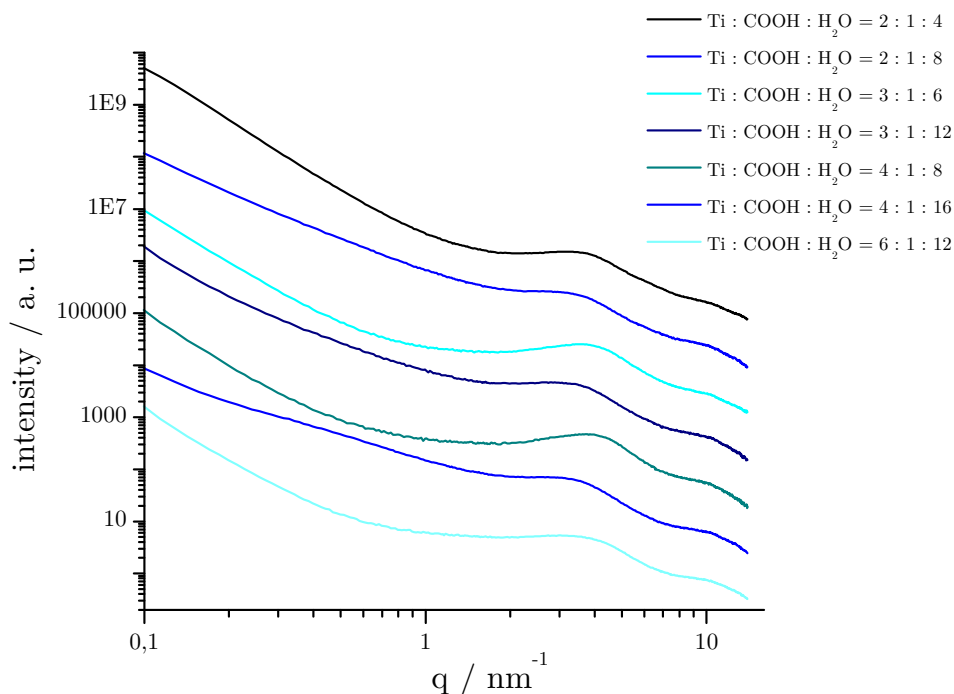


Figure 4.30: SAXS patterns of TiO\_BT-4 (the SAXS patterns are plotted with an offset of 50% on the y axis)

However, samples with Ti:H<sub>2</sub>O=1:4 showed a slope (linear part of the SAXS patterns between 0.1 and 1 nm<sup>-1</sup>) between  $q^{-2.0}$  and  $q^{-2.7}$ , which was assigned to a 2D layered structure. If the Ti:COOH ratio was increased, the hard sphere volume fraction revealed an enhanced ordering. The periodic assemblies were of 0.66 nm in radius. The distance between the periodic moieties was between 1.48 and 1.60 nm, which was in a comparable range with previously investigated TiO\_BT-3. The nearly planar geometry of BTB-4 additionally supported the 2D structure. The structure parameters derived from the SAXS patterns are summarised in Table 4.5.



**Table 4.5: Parameters of TiO\_BTBT-4 derived from the SAXS patterns**

Ti:COOH:H <sub>2</sub> O	R <sub>2</sub> / nm	d <sub>2</sub> / nm	$\eta$	Slope q <sup>-n</sup>
2:1:4	0.62	1.40	0.134	3.5
2:1:8	0.65	1.52	0.118	2.5
3:1:6	0.63	1.34	0.194	3.3
3:1:12	0.66	1.48	0.132	2.7
4:1:8	0.60	1.32	0.192	3.3
4:1:16	0.65	1.60	0.165	2.0
6:1:12	0.68	1.28	0.159	3.2

It was assumed that structural features were obtained, which were similar to the previously described MOF structures in Chapter 1.3.4. There, each BTB-4 ligand interconnected four metal ions. These assemblies were additionally interconnected by diamino ligands. In case of TiO\_BTBT-4, each tetracarboxylate connected four titanium building blocks. These titanium assemblies were additionally linked by Ti-O-Ti bridges. Varying the Ti:H<sub>2</sub>O ratio resulted in either planar or 3-dimensional interconnections by Ti-O-Ti bridges. Thus, various structural features were possible with the same titanium alkoxide/ligand system.

Additional investigations were done by nitrogen sorption measurements. Figure 4.31 summarizes all experiments with TiO\_BTBT-4. All investigated materials showed a high gas uptake at very low relative pressure, which was typical of micropores. A clear trend was observed with this material. Very high microporous surface areas were observed for Ti:H<sub>2</sub>O=1:4. Hereby, microporous surface areas up to 280 m<sup>2</sup>/g were determined. If a smaller Ti:H<sub>2</sub>O ratio was used, the surface area fell by around 100 m<sup>2</sup>/g. Microporous surface areas above 180 m<sup>2</sup>/g were observed for samples with Ti:H<sub>2</sub>O=1:2. Additionally, if the Ti:COOH ratio was risen, the surface areas stayed nearly constant.

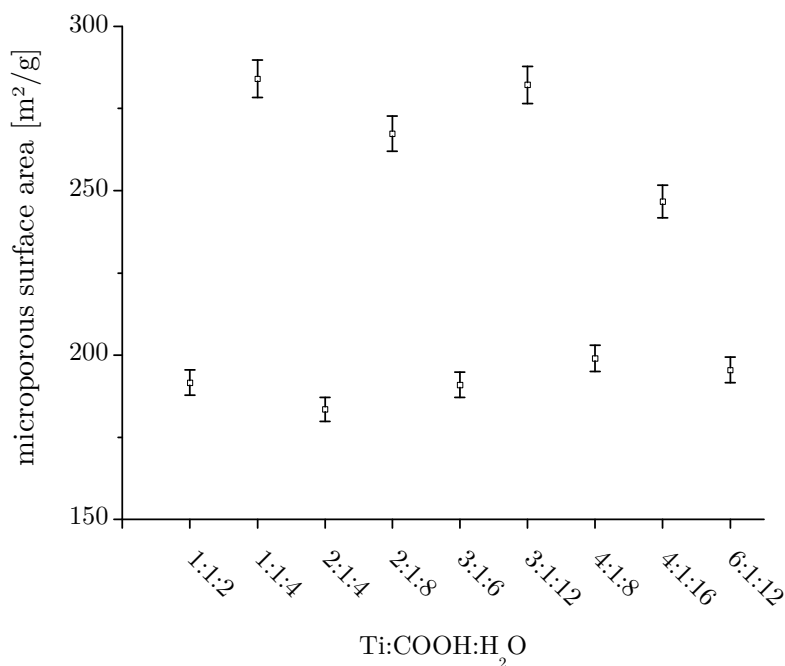


**Figure 4.31: Microporous surface area of TiO\_BT-4**

The nitrogen sorption experiments proved that ligands with more coordinating groups did not influence the obtained surface area. Moreover, the microporous surface areas decreased in comparison to TiO\_BT-3 by around 70 m<sup>2</sup>/g. It was assumed that the additional carboxylate groups increased the steric strain in the material. The fourth carboxylate group permitted another connection between the titanium building blocks and therefore decreased the pore volume and the corresponding microporous surface area.

## 4.6 Modification of Ti(O<sup>i</sup>Pr)<sub>4</sub> with tetrakis(4-carboxyphenyl)silane

Tetrakis(4-carboxyphenyl)silane was chosen because of the tetrahedral assembly of the carboxylate groups. It is a counterpart to BTB-4, where the four carboxylic groups were nearly in one plane. Reactions of TCPS with Ti(O<sup>i</sup>Pr)<sub>4</sub> yielded insoluble precipitates. (Figure 4.32)

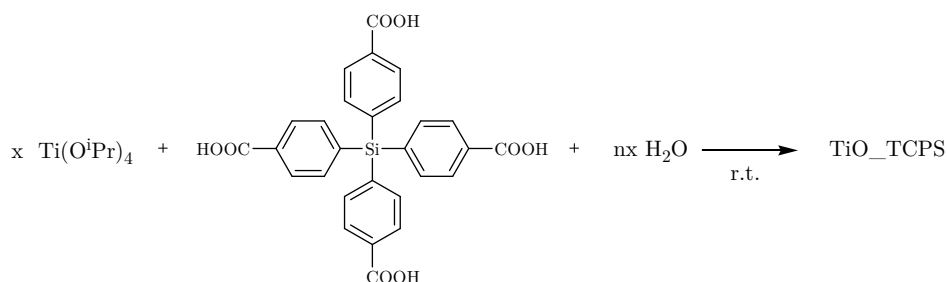


**Figure 4.32: Synthesis of TiO\_TCPS**

The materials were investigated by IR spectroscopic measurements. (Figure 4.33) The asymmetric C=O stretching frequency shifted from  $1680\text{ cm}^{-1}$  to  $1578$  and  $1524\text{ cm}^{-1}$  in the final material. Furthermore, a slight shift of the symmetric C=O stretching frequency from  $1420$  to  $1402\text{ cm}^{-1}$  was observed. An additional intensive band appeared at  $1100\text{ cm}^{-1}$ . This was in line with a coordination of all carboxylate groups to the titanium centres. The IR spectra were independent of the used  $\text{Ti}(\text{O}^i\text{Pr})_4$  proportions. No hints of uncoordinated carboxylic groups or ester groups were present in the IR spectra.

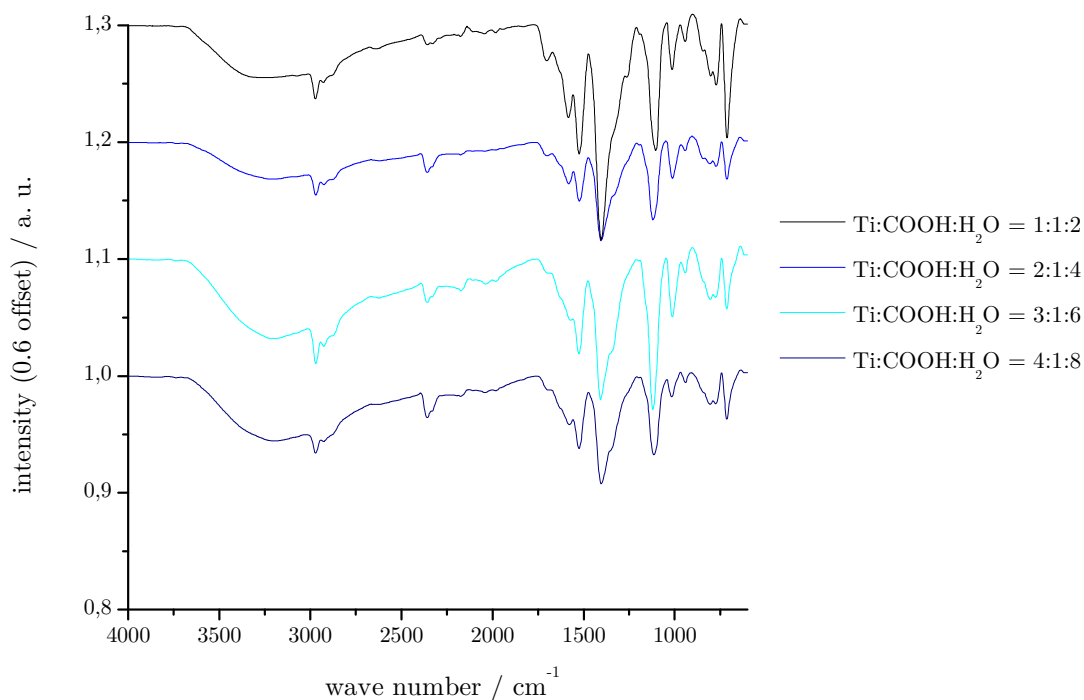


**Figure 4.33:** IR spectra of  $\text{TiO\_TCPS}$  (the spectra are plotted with an offset of 0.6 on the y axis)

Figure 4.34 shows the SAXS patterns of all  $\text{TiO\_TCPS}$  materials. The scattering maxima were in the similar  $q$  regions with BTB-3 and BTB-4. The ligand was of approximately comparable size, thus if the ligand molecules were ordered, a similar scattering maximum was expected. When the  $\text{Ti}:\text{H}_2\text{O}$  ratio was changed, slight differences were observed in the patterns. The SAXS patterns showed slopes in the range between  $q^{-3.1}$  and  $q^{-3.7}$  for the samples with  $\text{Ti}:\text{H}_2\text{O}$  ratio of 1:2 and 1:4. Slightly smaller slopes were observed in  $\text{Ti}:\text{H}_2\text{O}=1:2$ . Therefore, a 3D structure was assumed for all samples of  $\text{TiO\_TCPS}$ . The SAXS patterns revealed no influence of the  $\text{Ti}:\text{COOH}$  ratio. The hard sphere volume fraction, a hint for the ordering of the structure, remained constant around 0.2 for all investigated samples. The structure parameters derived from the SAXS patterns that are summarised in Table 4.6.

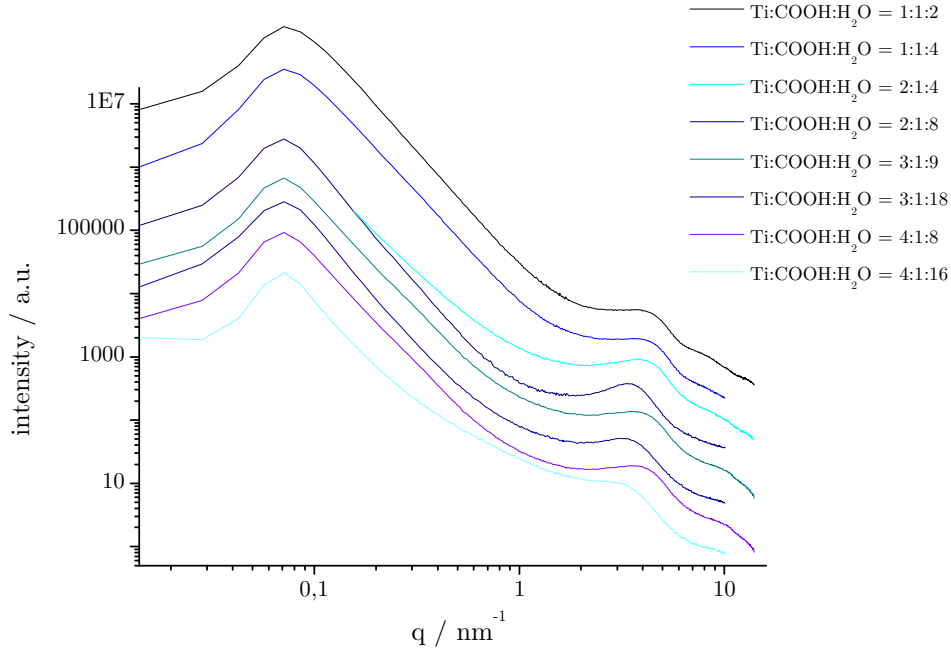


Figure 4.34: SAXS patterns of TiO\_TCPS (the SAXS patterns are plotted with an offset of 40% on the y axis)

Table 4.6: Parameters of TiO\_TCPS derived from SAXS patterns

Ti:COOH:H <sub>2</sub> O	R <sub>2</sub> / nm	d <sub>2</sub> / nm	$\eta$	Slope q <sup>-n</sup>
1:1:2	0.62	1.32	0.192	3.5
1:1:4	0.68	1.26	0.199	3.5
2:1:4	0.65	1.28	0.207	3.1
2:1:8	0.75	1.56	0.243	3.7
3:1:6	0.62	1.32	0.176	3.3
3:1:12	0.79	1.40	0.194	3.5
4:1:8	0.65	1.28	0.207	3.3
4:1:16	0.76	1.46	0.122	2.5

The periodic units were between 0.64 and 0.79 nm in radius and therefore slightly larger than those of TiO\_BT3 or TiO\_BT4. Materials with Ti:H<sub>2</sub>O=1:2 showed smaller periodic assemblies. The distances between these periodic assemblies were between 1.26 and 1.56 nm, which was in good agreement with previously investigated materials. Similar to TiO\_BT4, the titanium building blocks seemed to be interconnected by the TCPS ligand in all dimensions. In contrary to TiO\_BT4, it was not possible to adjust the obtained structure by applying the suitable Ti:H<sub>2</sub>O ratio. The tetrahedral orientation of TCPS probably prevented 2D layered structures.

Nitrogen sorption measurements (Figure 4.35) were performed to check whether trends, similar to TiO\_BT4, were observed with TiO\_TCPS. Most samples were microporous. Whereas all samples with Ti:H<sub>2</sub>O=2:1 showed a microporous surface area above 200 m<sup>2</sup>/g, the sample with risen Ti:H<sub>2</sub>O ratios resulted in dense materials or compounds with smaller surface area. The tendency was in contrary to the observations of TiO\_BT4, where higher microporous surface areas were obtained with Ti:H<sub>2</sub>O=4:1. It was assumed that the different ligand geometry led to this trend.

The tetrahedral positioning of the carboxylate groups enabled a better interconnection between titanium moieties. Compared to TiO\_BT-4, less water was needed for a 3D structure. The microporous surface area fell by a higher Ti:COOH ratio for compounds with Ti:H<sub>2</sub>O=2:1. This was in line with previously described observations of TiO\_BT-3. It was assumed that the decreased porosity was caused by the formation of a TiO<sub>2</sub> matrix.

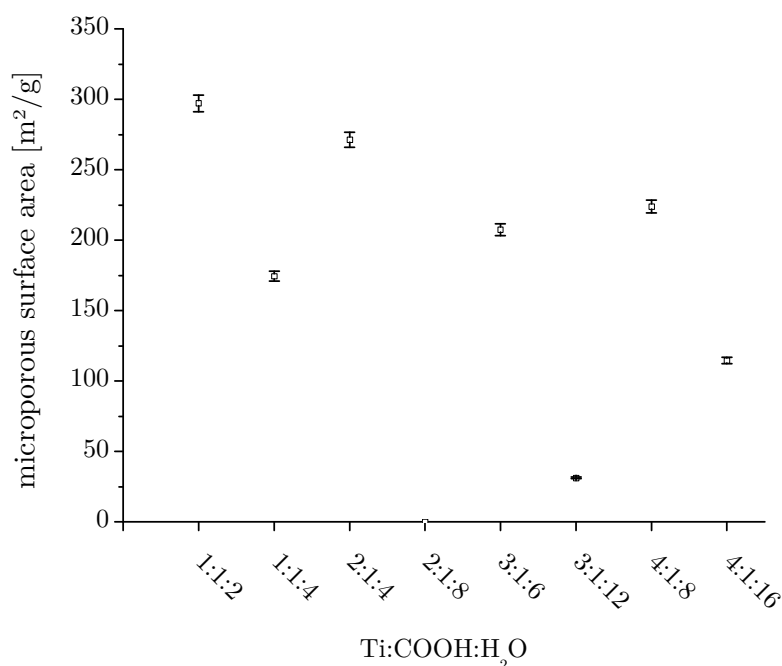


Figure 4.35: Microporous surface area of TiO\_TCPS

#### 4.7 Modification of Ti(OEt)<sub>4</sub> with adamantyl tetracarboxylic acid

Starting from the results of TiO\_BT-4 and TiO\_TCPS, a third tetracarboxylic acid was applied in the modification of Ti(OR)<sub>4</sub>. Adamantyl tetracarboxylic acid (ATC) was chosen because of its tetrahedral orientation of the carboxylic groups and the smaller linker. Reactions of Ti(OEt)<sub>4</sub> with ATC yielded off-white precipitates were insoluble in common organic solvents. (Figure 4.36)

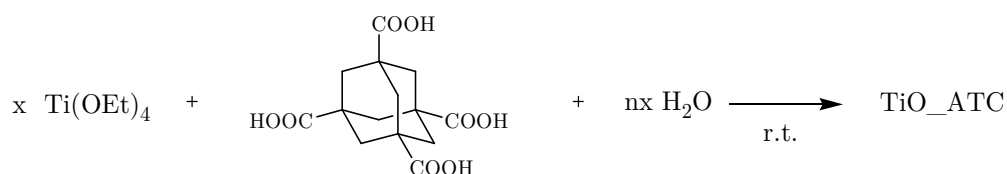


Figure 4.36: Synthesis of TiO\_ATC

SAXS investigations should again get insights in the structural features of TiO\_ATC. Figure 4.37 shows four nearly identical SAXS patterns. They all had slopes (linear part of the SAXS patterns

between 0.1 and 1 nm<sup>-1</sup>) between  $q^{-3.7}$  and  $q^{-4}$  in common, indicating a 3D structure. The structure was highly ordered; the hard sphere volume fraction was calculated around 0.2. The distance between the periodic assemblies depended on the Ti:COOH ratios. Ratios with Ti:COOH=2:1 and 4:1 resulted in short distances of around 0.70 to 0.96 nm, whereas ratios with Ti:COOH=1:1 and 3:1 resulted in longer distances around 1.34 to 1.72. Distances around 0.70 nm had never been observed before. However, the size of the periodic assembly was independent of the applied Ti:COOH ratio and remained constant between 0.34 and 0.50 nm in radius. Furthermore, the SAXS pattern of Ti:COOH=4:1 showed the known scattering maximum.

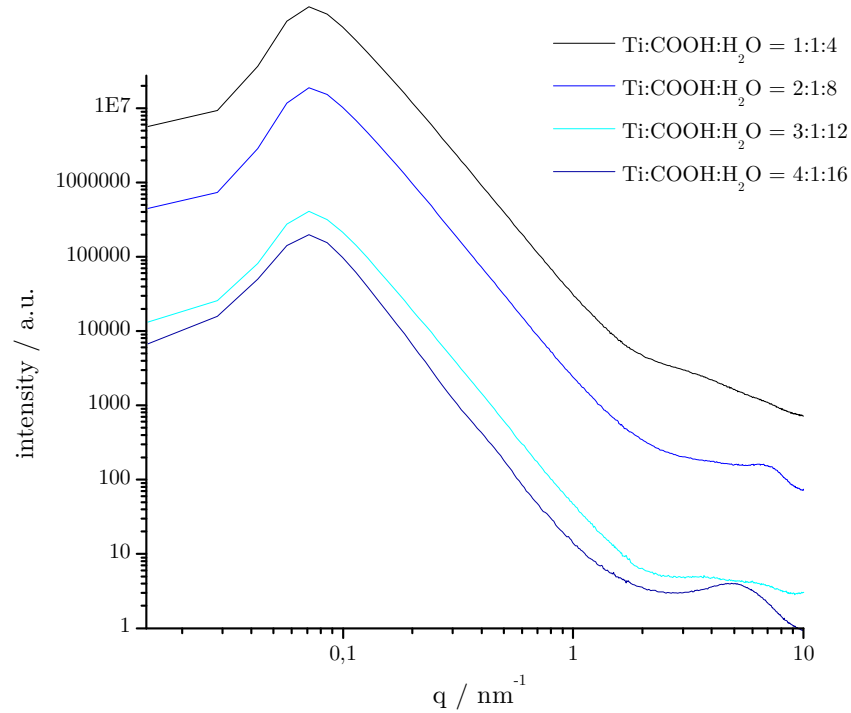


Figure 4.37: SAXS patterns of TiO\_ATC (the SAXS patterns are plotted with an offset of 40% on the y axis)

Table 4.7: Parameters of TiO\_ATC derived from SAXS patterns

Ti:COOH:H <sub>2</sub> O	R <sub>2</sub> / nm	d <sub>2</sub> / nm	$\eta$	Slope $q^{-n}$
1:1:4	0.50	1.72	0.070	3.7
2:1:8	0.46	0.70	0.226	3.7
3:1:12	0.34	1.34	0.196	3.7
4:1:16	0.48	0.96	0.21	4.0

Additional gas sorption experiments should check whether porosity and surface area were similar to TiO\_TCPS. According to the good results of TiO\_BTb-4 with Ti:H<sub>2</sub>O=1:4, samples were only prepared with this Ti:H<sub>2</sub>O ratio. Nitrogen sorption measurements (Figure 4.38) revealed microporosity for all investigated samples. The microporous surface areas were above 100 m<sup>2</sup>/g; a maximum was reached for Ti:COOH= 3:1 with 126 m<sup>2</sup>/g. Furthermore, a high external surface area was determined for Ti:COOH=2:1 and Ti:COOH=4:1. The surface areas were significantly

lower than those of TiO\_TCPS and TiO\_BTb-4. It was assumed that the fallen surface area was caused by the smaller linker of the ATC ligand.

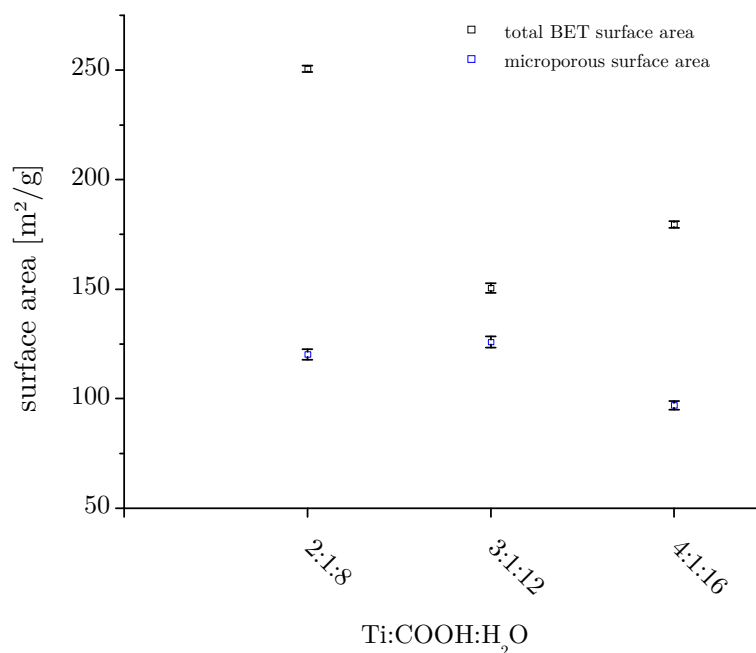
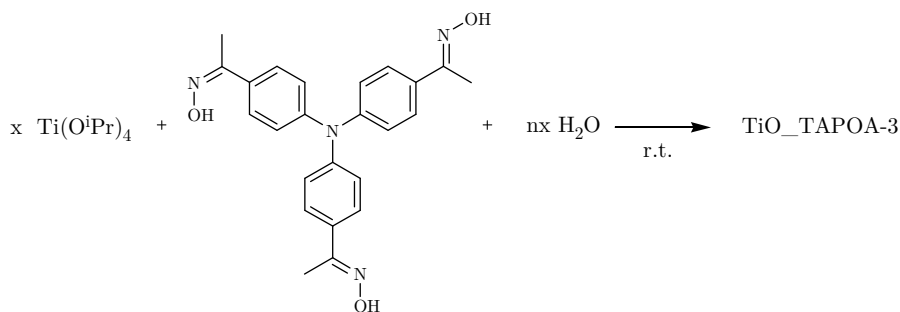


Figure 4.38: Surface area of TiO\_ATC

#### 4.8 Modification of Ti(O<sup>i</sup>Pr)<sub>4</sub> with tri(4-acetylphenyl-4-oxime)amine

All previous investigations only used tri- or tetracarboxylic acids for metal alkoxide modification. The experiments proved that all carboxylates were coordinated to the titanium building blocks. Porous and structured materials were obtained. Additional investigations should be carried out or taken under consideration with alternative functional groups with a comparable linker to check whether the functional groups would influence the obtained structural features.

Therefore, a trioxime was synthesised. The Ti-oximate bonds are known to retain the hydrolysis process. The dropwise addition of Ti(O<sup>i</sup>Pr)<sub>4</sub> to a solution of tri(4-acetylphenyl-4-oxime)amine (TAPOA-3) resulted in the formation of a yellow-coloured precipitate. Furthermore, an addition of stoichiometric proportions of water yielded TiO\_TAPOA-3, which was isolated by solvent evaporation. (Figure 4.39)



**Figure 4.39: Synthesis of TiO\_TAPOA-3**

The IR spectra (Figure 4.40) revealed two intensive bonds at 1598 and 1508  $\text{cm}^{-1}$ . They were in line with the IR spectra of the uncoordinated trioxime. Additional intensive bonds at 1276, 1008 and 935  $\text{cm}^{-1}$  matched well with the trioximate spectrum. This would indicate that the trioximate was not coordinated. Previous investigations with dioximes and  $\text{Ti}(\text{O}^i\text{Pr})_4$  had shown a similar behaviour (Chapter 3.9 and 3.10). There, no shifts of the  $\text{C}=\text{N}$  stretching frequency had been observed, although coordination had been proven by diffraction and spectroscopic methods.

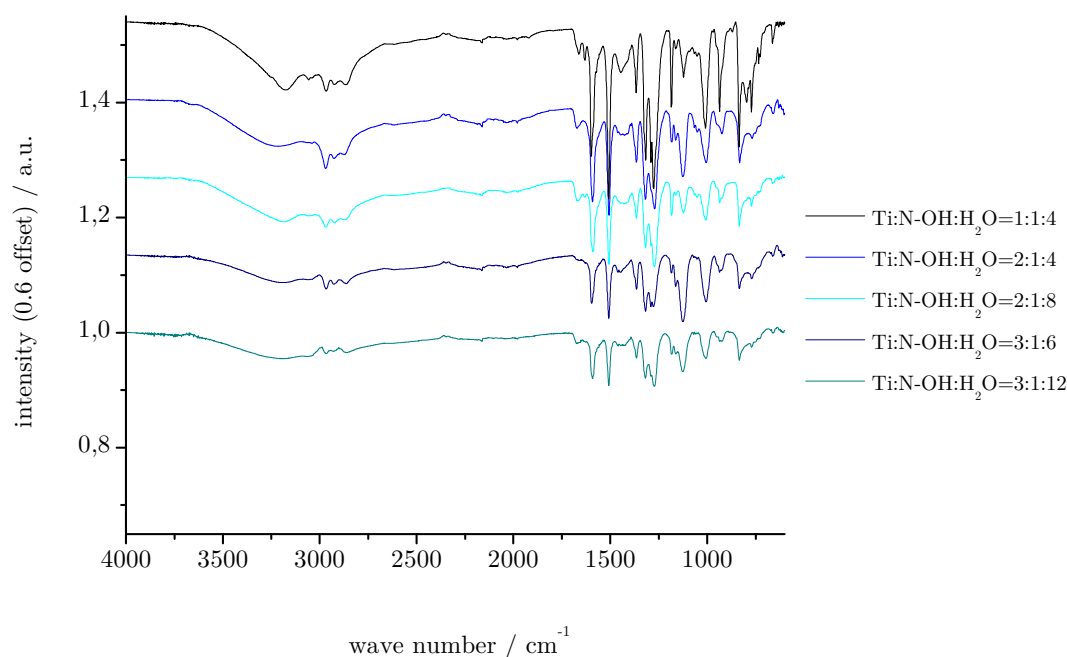


**Figure 4.40: IR spectra of TiO\_TAPOA-3 (the spectra are plotted with an offset of 0.6 on the y axis)**

Additional structure elucidation was carried out by SAXS measurements. (Figure 4.41) The SAXS patterns of all investigated samples showed a slope (linear part of the SAXS patterns between 0.1 and 1  $\text{nm}^{-1}$ ) in the range of  $q^{-2.7}$  and  $q^{-3.5}$ , which was in line with 2D to 3D structures for all materials. The hard sphere volume fraction was very low. No tendency was observed whether the ordering became better or worse with increasing Ti:N-OH or Ti:H<sub>2</sub>O ratio. The parameters, which were derived from the SAXS patterns, are shown in Table 4.8.



All samples showed a scattering maximum between 3 and 4 nm<sup>-1</sup>, which was previously observed in the carboxylate-based materials. In contrary to TiO\_BTb-3 and other carboxylate-based materials, the scattering maximum was also less defined with low Ti:N-OH ratios. The position of the scattering maxima seemed to be independent of the used functionality. Thus, the scattering maxima were derived from comparable ligand organisation.

In TiO\_TAPOA-3, the distances between the periodic assemblies varied between 1.34 and 1.38. No trend was observed, whether the distances became larger with increased Ti:N-OH:H<sub>2</sub>O ratios. The assemblies were 0.65 nm in diameter. The size of the assemblies remained constant with risen Ti:N-OH:H<sub>2</sub>O ratios. The size of the periodic building blocks was comparable with those of TiO\_BTb-3. This observation confirmed the postulation that the scattering maximum was caused by an organisation of the ligands and depended on the linker. The overall structure and the porosity depended on the used functionalities.

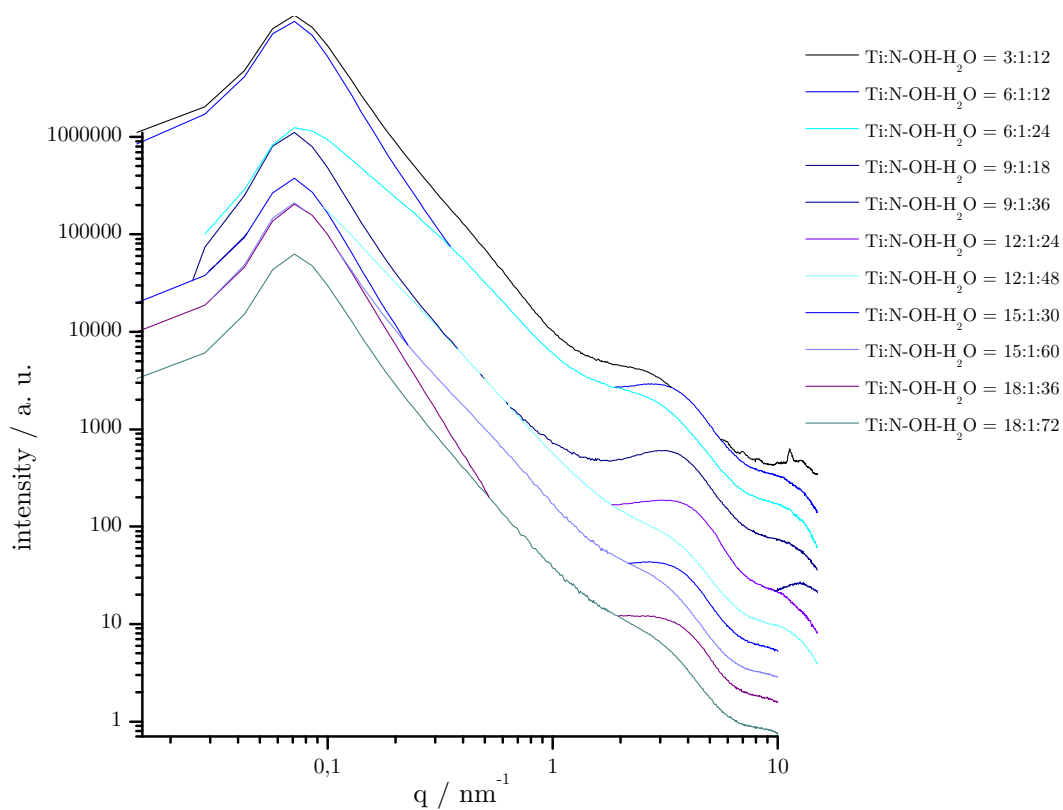


Figure 4.41: SAXS patterns of TiO\_TAPOA-3 (the SAXS patterns are plotted with an offset of 40% on the y axis)

**Table 4.8: Parameters of TiO\_TAPOA-3**

Ti:N-OH:H <sub>2</sub> O	R <sub>2</sub> /nm	d <sub>2</sub> / nm	$\eta$	Slope q <sup>-n</sup>
1:1:4	0.67	2.00	0.113	3.0
2:1:4	0.65	1.48	0.133	3.5
2:1:8	0.70	1.82	0.117	2.5
3:1:6	0.68	1.44	0.186	3.2
3:1:12	0.65	1.76	0.090	2.7
4:1:8	0.67	1.34	0.190	2.7
4:1:16	0.67	1.38	0.065	2.7
5:1:10	0.65	1.52	0.134	3.5
5:1:20	0.72	1.72	0.082	2.8
6:1:12	0.70	1.44	0.139	3.7
6:1:24	0.81	0.94	0.043	3.0

Nitrogen sorption measurements (Figure 4.42) showed an unexpected behaviour. Samples with low Ti:N-OH ratio showed no porosity. When the Ti:H<sub>2</sub>O ratio was varied, the surface area did not change. If the Ti:N-OH ratio was raised above 3:1, the samples became slightly porous. BET total surface areas above 150 m<sup>2</sup>/g were measured. In contrary to TiO\_BTBA-3 and other tri and tetracarboxylate-based hybrid materials, the samples were no longer microporous. Only TiO\_TAPOA-3 materials with Ti:N-OH ratios above 3:1 showed a microporous behaviour. It was assumed, that the controlled hydrolysis of unsubstituted Ti(O<sup>i</sup>Pr)<sub>4</sub>, which had to be present in the reactions with Ti:N-OH ratios up to 3:1, led to the observed porosity. Controlled hydrolysis experiments with Ti(O<sup>i</sup>Pr)<sub>4</sub> in THF proved this assumption.

The nitrogen sorption measurements proved that when other functional groups were used, significant differences were present. The structure of the titanium carboxylate materials was assumed to consist of titanium oxo clusters interconnected by the tri- and tetracarboxylate ligands. The clusters provided free space between the ligands, therefore pores were obtained. Titanium oxo clusters were also assumed as corresponding building blocks for oximate-based materials. Several titanium oxo oximate clusters had been reported.<sup>43</sup> It was assumed that similar structures and corresponding porosity could be observed with TiO\_TAPOA-3, and the titanium oxo oximate clusters led to a comparable interconnected structure. Investigations proved that these structural features could not be transferred from carboxylate- to oximate- based materials. This was either caused by a different interconnection of the trioximates or different titania-based building blocks.

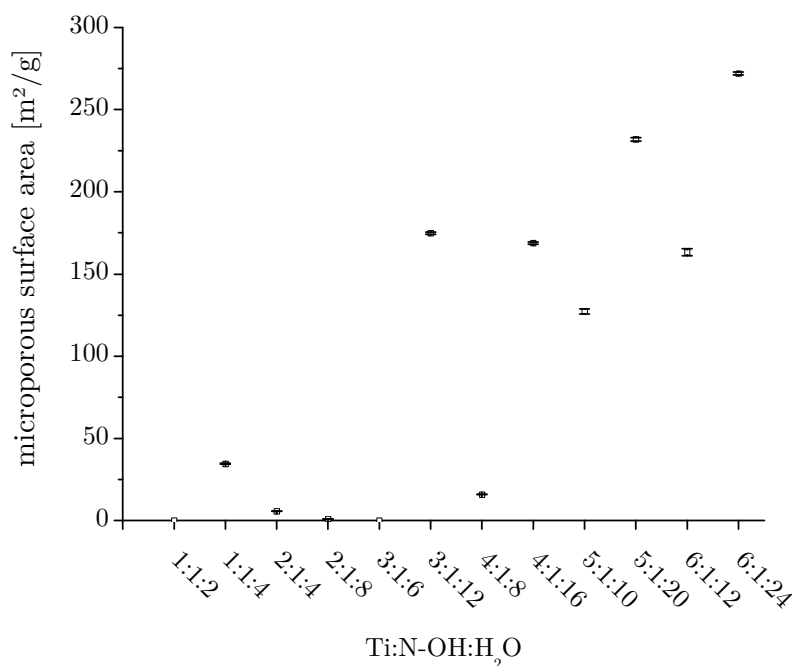


Figure 4.42: Total BET surface area of TiO\_TAPOA-3

## 4.9 Conclusions

Modification of titan alkoxides with tri- and tetrafunctional compounds resulted in insoluble residues, which were non-structured as well as non-porous. Nevertheless, the obtained complexes showed microporosity and 2D/3D structure if the coordination compounds were partially hydrolysed. Microporous surface areas up to 350 m<sup>2</sup>/g were observed in the nitrogen sorption measurements of these materials. IR spectroscopic investigations of the non-hydrolysed as well as the hydrolysed materials proved that the carboxylate groups remained coordinated to the titanium centres. Structure elucidation by small angle scattering showed, that the structure depended on the used ligand. Planar ligands preferred 2D layered as well as 3D structures, whereas a tetrahedral orientation of the carboxylate groups resulted more or less in 3D structured materials. Best results concerning porosity and structuring was achieved for TiO\_BTb-3. A network-like structure was assumed for all materials, in which tri-/tetracarboxylates bridged the titanium building blocks. It was assumed that dimeric titanium complexes or titanium oxo clusters were the building blocks.

Investigations with varying Ti:COOH and Ti:H<sub>2</sub>O ratios showed a certain tendency, which was observed for all titania-based materials. The higher the Ti:COOH ratio, the lower the microporous surface area was. This was caused by an additional TiO<sub>2</sub> matrix, which was formed around the Ti-carboxylate network and blocked the pores. Very low Ti:COOH ratios also resulted in materials with decreased surface areas as titanium precursor was missing to link the tri-/tetracarboxylates. Concerning the Ti:H<sub>2</sub>O ratio, a tendency was only observed with specific ligands, but no general trend was observed. Experiments with different ligand linkers showed a

shifting of the scattering maximum according to the size of the linker. Therefore, the observed scattering maxima were attributed an organisation of the ligands.

Investigations with the same ligand, BTB-3, and zirconium alkoxides resulted in similar materials. The microporous surface area was significantly smaller than that of the corresponding titanium material. Only 3D structured materials were obtained. The structuring itself was independent of the used metal alkoxide.

Experiments with other functional groups, such as oximates, showed completely different results in contrary to that of TiO<sub>2</sub>\_BTB-3. No microporosity was observed for these materials. The materials only became porous at higher Ti:COOH ratios, which was mainly caused by a porous unmodified TiO<sub>2</sub> network. It was assumed, that the oximates did not form similar building blocks as in the carboxylate-based materials. Additional experiments with tris[bis(*β*-diketones)] failed because of the inability to isolate the corresponding ligands. The investigations proved that the structure of these titania-based materials highly depended on the functional groups used for modification.

## 5 Summary

This thesis dealt with the pre-organisation of group(IV) metal alkoxides. These pre-structured precursors should be used for the formation of structured metal oxide materials, where the structuring was achieved without using any structure-directing agents (templates). Moreover, the pre-organisation should be achieved by a defined modification of the group(IV) metal alkoxides, which was stable during the sol-gel processing.

First access was given by the modification with bifunctional ligands, for which a polymeric or oligomeric structure would be possible. Bis( $\beta$ -diketones) were used, as they are known for their strong coordination to group(IV) metal centres. Reactions of numerous bis( $\beta$ -diketones) with different titanium alkoxides yielded metallacyclic structures of the type  $\{\text{Ti}[\text{bis}(\beta\text{-diketonate})](\text{O}^i\text{Pr})_2\}_2$ , the composition of which was elucidated by ESI mass spectrometry. In these metallacycles, both titanium centres were bridged by two bifunctional ligands. Additional low energy CID MS/MS scans proved that the remaining two alkoxo groups were in terminal position. DFT calculations were performed to check, which configuration was obtained. They proved that the *cis/cis*-configuration was the thermodynamically more stable isomer. Furthermore, the calculations only showed a small difference of 60 kJ/mol in Gibbs free energy between both isomers. Therefore, both isomers should exist at room temperature. Exemplarily, the *cis/cis* isomer is shown in Figure 5.1.

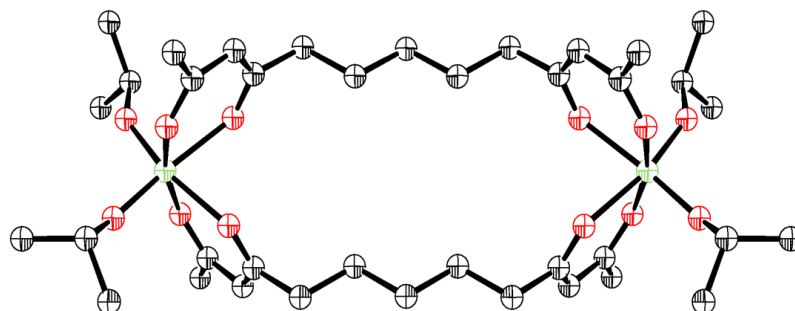


Figure 5.1: *Cis/cis* isomer of 4

When the experiments were extended to zirconium alkoxides, different structural features were observed with the alkylene-bridged bis( $\beta$ -diketones). While the pentylene-linked ligand resulted in a similar metallacycle with one additionally coordinated 2-propanol per zirconium centre, the hexylene- and octylene-linked ligand yielded dimeric complexes with three and four bridging bis( $\beta$ -diketonates). The structures of both complexes were confirmed by ESI-MS experiments.

Modification of group(IV) metal alkoxides with bis( $\beta$ -ketoesters) resulted in the same metallacyclic structures for titanium and zirconium alkoxides. In each case, a dimeric metallacycle with two bridging bis( $\beta$ -ketoesterates) and two residual, terminal alkoxides per metal centre was obtained. Solution NMR spectroscopy and ESI mass spectrometry were used for structure/composition elucidation. These complexes revealed an unexpected fragmentation pattern in

MS/MS scans, as no monomeric complex was formed, however, a partial cleavage of the  $\beta$ -ketoester groups occurred. Reactions of a mixture of  $\text{Ti}(\text{O}^i\text{Pr})_4$  and  $\text{Zr}(\text{O}^i\text{Pr})_4 \cdot {}^i\text{PrOH}$  with bis( $\beta$ -ketoesters) resulted in the partial formation of mixed metal metallacycles, as evidenced by the ESI full scan mass spectrum.

When dioximes were used for the modification of titanium alkoxide, different structural motives were observed. Crystals were obtained for two titanium alkoxo dioximates. Single crystal XRD showed a dimeric complex, in which both metal centres were bridged by two dioximate ligands and two additional alkoxo groups. One alkoxo group per titanium remained in terminal position. Each titanium atom was 7-fold coordinated. This was possible due to the lower bite angle of the oximate groups. Therefore, the titanium centre was not overcrowded. An example of alkoxo and dioximate bridged titanium complexes is given in Figure 5.2.

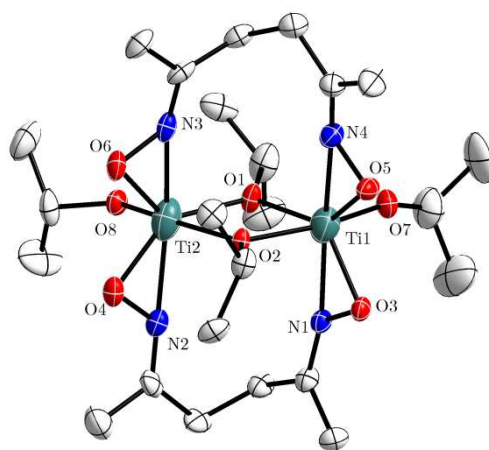


**Figure 5.2:** Molecular structure of **22** (the ellipsoids are drawn at 50% of the probability density function)

Mass spectrometric investigations confirmed the same structure from alcoholic solutions. Compared to titanium alkoxo bis( $\beta$ -diketonates), low energy CID MS/MS showed a different fragment pathway for the alkoxo bridged complexes. Product ions of type  $[\text{TiL}_2\text{Na}]^+$  were observed for both compounds. Solution NMR spectroscopy resulted in a similar structure in solution. 2D NMR experiments proved that the complex was highly dynamic.

Modification reactions were extended to arylene- and cyclohexylene-linked dioximes. Each of them resulted in titanium alkoxo complexes, which were hardly soluble in common organic solvents, excluding the corresponding alcohol. Although carbon and nitrogen solid state CP-MAS NMR spectroscopy proved the coordination of the ligand, MALDI- and ESI-MS remained unsuccessfully in the detection of the molecular composition. DSC measurements of one titanium cyclohexylene-linked dioximate complexes showed a glass transition, which was evidence of a polymeric arrangement. Numerous arylene-linked dioximes with less polar substituents were synthesised to improve the solubility, but all of them failed to result in complexes with increased solubility. Additional experiments were done in the field of tetradentate Schiff bases. Several bis(salicylaldiminate) ligands with flexible or rigid linkers were synthesised and applied in the

modification of group(IV) metal alkoxides. The reactions resulted in complexes of the same composition, which was also observed for the titanium alkoxo bis( $\beta$ -diketonates). A metallacyclic structure was obtained for zirconium as well as for titanium, in which the bis(salicylaldiminate) ligands bridged the  $M(OR)_2$  moieties. MS/MS scans proved that both alkoxo groups were in terminal positions. Surprisingly, the zirconium complexes were detected as the chloride-adduct and no third or fourth bridging bis(salicylaldiminate) ligand was observed, although quite flexible linkers were used. Additionally, NMR spectroscopy showed similar structural features in solution. Postulated structures for zirconium and titanium alkoxides with selected bis(salicylaldiminate) ligands are shown in Figure 5.3.

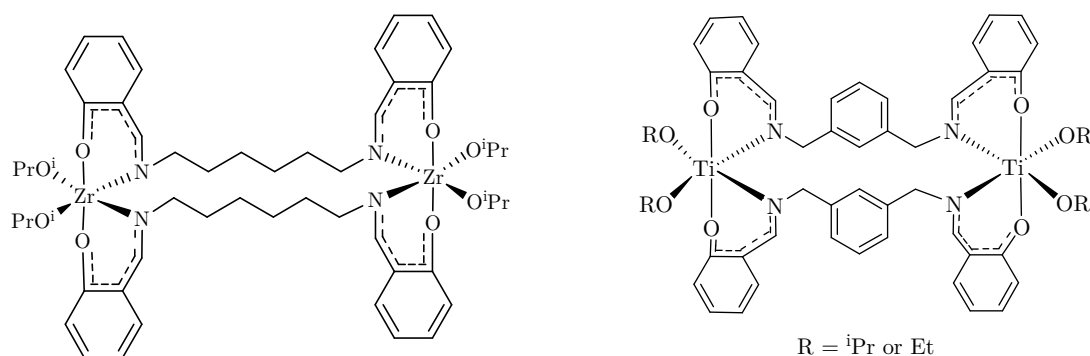


**Figure 5.3: Postulated structure of zirconium and titanium bis(salicylaldiminate) complexes**

Investigations with difunctional ligands resulted in numerous new dimeric complexes, the structural features of which, *i.e.* metallacycles with or without bridging alkoxo groups, had never been observed before in metal alkoxides. Dimeric complexes were the thermodynamically most stable configuration, however, and no polymers were observed with this approach except the complexes with cyclic-linked dioximates.

Another access for pre-structured group(IV) metal alkoxide precursors was the use of tri- and tetrafunctional ligands, with which network-like or MOF-like structures were formed with other transition metals. First reactions of  $Ti(O^iPr)_4$  with benzenetribenzoic acid resulted in precipitates, which were insoluble in common organic solvents. Nitrogen sorption and SAXS measurements resulted in non-porous and non-structured materials. It was assumed that a link between the titanium carboxylate moieties was missing due to non-hydrolysed alkoxo groups, and single layers of a titanium carboxylate network were formed. Therefore, partial hydrolysis was applied. IR spectroscopic measurements proved the coordination of the carboxylate groups. Nitrogen sorption measurements resulted in a microporous surface area up to 340 m<sup>2</sup>/g. The measurements showed the highest porosity with a Ti:COOH ratio of 1:1. SAXS investigations showed a 2D layered to a 3D structure, the ordering of which was lowered with increasing Ti:COOH ratio. A network-like structure was assumed, in which the tricarboxylates interconnected the titanium building blocks. Similar behaviour was also obtained for zirconia-based materials, although slightly lower surface areas were observed.

When the experiments were extended to tetracarboxylic acids, two different arrangements of the carboxylate groups were possible. The carboxylic groups were either in plane or tetrahedrally orientated. Reactions of benzenetetrabenzoic acid with  $\text{Ti}(\text{O}^i\text{Pr})_4$  resulted in titania-based materials with significantly lower surface areas compared to benzenetribenzoate-based materials. The microporous surface area additionally depended on the  $\text{Ti}:\text{H}_2\text{O}$  ratio. The higher the  $\text{Ti}:\text{H}_2\text{O}$  ratio the larger the surface area. The results were confirmed by SAXS measurements, where materials with  $\text{Ti}:\text{H}_2\text{O}=1:2$  showed a 3D structure, whereas  $\text{Ti}:\text{H}_2\text{O}=1:4$  showed a 2D structure.

Tetrakis(4-carboxyphenyl)silane was used as a ligand with tetrahedrally orientated carboxylate groups. The corresponding materials were all 3D structured with risen porosity with  $\text{Ti}:\text{H}_2\text{O}=1:2$ . More generally, materials with 2D structure had higher surface areas than the ones with a 3D structure.

Reactions with other polyfunctional compounds, such as trioximes, resulted in dense materials. Porosity was only observed for  $\text{Ti}:\text{N-OH}$  ratios up to 3:1. It was assumed that the functional group affected the formed titania-based building block.

When ligands with similar linker were used, SAXS measurements showed the same scattering maxima for all investigated carboxylate-based materials. It was assumed that these scattering maxima were caused by the same ordering of the ligands. Experiments with larger and smaller linkers led to a shift of the scattering maximum, which proved the dependence on the used ligands. Considering known MOF-like structures with titanium and zirconium, a group(IV) metal oxo cluster was assumed to be a potential building block, which was interconnected by the carboxylate ligands.



## 6 Experimental Section

### 6.1 General methods and materials

All manipulations were carried out in moisture- and oxygen-free atmosphere of dry argon using standard Schlenk or glove box techniques. Solvents were purified and desiccated by standard methods and stored under argon atmosphere over 4 Å molecular sieve.<sup>154</sup> The solvents for NMR spectroscopy (Eurisotop or Aldrich) were degassed prior to use and stored over molecular sieve. Titanium isopropoxide (Aldrich, 97 %), titanium ethoxide (Aldrich, techn.), titanium butoxide (Aldrich, 97 %), titanium tert-butoxide (Aldrich, purum), titanium tetrachloride (Aldrich, 98 %), titanium methoxide (95 %, Aldrich), zirconium isopropoxide iso-propanol adduct (ABCR, 99.9 %), zirconium butoxide (Aldrich, 80 % in butanol), acetone oxime (Aldrich, 99 %), acetophenone (Aldrich, 99 %), acetylacetone (Aldrich, 99 %), 4-acetylbiphenyl (Fluka, 99 %), acetyl chloride (Fluka, 99 %), 1,3,5,7-adamantanetetracarboxylic acid (ATC) (Waco, 92 %), 2-aminoethanol (Loba, p.a.), aluminium chloride (Fluka, 99 %), 1,4-benzenedimethanol (TCI, 99 %), benzoyl acetone (Aldrich, 99 %), bismuth triflate (Aldrich), 4-bromotoluene (Aldrich, 98 %), n-butyl lithium (Aldrich, 2.5 M in hexane), copper sulfate (Merck, p.a.), cyclohexanediol (Janssen, 99 %), 1,3-cyclohexanedione (Aldrich, 97 %), 1,4-cyclohexanedione (Aldrich, 98 %), 1,4-diacetylbenzene (Aldrich, 98 %), 1,4-diaminobenzene (Aldrich, 97 %), 1,6-diaminohexane (Aldrich, 98 %), 4,4'-diaminodicyclohexylmethane (BASF),  $\alpha,\alpha'$ -diamino-p-oxylen (Fluka, 98 %), 1,4-dibromobutane (Janssen, 97 %), 1,6-dibromohexane (Aldrich, 96 %), diethyl oxalate (Loba, purum), 4,4'-dihydroxy-3,3',5,5'-tetramethylbiphenyl (Aldrich, 98%), dimethyl isophthalate (Fluka, pur), dimethyl terephthalate (Aldrich, 99 %) 1,3-diiodopropane (Aldrich, 99 %), glutaraldehyde (25 % aqueous solution), hexabromobenzene (Aldrich, 98 %), 2,5-hexanedion (Fluka, 97 %), hydroxylamine hydrochloride (Loba, 98 %), isophthalaldehyde (Aldrich, 97 %), magnesium (Aldrich, 99 %), methylacetoacetate (Aldrich, 99 %), 4-methylacetophenon (EGA, 95 %), methyl benzoate (Aldrich, 99 %), dimethyl-2,6-naphthalenedicarboxylate (Aldrich, 98 %), potassium carbonate (Fluka, purum), salicylaldehyde (Fluka, purum), silicon tetrachloride (Aldrich, 99 %), sodium amide (Aldrich, 95 %), terephthalaldehyde (Aldrich, 99 %), terephthaloyl chloride (Fluka, purum), p-toluenesulfonic acid (Riedel de Haen, 99 %) were used as received.

### 6.2 Analytical techniques

#### 6.2.1 Single crystal X-ray diffraction

Single crystal X-ray diffraction experiments were performed at 100K on a Bruker-AXS SMART APEX II diffractometer with a CCD area detector and a crystal-to-detector distance of 5.0 cm using graphite-monochromated Mo- $K_\alpha$  radiation ( $\lambda = 71.073$  pm). Data were collected with  $\varphi$  and  $\omega$ -scans and 0.5° frame width. The data were corrected for polarization and Lorentz effects, and an empirical absorption correction (SADABS) was applied. The cell dimensions were refined with

all unique reflections. The structures were solved with direct methods (SHELXS97), and refinement to convergence was carried out with the full-matrix least squares method based on  $F^2$  (SHELXL97) with anisotropic structure parameters for all non-hydrogen atoms. The hydrogen atoms were placed on calculated positions and refined riding on their parent atoms.<sup>155,156,157</sup>

### 6.2.2 Nuclear magnetic resonance spectroscopy

$^1\text{H}$  and  $^{13}\text{C}$  solution NMR spectra were recorded on a Bruker AVANCE 250 (250.13 MHz  $\{^1\text{H}\}$ , 62.86 MHz  $\{^{13}\text{C}\}$ ) and a Bruker AVANCE DPX 300 spectrometer (300.13 MHz  $\{^1\text{H}\}$ , 75.47 MHz  $\{^{13}\text{C}\}$ ) equipped with a 5 mm inverse-broadband probe head and a  $z$ -gradient unit. 2D NMR spectra were measured with Bruker standard pulse programs COSY (Correlation Spectroscopy), TOCSY (Total Correlation Spectroscopy), HSQC (Heteronuclear Single Quantum Correlation), and HMBC (Heteronuclear Multiple-Bond Correlation). Solid state  $^{13}\text{C}$  and  $^{15}\text{N}$  NMR spectra were recorded on a Bruker AVANCE 300 (75.40 MHz  $\{^{13}\text{C}\}$ , 30.38 MHz  $\{^{15}\text{N}\}$ ,  $\delta_{\text{N}}(\text{NH}_4\text{Cl}) = 0$  ppm) equipped with a 4 mm broadband MAS probe head. The spectra were recorded with ramped CP/MAS spectra (cross-polarization and magic angle spinning) with a rotor spinning speed of 6–8 kHz.

### 6.2.3 Mass spectrometry

Electrospray Ionization Mass Spectrometry were performed on a Bruker Daltonics Esquire 3000plus 3D-ion trap mass spectrometer fitted with an orthogonal electrospray ion source and operated in the positive-ion mode. The spray voltage was maintained at -4 kV, the drying gas temperature was set to 200°C and all source voltages were optimized for maximum molecular ion transmission (i. e. the sodiated molecule). In the low energy CID MS/MS experiments, the isolation width was typical set to 10 Da in order to cover to entire isotopic distribution of the selected precursor ion. The fragmentation amplitude was manually set to 0.5-1 V in order to induce abundant product ion formation. The samples were prepared either in pure 2-propanol, ethanol or in a chloroform/alcohol mixture at a concentration of 1 mg/mL. The solutions were directly infused via a syringe pump into the ESI-source at a flow rate of 3  $\mu\text{L}/\text{min}$ . All calculated  $m/z$  values of the titanium complexes were based on the naturally most abundant  $^{48}\text{Ti}$  isotope, the ones of the zirconium complexes based on the most abundant  $^{90}\text{Zr}$  isotope.

MALDI-MS evaluation (for **25** and **26**) was performed by means of a Shimadzu Kratos Analytical Axima CFR<sup>+</sup> in the positive ion mode applying standard MALDI matrices.

#### 6.2.4 Infrared spectroscopy

FT-IR spectra were recorded on a Bruker Tensor 27 working in ATR MicroFocusing MVP-QL with a diamond crystal or in d<sup>1</sup>-Chloroform solution, using OPUS version 4.0 software for analysis. Resolution was set to 2-4 cm<sup>-1</sup> in a range from 4000 to 600 cm<sup>-1</sup>.

#### 6.2.5 Gas sorption measurement

Nitrogen sorption measurements were carried out on a Micromeritics ASAP 2020 or an ASAP 2010 instrument at 77 K. The samples were degassed at 50°C prior to measurement to reach a pressure below 9 µmHg. The total surface area was calculated using the adsorption model by Brunauer, Emmet and Teller (BET), the microporous surface area was calculated by the t-plot method. The argon sorption measurements were carried out on a Micromeritics ASAP 2020 with microporous option. The measurements were performed as described for nitrogen. Total surface area and microporous surface area were calculated in a similar way, the pore size distribution was calculated by the method of Horvath-Kawazoe for slit-like pores.

#### 6.2.6 Small angle X-ray scattering

SAXS was performed with a rotating anode generator (Bruker Nanostar, turbospeed solution), CuK<sub>α</sub> radiation monochromatized and collimated with crossed Goebel mirrors and equipped with a pinhole camera. The patterns were detected with a 2D position sensitive detector (Vantec 2000) and radially averaged to obtain the scattering intensity in dependence on the scattering vector  $q=4\pi/\lambda \sin(\theta)$ . The wavelength is 0.1542 nm and  $2\theta$  is the scattering angle.

The SAXS patterns were fitted by a Beaucage function. The radius of the periodic assembly  $R_2$  was derived from the resulting radius of gyration. The distance between the periodic assemblies  $d_2$  was calculated from the hard-sphere radius, which was derived from the structure factor of the Beaucage function. The standard deviation the fits is known to be around 5%.

#### 6.2.7 X-ray powder diffraction

X-ray diffraction (XRD) analyses of powders were carried out on a Philips X-Pert Pro diffractometer system [Cu K<sub>α1,2</sub> radiation ( $\lambda=1.54060, 1.54439$  Å) equipped with an X-Celerator multi-channel detector, Bragg Brentano geometry, silicon single crystal sample holder]. The diffraction pattern was recorded between 5 and 70° ( $2\theta$ ) with 0.2 s/step and a step size of 0.02°.

### 6.2.8 Dynamic light scattering

Dynamic light scattering (DLS) measurements were carried out using an ALV/CGS-3 Compact Goniometer controlled by an ALV/LSE-5003 Multiple Tau Digital Correlator (ALV-GmbH, Germany) at a scattering angle of 90° under temperature control.

### 6.2.9 Density functional calculations

All geometries were optimized at the B3LYP/6-31G(d,p) level of theory<sup>158,159</sup> known to produce reliable results with regard to convergence of structural parameters.<sup>160,161</sup> The basis sets used in this study are provided at <https://bse.pnl.gov/bse/portal>. Geometry optimizations were carried out of compound **4**, and additional frequency calculations were carried out to ensure that the resulting geometries were minima on the potential energy surface. The <sup>13</sup>C NMR shielding calculations were carried out using the gauge including atomic orbital (GIAO) method, again in conjunction with the hybrid B3LYP functional and the 6-31G(d,p) basis set.<sup>162</sup> To facilitate the comparison of calculated and experimental chemical shifts, the calculated isotropic shielding constants were converted into chemical shifts using tetramethylsilane (TMS) as a reference: for this purpose, the shielding constants for TMS were calculated at the same level of theory used in the study. All calculations were carried out with the Gaussian 03 suite of programs (revision D.01).<sup>163</sup>

## 6.3 Synthesis of the ligands

### 6.3.1 Synthesis of arylene-bridged bis(*β*-diketones)

1,1-(1,3-Phenylene)-bis-butane-1,3-dione and 1,1-(1,4-phenylene)-bis-butane-1,3-dione were synthesised according to references 164 and 51. 1,1-(1,6-Naphtylene)-bis-butane-1,3-dione was synthesised by the same procedure.

### 6.3.2 Synthesis of alkylene-bridged bis(*β*-diketones)

2,4,10,12-Tridecanetetrone was synthesised by a modified method according to Ref. 165.

A solution of 4.4 mL (43 mmol) of 2,4-pentandione in dry THF (100 mL) was cooled to 0 °C and 1.25 g (52 mmol) of NaH was added stepwise. After stirring this white suspension for 20 min, 19 mL of n-butyllithium (2.5 M in hexane) was added dropwise at 0 °C over 10 min. The clear yellow solution was allowed to react with 2.5 mL (21.5 mmol) of 1,3-diiodopropane over a period of 20 min. The reaction was allowed to warm to room temperature and stirred for 4 h. The solution was poured into an acidic ice/water mixture (pH=2). The organic layer was extracted with diethylether, washed with brine and water and dried over sodium sulphate. The solvent was re-

moved by evaporation in a rotary evaporator, which gave a yellowish solid residue. After recrystallisation from methanol a white crystalline solid was obtained.

$^1\text{H}$  NMR (250 MHz,  $\text{CDCl}_3$ ):  $\delta$  5.49 (s, 2H,  $\text{COCHCO}$ ), 2.26 (t, 4H,  $\text{CH}_2\text{CH}_2\text{CO}$ ), 2.05 (s, 6H,  $\text{COCH}_3$ ), 1.55 (t, 4H,  $\text{COCH}_2\text{CH}_2$ ), 1.30 (m, 2H) ppm.  $^{13}\text{C}$  NMR (62.86 MHz,  $\text{CDCl}_3$ ):  $\delta$  194.2 ( $\text{CHCOHCH}_2$ ), 191.4 ( $\text{CHCOHCH}_3$ ), 99.7 ( $\text{COCHCO}$ ), 38.2 ( $\text{COCH}_2\text{CH}_2$ ), 29.1 ( $\text{CH}_3\text{CO}$ ), 25.6 ( $\text{CH}_2$ ), 24.9 ( $\text{CH}_2$ ) ppm. IR ( $\text{cm}^{-1}$  ATR):  $\nu$  = 2930, 2850, 1624 ( $\text{C=O}$ ), 1596 ( $\text{C=C}$ ), 1411, 1214, 1129, 901, 781.

2,4,11,13-Tetradecanetetron and 2,4,13,15-hexadecanetetron were synthesised in a similar manner by using 1,4-dibromobutane and 1,6-dibromohexane instead of 1,3-diiodopropane.

### 6.3.3 Synthesis of 1,1,2,2-tetraacetyethane (taet)

This ligand was synthesised according to reference 64.

### 6.3.4 Synthesis of bis( $\beta$ -ketoester)

Bis-3-oxo-butanoic acid-1,1'-[1,4-phenylenebis(methylene)] ester { $\beta$ -ketoester 1} and bis-3-oxo-butanoic acid-1,4-cyclohexanediyl ester { $\beta$ -ketoester 2} were synthesised according to reference 166.

#### 6.3.4.1 Synthesis of 3-Oxo-butyric acid-1,1'-(1,5-pentyl) ester [ $\beta$ -ketoester-3]

5 g (0.048 mmol) of 1,5-pentandiole and 11.37 ml (106 mmol) of methyl acetoacetate were dissolved in 20 ml of THF, and 0.804 g (3 mmol) of iodine was added. The solution was heated under reflux over night. The reaction mixture was washed with sodium thiosulfate solution and brine and dried over sodium sulfate. Evaporation of the solvent yielded a brown oily residue, which was purified by column chromatography.

$^1\text{H}$  NMR (250 MHz,  $\text{CDCl}_3$ ):  $\delta$  3.92 (t, 4H,  $\text{OCH}_2\text{CH}_2$ ), 3.45 (s, 4H,  $\text{COCH}_2\text{COO}$ ), 2.04 (s, 6H,  $\text{CH}_3\text{CO}$ ), 1.45 (m, 4H,  $\text{CH}_2\text{CH}_2\text{CH}_2$ ), 1.20 (m, 2H,  $\text{CH}_2\text{CH}_2\text{CH}_2$ ) ppm.  $^{13}\text{C}$  NMR (62.86 MHz,  $\text{CDCl}_3$ ):  $\delta$  200.8 ( $\text{CH}_3\text{COCH}_2$ ), 167.1 ( $\text{CH}_2\text{COOCH}_2$ ), 65.0 ( $\text{COOCH}_2\text{CH}_2$ ), 49.8 ( $\text{COCH}_2\text{CO}$ ), 29.9 ( $\text{CH}_2\text{CH}_2\text{CH}_2$ ), 28.1 ( $\text{CH}_2\text{CH}_2\text{CH}_2$ ), 25.2 ( $\text{CH}_3\text{CO}$ ) ppm.

#### 6.3.4.2 Synthesis of 3-Oxo-butyric acid-1,1'-[4,4'-(3,5,3',5'-tetramethyl)biphenyl] ester { $\beta$ -ketoester 4}

5.78 ml (98.8 mmol) of diketene was diluted in 50 ml of THF and 0.44 ml (3.18 mmol) of triethylamine was added. The solution was cooled to 0 °C and 4.91 g (22.7 mmol) of 4,4'-dihydroxy-3,3',5,5'-tetramethylbiphenyl was added in small portions. The reaction mixture was

stirred at this temperature for 30 min and was then allowed to warm up to room temperature. After stirring over night the suspension was poured in a dichloromethane/water mixture. After extraction with dichloromethane the combined organic phases were washed with water and brine and dried over sodium sulfate. Evaporation of the solvent and recrystallisation in toluene yielded a white crystalline powder.

$^1\text{H}$  NMR (250 MHz,  $\text{C}_6\text{D}_6$ ):  $\delta$  7.13 (s, 4H, aryl-CH), 3.10 (s, 4H,  $\text{COCH}_2\text{COO}$ ), 2.21 (s, 6H,  $\text{CH}_3\text{CO}$ ), 1.67 (s, 12H,  $\text{CH}_3\text{-C-aryl}$ ) ppm.  $^{13}\text{C}$  NMR (62.86 MHz,  $\text{d}^6\text{-DMSO}$ ):  $\delta$  201.6 ( $\text{CH}_3\text{COCH}_2$ ), 165.8 ( $\text{CH}_2\text{COOCH}_2$ ), 147.7 (aryl-C), 137.7 (aryl-C), 130.7 (aryl-C), 127.5 (aryl-CH), 49.5 ( $\text{OCH}_2\text{CH}_2$ ), 30.8 ( $\text{CH}_3\text{CO}$ ), 15.6 ( $\text{CH}_3\text{-C-aryl}$ ) ppm.

### 6.3.5 Synthesis of butanoic acid-3-oxo-3-(triethoxysilyl)propyl ester { $\beta$ -ketoester 5}

4.15 g (30.5 mmol) of allyl acetoacetate and 5 g (30.5 mmol) of triethoxysilane were dissolved in 30 ml toluene. After addition of three drops Karstedt catalyst the reaction solution was stirred for 48 h at 50 °C. The remaining solvent and reactants were removed by distillation. The crude product was dissolved in toluene again and filtered over charcoal to get rid of the catalyst.

Evaporation of the solvent resulted in an oily product.

$^1\text{H}$  NMR (250 MHz,  $\text{CDCl}_3$ ):  $\delta$  4.08 (t, 2H,  $\text{OCH}_2\text{CH}_2$ ), 3.77 (q, 6H,  $\text{CH}_3\text{CH}_2\text{O}$ ), 3.41 (s, 2H,  $\text{COCHCOO}$ ), 2.25 (s, 3H,  $\text{CH}_3\text{CO}$ ), 1.71 (m, 2H,  $\text{CH}_2\text{CH}_2\text{CH}_2$ ), 1.18 (t, 9H,  $\text{CH}_3\text{CH}_2\text{O}$ ), 0.60 (t, 2H,  $\text{SiCH}_2\text{CH}_2$ ) ppm. IR ( $\text{cm}^{-1}$  ATR):  $\nu$  = 2975 (C-H), 1717 (C=O), 1650 (C=O), 1239, 1151, 1073 (Si-O), 956, 791.

### 6.3.6 Synthesis of 1,5-diphenyl-pentane-1,3,5-trione

The synthesis was done in a modified method described by Miles *et al.*<sup>167</sup>

2.47 g (103 mmol) of sodium hydride was suspended in 40 ml of THF and heated a reflux. A solution of 5 g (30.8 mmol) of benzoylacetone in 25 ml of THF was added dropwise. The suspension was stirred for 30 min, meanwhile it turned orange. Afterwards 3.2 ml (25.7 mmol) of methyl benzoate was added and the reaction mixture was heated at reflux over night. After addition of further diethylether the remaining sodium hydride was quenched with ethanol/water. The solution was extracted with diethylether, and the combined organic phases were washed with 1% sodium hydroxide solution and water. The organic phase was poured on an HCl/ ice mixture. The precipitation was collected by filtration and purified by recrystallisation from ethanol.

$^1\text{H}$  NMR (250 MHz,  $\text{CDCl}_3$ ):  $\delta$  14.73 (s, C-OH), 7.98 (d, aryl-CH), 7.81 (d, aryl-CH), 7.34-7.57 (m, aryl-CH), 6.29 (s,  $\text{COCHCO}$ ), 6.00 (s,  $\text{COCHCO}$ ), 4.08 (s,  $\text{COCH}_2\text{CO}$ ) ppm.  $^{13}\text{C}$  NMR (62.86 MHz,  $\text{CDCl}_3$ ):  $\delta$  194.1 (C=O), 191.0 (C=O), 182.1 (C=O), 173.7 (C-OH), 136.3 (aryl-C), 134.0 (aryl-C), 133.8 (aryl-C), 133.7 (aryl-C), 132.6 (aryl-C), 131.7 (aryl-C), 128.8 (aryl-CH), 128.7 (aryl-CH), 127.1 (aryl-C), 126.4 (aryl-CH), 96.8 ( $\text{COCHCO}$ ), 50.6 ( $\text{COCH}_2\text{CO}$ ) ppm.

### 6.3.7 Synthesis of 1,6-diphenyl-hexane-1,3,4,6-tetraone

3.00 g (40 mmol) of sodium ethoxide was suspended in diethylether and a mixture of 5.2 ml (44 mmol) of acetophenone and 3.00 ml (22 mmol) of diethyl oxalate was added. The suspension turned yellow immediately. Stirring at room temperature was continued for 96 h. The product was precipitated by addition of petroleum ether. The dry product was stirred in 1 M acetic acid. Filtration of the crude product and recrystallisation from chloroform/ethanol yielded yellow needle like crystal.

$^1\text{H}$  NMR (250 MHz,  $\text{CDCl}_3$ ):  $\delta$  8.00 (d, 4H, aryl-CH), 7.55 (t, 2H, aryl-CH), 7.48 (d, 4H, aryl-CH), 7.11 (s, 2H, COCHCO) ppm.

### 6.3.8 Synthesis of dioximes

All oximes were synthesised in a modified method described by Bousquet.<sup>168</sup>

In a typical procedure 14.5 g (209 mmol) of hydroxylamine hydrochloride was dissolved in 50 mL of deionized water, and the solution was cooled to 0°C. 87 mmol of the diketone/ dialdehyde was added dropwise. After 30 min of stirring at room temperature a solution of 14.4 g (104 mmol) of potassium carbonate in 25 ml of deionized water was added. The solution was stirred at ambient temperature over night. The formed precipitates was filtered off and recrystallised from EtOH or  $^i\text{PrOH}$ .

#### 6.3.8.1 1,5-Pentanedial-1,5-dioxime

$^1\text{H}$  NMR (250 MHz,  $\text{d}^6\text{-DMSO}$ ):  $\delta$  10.77 (s, 2H, N-OH), 6.64 (s, 2H  $\text{CH}=\text{N}$ ), 2.20 (t, 4H,  $\text{CH}_2\text{CH}_2\text{CN}$ ), 1.54 (m, 2H,  $\text{CH}_2\text{CH}_2\text{CH}_2$ ) ppm.  $^{13}\text{C}$  NMR (62.86 MHz,  $\text{d}^6\text{-DMSO}$ ):  $\delta$  150.5 ( $\text{CHNCH}_2$ ), 25.7 ( $\text{CNCH}_2\text{CH}_2$ ), 23.0 ( $\text{CH}_2\text{CH}_2\text{CH}_2$ ) ppm. IR ( $\text{cm}^{-1}$ , ATR):  $\nu$  = 3182, 2080, 2932, 2863, 1665, 1439, 1326, 1292, 1225, 1037, 933, 914, 856, 811, 751, 721, 709.

#### 6.3.8.2 2,5-Hexanedione-2,5-dioxime

$^1\text{H}$  NMR (250 MHz,  $\text{d}^6\text{-DMSO}$ ):  $\delta$  10.3 (s, 2H, N-OH), 2.25 (s, 4H,  $\text{CH}_2\text{CH}_2\text{CN}$ ), 1.69 ppm (s, 6H,  $\text{CH}_3\text{CN}$ ).  $^{13}\text{C}$  NMR (62.86 MHz,  $\text{d}^6\text{-DMSO}$ ):  $\delta$  155.3 ( $\text{CH}_3\text{CNCH}_2$ ), 32.5 ( $\text{CNCH}_2\text{CH}_2$ ), 13.5 ( $[\text{CH}_3]_2\text{CN}$ ) ppm. IR ( $\text{cm}^{-1}$ , ATR):  $\nu$  = 3228, 3175, 2917, 1675, 1459, 1428, 1371, 1306, 1202, 998, 943, 823, 760, 727, 615.

#### 6.3.8.3 1,4-cyclohexanedione-1,4-dioxime

$^1\text{H}$  NMR (250 MHz,  $\text{d}^6\text{-DMSO}$ ):  $\delta$  10.33 (s, 2H, N-OH), 2.43 (t, 4H,  $\text{CH}_2$ ), 2.34 (t, 4H,  $\text{CH}_2$ ) ppm.  $^{13}\text{C}$  NMR (62.86 MHz,  $\text{d}^6\text{-DMSO}$ ):  $\delta$  156.6 ( $(\text{CH}_2)_2\text{CN}$ ), 26.9 ( $\text{CH}_2\text{CH}_2\text{C}$ ), 23.9 ( $\text{CH}_2\text{CH}_2\text{C}$ ) ppm.



$^{13}\text{C}$ -CPMAS NMR:  $\delta$  157.8 ( $\text{CH}_2\text{CNCH}_2$ ), 36.5 ( $\text{CH}_2\text{CH}_2\text{C}$ ), 24.6 ( $\text{CH}_2\text{CH}_2\text{C}$ ) ppm.  $^{15}\text{N}$ -CPMAS NMR:  $\delta$  278.1, 221.4 ppm. IR ( $\text{cm}^{-1}$ , ATR):  $\nu$  = 3182, 2858, 1658, 1485, 1432, 1405, 1324, 1277, 1212, 1175, 1055, 955, 972, 952, 926, 838, 778, 712, 638.

#### 6.3.8.4 1,3-cyclohexanedione-1,3-dioxime

$^1\text{H}$  NMR (250 MHz,  $\text{d}_6$ -DMSO):  $\delta$  10.42 (s, 2H, N-OH), 3.42 (s, 2H,  $\text{CNCH}_2\text{CN}$ ), 2.29 (t, 4H,  $\text{CNCH}_2\text{CH}_2$ ), 1.62 (m, 2H,  $\text{CH}_2\text{CH}_2\text{CH}_2$ ) ppm.  $^{13}\text{C}$  NMR (62.86 MHz,  $\text{d}_6$ -DMSO):  $\delta$  153.6 ( $((\text{CH}_2)_2\text{CN})$ ), 31.0 ( $\text{CH}_2\text{CH}_2\text{C}$ ), 24.4 ( $\text{CCH}_2\text{C}$ ), 23.7 ( $\text{CH}_2\text{CH}_2\text{CH}_2$ ) ppm.  $^{13}\text{C}$ -CPMAS NMR:  $\delta$  152.9 ( $\text{CH}_2\text{CNCH}_2$ ), 31.4 ( $\text{CH}_2\text{CH}_2\text{C}$ ,  $\text{CH}_2\text{CH}_2\text{CH}_2$ ,  $\text{CNCH}_2\text{CN}$ ) ppm.  $^{15}\text{N}$ -CPMAS NMR:  $\delta$  278.8 ppm. IR ( $\text{cm}^{-1}$ , ATR):  $\nu$  = 3175, 3080, 2878, 1661, 1474, 1433, 1336, 1255, 1043, 993, 958, 894, 872, 811, 749, 660, 630.

#### 6.3.8.5 Isophthaldialdehyde-1,3-dioxime

$^1\text{H}$  NMR (250 MHz,  $\text{d}_6$ -DMSO):  $\delta$  10.98 (s, 2H, N-OH), 8.59 (s, 2H,  $\text{CH}=\text{N}$ ), 8.31 (s, 1H, aryl- $\text{CCHC}$ ), 8.06 (d, 2H, aryl- $\text{CCHCH}$ ), 7.85 (t, 1H, aryl- $\text{CHCHCH}$ ) ppm.  $^{13}\text{C}$  NMR (62.86 MHz,  $\text{d}_6$ -DMSO):  $\delta$  148.5 ( $\text{CCHN}$ ), 133.7 (aryl- $\text{CH}$ ), 129.7 (aryl- $\text{CH}$ ), 127.7 (aryl- $\text{C}$ ), 124.4 (aryl- $\text{CH}$ ) ppm. IR ( $\text{cm}^{-1}$ , ATR):  $\nu$  = 3107, 3000, 1491, 1319, 1170, 1083, 968, 946, 843, 790, 712, 678.

#### 6.3.8.6 Terephthaldialdehyde-1,4-dioxime

$^1\text{H}$  NMR (250 MHz,  $\text{d}_6$ -DMSO):  $\delta$  11.10 (s, 2H, N-OH), 8.30 (s, 2H,  $\text{CH}=\text{N}$ ), 7.98-7.40 (d, 4H, aryl- $\text{CHCHC}$ ) ppm.  $^{13}\text{C}$  NMR (62.86 MHz,  $\text{d}_6$ -DMSO):  $\delta$  147.6 ( $\text{CCHN}$ ), 133.7 (aryl- $\text{C}$ ), 126.5 (aryl- $\text{CH}$ ) ppm. IR ( $\text{cm}^{-1}$ , ATR):  $\nu$  = 3142, 2987, 2876, 1624 ( $\text{C}=\text{N}$ ), 1518, 1455, 1407, 1323, 1296, 1214, 1113, 976, 963, 854, 822.

#### 6.3.8.7 2,3,5,6-Tetramethylterephthaldialdehyde-1,4-dioxime

2,3,5,6-Tetramethylterephthaldialdehyde was prepared in a similar way described by Chan *et al.*

The oxime was synthesised in the similar way as described above.

$^{13}\text{C}$  NMR (62.86 MHz,  $\text{d}_6$ -DMSO):  $\delta$  153.2 ( $\text{CH}=\text{N}$ ), 138.2 (aryl- $\text{C}$ ), 134.7 (aryl- $\text{C}$ ), 15.3 ( $\text{CH}_3\text{-C}$ ) ppm.

#### 6.3.8.8 1,4-Diacetyl-dioxime-benzene

$^1\text{H}$  NMR (250 MHz,  $\text{d}_6$ -DMSO):  $\delta$  7.61 (s, 4H, aryl- $\text{CH}$ ), 2.11 (s, 6H,  $\text{CH}_3\text{C}=\text{N}$ ) ppm.  $^{13}\text{C}$  NMR (62.86 MHz,  $\text{d}_6$ -DMSO):  $\delta$  153.2 ( $\text{CH}=\text{N}$ ), 137.4 (aryl- $\text{C}$ ), 125.8 (aryl- $\text{CH}$ ), 11.6 ( $\text{CH}_3\text{C}=\text{N}$ ) ppm.



*6.3.8.9 1,4-Bis(benzoyl-oxime)benzene*

4 g (20 mmol) of terephthaloyl chloride was dissolved in 40 ml of benzene. 5.4 g (41 mmol) of aluminium chloride was added in small portions, while the reaction mixture turned orange. The suspension was stirred over night. After quenching the reaction with ice, the mixture was extracted with toluene several times. The combined organic phases were washed with diluted sodium hydroxide solution, water and brine and dried over sodium sulfate. Evaporation of the solvent yielded an off-white product.

$^1\text{H}$  NMR (250 MHz,  $\text{d-CDCl}_3$ ):  $\delta$  7.89 (s, 4H, aryl-CH), 7.84 (d, 4H, aryl-CH), 7.63 (d, 2H, aryl-CH), 7.51 (t, 4H, aryl-CH) ppm.  $^{13}\text{C}$  NMR (62.86 MHz,  $\text{CDCl}_3$ ):  $\delta$  196.1 (C=O), 140.6 (aryl-C), 136.9 (aryl-C), 133.0 (aryl-CH), 130.1 (aryl-CH), 129.7 (aryl-CH), 128.5 (aryl-CH) ppm.

1,4-Bis(4-tert-butylbenzoyl)benzene, 1,3-bis(4-tert-butylbenzoyl)benzene and 1,6-bis(benzoyl)hexane were synthesised in a similar way.

The oxime was synthesised by a modified method described in reference 168. In a typical reaction 4.29 (15 mmol) of 1,4-bis(benzoyl-oxime)benzene were suspended in 200 ml ethanol. 2.59 g (37.2 mmol) of hydroxylamine hydrochloride and 2.57 g (18.6 mmol) of potassium carbonate were each dissolved in 10 ml water, each, and added to the suspension. Heating the reaction mixture at reflux resulted in the formation of a clear solution first. Further heating led to the formation of a precipitate. The suspension was filtered after 48h, and the precipitate washed with water several times. The product was purified by recrystallisation from a methanol/ethanol mixture.

$^1\text{H}$  NMR (250 MHz,  $\text{d}^6\text{-DMSO}$ ):  $\delta$  7.14-7.85 (m, 12H, aryl-CH) ppm.  $^{13}\text{C}$  NMR (62.86 MHz,  $\text{d}^6\text{-DMSO}$ ):  $\delta$  155.3 (CH=N), 137.0 (aryl-C), 133.8 (aryl-C), 129.2 (aryl-CH), 128.8 (aryl-CH), 127.4 (aryl-CH) ppm.

1,4-Bis(4-tert-butylbenzoyl-oxime)benzene, 1,3-bis(4-tert-butylbenzoyl-oxime)benzene and 1,6-bis(benzoyl-oxime)hexane were synthesised in a similar way.

*6.3.8.10 Naphthalene-1,5-dicarbaldehyde-1,5-dioxime*

To a solution of 2.0 g (12.8 mmol) of 1,5-dimethylnaphthalene in 50 ml of chloroform, 6.85 g (38.5 mmol) of N-bromosuccinimide and 0.31 g (1.28 mmol) of dibenzoyl peroxide were added and the suspension was heated under reflux for 4 h. After cooling to room temperature the precipitated succinimide was filtrated and washed with chloroform. Afterwards the filtrate was extracted with hydrochloride acid, diluted sodium hydroxide solution and brine. The combined organic phases were dried over sodium sulfate and yielded an off-white solid product.

$^1\text{H}$  NMR (250 MHz,  $\text{CDCl}_3$ ):  $\delta$  8.96 (d, 2H, aryl-CH), 7.70-7.40 (m, 4H, aryl-CH), 4.96 (s, 4H,  $\text{BrCH}_2\text{C}$ ) ppm.

2.63 g (8.4 mmol) 1,5-bis(bromomethyl)naphthalene were dissolved in 120 ml of acetonitrile and 15 g of 4 Å molecular sieves was suspended in the solution. Adding 3.92 g (33.5 mmol) of N-Methylmorpholin-N-oxide led to a colour change from clear to yellow. After heating at reflux over night the suspension was cooled to room temperature and filtered. The filtrate was concentrated and cooled to give the raw product as brown crystals. After filtration and washing with n-hexane the product was recrystallised from ethanol.

$^1\text{H}$  NMR (250 MHz,  $\text{CDCl}_3$ ):  $\delta$  10.42 (s, 2H,  $\text{COCH}$ ), 9.58 (d, 2H, aryl- $\text{CH}$ ), 8.15 (d, 2H, aryl- $\text{CH}$ ), 7.86 (t, 2H, aryl- $\text{CH}$ ) ppm.

Finally, the oxime was synthesised in the modified way of Bousquet described in chapter 6.3.8.9.

$^{13}\text{C}$  NMR (62.86 MHz,  $\text{d}^6\text{-DMSO}$ ):  $\delta$  148.5 ( $\text{CH}=\text{N}$ ), 130.9 (aryl- $\text{C}$ ), 129.9 (aryl- $\text{C}$ ), 127.1 (aryl- $\text{CH}$ ), 126.9 (aryl- $\text{CH}$ ), 126.6 (aryl- $\text{CH}$ ) ppm.

#### 6.3.8.11 1,1'-(1,4-Phenylene)dipropan-2-on-dioxime

3.12 g (9.5 mmol) of 1,4-diiodobenzene, 5.71 ml (56.8 mmol) of acetylacetone and 21.6 g of (56.8 mmol) sodium phosphate dodecahydrate were dissolved in 30 ml of DMSO and 0.36 g (1.9 mmol) of copper(I) iodide was added. While heating to 90 °C the solution changed its colour from blue to green in 30 minutes. After stirring the mixture at temperature over night it was quenched with 20 ml of diluted 2M hydrochloride acid. The solution was extracted with ethyl acetate. The organic layers were combined and dried over  $\text{Na}_2\text{SO}_4$ . Evaporation of the solvent yielded the crude product, which was purified by column chromatography (PE/EE 4:1).

$^1\text{H}$  NMR (250 MHz,  $\text{CDCl}_3$ ):  $\delta$  7.10 (s, 4H, aryl- $\text{CH}$ ), 3.61 (s, 4H,  $\text{CCH}_2\text{CO}$ ), 2.09 (s, 6H,  $\text{COCH}_3$ ) ppm.

Finally, the oxime was synthesised in the modified way of Bousquet *et al.* described in chapter 6.3.8.9.

$^{13}\text{C}$  NMR (62.86 MHz,  $\text{d}^6\text{-DMSO}$ ):  $\delta$  150.5 ( $\text{C}=\text{N}$ ), 132.92 (aryl- $\text{C}$ ), 129.60 (aryl- $\text{CH}$ ), 50.43 ( $\text{CCH}_2\text{CN}$ ), 29.30 ( $\text{CH}_3\text{CN}$ ) ppm.

### 6.3.9 Synthesis of 1,3-bis-[(2-hydroxy-ethylimino)-methyl]-benzene

1.36 g (10 mmol) of isophthalaldehyde was dissolved in ethanol, and 0.62 g (20 mmol) of 2-aminoethanol was added. The solution was held under reflux over night. After evaporation of the solvent, an off-white residue was observed. The crude product was purified by recrystallisation from chloroform.

$^1\text{H}$  NMR (250 MHz,  $\text{CDCl}_3$ ):  $\delta$  8.31 (s, 2H,  $\text{CH}=\text{N}$ ), 8.01 (s, 1H, aryl- $\text{CCH}$ ), 7.74 (d, 2H, aryl- $\text{CCH}$ ), 7.42 (t, 1H, aryl- $\text{CHCH}$ ), 3.93 (t, 4H,  $\text{CH}_2\text{CH}_2\text{OH}$ ), 3.76 (t, 4H,  $\text{CH}_2\text{CH}_2\text{N}=\text{CH}$ ) ppm.

1,4-Bis-[(2-hydroxy-ethylimino)-methyl]-benzene was synthesised in a similar way using terephthalaldehyde.

### 6.3.10 Synthesis of bis(salicylaldiminate) ligands

All bis(salicylaldiminate) ligands were synthesised in a comparable way as described in reference 91.

#### 6.3.10.1 1,6-bis(salicylideneamino)hexane

$^1\text{H}$  NMR (250 MHz,  $\text{d}^6\text{-DMSO}$ ):  $\delta$  8.33 (s, 2H,  $\text{CH}=\text{N}$ ), 7.31 (t, 2H, aryl- $\text{CHCHCH}$ ), 7.24 (d, 2H, aryl- $\text{CCHCH}$ ), 6.96 (d, 2H, aryl- $\text{CCHCH}$ ), 6.87 (t, 2H, aryl- $\text{CHCHCH}$ ), 3.59 (t, 4H,  $\text{CH}=\text{NCH}_2$ ), 1.72 (m, 4H,  $\text{CH}_2\text{CH}_2\text{CH}_2$ ), 1.44 (m, 4H,  $\text{CH}_2\text{CH}_2\text{CH}_2$ ) ppm.

#### 6.3.10.2 1,4-bis(salicylideneamino)-benzene

$^1\text{H}$  NMR (250 MHz,  $\text{d}^6\text{-DMSO}$ ):  $\delta$  9.01 (s, 2H,  $\text{CH}=\text{N}$ ), 7.66 (d, 2H, aryl- $\text{CCHCH}$ ), 7.53 (s, 4H, aryl- $\text{CCHCH}$ ), 7.41 (t, 2H, aryl- $\text{CHCHCH}$ ), 6.98 (t, 2H, aryl- $\text{CHCHCH}$ ; d, 2H, aryl- $\text{CCHCH}$ ) ppm.

#### 6.3.10.3 1,3-bis(salicylideneamino)-xylene

$^1\text{H}$  NMR (250 MHz,  $\text{d}^6\text{-DMSO}$ ):  $\delta$  8.46 (s, 2H,  $\text{CH}=\text{N}$ ), 7.24-7.36 (m, 8H, aryl- $\text{CH}$ ), 6.86-6.99 (m, 4H, aryl- $\text{CH}$ ), 4.81 (s, 4H,  $\text{CH}=\text{N-CH}_2\text{C}$ ) ppm.

#### 6.3.10.4 4,4'-bis(salicylideneamino)-dicyclohexylmethane

$^1\text{H}$  NMR (250 MHz,  $\text{d-CDCl}_3$ ):  $\delta$  8.38 (s, 2H,  $\text{CH}=\text{N}$ ), 7.24-7.36 (m, 4H, aryl- $\text{CH}$ ), 6.95 (d, 2H, aryl- $\text{CCHCH}$ ), 6.86 (t, 2H, aryl- $\text{CHCHCH}$ ), 3.17 (m, 2H,  $\text{NCH}(\text{CH}_2)_2$ ), 0.89-1.95 (m, 20H, cyclohexyl- $\text{CH}_2/\text{CH}$ ) ppm.

### 6.3.11 Synthesis of Benzenetribenzoate (BTB-3)

#### 6.3.11.1 Synthesis of 1,3,5-tri(4-methylphenyl)benzene

The synthesis was performed in a modified way described by Zhao *et al.*<sup>170</sup>

7.20 g (60 mmol) of 4-methylacetophenone was added to 1.14 g (6 mmol) of p-toluenesulphonic acid. The reaction mixture was stirred under reflux for 48 h. The residue was dissolved in dichloromethane and extracted with a saturated sodium hydrogen carbonate solution. The organic phases

were combined and the solvent was removed by evaporation. Addition of 100 ml of ethanol resulted in an off-white precipitation, which was collected by filtration and dried in vacuum.

$^1\text{H}$  NMR (250 MHz,  $\text{d-CDCl}_3$ ):  $\delta$  7.77 (s, 3H, aryl- $\text{CCHC}$ ), 7.61 (d, 6H, aryl- $\text{CCHCH}$ ), 7.32 (d, 6H, aryl- $\text{CCHCH}$ ), 2.45 (s, 9 H,  $\text{CH}_3\text{C}$ ) ppm.

#### 6.3.11.2 Synthesis of 1,3,5-Benzenetribenzoate

1 g (2.9 mmol) of 1,3,5-tri(4-methylphenyl)benzene was placed in a 9 ml teflon autoclave inlet. 1.5 ml of nitric acid and 6 ml of water were added. The autoclave was sealed and heated at 170 °C over night. After cooling the autoclave, the crude product was collected by filtration and washed several times with water. The product was purified by precipitation of a THF solution of the crude product in excess petroleum ether.

$^1\text{H}$  NMR (250 MHz,  $\text{d}^6\text{-DMSO}$ ):  $\delta$  8.07 (s, 3H, aryl- $\text{CCHC}$ ), 8.04 (d, 12H, aryl- $\text{CCHCH}$ ) ppm.  $^{13}\text{C}$  NMR (62.86 MHz,  $\text{d}^6\text{-DMSO}$ ):  $\delta$  167.7 ( $\text{COOH}$ ), 144.3 (aryl- $\text{C}$ ), 141.1 (aryl- $\text{CH}$ , inner aromatic ring), 130.4 (aryl- $\text{CH}$ , aryl- $\text{C}$ ), 127.8 (aryl- $\text{CH}$ ), 126.0 (aryl- $\text{C}$ ) ppm. IR ( $\text{cm}^{-1}$ , ATR):  $\nu$  = 2988 (C-H), 1687 (C=O), 1608 (C=O), 1420 (C-O), 1286, 1182, 1107, 1017, 849, 765, 699.

#### 6.3.12 Synthesis of 1,3,5-tri(4-acetylphenyl-4-oxime)benzene (TAPOB-3)

##### 6.3.12.1 Synthesis of 1,3,5-tri(4-acetylphenyl)benzene

3.12 g (24 mmol) of aluminium chloride was added to 17 ml (238 mmol) of acetyl chloride in small portions at 0 °C. A solution of 0.889 g (3 mmol) of 1,3,5-triphenylbenzene in dichloromethane was added dropwise to the clear solution. The dark, red coloured reaction mixture was stirred for 2 h at room temperature. The solution was quenched with ice and stirred over night. Afterwards the mixture was extracted with chloroform several times. The combined organic phases were washed with a saturated sodium hydrogen carbonate solution and brine. Drying the solution over sodium sulfate and evaporation of the solvent afterwards yielded an off-white product.

$^1\text{H}$  NMR (250 MHz,  $\text{d-CDCl}_3$ ):  $\delta$  8.09 (d, 6H, aryl- $\text{CHCHC}$ ), 7.87 (s, 3H, aryl- $\text{CCHC}$ ), 7.80 (d, 6H, aryl- $\text{CCHCH}$ ), 2.67 (s, 9H,  $\text{CH}_3\text{C=O}$ ) ppm.

##### 6.3.12.2 Synthesis of 1,3,5-tri(4-acetylphenyl-4-oxime)benzene

0.65 g (1.5 mmol) of 1,3,5-tri(4-acetylphenyl)benzene was suspended in 200 ml of THF. 0.39 g (5.5 mmol) of hydroxylamine hydrochloride and 0.39 g (3 mmol) potassium carbonate were dissolved, in 10 ml water each, and added to the suspension. The reaction mixture was heated at reflux for 72 h and became a clear solution after some hours. After cooling, a white precipitate was formed, evaporation of half of the solvent raised the amount of the precipitate. The product was collected by filtration and dried in vacuum.

$^1\text{H}$  NMR (250 MHz,  $\text{d}^6\text{-DMSO}$ ):  $\delta$  8.04 (s, 3H, aryl- $\text{CCHC}$ ), 7.81 (d, 6H, aryl- $\text{CHCHC}$ ), 7.78 (d, 6H, aryl- $\text{CCHCH}$ ), 2.19 (s, 9H,  $\text{CH}_3\text{C}=\text{O}$ ) ppm.  $^{13}\text{C}$  NMR (62.86 MHz,  $\text{d}^6\text{-DMSO}$ ):  $\delta$  153.1 ( $\text{CH}=\text{N}$ ), 141.5 (aryl- $\text{C}$ ), 140.5 (aryl- $\text{CH}$ , inner aromatic ring), 136.9 (aryl- $\text{C}$ ), 127.5 (aryl- $\text{CH}$ ), 126.5 (aryl- $\text{CH}$ ), 124.7 (aryl- $\text{C}$ ), 12.2 ( $\text{CH}_3\text{C}=\text{N}$ ) ppm.

The synthesis of tri(4-acetylphenyl-4-oxime)amine (TAPOA-3) was done in a similar way starting from triphenylamine.

### 6.3.13 Synthesis of Benzenetetra benzoate (BTB-4)

#### 6.3.13.1 Synthesis of 1,2,4,5-tetra(4-methylphenyl)benzene

The synthesis was done in a modified method described by Farha *et al.*<sup>171</sup>

2.5 g (0.1 mol) of magnesium was covered with absolute THF; then 16.9 g of (0.1 mol) 4-bromotoluene was added dropwise until the Grignard reaction started. The remaining bromide was diluted with further THF and added continuously. After full addition of the reactant, the reaction mixture was heated at reflux over night. The greenish Grignard solution was added to 2.5 g (4.53 mmol) of hexabromobenzene dropwise. The suspension was stirred over night at room temperature. The reaction mixture was poured on an ice/HCl mixture. The aqueous phase was extracted with hexane several times; the organic phases were combined and washed with brine. After drying over sodium sulfate and evaporation of the solvent, a white product was obtained, which was purified by recrystallisation from ethyl acetate.

$^1\text{H}$  NMR (250 MHz,  $\text{d-CDCl}_3$ ):  $\delta$  7.47 (s, 2H, aryl- $\text{CCHC}$ ), 7.12 (d, 8H, aryl- $\text{CCHCH}$ ), 7.04 (d, 8H, aryl- $\text{CCHCH}$ ), 2.32 (s, 12H,  $\text{CH}_3\text{C}$ ) ppm.

#### 6.3.13.2 Synthesis of 1,2,4,5-benzenetetra benzoate

The synthesis was done according to reference 171.

### 6.3.14 Synthesis of tetrakis(4-carboxyphenyl)silane (TCPS)

#### 6.3.14.1 Synthesis of tetra(4-methylphenyl)silan

2.5 g (0.1 mol) of magnesium was covered with absolute THF; then 16.9 g (0.1 mol) of 4-bromotoluene was added dropwise until the Grignard reaction started. The remaining bromide was diluted with further THF and added continuously. After complete addition of the reactant, the reaction mixture was heated at reflux over night. 1.56 ml (14 mmol) of silicon tetrachloride was added dropwise to the greenish Grignard solution. The solution was stirred for 3 h at room temperature and heated at reflux over night. The reaction was quenched with 1 M aqueous HCl and extracted with chloroform several times. The combined organic phases were washed with a

saturated sodium bicarbonate solution and brine and dried over sodium sulfate. Removing the solvent resulted in an oily residue, which was purified by column chromatography with petroleum ether. Evaporation of the solvent yielded a white crystalline product.

$^1\text{H}$  NMR (250 MHz,  $\text{d-CDCl}_3$ ):  $\delta$  7.41 (d, 8H, aryl- $\text{CCHCH}$ ), 7.14 (d, 8H, aryl- $\text{CCHCH}$ ), 2.33 (s, 12H,  $\text{CH}_3\text{C}$ ) ppm.

#### 6.3.14.2 Synthesis of tetrakis(4-carboxyphenyl)silane

The oxidation reaction was done following the method of Farha.<sup>171</sup>

### 6.3.15 Synthesis of 1,3,5-tris(4-carboxybiphenyl)benzene (TCBB)

#### 6.3.15.1 Synthesis of 1,3,5-tris(biphenyl)benzene

0.08 g (0.12 mmol) of bismuth triflate was dissolved in 3 ml of toluene, and 1.18 g (6 mmol) of 4-acetylbiphenyl was added. The suspension, which turned to a reddish solution at elevated temperature, was heated at reflux over night. Afterwards it was quenched with saturated sodium bicarbonate solution. The suspension was extracted with dichloromethane several times; the combined organic phases were washed with water and brine and dried over sodium sulfate. Evaporation of the solvent resulted in an off-white residue. The product was dissolved again stirred 10 min with charcoal for further purification. Filtration and solvent evaporation yielded a colourless product.

$^1\text{H}$  NMR (250 MHz,  $\text{d-CDCl}_3$ ):  $\delta$  7.90 (s, 3H, aryl- $\text{CH}$ ), 7.67-7.84 (m, aryl- $\text{CH}$ ), 7.38-7.51 (m, aryl- $\text{CH}$ ) ppm.

#### 6.3.15.2 Synthesis of 1,3,5-tris(4-methylbiphenyl)benzene

1.25 g (9.68 mmol) of aluminium chloride was dissolved in 6.8 ml (96.8 mmol) of acetyl chloride at 0 °C. 1.21 g (2.25 mmol) 1,3,5-tris(biphenyl)benzene was dissolved in dichloromethane and added dropwise to the clear solution. After stirring the reaction at room temperature for 4 h the reaction mixture was quenched with ice and stirred over night. The residue was extracted with dichloromethane. The combined organic phases were washed with saturated sodium hydrogen carbonate solution and dried over sodium sulfate. Evaporation of the solvent yielded an off-white solid.

$^1\text{H}$  NMR (250 MHz,  $\text{d-CDCl}_3$ ):  $\delta$  8.07 (d, 6H, aryl- $\text{CH}$ ), 7.89 (s, 3H, aryl- $\text{CH}$ ), 7.75-7.82 (m, 18H, aryl- $\text{CH}$ ), 2.66 (s, 9H,  $\text{CH}_3\text{CO}$ ) ppm.

### 6.3.15.3 Synthesis of 1,3,5-tris(4-carboxybiphenyl)benzene

1.12 g (28 mmol) of sodium hydroxide was dissolved in 10 ml of water, and 0.5 ml (10 mmol) of bromine was added dropwise at 0 °C. After further 15 min stirring at room temperature the yellowish solution was added slowly to a solution of 0.487 g (0.74 mmol) of 1,3,5-tris(4-methylbiphenyl)benzene in THF. The solution was stirred for 3 h at 60 °C. After acidification with HCl a white precipitation was formed, which was collected by filtration, washed with water and dried in vacuum.

$^1\text{H}$  NMR (250 MHz,  $\text{d}^6\text{-DMSO}$ ):  $\delta$  7.99 (s, 3H, aryl  $\text{CH}$ ), 7.64-7.82 (m, 24H, aryl- $\text{CH}$ ) ppm.  $^{13}\text{C}$  NMR (62.86 MHz,  $\text{d}^6\text{-DMSO}$ ):  $\delta$  167.8 ( $\text{COOH}$ ), 144.1 (aryl- $\text{C}$ ), 141.4 (aryl- $\text{C}$ ), 140.2 (aryl- $\text{CH}$ ), 138.7 (aryl- $\text{C}$ ), 130.5 (aryl- $\text{CH}$ ), 130.2 (aryl- $\text{C}$ ), 129.3 (aryl- $\text{C}$ ), 128.3 (aryl- $\text{CH}$ ), 127.9 (aryl- $\text{CH}$ ), 127.1 (aryl- $\text{CH}$ ), 124.8 (aryl- $\text{C}$ ) ppm.

## 6.4 Synthesis of complexes

### 6.4.1 Synthesis of $\{\text{Ti}[\text{bis}(\beta\text{-diketonate})](\text{O}^i\text{Pr})_2\}_n$

To a solution of 0.66 mmol of bis( $\beta$ -diketone) in 3 mL of 1,2-dichloroethane, 0.2 mL (0.66 mmol) of  $\text{Ti}(\text{O}^i\text{Pr})_4$  was added dropwise at room temperature. The yellow solution was stirred 15 min. After removing the solvent a yellowish oily product was obtained.

#### 6.4.1.1 $\{\text{Ti}[1,1\text{-(1,4-phenylene)-bis-butane-1,3-dionate}](\text{O}^i\text{Pr})_2\}_3$ (**1**)

$^1\text{H}$  NMR (250 MHz,  $\text{CDCl}_3$ ):  $\delta$  8.03 (d, 12H, aryl- $\text{CH}$ ), 6.20 (s, 6H,  $\text{COCHCO}$ ), 4.80 (m, 6H,  $[\text{CH}_3]_2\text{CH}$ ), 2.19 (s, 9H,  $\text{CH}_3\text{CO}$ ), 2.00 (s, 9H,  $\text{CH}_3\text{CO}$ ), 1.22 (d, 36H,  $[\text{CH}_3]_2\text{CH}$ ) ppm.  $^{13}\text{C}$  NMR (62.86 MHz,  $\text{CDCl}_3$ ):  $\delta$  193.4 ( $\text{CH}_3\text{COCH}$ ), 190.3 ( $\text{CH}_3\text{COCH}$ ), 182.0 ( $\text{CHCOC}$ ), 178.5 ( $\text{CHCOC}$ ), 140.2 (aryl- $\text{C}$ ), 127.6 (aryl- $\text{CH}$ ), 99.3 ( $\text{COCHCO}$ ), 78.8 ( $[\text{CH}_3]_2\text{CH}$ ), 27.7 ( $\text{CH}_3\text{CO}$ ), 25.2 ( $[\text{CH}_3]_2\text{CH}$ ) ppm. IR ( $\text{cm}^{-1}$ , liquid  $[\text{CDCl}_3]$ ):  $\nu$  = 2972 (C-H), 1711, 1581 (C=O), 1517 (C=C), 1491 (C=C), 1362, 1120, 1007, 910, 619. ESI-MS ( $m/z$ ) found (calc.): 1253.7 (1253.4)  $\{\text{[TiL(O}^i\text{Pr)}_2\text{]}_3\text{Na}\}^+$ ; 1171.6 (1171.5)  $\{\text{[TiL(O}^i\text{Pr)}_3\text{(O}^i\text{Pr)}_2\text{]}^+\}$ .

#### 6.4.1.2 $\{\text{Ti}[1,1\text{-(1,3-phenylene)-bis-butane-1,3-dionate}](\text{O}^i\text{Pr})_2\}_2$ (**2**)

$^1\text{H}$  NMR (250 MHz,  $\text{CDCl}_3$ ):  $\delta$  7.31-8.02 (d, 8H, aryl- $\text{CH}$ ), 6.19 (s, 4H,  $\text{COCHCO}$ ), 4.71 (m, 4H,  $[\text{CH}_3]_2\text{CH}$ ), 2.11 (s, 6H,  $\text{CH}_3\text{CO}$ ), 1.92 (s, 6H,  $\text{CH}_3\text{CO}$ ), 1.10 (d, 24H,  $[\text{CH}_3]_2\text{CH}$ ) ppm.  $^{13}\text{C}$  NMR (62.86 MHz,  $\text{CDCl}_3$ ):  $\delta$  193.2 ( $\text{CH}_3\text{COCH}$ ), 189.9 ( $\text{CH}_3\text{COCH}$ ), 181.7 ( $\text{CHCOC}$ ), 178.5 ( $\text{CHCOC}$ ), 137.2 (aryl- $\text{C}$ ), 130.7 (aryl- $\text{CH}$ ), 128.2 (aryl- $\text{CH}$ ), 126.5 (aryl- $\text{CH}$ ), 98.8 ( $\text{COCHCO}$ ), 78.7 ( $[\text{CH}_3]_2\text{CH}$ ), 27.9 ( $\text{CH}_3\text{CO}$ ), 26.8 ( $\text{CH}_3\text{CO}$ ), 25.2 ( $[\text{CH}_3]_2\text{CH}$ ) ppm. IR ( $\text{cm}^{-1}$ , liquid  $[\text{CDCl}_3]$ ):  $\nu$  = 2971 (C-H), 2930 (C-H), 1665, 1573 (C=O), 1512 (C=C), 1369, 1264, 1162, 1010. ESI-MS ( $m/z$ )

found (calc.): 1253.6 (1253.4)  $\{[\text{TiL}(\text{O}^i\text{Pr})_2]_3\text{Na}\}^+$ ; 843.5 (843.2)  $\{[\text{TiL}(\text{O}^i\text{Pr})_2]_2\text{Na}\}^+$ ; 761.4 (761.2)  $\{[\text{TiL}(\text{O}^i\text{Pr})]_2(\text{O}^i\text{Pr})\}^+$ ; 351.0 (351.1)  $\{\text{TiL}(\text{O}^i\text{Pr})\}^+$ .

#### 6.4.1.3 $\{\text{Ti}[1,1-(1,6\text{-naphthylene})\text{-bis-butane-1,3-dionate}](\text{O}^i\text{Pr})_2\}_3$ (**3**)

$^1\text{H}$  NMR (250 MHz,  $\text{CDCl}_3$ ):  $\delta$  8.49 (s, 6H, aryl-CH), 7.80-8.23 (m, 12H, aryl-CH), 6.39 (s, 6H, COCHCO), 4.79 (m, 3H,  $[\text{CH}_3]_2\text{CH}$ ), 4.39 (m, 3H,  $[\text{CH}_3]_2\text{CH}$ ), 2.20 (s, 9H,  $\text{CH}_3\text{CO}$ ), 1.98 (s, 9H,  $\text{CH}_3\text{CO}$ ), 1.18 (d, 36H,  $[\text{CH}_3]_2\text{CH}$ ) ppm.  $^{13}\text{C}$  NMR (62.86 MHz,  $\text{CD}_2\text{Cl}_2$ ):  $\delta$  193.7 ( $\text{CH}_3\text{CO}$ ), 190.1 ( $\text{CH}_3\text{CO}$ ), 182.5 ( $\text{CHCO}$ ), 178.8 ( $\text{CHCO}$ ), 136.2 (aryl-C), 134.4 (aryl-C), 129.4 (aryl-CH), 128.2 (aryl-CH), 124.7 (aryl-CH), 99.7 (COCHCO), 78.8 ( $[\text{CH}_3]_2\text{CH}$ ), 76.2 ( $[\text{CH}_3]_2\text{CH}$ ), 26.4 ( $[\text{CH}_3]_2\text{CH}$ ), 25.2 ( $\text{CH}_3\text{CO}$ ) ppm.

#### 6.4.1.4 $\{\text{Ti}(2,4,10,12\text{-tridecanetetronate})(\text{O}^i\text{Pr})_2\}_2$ (**4**)

$^1\text{H}$  NMR (250 MHz,  $\text{CDCl}_3$ ):  $\delta$  5.55 (s, 4H, COCHCO); 4.71 (m, 4H,  $[\text{CH}_3]_2\text{CH}$ ), 2.43 (t, 8H,  $\text{CH}_2\text{CH}_2\text{CO}$ ), 2.11 (s, 6H,  $\text{CH}_3\text{CO}$ ), 1.98 (s, 6H,  $\text{CH}_3\text{CO}$ ), 1.69 (m, 4H,  $\text{CH}_2\text{CH}_2\text{CH}_2$ ), 1.34 (d, 24H,  $[\text{CH}_3]_2\text{CH}$ , m, 8H,  $\text{CH}_2\text{CH}_2\text{CH}_2$ ) ppm.  $^{13}\text{C}$  NMR (62.86 MHz,  $\text{CDCl}_3$ ):  $\delta$  193.7 ( $\text{CH}_2\text{COCH}$ ), 191.0 ( $\text{CH}_2\text{COCH}$ ), 189.9 ( $\text{CH}_3\text{COCH}$ ), 187.0 ( $\text{CH}_3\text{COCH}$ ), 101.9 (COCHCO), 78.4 ( $[\text{CH}_3]_2\text{CH}$ ), 39.7 ( $\text{CH}_2\text{CH}_2\text{CO}$ ), 38.9 ( $\text{CH}_2\text{CH}_2\text{CO}$ ), 28.7 ( $\text{CH}_2\text{CH}_2\text{CH}_2$ ), 26.8 ( $\text{CH}_2\text{CH}_2\text{CH}_2$ ), 25.8 ( $\text{CH}_3\text{CO}$ ), 25.0 ( $[\text{CH}_3]_2\text{CH}$ ) ppm. IR ( $\text{cm}^{-1}$ , ATR):  $\nu$  = 2969 (C-H), 1584 (C=O), 1520 (C=C), 1362, 1124, 1001, 852. ESI-MS ( $m/z$ ) found (calc.): 831.4 (831.3)  $\{[\text{TiL}(\text{O}^i\text{Pr})_2]_2\text{Na}\}^+$ ; 427.2 (427.2)  $[\text{TiL}(\text{O}^i\text{Pr})_2\text{Na}]^+$ ; 307.1 (307.1)  $[\text{Ti}(\text{O}^i\text{Pr})_4\text{Na}]^+$ .

#### 6.4.1.5 $\{\text{Ti}(2,4,11,13\text{-tetradecanetetronate})(\text{O}^i\text{Pr})_2\}_2$ (**5**)

$^1\text{H}$  NMR (250 MHz,  $\text{CDCl}_3$ ):  $\delta$  5.39 (s, 4H, COCHCO); 4.66 (m, 4H,  $[\text{CH}_3]_2\text{CH}$ ), 2.23 (t, 8H,  $\text{CH}_2\text{CH}_2\text{CO}$ ), 2.06 (s, 6H,  $\text{CH}_3\text{CO}$ ), 1.93 (s, 6H,  $\text{CH}_3\text{CO}$ ), 1.55 (m, 4H,  $\text{CH}_2\text{CH}_2\text{CH}_2$ ), 1.30 (m, 8H,  $\text{CH}_2\text{CH}_2\text{CH}_2$ ), 1.20 (d, 24H,  $[\text{CH}_3]_2\text{CH}$ ) ppm.  $^{13}\text{C}$  NMR (62.86 MHz,  $\text{CDCl}_3$ ):  $\delta$  193.8 ( $\text{CH}_2\text{COCH}$ ), 191.0 ( $\text{CH}_2\text{COCH}$ ), 190.0 ( $\text{CH}_3\text{COCH}$ ), 187.0 ( $\text{CH}_3\text{COCH}$ ), 101.9 (COCHCO), 78.4 ( $[\text{CH}_3]_2\text{CH}$ ), 39.8 ( $\text{CH}_2\text{CH}_2\text{CO}$ ), 39.1 ( $\text{CH}_2\text{CH}_2\text{CO}$ ), 29.0 ( $\text{CH}_2\text{CH}_2\text{CH}_2$ ), 26.8 ( $\text{CH}_2\text{CH}_2\text{CH}_2$ ), 25.8 ( $\text{CH}_3\text{CO}$ ), 25.0 ( $[\text{CH}_3]_2\text{CH}$ ) ppm. IR ( $\text{cm}^{-1}$ , ATR):  $\nu$  = 2968 (C-H), 1583 (C=O), 1520 (C=C), 1391, 1124, 999, 852. ESI-MS ( $m/z$ ) found (calc.): 859.4 (859.4)  $\{[\text{TiL}(\text{O}^i\text{Pr})_2]_2\text{Na}\}^+$ ; 441.2 (441.2)  $\{[\text{TiL}(\text{O}^i\text{Pr})_2]\text{Na}\}^+$ , 307.1 (307.1)  $[\text{Ti}(\text{O}^i\text{Pr})_4\text{Na}]^+$ .

#### 6.4.1.6 $\{\text{Ti}(2,4,13,15\text{-hexadecanetetronate})(\text{O}^i\text{Pr})_2\}_2$ (**6**)

$^1\text{H}$  NMR (250 MHz,  $\text{CDCl}_3$ ):  $\delta$  5.48 (s, 4H, COCHCO); 4.72 (m, 4H,  $[\text{CH}_3]_2\text{CH}$ ), 2.23 (t, 8H,  $\text{CH}_2\text{CH}_2\text{CO}$ ), 2.13 (s, 6H,  $\text{CH}_3\text{CO}$ ), 1.98 (s, 6H,  $\text{CH}_3\text{CO}$ ), 1.59 (m, 4H,  $\text{CH}_2\text{CH}_2\text{CH}_2$ ), 1.12 (d, 24H,  $[\text{CH}_3]_2\text{CH}$ , m, 8H,  $\text{CH}_2\text{CH}_2\text{CH}_2$ ) ppm.  $^{13}\text{C}$  NMR (62.86 MHz,  $\text{CDCl}_3$ ):  $\delta$  193.9  $\text{CH}_2\text{COCH}$ ),



190.8 ( $\text{CH}_2\text{COCH}$ ), 190.1 ( $\text{CH}_3\text{COCH}$ ), 186.9 ( $\text{CH}_3\text{COCH}$ ), 102.0 ( $\text{COCHCO}$ ), 78.0 ( $\text{CH}_3\text{CH}$ ), 39.8 ( $\text{CH}_2\text{CH}_2\text{CO}$ ), 39.1 ( $\text{CH}_2\text{CH}_2\text{CO}$ ), 29.3 ( $\text{CH}_2\text{CH}_2\text{CH}_2$ ), 26.7 ( $\text{CH}_2\text{CH}_2\text{CH}_2$ ), 25.8 ( $\text{CH}_3\text{CO}$ ), 25.0 ( $[\text{CH}_3]_2\text{CH}$ ) ppm. IR ( $\text{cm}^{-1}$ , ATR):  $\nu$  = 2968 (C-H), 1583 (C=O), 1520 (C=C), 1395, 1125, 997, 851. ESI-MS ( $m/z$ ) found (calc.): 915.4 (915.4)  $\{[\text{TiL}(\text{O}^i\text{Pr})_2]_2\text{Na}\}^+$ ; 469.2 (469.2)  $[\text{TiL}(\text{O}^i\text{Pr})_2\text{Na}]^+$ ; 387.1 (387.2)  $[\text{TiL}(\text{O}^i\text{Pr})]^+$ ; 307.1 (307.1)  $[\text{Ti}(\text{O}^i\text{Pr})_4\text{Na}]^+$ .

#### 6.4.2 Synthesis of $\text{Zr}_2[\text{bis}(\beta\text{-diketonate})]_{4-x}(\text{O}^i\text{Pr})_x$

To a solution of 256 mg (0.66 mmol) of  $\text{Zr}(\text{O}^i\text{Pr})_4 \cdot i\text{PrOH}$  in 3 ml of toluene, 0.66 mmol of bis( $\beta$ -diketone) was added in small portions. The clear solution was stirred for 15 min. After removing the solvent a white solid product was obtained.

##### 6.4.2.1 $\{\text{Zr}(2,4,10,12\text{-tridecanetetronate})(\text{O}^i\text{Pr})_2\}_2$ (**7**)

$^1\text{H}$  NMR (250 MHz,  $\text{C}_6\text{D}_6$ ):  $\delta$  5.47 (s, 2H,  $\text{COCHCO}$ ), 5.43 (s, 2H,  $\text{COCHCO}$ ), 4.71 (m, 4H,  $[\text{CH}_3]_2\text{CH}$ ), 2.22 (t, 4H,  $\text{COCH}_2\text{CH}_2$ ), 2.14 (t, 4H,  $\text{COCH}_2\text{CH}_2$ ), 1.82 (s, 12H,  $\text{CH}_3\text{CO}$ ), 1.62 (m, 8H,  $\text{CH}_2\text{CH}_2\text{CH}_2$ ), 1.50 (d, 24H,  $[\text{CH}_3]_2\text{CH}$ , m, 4H,  $\text{CH}_2\text{CH}_2\text{CH}_2$ ) ppm.  $^{13}\text{C}$  NMR (62.86 MHz,  $\text{C}_6\text{D}_6$ ):  $\delta$  195.1 ( $\text{CHCOCH}_2$ ), 193.9 ( $\text{CHCOCH}_2$ ), 190.2 ( $\text{CH}_3\text{COCH}$ ), 186.9 ( $\text{CH}_3\text{COCH}$ ), 102.7 ( $\text{COCHCO}$ ), 102.1 ( $\text{COCHCO}$ ), 70.5 ( $[\text{CH}_3]_2\text{CH}$ ); 39.7 ( $\text{COCH}_2\text{CH}_2$ ), 38.2 ( $\text{COCH}_2\text{CH}_2$ ), 27.3 ( $\text{CH}_3\text{CO}$ ), 27.0 ( $\text{CH}_3\text{CO}$ ), 26.5 ( $[\text{CH}_3]_2\text{CH}$ ), 26.1 ( $\text{CH}_2$ ), 24.7 ( $\text{CH}_2$ ) ppm. ESI-MS ( $m/z$ ) found (calc.): 1035.2 (1035.4)  $\{[\text{ZrL}(\text{O}^i\text{Pr})_2]_2(i\text{PrOH})_2\text{Na}\}^+$ ; 953.2 (953.4)  $\{[\text{ZrL}(\text{O}^i\text{Pr})]_2(\text{O}^i\text{Pr})(i\text{PrOH})_2\}^+$ ; 915.2 (915.2)  $\{[\text{ZrL}(\text{O}^i\text{Pr})_2]_2\text{Na}\}^+$ ; 833.2 (833.2)  $\{[\text{ZrL}(\text{O}^i\text{Pr})]_2(\text{O}^i\text{Pr})\}^+$ .

##### 6.4.2.2 $\text{Zr}_2(2,4,11,13\text{-tetradecanetetronate})_3(\text{O}^i\text{Pr})_2$ (**8**)

$^1\text{H}$  NMR (250 MHz,  $\text{C}_6\text{D}_6$ ):  $\delta$  5.55 (s, 3H,  $\text{COCHCO}$ ), 5.47 (s, 3H,  $\text{COCHCO}$ ), 4.66 (m, 2H,  $[\text{CH}_3]_2\text{CH}$ ), 2.22 (t, 6H,  $\text{COCH}_2\text{CH}_2$ ), 1.97 (s, 9H,  $\text{CH}_3\text{CO}$ ), 1.84 (s, 9H,  $\text{CH}_3\text{CO}$ ), 1.64 (m, 12H,  $\text{CH}_2\text{CH}_2\text{CH}_2$ ), 1.45 (d, 12H,  $[\text{CH}_3]_2\text{CH}$ , m, 12H,  $\text{CH}_2\text{CH}_2\text{CH}_2$ ) ppm.  $^{13}\text{C}$  NMR (62.86 MHz,  $\text{C}_6\text{D}_6$ ):  $\delta$  194.0 ( $\text{CHCOCH}_2$ ), 191.9 ( $\text{CHCOCH}_2$ ), 190.1 ( $\text{CH}_3\text{COCH}$ ), 189.3 ( $\text{CH}_3\text{COCH}$ ), 102.7 ( $\text{COCHCO}$ ), 102.1 ( $\text{COCHCO}$ ), 72.0 ( $[\text{CH}_3]_2\text{CH}$ ); 39.9 ( $\text{COCH}_2\text{CH}_2$ ), 29.3 ( $\text{CH}_3\text{CO}$ ), 26.6 ( $[\text{CH}_3]_2\text{CH}$ ), 26.3 ( $\text{CH}_2$ ) ppm. ESI-MS ( $m/z$ ) found (calc.): 1077.6 (1077.3)  $\{[\text{Zr}_2\text{L}_3(\text{O}^i\text{Pr})_2]\text{Na}\}^+$ ; 995.6 (995.3)  $\{[\text{Zr}_2\text{L}_3(\text{O}^i\text{Pr})]\}^+$ ; 677.5 (677.3)  $\{[\text{ZrL}_2](i\text{PrOH})\text{Na}\}^+$ .

##### 6.4.2.3 $\text{Zr}_2(2,4,13,15\text{-hexadecanetetronate})_4$ (**9**)

$^1\text{H}$  NMR (250 MHz,  $d^8$ -toluene):  $\delta$  5.44 (s, 4H,  $\text{COCHCO}$ ), 5.34 (s, 4H,  $\text{COCHCO}$ ), 2.22 (t, 8H,  $\text{COCH}_2\text{CH}_2$ ), 2.15 (t, 8H,  $\text{COCH}_2\text{CH}_2$ ), 1.85 (s, 12H,  $\text{CH}_3\text{CO}$ ), 1.77 (s, 12H,  $\text{CH}_3\text{CO}$ ), 1.46 (m, 16H,  $\text{CH}_2\text{CH}_2\text{CH}_2$ ), 1.33 (m, 16H,  $\text{CH}_2\text{CH}_2\text{CH}_2$ ) ppm.  $^{13}\text{C}$  NMR (62.86 MHz,  $d^8$ -toluene):  $\delta$  194.4 ( $\text{CHCOCH}_2$ ), 192.2 ( $\text{CHCOCH}_2$ ), 191.8 ( $\text{CH}_3\text{COCH}$ ), 188.9 ( $\text{CH}_3\text{COCH}$ ), 102.5 ( $\text{COCHCO}$ ), 39.9

(COCH<sub>2</sub>CH<sub>2</sub>), 38.6 (COCH<sub>2</sub>CH<sub>2</sub>), 29.6 (CH<sub>3</sub>CO), 25.9 (CH<sub>2</sub>), 25.7 (CH<sub>2</sub>) ppm. ESI-MS (*m/z*) found (calc.): 1323.7 (1323.5) {[ZrL<sub>2</sub>]<sub>2</sub>Na}<sup>+</sup>; 1079.6 (1079.4) {[Zr<sub>2</sub>L<sub>3</sub>(O<sup>i</sup>Pr)]<sup>+</sup>}; 673.4 (673.2) {[ZrL<sub>2</sub>]<sub>2</sub>Na}<sup>+</sup>.

#### 6.4.3 Synthesis of [Ti(taet)(O<sup>i</sup>Pr)<sub>2</sub>]<sub>2</sub> (**10**)

0.131 g (0.66 mmol) of 1,1,2,2-tetraacetyethane was dissolved in 4 ml of toluene/1,2-dichloroethane mixture (1:1) at 70 °C. 0.2 ml of (0.66 mmol) Ti(O<sup>i</sup>Pr)<sub>4</sub> was added dropwise. The reaction mixture was stirred for 10 min at room temperature. Evaporation of the solvent yielded a white, solid residue.

<sup>1</sup>H NMR (250 MHz, d<sup>6</sup>-benzene): δ 4.95 (m, [CH<sub>3</sub>]<sub>2</sub>CH), 1.86 (s, CH<sub>3</sub>CO), 1.72 (s, CH<sub>3</sub>CO), 1.27 (m, [CH<sub>3</sub>]<sub>2</sub>CH) ppm. <sup>13</sup>C NMR (62.86 MHz, d<sup>6</sup>-benzene): δ 190.7 (CH<sub>3</sub>COC), 187.7 (CH<sub>3</sub>COC), 112.7 (COC(C)CO), 78.5 ([CH<sub>3</sub>]<sub>2</sub>CH), 26.1 (CH<sub>3</sub>CO), 25.2 ([CH<sub>3</sub>]<sub>2</sub>CH), 24.8 (CH<sub>3</sub>CO) ppm.

#### 6.4.4 Synthesis of {Ti[bis(β-ketoesterate)](O<sup>i</sup>Pr)<sub>2</sub>}, {Zr[bis(β-ketoesterate)](O<sup>i</sup>Pr)<sub>2</sub>} and ZrTi[bis(β-ketoesterate)]<sub>2</sub>(O<sup>i</sup>Pr)<sub>4</sub>

To a solution of 0.66 mmol of bis(β-ketoester) in 3 mL of 1,2-dichloroethane, 0.2 mL (0.66 mmol) of Ti(O<sup>i</sup>Pr)<sub>4</sub>/ 256 mg (0.66 mmol) of Zr(O<sup>i</sup>Pr)<sub>4</sub> · <sup>i</sup>PrOH (diluted in 4 ml of toluene or chloroform/isopropanol mixture) was added dropwise at room temperature. The yellow solution was stirred 15 min. After removing the solvent an off-white solid product was obtained.

##### 6.4.4.1 {Ti[bis(β-ketoesterate 1)](O<sup>i</sup>Pr)<sub>2</sub>}<sub>2</sub> (**11**)

<sup>1</sup>H NMR (250 MHz, C<sub>6</sub>D<sub>6</sub>): δ 6.99 (d, 8H, aryl-CH), 5.11 (s, 4H, COCHCO), 4.90 (m, 4H, [CH<sub>3</sub>]<sub>2</sub>CH), 2.92 (s, 8H, COOCH<sub>2</sub>C), 1.80 (s, 12H, CH<sub>3</sub>CO), 1.34 (d, 24H, [CH<sub>3</sub>]<sub>2</sub>CH) ppm. <sup>13</sup>C NMR (62.86 MHz, C<sub>6</sub>D<sub>6</sub>): δ 185.6 (CH<sub>3</sub>COCH), 172.5 (CHCOOCH<sub>2</sub>), 136.3 (aryl-C), 125.4 (aryl-CH), 88.4 (COCHCOO), 79.6 ([CH<sub>3</sub>]<sub>2</sub>CH); 65.0 (COOCH<sub>2</sub>C), 25.3 (CH<sub>3</sub>CO), 25.1 ([CH<sub>3</sub>]<sub>2</sub>CH) ppm. ESI-MS (*m/z*) found (calc.): 963.2 (963.3) {[TiL(O<sup>i</sup>Pr)<sub>2</sub>]<sub>2</sub>Na}<sup>+</sup>; 307.1 (307.1) {[Ti(O<sup>i</sup>Pr)<sub>4</sub>]<sub>2</sub>Na}<sup>+</sup>. ESI-MS/MS (*m/z*) found (calc.): 963.2 (963.3) {[TiL(O<sup>i</sup>Pr)<sub>2</sub>]<sub>2</sub>Na}<sup>+</sup>; 879.2 (879.3) {Ti<sub>2</sub>L[OCH<sub>2</sub>(C<sub>6</sub>H<sub>4</sub>)CH<sub>2</sub>OOCCHCOCH<sub>3</sub>](O<sup>i</sup>Pr)<sub>4</sub>Na}<sup>+</sup>; 795.2 (795.2) {Ti<sub>2</sub>L[CH<sub>2</sub>O(C<sub>6</sub>H<sub>4</sub>)CH<sub>2</sub>O](O<sup>i</sup>Pr)<sub>4</sub>Na}<sup>+</sup>; 711.2 (711.2) {Ti<sub>2</sub>[OCH<sub>2</sub>(C<sub>6</sub>H<sub>4</sub>)CH<sub>2</sub>O][OCH<sub>2</sub>(C<sub>6</sub>H<sub>4</sub>)CH<sub>2</sub>OOCCHCOCH<sub>3</sub>](O<sup>i</sup>Pr)<sub>4</sub>Na}<sup>+</sup>; 627.2 (627.2) {[Ti[OCH<sub>2</sub>(C<sub>6</sub>H<sub>4</sub>)CH<sub>2</sub>O](O<sup>i</sup>Pr)<sub>2</sub>]<sub>2</sub>Na}<sup>+</sup>.

##### 6.4.4.2 {Ti[bis(β-ketoesterate 2)](O<sup>i</sup>Pr)<sub>2</sub>}<sub>2</sub> (**12**)

<sup>1</sup>H NMR (250 MHz, CDCl<sub>3</sub>): δ 4.85 (m, 4H, COCH[CH<sub>2</sub>]<sub>2</sub>), s, 4H, COCHCOO), 4.68 (m, 4H, [CH<sub>3</sub>]<sub>2</sub>CH), 1.83 (s, 12H, CH<sub>3</sub>CO), 1.40 (m, 16 H, CH<sub>2</sub>-cyclo-hexyl), 1.12 (d, 24H, [CH<sub>3</sub>]<sub>2</sub>CH) ppm.

$^{13}\text{C}$  NMR (62.86 MHz,  $\text{CDCl}_3$ ):  $\delta$  184.8 ( $\text{CH}_3\text{COCH}$ ), 172.0 ( $\text{CHCOOCH}$ ), 88.4 ( $\text{COCHCOO}$ ), 79.1 ( $[\text{CH}_3]_2\text{CH}$ ), 70.9 ( $\text{COOCH}[\text{CH}_2]_2$ ), 27.6 ( $\text{CH}_3\text{CO}$ ), 25.1 ( $\text{CH}_2$ ), 24.9 ( $[\text{CH}_3]_2\text{CH}$ ) ppm. IR ( $\text{cm}^{-1}$  liquid [ $\text{CDCl}_3$ ]):  $\nu$  = 2972 (C-H), 1580 (C=O), 1517 (C=C), 1493, 1372, 1124, 1016, 906. ESI-MS ( $m/z$ ) found (calc.): 919.3 (919.3)  $\{[\text{TiL}(\text{O}^i\text{Pr})_2]_2\text{Na}\}^+$ ; 307.1 (307.1)  $\{\text{Ti}(\text{O}^i\text{Pr})_4\text{Na}\}^+$ . ESI-MS/MS ( $m/z$ ) found (calc.): 919.3 (919.3)  $\{[\text{TiL}(\text{O}^i\text{Pr})_2]_2\text{Na}\}^+$ ; 835.3 (835.3)  $\{\text{Ti}_2\text{L}[\text{O}(\text{C}_6\text{H}_{10})\text{OOCCHCOCH}_3](\text{O}^i\text{Pr})_4\text{Na}\}^+$ ; 751.3 (751.3)  $\{\text{Ti}_2\text{L}[\text{O}(\text{C}_6\text{H}_{10})\text{O}](\text{O}^i\text{Pr})_4\text{Na}\}^+$ ; 667.3 (667.3)  $\{\text{Ti}_2[\text{O}(\text{C}_6\text{H}_{10})\text{O}][\text{O}(\text{C}_6\text{H}_{10})\text{OOCCHCOCH}_3](\text{O}^i\text{Pr})_4\text{Na}\}^+$ ; 583.3 (583.4)  $\{\{\text{Ti}[\text{O}(\text{C}_6\text{H}_{10})\text{O}](\text{O}^i\text{Pr})_2\}_2\text{Na}\}^+$ .

#### 6.4.4.3 $\{\text{Ti}[\text{bis}(\beta\text{-ketoesterate } 3)](\text{O}^i\text{Pr})_2\}_2$ (**13**)

$^1\text{H}$  NMR (250 MHz,  $\text{CDCl}_3$ ):  $\delta$  4.79 (s, 4H,  $\text{COCHCOO}$ ), 4.61 (m, 4H,  $[\text{CH}_3]_2\text{CH}$ ), 3.81 ( $\text{COOCH}_2\text{CH}_2$ ), 1.79 ( $\text{CH}_3\text{CO}$ ), 1.40 (m, 8H,  $\text{CH}_2\text{CH}_2\text{CH}_2$ ), 1.05 (m, 4H,  $\text{CH}_2\text{CH}_2\text{CH}_2$ ; d, 24H,  $[\text{CH}_3]_2\text{CH}$ ) ppm.  $^{13}\text{C}$  NMR (62.86 MHz,  $\text{CDCl}_3$ ):  $\delta$  184.8 ( $\text{CH}_3\text{COCH}$ ), 172.5 ( $\text{CHCOOCH}$ ), 88.3 ( $\text{COCHCOO}$ ), 79.1 ( $[\text{CH}_3]_2\text{CH}$ ), 64.2 ( $\text{COOCH}_2\text{CH}_2$ ), 28.6 ( $\text{CH}_2\text{CH}_2\text{CH}_2$ ), 25.5 ( $\text{CH}_2\text{CH}_2\text{CH}_2$ ), 25.3 ( $[\text{CH}_3]_2\text{CH}$ ), 24.9 ( $\text{CH}_3\text{CO}$ ) ppm. IR ( $\text{cm}^{-1}$  ATR):  $\nu$  = 2973, 1717, 1632, 1616, 1528, 1465, 1382, 1265, 1127, 1072, 997, 946.

#### 6.4.4.4 $\{\text{Ti}[\text{bis}(\beta\text{-ketoesterate } 4)](\text{O}^i\text{Pr})_2\}_2$ (**14**)

$^1\text{H}$  NMR (250 MHz,  $\text{CD}_2\text{Cl}_2$ ):  $\delta$  6.90-7.31 (s, 16H, aryl-CH), 5.22 (s, 4H,  $\text{COCHCOO}$ ), 4.67/4.40 (m, 4H,  $[\text{CH}_3]_2\text{CH}$ ), 2.07 (s, 6H,  $\text{CH}_3\text{CO}$ ), 1.92 (s, 6H,  $\text{CH}_3\text{CO}$ ), 1.16 (d, 24H,  $[\text{CH}_3]_2\text{CH}$ ), 1.00 ( $\text{CH}_3\text{-C-aryl}$ ) ppm.  $^{13}\text{C}$  NMR (62.86 MHz,  $\text{CD}_2\text{Cl}_2$ ):  $\delta$  190.0/186.4 ( $\text{CH}_3\text{COCH}$ ), 171.6/170.7 ( $\text{CHCOOC}$ ), 147.9 (C-O), 138.0 (aryl-C), 130.9 (aryl-C), 126.7 (aryl-CH), 88.0/86.0 ( $\text{COCHCOO}$ ), 80/77.3 ( $[\text{CH}_3]_2\text{CH}$ ), 26.1 ( $[\text{CH}_3]_2\text{CH}$ ), 24.8 ( $\text{CH}_3\text{CO}$ ), 16.1 ( $\text{CH}_3\text{-C-aryl}$ ) ppm.

#### 6.4.4.5 $\{\text{Zr}[\text{bis}(\beta\text{-ketoesterate } 1)](\text{O}^i\text{Pr})_2\}_2$ (**15**)

$^1\text{H}$  NMR (250 MHz,  $\text{C}_6\text{D}_6$ ):  $\delta$  6.99 (d, 8H, aryl-CH), 5.32 (s, 4H,  $\text{COCHCO}$ ), 5.21 (s, 8H,  $\text{COOCH}_2\text{C}$ ), 4.55 (m, 4H,  $[\text{CH}_3]_2\text{CH}$ ), 1.80 (s, 12H,  $\text{CH}_3\text{CO}$ ), 1.37 (d, 24H,  $[\text{CH}_3]_2\text{CH}$ ) ppm.  $^{13}\text{C}$  NMR (62.86 MHz,  $\text{C}_6\text{D}_6$ ):  $\delta$  186.3 ( $\text{CH}_3\text{COCH}$ ), 172.7 ( $\text{CHCOOCH}_2$ ), 136.4 (aryl-C), 124.7 (aryl-CH), 88.0 ( $\text{COCHCOO}$ ), 71.0 ( $[\text{CH}_3]_2\text{CH}$ ), 65.6 ( $\text{COOCH}_2\text{C}$ ), 26.3 ( $\text{CH}_3\text{CO}$ ), 25.3 ( $[\text{CH}_3]_2\text{CH}$ ) ppm. ESI-MS ( $m/z$ ) found (calc.): 1047.3 (1047.2)  $\{[\text{ZrL}(\text{O}^i\text{Pr})_2]_2\text{Na}\}^+$ . ESI-MS/MS ( $m/z$ ) found (calc.): 1047.3 (1047.2)  $\{[\text{ZrL}(\text{O}^i\text{Pr})_2]_2\text{Na}\}^+$ , 963.2 (963.2)  $\{[\text{Zr}_2\text{L}[\text{OCH}_2(\text{C}_6\text{H}_4)\text{CH}_2\text{OOCCHCOCH}_3](\text{O}^i\text{Pr})_4\text{Na}\}^+$ ; 879.3 (879.2)  $\{[\text{Zr}_2\text{L}[\text{OCH}_2(\text{C}_6\text{H}_4)\text{CH}_2\text{O}](\text{O}^i\text{Pr})_4\text{Na}\}^+$ ; 795.2 (795.1)  $\{[\text{Zr}_2[\text{OCH}_2(\text{C}_6\text{H}_4)\text{CH}_2\text{O}][\text{OCH}_2(\text{C}_6\text{H}_4)\text{CH}_2\text{OOCCHCOCH}_3](\text{O}^i\text{Pr})_4\text{Na}\}^+$ ; 711.2 (711.1)  $\{[\text{Zr}[\text{OCH}_2(\text{C}_6\text{H}_4)\text{CH}_2\text{O}](\text{O}^i\text{Pr})_2\}_2\text{Na}\}^+$ .

#### 6.4.4.6 $\{Zr[bis(\beta\text{-ketoesterate } 2)](O^iPr)_2\}_2$ (**16**)

$^1H$  NMR (250 MHz,  $CDCl_3$ ):  $\delta$  5.34 (m, 4H,  $COCH[CH_2]_2$ ), 5.05 (s, 4H,  $COCHCOO$ ), 4.72 (m, 4H,  $[CH_3]_2CH$ ), 1.94 (s, 12H,  $CH_3CO$ ), 1.56 (m, 16 H,  $CH_2$ -cyclo-hexyl), 1.17 (d, 24H,  $[CH_3]_2CH$ ) ppm.  $^{13}C$  NMR (62.86 MHz,  $CD_2Cl_2$ ):  $\delta$  186.3 ( $CH_3COCH$ ), 172.7 ( $CHCOOCH$ ), 88.7 ( $COCHCOO$ ), 71.1 ( $[CH_3]_2CH$ ,  $COOCH[CH_2]_2$ ), 28.2 ( $CH_3CO$ ), 26.2 ( $[CH_3]_2CH$ ), 25.4 ( $CH_2$ ) ppm. ESI-MS ( $m/z$ ) found (calc.): 1003.3 (1003.2)  $\{[ZrL(O^iPr)_2]_2Na\}^+$ ; 307.1 (307.1)  $\{[Zr(O^iPr)_4]Na\}^+$ . ESI-MS/MS ( $m/z$ ) found (calc.): 1003.3 (1003.2)  $\{[ZrL(O^iPr)_2]_2Na\}^+$ ; 919.2 (919.2)  $[Zr_2L[O(C_6H_{10})OOCCHCOCH_3](O^iPr)_4Na]^+$ ; 835.3 (835.2)  $[Zr_2L[O(C_6H_{10})O](O^iPr)_4]Na]^+$ ; 795.2 (795.1)  $[Zr_2L[O(C_6H_{10})OOCCHCOCH_3](O^iPr)](^iPrOH)]^+$ .

#### 6.4.4.7 $ZrTi[bis(\beta\text{-ketoesterate } 1)]_2(O^iPr)_4$ (**17**)

Hereby, 128 mg (0.33 mmol) of  $Zr(O^iPr)_4 \cdot ^iPrOH$  was dissolved in a 5 ml of a mixture of chloroform/isopropanol, and 0.1 ml (0.33 mmol) of  $Ti(O^iPr)_4$  was added dropwise. The solution was stirred for 5 min and 0.202 g (0.66 mmol) of ketoester 1 was added in small portions. The solution was stirred for further 10 min at room temperature, and the solvent was removed by evaporation afterwards.

$^1H$  NMR (250 MHz,  $CDCl_3$ ):  $\delta$  7.11 (d, 8H, aryl- $CH$ ), 4.84 (s, 8H,  $COOCH_2C$ ; s, 4H,  $COCHCO$ ), 4.36 (m, 4H,  $[CH_3]_2CH$ ), 1.84 (s, 6H,  $CH_3CO$ ), 1.75 (s, 6H,  $CH_3CO$ ), 1.13 (d, 24H,  $[CH_3]_2CH$ ) ppm.  $^{13}C$  NMR (62.86 MHz,  $CDCl_3$ ):  $\delta$  185.3 ( $CH_3COCH$ ), 172.2 ( $CHCOOCH_2$ ), 136.2 (aryl- $C$ ), 128.2 (aryl- $CH$ ), 88.2 ( $COCHCOO$ ), 76.2 ( $[CH_3]_2CH$ ), 70.8 ( $[CH_3]_2CH$ ), 65.7 ( $COOCH_2C$ ), 26.5 ( $[CH_3]_2CH$ ) 25.7 ( $CH_3CO$ ), 25.0 ( $CH_3CO$ ) ppm. ESI-MS ( $m/z$ ) found (calc.): 1005.5 (1005.2)  $\{TiZrL_2(O^iPr)_4Na\}^+$ ; 963.2 (963.3)  $\{[TiL(O^iPr)_2]_2Na\}^+$ .

#### 6.4.5 Synthesis of $[Ti(\beta\text{-ketoesterate } 5)(O^iPr)_2]_2$ (**18**)

0.2 ml (0.66 mmol) of  $Ti(O^iPr)_4$  was dissolved in 5 mL of 1,2-dichloroethane. 0.2 g (0.66 mmol) of butanoic acid-3-oxo-3-(triethoxysilyl)propyl ester was added dropwise, and the solution turned greenish in the meantime. The reaction mixture was stirred for 30 min at room temperature. After removing the solvent an oily off-white residue was obtained.

$^1H$  NMR (250 MHz,  $CDCl_3$ ):  $\delta$  4.92 (s, 2H ( $COCHCO$ ), 4.73 (m, 2H,  $[CH_3]_2CH$ ), 4.47 (t, 2H,  $OCH_2CH_2$ ), 4.21 (m, 4H,  $[CH_3]_2CH$ ), 3.77 (q, 12H,  $OCH_2CH_3$ ), 1.90 (s, 3H,  $CH_3CO$ ), 1.84 (s, 3H,  $CH_3CO$ ), 1.66 (m, 4H,  $CH_2CH_2CH_2$ ), 1.18 (d, 36H,  $[CH_3]_2CH$ ); t, 18H  $OCH_2CH_3$ ) 0.55 (t, 4H,  $SiCH_2CH_2$ ) ppm.  $^{13}C$  NMR (62.86 MHz,  $CDCl_3$ ):  $\delta$  184.6 ( $CH_3COCH$ ), 172.4 ( $CHCOOCH_2$ ), 88.2 ( $COCHCOO$ ), 78.8 ( $[CH_3]_2CH$ ), 66.5 ( $OCH_2CH_2$ ), 65.0 ( $OCH_2CH_3$ ), 58.1, 25.4 ( $[CH_3]_2CH$ ), 22.5 ( $CH_2CH_2CH_2$ ), 18.3 ( $OCH_2CH_3$ ), 7.5 ( $SiCH_2CH_2$ ) ppm. IR ( $cm^{-1}$ , ATR):  $\nu$  = 2970 (C-H), 2927.8 (C-H), 1631 (C=O), 1611 (C=O), 1526, 1466, 1377, 1269, 1165, 1117, 1038, 996, 952, 785.

#### 6.4.6 Synthesis of $[\text{Ti}_2\text{O}(\text{O}^i\text{Pr})_4(1,5\text{-diphenyl-pentane-1,3,5-trione})]_2$ (**19**)

0.176 g (0.66 mmol) of 1,5-diphenyl-pentane-1,3,5-trione was dissolved in 4 ml of dichloromethane, and 0.4 ml (1.32 mmol) of  $\text{Ti}(\text{O}^i\text{Pr})_4$  was added dropwise. The reaction mixture was stirred for 10 min and kept at room temperature for crystallisation. After 24 h upon slow diffusion of water, first crystals of **19**  $\cdot \text{CH}_2\text{Cl}_2$  were obtained from the solution.

$^{13}\text{C}$  NMR (62.86 MHz,  $\text{CD}_2\text{Cl}_2$ ):  $\delta$  182.4 ( $\text{CH}_3\text{COCH}$ ), 176.2 ( $\text{CHCOCH}$ ), 138.6 (aryl- $\text{C}$ ), 131.5 (aryl- $\text{C}$ ), 130.4 (aryl- $\text{CH}$ ), 128.3 (aryl- $\text{CH}$ ), 126.9 (aryl- $\text{CH}$ ), 97.9 ( $\text{COCHCO}$ ), 76.0 ( $[\text{CH}_3]_2\text{CH}$ ), 25.4 ( $[\text{CH}_3]_2\text{CH}$ ) ppm.

#### 6.4.7 Synthesis of $\text{Ti}_2(1,6\text{-diphenyl-hexane-1,3,4,6-tetraone})(\text{OEt})_6$ (**20**)

0.194 g (0.66 mmol) of 1,6-diphenyl-hexane-1,3,4,6-tetraone was suspended in a chloroform/ethanol mixture and 0.14 ml (0.66 mmol) of  $\text{Ti}(\text{OEt})_4$  was added dropwise. After some minutes the reaction mixture became a clear solution. The solution was stirred for 10 min at room temperature and was then further diluted for MS measurements.

ESI-MS ( $m/z$ ) found (calc.): 681.2 (681.2)  $\{[\text{Ti}_2(\text{OEt})_6\text{L}]\text{Na}\}^+$ , 453.1 (453.1)  $\{[\text{Ti}(\text{OEt})_2\text{L}]\text{Na}\}^+$ .

#### 6.4.8 Synthesis of $[\text{Ti}(1,5\text{-pentanedial-1,5-dioximate})_2(\text{OEt})_2]_2$ (**21**)

86 mg (0.66 mmol) of 1,5-pentanedioxime was dissolved in 3 ml of ethanol, and 0.2 ml (0.66 mmol) of  $\text{Ti}(\text{OEt})_4$  was added dropwise. The solution was stirred for 30 min at room temperature. Colourless crystals of **21** were obtained after two weeks by slow evaporation of the solvent.

$^1\text{H}$  NMR (250 MHz,  $\text{CDCl}_3$ ):  $\delta$  4.34 (m, 4H,  $\text{CH}_3\text{CH}_2$ ), 3.64 (m, 4H,  $\text{CH}_3\text{CH}_2$ ), 2.50 (t, 8H,  $\text{CH}_2\text{CH}_2\text{CN}$ ), 1.84 (m, 4H,  $\text{CH}_2\text{CH}_2\text{CH}_2$ ), 1.16/0.84 (d, 12H,  $\text{CH}_3\text{CH}_2$ ) ppm.  $^{13}\text{C}$  NMR (62.86 MHz,  $\text{CDCl}_3$ ):  $\delta$  139.4 ( $\text{CHNCH}_2$ ), 71.7/68.2 ( $\text{CH}_3\text{CH}_2$ ), 58.3 ( $\text{CNCH}_2\text{CH}_2$ ), 27.9 ( $\text{CH}_2\text{CH}_2\text{CH}_2$ ), 22.2/18.0 ( $\text{CH}_3\text{CH}_2$ ), ppm. ESI-MS ( $m/z$ ) found (calc.): 555.2 (555.1)  $\{[\text{TiL}(\text{OEt})_2]_2\text{Na}\}^+$ . IR ( $\text{cm}^{-1}$ , ATR): 2966 (C-H), 2919, 2859 (C-H), 1631 (C=N), 1437 (C-C), 1374 (C-O-Ti), 1114 (C-O), 1095, 1069, 1045 (C-O), 919, 887, 799.

#### 6.4.9 Synthesis of $[\text{Ti}(2,5\text{-hexanedione-2,5-dioximate})_2(\text{OR})_2]_2$

95 mg (0.66 mmol) of 2,5-hexanedione-2,5-dioxime was dissolved in 3 ml of 1,2-dichloroethane, and 0.66 mmol of  $\text{Ti}(\text{O}^i\text{Pr})_4/\text{Ti}(\text{OEt})_4$  was added dropwise. The solution was stirred for 30 min at room temperature.

##### 6.4.9.1 $[\text{Ti}(2,5\text{-hexanedione-2,5-dioximate})_2(\text{O}^i\text{Pr})_2]_2$ (**22**)

Colourless crystals of **22** were obtained after two weeks by slow evaporation of the solvent.

$^1\text{H}$  NMR (250 MHz,  $\text{CDCl}_3$ ):  $\delta$  4.47 (m, 2H,  $[\text{CH}_3]_2\text{CH}$ ), 3.37 (m, 2H,  $[\text{CH}_3]_2\text{CH}$ ), 3.12 (m, 4H,  $\text{CH}_2\text{CH}_2\text{CN}$ ), 2.12 (m, 4H,  $\text{CH}_2\text{CH}_2\text{CN}$ ), 1.82 (s, 12H,  $\text{CH}_3\text{CN}$ ), 1.28 (d, 12H,  $[\text{CH}_3]_2\text{CH}$ ), 1.17 (d, 12H,  $[\text{CH}_3]_2\text{CH}$ ) ppm.  $^{13}\text{C}$  NMR (62.86 MHz,  $\text{CDCl}_3$ ):  $\delta$  144.8 ( $\text{CH}_3\text{CNCH}_2$ ), 77.1/75.9 ( $[\text{CH}_3]_2\text{CH}$ ), 30.5 ( $\text{CNCH}_2\text{CH}_2$ ), 26.2/25.7 ( $[\text{CH}_3]_2\text{CH}$ ), 19.9/17.0 ( $[\text{CH}_3]_2\text{CN}$ ) ppm. IR ( $\text{cm}^{-1}$ , ATR): 2967 (C-H), 2918 (C-H), 1658 (C=N), 1428 (C-C), 1360 (C-O-Ti), 1121 (C-O), 995 (C-O), 934, 849, 819.

#### 6.4.9.2 $[\text{Ti}(2,5\text{-hexanedione-2,5-dioximate})_2(\text{OEt})_2]_2$ (**23**)

The solvent was removed by evaporation resulted in a solid residue, from which the analysis was performed.

$^1\text{H}$  NMR (250 MHz,  $\text{CDCl}_3$ ):  $\delta$  4.35 (q, 4H,  $\text{CH}_3\text{CH}_2$ ), 3.91 (q, 4H,  $\text{CH}_3\text{CH}_2$ ), 2.77/2.57 (s, 8H,  $\text{CH}_2\text{CH}_2\text{CN}$ ), 1.98 (s, 12H,  $\text{CH}_3\text{CN}$ ), 1.45/1.21/0.94 (d, 12H,  $\text{CH}_3\text{CH}_2$ ) ppm.  $^{13}\text{C}$  NMR (62.86 MHz,  $\text{CDCl}_3$ ):  $\delta$  146.0 ( $\text{CH}_3\text{CNCH}_2$ ), 71.0/70.1 ( $\text{CH}_3\text{CH}_2$ ), 30.7 ( $\text{CNCH}_2\text{CH}_2$ ), 19.0/18.0 ( $\text{CH}_3\text{CH}_2$ ), 16.7/13.1 ( $\text{CH}_3\text{CN}$ ) ppm. ESI-MS ( $m/z$ ) found (calc.): 583.2 (583.2)  $\{[\text{TiL}^1(\text{OEt})_2]_2\text{Na}\}^+$ .

### 6.4.10 Synthesis of $[\text{Ti}(\text{aryl-dioximate})(\text{OR})]_x$ and $[\text{Ti}(\text{cyclohexyl-dioximate})(\text{OR})]_x$

0.66 mmol of the dioxime was dissolved in 6 ml of ethanol at 70 °C, and 0.14 ml (0.66 mmol) of  $\text{Ti}(\text{OEt})_4$  was added dropwise. The solution was stirred for 30 min at room temperature, while a precipitation was formed, which was collected by filtration or by evaporation of the solvent.

#### 6.4.10.1 $[\text{Ti}(1,4\text{-cyclohexanedione-1,4-dioximate})(\text{OEt})_2]_x$ (**24**)

IR ( $\text{cm}^{-1}$ , ATR): 2967 (C-H), 2926 (C-H), 1653 (C=N), 1437 (C-C), 1374 (C-O-Ti), 1359, 1327, 1122 (C-O), 996 (C-O), 943, 849, 824.

#### 6.4.10.2 $[\text{Ti}(1,3\text{-cyclohexanedione-1,4-dioximate})(\text{OEt})_2]_x$ (**25**)

$^{13}\text{C}$ -CPMAS NMR:  $\delta$  = 143.0 ( $\text{CH}_2\text{CNCH}_2$ ), 68.7 ( $\text{CH}_2\text{CH}_3$ ), 16.5 ( $\text{CH}_2\text{CH}_2\text{C}$ ,  $\text{CH}_2\text{CH}_2\text{CH}_2$ ,  $\text{CNCH}_2\text{CN}$ ,  $\text{CH}_2\text{CH}_3$ ) ppm.  $^{15}\text{N}$ -CPMAS NMR:  $\delta$  = 274.0 ppm. IR ( $\text{cm}^{-1}$ , ATR): 3247, 2966 (C-H), 2926 (C-H), 2864 (C-H), 1640 (C=N), 1452 (C-C), 1376 (C-O-Ti), 1125 (C-O), 1003 (C-O), 951, 851, 753.

#### 6.4.10.3 $[\text{Ti}(\text{isophthaldialdehyde-1,3-dioximate})(\text{OEt})_2]_x$ (**26**)

IR ( $\text{cm}^{-1}$ , ATR): 2968 (C-H), 2861 (C-H), 1376 (C-O-Ti), 1354, 1327, 1112 (C-O), 1067, 1038 (C-O), 920, 883, 852, 827.

#### 6.4.10.4 $[Ti(\textit{terephthaldialdehyde-1,4-dioximate})(OEt)_2]_x$ (**27**)

IR (cm<sup>-1</sup>, ATR): 2966 (C-H), 2848 (C-H), 1376 (C-O-Ti), 1354, 1327, 1112 (C-O), 1038 (C-O), 999, 917, 883, 852.

#### 6.4.10.5 $[Ti(2,3,5,6\text{-Tetramethylterephthaldialdehyde-1,4-dioximate})(OEt)_2]_x$ (**28**)

IR (cm<sup>-1</sup>, ATR): 2986 (C-H), 2926 (C-H), 2864 (C-H), 1449, 1374 (C-O-Ti), 1359 (C=C), 1327 (C-N), 1162 (C-O), 1115 (C-O), 987 (C-O), 937, 877, 849, 821, 682, 632.

### 6.4.11 Synthesis of $Ti_2\{1,4\text{-bis}[(2\text{-hydroxy-ethylimino)-methyl-benzene}]_2(OEt)_4$ (**29**)

0.145 g (0.66 mmol) of 2-hydroxy-ethylimino)-methyl]-benzene was dissolved in ethanol at elevated temperature. To the clear solution, 0.28 ml (1.32 mmol) of  $Ti(OEt)_4$  was added. Addition of additional ethanol and heating at reflux kept the product in solution, which was stirred for 10 min at room temperature. Removing the solvent resulted in an oily product.

<sup>13</sup>C NMR (62.86 MHz, CDCl<sub>3</sub>):  $\delta$  161.7 (CH=N), 138.0 (aryl-C), 128.2 (aryl-CH), 70.0 (CH<sub>2</sub>CH<sub>3</sub>, OCH<sub>2</sub>CH<sub>2</sub>N), 64.4 (CH<sub>2</sub>CH<sub>2</sub>N), 19.0 (CH<sub>3</sub>CH<sub>2</sub>) ppm.

### 6.4.12 Synthesis of $\{Ti[\textit{bis}(\textit{salicylaldiminate})](OR)_2\}_2$ and $\{Zr[\textit{bis}(\textit{salicylaldiminate})](O^iPr)_2\}_2$

0.66 mmol of bis(salicylaldiminate) ligand was dissolved in 3 mL of 1,2-dichloroethane and 0.66 mmol of  $Ti(OR)_4 / Zr(O^iPr)_4 \cdot ^iPrOH$  (diluted in 4 ml of toluene) was added dropwise. The coloured solution was stirred for 20 min at room temperature. Removing the solvent in vacuum succeeded in a yellow solid residue.

#### 6.4.12.1 $\{Ti[1,6\text{-bis}(\textit{salicylideneamino})\textit{hexane}](O^iPr)_2\}_2$ (**30**)

<sup>1</sup>H NMR (250 MHz, CDCl<sub>3</sub>):  $\delta$  7.92 (s, 4H, CH=N), 7.25 (d, 2H, aryl-H), 7.14 (m, 2H, aryl-H), 6.73 (m, 4H, aryl-H), 4.63 (m, 2H, [CH<sub>3</sub>]<sub>2</sub>CH), 4.47 (m, 2H, [CH<sub>3</sub>]<sub>2</sub>CH), 3.18 (t, 8H, CNCH<sub>2</sub>CH<sub>2</sub>), 1.23 (d, 24H, [CH<sub>3</sub>]<sub>2</sub>CH), 1.03 (m, 16H, CH<sub>2</sub>CH<sub>2</sub>CH<sub>2</sub>) ppm. <sup>13</sup>C NMR (62.86 MHz, CDCl<sub>3</sub>):  $\delta$  164.3 (aryl-CHN), 163.8 (aryl-CO), 134.2 (aryl-CH), 133.2 (aryl-CH), 122.2 (aryl-C-CHN), 118.8 (aryl-CH), 117.0 (aryl-CH), 77.9/76.0 ([CH<sub>3</sub>]<sub>2</sub>CH), 62.2 (CNCH<sub>2</sub>CH<sub>2</sub>), 31.3 (CH<sub>2</sub>CH<sub>2</sub>CH<sub>2</sub>), 26.9 (CH<sub>2</sub>CH<sub>2</sub>CH<sub>2</sub>), 26.5/25.3 ([CH<sub>3</sub>]<sub>2</sub>CH) ppm. ESI-MS ( $m/z$ ) found (calc.): 999.5 (999.4)  $\{[TiL(O^iPr)_2]_2Na\}^+$ , 775.4 (775.3)  $\{[(TiL_2)^iPrOH\}Na^+$ , 511.2 (511.2)  $[TiL(O^iPr)_2Na]^+$ , 307.1 (307.1)  $[Ti(O^iPr)_4Na]^+$ .



#### 6.4.12.2 $\{Ti[1,4\text{-bis(salicylideneamino)-benzene}](O^iPr)_2\}_2$ (**31**)

$^1H$  NMR (250 MHz,  $d^8$ -toluene):  $\delta$  7.73 (s, 2H,  $CH=N$ ), 7.62 (s, 2H,  $CH=N$ ), 6.99 (s, 8H, aryl- $CH$ ), 6.90 (m, 8H, aryl- $CH$ ), 6.28-6.56 (m, 8H, aryl- $CH$ ), 5.12 (m, 2H,  $[CH_3]_2CH$ ), 4.52 (m, 2H,  $[CH_3]_2CH$ ), 1.42/ 1.27 (d, 24H,  $[CH_3]_2CH$ ) ppm.  $^{13}C$  NMR (62.86 MHz,  $d^8$ -toluene):  $\delta$  164.6 (aryl- $CHN$ ), 163.7 (aryl-CO), 133.8 (aryl- $CH$ ), 128.8 (aryl- $CH$ ), 122.6 (aryl- $C-CHN$ ), 119.4 (aryl- $CH$ ), 116.7 (aryl- $CH$ ), 78.7 ( $[CH_3]_2CH$ ), 76.0 ( $[CH_3]_2CH$ ), 26.3 ( $[CH_3]_2CH$ ), 25.7 ( $[CH_3]_2CH$ ) ppm.

#### 6.4.12.3 $\{Ti[1,3\text{-bis(salicylideneamino)-xylene}](O^iPr)_2\}_2$ (**32**)

$^1H$  NMR (250 MHz,  $CDCl_3$ ):  $\delta$  7.70 (s, 4H,  $CH=N$ ), 7.36 (d, 4H, aryl-H), 7.00 (d, 4H, aryl-H), 6.80 – 6.70 (m, 16H, aryl-H), 4.51 (m, 4H,  $[CH_3]_2CH$ ), 4.00 (s, 8H,  $CNCH_2$ aryl), 1.26 (d, 24H,  $[CH_3]_2CH$ ) ppm.  $^{13}C$  NMR (62.86 MHz,  $CDCl_3$ ):  $\delta$  165.8 (aryl- $CHN$ ), 164.0 (aryl-CO), 137.2 (aryl-C), 134.4 (aryl- $CH$ ), 133.7 (aryl- $CH$ ), 129.6 (aryl- $CH$ ), 127.0 (aryl- $CH$ ), 122.2 (aryl- $C-CHN$ ), 118.9 (aryl- $CH$ ), 117.1 (aryl- $CH$ ), 78.0 ( $[CH_3]_2CH$ ), 76.2 ( $[CH_3]_2CH$ ), 63.6 ( $CNCH_2$ ), 26.5 ( $[CH_3]_2CH$ ), 25.1 ( $[CH_3]_2CH$ ) ppm. ESI-MS ( $m/z$ ) found (calc.): 1039.3 (1039.4)  $\{[TiL(O^iPr)_2]_2Na\}^+$ , 957.3 (957.3)  $\{[TiL(O^iPr)_2](O^iPr)\}^+$ .

#### 6.4.12.4 $\{Ti[4,4'\text{-bis(salicylideneamino)-dicyclohexylmethane}](OEt)_2\}_2$ (**33**)

$^1H$  NMR (250 MHz,  $CD_2Cl_2$ ):  $\delta$  8.23/8.03 (s, 4H,  $CH=N$ ), 7.31-7.43 (m, 4H, aryl- $CH$ ), 7.19 (m, 4H, aryl- $CH$ ), 6.73-6.90 (m, 8H, aryl- $CH$ ), 4.51/4.36 (q, 8H,  $CH_3CH_2$ ), 3.68 (m, 4H,  $[CH_2]_2CHN$ ), 0.54-1.89 (m, 34H, cyclohexyl- $CH_2$ ), 1.25 (t, 12H,  $CH_3CH_2$ ; m, 2H, cyclohexyl- $CH$ ) ppm.  $^{13}C$  NMR (62.86 MHz,  $CD_2Cl_2$ ):  $\delta$  163.1 (aryl- $CHN$ ), 162.2/161.9 (aryl-CO), 133.9/133.2 (aryl- $CH$ ), 123.8 (aryl- $C-CHN$ ), 122.4 (aryl- $CH$ ), 118.9/118.6 (aryl- $CH$ ), 117.8/117.2 (aryl- $CH$ ), 71.6 ( $CH_3CH_2$ ), 70.3 ( $CH_3CH_2$ ), 63.0 ( $[CH_2]_2CHN$ ), 34.6 (cyclohexyl- $CH_2$ ), 34.1 (cyclohexyl- $CH_2$ ), 33.9 (cyclohexyl- $CH_2$ ), 33.5 (cyclohexyl- $CH_2$ ), 32.8 (cyclohexyl- $CH_2$ ), 31.7 (cyclohexyl- $CH_2$ ), 19.0 ( $CH_3CH_2$ ) ppm.

#### 6.4.12.5 $\{Zr[1,6\text{-bis(salicylideneamino)hexane}](O^iPr)_2\}_2$ (**34**)

$^1H$  NMR (250 MHz,  $C_6D_6$ ):  $\delta$  7.83 (s, 4H,  $CH=N$ ), 7.30 (d, 2H, aryl-H), 7.19 – 7.05 (m, 4H, aryl-H), 6.73 (m, 2H, aryl-H), 4.63 (m, 4H,  $[CH_3]_2CH$ ), 3.42 (t, 8H,  $CNCH_2CH_2$ ), 1.86 (m, 8H,  $CH_2CH_2CH_2$ ), 1.48 (d, 24H,  $[CH_3]_2CH$ ), 1.16 (m, 8H,  $CH_2CH_2CH_2$ ) ppm.  $^{13}C$  NMR (62.86 MHz,  $C_6D_6$ ):  $\delta$  167.0 (aryl- $CHN$ ), 163.7 (aryl-CO), 134.6 (aryl- $CH$ ), 134.2 (aryl- $CH$ ), 122.4 (aryl- $C-CHN$ ), 120.3 (aryl- $CH$ ), 117.0 (aryl- $CH$ ), 71.4 ( $[CH_3]_2CH$ ), 62.8 ( $CNCH_2CH_2$ ), 31.3 ( $CH_2CH_2CH_2$ ), 26.7 ( $[CH_3]_2CH$ ), 21.8 ( $CH_2CH_2CH_2$ ) ppm. ESI-MS ( $m/z$ ) found (calc.): 1095.3 (1095.3)  $\{[ZrL(O^iPr)_2]_2Cl\}^-$ , 1083.4 (1083.3)  $\{[ZrL(O^iPr)_2]_2Na\}^+$ .



#### 6.4.12.6 $\{Zr[1,3\text{-bis(salicylideneamino)-xylene}](O^iPr)_2\}_2$ (**35**)

$^1H$  NMR (250 MHz,  $CDCl_3$ ):  $\delta$  7.67 (s, 4H,  $CH=N$ ), 7.29 (d, 4H, aryl-H), 6.95 (d, 4H, aryl-H), 6.79 – 6.70 (m, 12H, aryl-H), 6.59 (d, 4H, aryl-H), 4.39 (m, 4H,  $[CH_3]_2CH$ ), 4.00 (s, 8H,  $CNCH_2$ aryl), 1.10 (d, 12H,  $[CH_3]_2CH$ ), 0.94 (d, 12H,  $[CH_3]_2CH$ ) ppm.  $^{13}C$  NMR (62.86 MHz,  $CDCl_3$ ):  $\delta$  168.4 (aryl- $CHN$ ), 163.1 (aryl-CO), 137.1 (aryl-C), 134.6 (aryl- $CH$ ), 134.4 (aryl- $CH$ ), 129.6 (aryl- $CH$ ), 127.3 (aryl- $CH$ ), 122.2 (aryl- $C-CHN$ ), 120.4 (aryl- $CH$ ), 117.0 (aryl- $CH$ ), 71.3 ( $[CH_3]_2CH$ ), 63.0 ( $CNCH_2C$ ), 26.6 ( $[CH_3]_2CH$ ) ppm. ESI-MS ( $m/z$ ) found (calc.): 1135.2 (1135.3)  $\{[ZrL(O^iPr)_2]_2Cl\}^-$ .

#### 6.4.12.7 $\{Zr[4,4'\text{-bis(salicylideneamino)-dicyclohexylmethane}](O^iPr)_2\}_2$ (**36**)

$^1H$  NMR (250 MHz,  $C_6D_6$ ):  $\delta$  8.08 (s, 4H,  $CH=N$ ), 7.03-7.40 (m, 8H, aryl- $CH$ ), 6.77 (m, 8H, aryl- $CH$ ), 4.70 (q, 4H,  $[CH_3]_2CH$ ), 4.14 (m, 4H,  $[CH_2]_2CHN$ ), 1.03-1.72 (m, 36H, cyclohexyl- $CH_2/CH$ ), 1.50 (t, 24H,  $[CH_3]_2CH$ ) ppm.  $^{13}C$  NMR (62.86 MHz,  $C_6D_6$ ):  $\delta$  164.7 (aryl- $CHN$ ), 163.1 (aryl-CO), 134.2/134.5 (aryl- $CH$ ), 123.1 (aryl- $C$ ), 122.1 (aryl- $C-CHN$ ), 120.4 (aryl- $CH$ ), 117.1 (aryl- $CH$ ), 71.6 ( $[CH_3]_2CH$ ), 70.7 ( $[CH_3]_2CH$ ), 63.8 ( $[CH_2]CHN$ ), 32.7-33.8 (cyclohexyl- $CH_2$ ), 26.9 ( $[CH_3]_2CH$ ) ppm.

## 6.5 Synthesis of titanium/zirconium hybrid materials

### 6.5.1 Ti\_BT-3

In a typical procedure, BTB-3 was dissolved in 5 ml of THF,  $\text{Ti}(\text{O}^i\text{Pr})_4$  was added, and a precipitate was formed immediately. The suspension was stirred overnight at room temperature. After solvent evaporation an oily to solid residue was obtained.

**Table 6.1: Ti/COOH ratios used with Ti\_BT-3**

ratio Ti/COOH	$\text{Ti}(\text{O}^i\text{Pr})_4$	BTB-3
1:3	0.05 ml (0.165 mmol)	72 mg(0.165 mmol)
3:2	0.15 ml (0.495 mmol)	114 mg (0.33 mmol)
1:1	0.3 ml (0.99 mmol)	114 mg (0.33 mmol)
2:1	0.3 ml (0.99 mmol)	72 mg(0.165 mmol)
4:1	0.6 ml (1.98 mmol)	72 mg (0.165 mmol)

### 6.5.2 TiO\_BT-3

In a typical procedure, BTB-3 was dissolved in 5 ml of THF,  $\text{Ti}(\text{O}^i\text{Pr})_4$  was added, and a precipitate was formed immediately. The suspension was stirred for 10 min. Then a defined proportion of water was dissolved in 2ml of THF and added to the suspension. The reaction mixture was stirred overnight at room temperature. Solvent evaporation yielded an off-white powder.

**Table 6.2: Ti/COOH/H<sub>2</sub>O ratios used with TiO\_BT-3**

ratio Ti/COOH/H <sub>2</sub> O	$\text{Ti}(\text{O}^i\text{Pr})_4$	BTB-3	H <sub>2</sub> O
1:4:2	0.04 ml (0.124 mmol)	72 mg (0.165 mmol)	4.5 $\mu\text{l}$ (0.248 mmol)
1:4:4	0.04 ml (0.124 mmol)	72 mg (0.165 mmol)	9 $\mu\text{l}$ (0.496 mmol)
1:2:2	0.07 ml (0.248 mmol)	72 mg (0.165 mmol)	9 $\mu\text{l}$ (0.496 mmol)
1:2:4	0.07 ml (0.248 mmol)	72 mg (0.165 mmol)	18 $\mu\text{l}$ (0.99 mmol)
1:1:2	0.15 ml (0.496 mmol)	72 mg (0.165 mmol)	18 $\mu\text{l}$ (0.99 mmol)
1:1:4	0.15 ml (0.496 mmol)	72 mg (0.165 mmol)	36 $\mu\text{l}$ (1.98 mmol)
2:1:0.5	0.3 ml (0.99 mmol)	72 mg (0.165 mmol)	4.5 $\mu\text{l}$ (0.248 mmol)
2:1:1	0.3 ml (0.99 mmol)	72 mg (0.165 mmol)	9 $\mu\text{l}$ (0.496 mmol)
2:1:2	0.3 ml (0.99 mmol)	72 mg (0.165 mmol)	18 $\mu\text{l}$ (0.99 mmol)
2:1:4	0.3 ml (0.99 mmol)	72 mg (0.165 mmol)	36 $\mu\text{l}$ (1.98 mmol)
2:1:8	0.3 ml (0.99 mmol)	72 mg (0.165 mmol)	72 $\mu\text{l}$ (3.96 mmol)
3:1:3	0.225 ml (0.744 mmol)	36 mg (0.083 mmol)	13.5 $\mu\text{l}$ (0.744 mmol)

3:1:6	0.225 ml (0.744 mmol)	36 mg (0.083 mmol)	27 $\mu$ l (1.485 mmol)
3:1:12	0.225 ml (0.744 mmol)	36 mg (0.083 mmol)	54 $\mu$ l (2.97 mmol)
4:1:4	0.3 ml (0.99 mmol)	36 mg (0.083 mmol)	18 $\mu$ l (0.99 mmol)
4:1:8	0.3 ml (0.99 mmol)	36 mg (0.083 mmol)	36 $\mu$ l (1.98 mmol)
4:1:16	0.3 ml (0.99 mmol)	36 mg (0.083 mmol)	72 $\mu$ l (3.96 mmol)
6:1:6	0.45 ml (1.485 mmol)	36 mg (0.083 mmol)	27 $\mu$ l (1.485 mmol)
6:1:12	0.45 ml (1.485 mmol)	36 mg (0.083 mmol)	54 $\mu$ l (2.97 mmol)
6:1:24	0.45 ml (1.485 mmol)	36 mg (0.083 mmol)	107 $\mu$ l (5.94 mmol)

### 6.5.3 TiO\_TCB

The materials were synthesised in a similar way as described in chapter 6.5.2.

**Table 6.3: Ti/COOH/H<sub>2</sub>O ratios used with TiO\_TCB**

ratio Ti/COOH/H <sub>2</sub> O	Ti(O <sup>i</sup> Pr) <sub>4</sub>	TCBB	H <sub>2</sub> O
1:1:2	0.2 ml (0.66 mmol)	46 mg (0.22 mmol)	24 $\mu$ l (1.32 mmol)
1:1:4	0.2 ml (0.66 mmol)	46 mg (0.22 mmol)	48 $\mu$ l (2.64 mmol)
2:1:4	0.4 ml (1.32 mmol)	46 mg (0.22 mmol)	48 $\mu$ l (2.64 mmol)
2:1:8	0.4 ml (1.32 mmol)	46 mg (0.22 mmol)	96 $\mu$ l (5.28 mmol)
3:1:6	0.6 ml (1.98 mmol)	46 mg (0.22 mmol)	72 $\mu$ l (3.96 mmol)
4:1:8	0.8 ml (2.64 mmol)	46 mg (0.22 mmol)	96 $\mu$ l (5.28 mmol)
6:1:12	1.2 ml (3.96 mmol)	46 mg (0.22 mmol)	144 $\mu$ l (7.92 mmol)

### 6.5.4 TiO\_TCBB

The materials were synthesised in a similar way as described in chapter 6.5.2.

**Table 6.4: Ti/COOH/H<sub>2</sub>O ratios used with TiO\_TCBB**

ratio Ti/COOH/H <sub>2</sub> O	Ti(O <sup>i</sup> Pr) <sub>4</sub>	TCBB	H <sub>2</sub> O
1:1:2	0.1 ml (0.33 mmol)	55 mg (0.083 mmol)	12 $\mu$ l (0.66 mmol)
1:1:4	0.1 ml (0.33 mmol)	55 mg (0.083 mmol)	24 $\mu$ l (1.32 mmol)
2:1:4	0.2 ml (0.66 mmol)	55 mg (0.083 mmol)	24 $\mu$ l (1.32 mmol)
2:1:8	0.2 ml (0.66 mmol)	55 mg (0.083 mmol)	48 $\mu$ l (2.64 mmol)
3:1:6	0.3 ml (0.99 mmol)	55 mg (0.083 mmol)	36 $\mu$ l (1.98 mmol)
4:1:8	0.4 ml (1.32 mmol)	55 mg (0.083 mmol)	48 $\mu$ l (2.64 mmol)
6:1:12	0.6 ml (1.98 mmol)	55 mg (0.083 mmol)	72 $\mu$ l (3.96 mmol)

### 6.5.5 ZrO\_BT3

In a typical procedure, BTB-3 and  $\text{Zr}(\text{O}^i\text{Pr})_4 \cdot i\text{PrOH}$  were dissolved in each 5 ml of THF. The zirconium alkoxide solution was added to the ligand solution and a precipitate was formed. The suspension was stirred for 10 min. Then, a defined amount of water was dissolved in 2ml of THF and added to the suspension. Solvent evaporation after 24 h stirring yielded an off-white powder.

**Table 6.5: Zr/COOH/H<sub>2</sub>O ratios used with ZrO\_BT3**

ratio Zr/COOH/H <sub>2</sub> O	Zr(O <sup>i</sup> Pr) <sub>4</sub> ·( <sup>i</sup> PrOH)	BTB-3	H <sub>2</sub> O
1:4:2	24 mg (0.062 mmol)	36 mg (0.083 mmol)	2.3 µl (0.124 mmol)
1:4:4	24 mg (0.062 mmol)	36 mg (0.083 mmol)	4.5 µl (0.248 mmol)
1:2:2	48 mg (0.124 mmol)	36 mg (0.083 mmol)	4.5 µl (0.248 mmol)
1:2:4	48 mg (0.124 mmol)	36 mg (0.083 mmol)	9 µl (0.496 mmol)
1:1:2	96 mg (0.248 mmol)	36 mg (0.083 mmol)	9 µl (0.496 mmol)
1:1:4	96 mg (0.248 mmol)	36 mg (0.083 mmol)	18 µl (0.99 mmol)
2:1:4	192 mg (0.496 mmol)	36 mg (0.083 mmol)	18 µl (0.99 mmol)
2:1:8	192 mg (0.496 mmol)	36 mg (0.083 mmol)	36 µl (1.98 mmol)
3:1:6	288 mg (0.744 mmol)	36 mg (0.083 mmol)	27 µl (1.485 mmol)
3:1:12	288 mg (0.744 mmol)	36 mg (0.083 mmol)	54 µl (2.97 mmol)
4:1:8	384 mg (0.99 mmol)	36 mg (0.083 mmol)	36 µl (1.98 mmol)
4:1:16	384 mg (0.99 mmol)	36 mg (0.083 mmol)	72 µl (3.96 mmol)

### 6.5.6 TiO\_BT4

The materials were synthesised in a similar way as described in chapter 6.5.2.

**Table 6.6: Ti/COOH/H<sub>2</sub>O ratios used with TiO\_BT4**

ratio Ti/COOH/H <sub>2</sub> O	Ti(O <sup>i</sup> Pr) <sub>4</sub>	BTB-4	H <sub>2</sub> O
1:1:2	0.1 ml (0.33 mmol)	46 mg (0.083 mmol)	12 µl (0.66 mmol)
1:1:4	0.1 ml (0.33 mmol)	46 mg (0.083 mmol)	24 µl (1.32 mmol)
2:1:4	0.2 ml (0.66 mmol)	46 mg (0.083 mmol)	24 µl (1.32 mmol)
2:1:8	0.2 ml (0.66 mmol)	46 mg (0.083 mmol)	48 µl (2.64 mmol)
3:1:6	0.3 ml (0.99 mmol)	46 mg (0.083 mmol)	36 µl (1.98 mmol)
3:1:12	0.3 ml (0.99 mmol)	46 mg (0.083 mmol)	72 µl (3.96 mmol)
4:1:8	0.4 ml (1.32 mmol)	46 mg (0.083 mmol)	48 µl (2.64 mmol)
4:1:16	0.4 ml (1.32 mmol)	46 mg (0.083 mmol)	96 µl (5.28 mmol)
6:1:12	0.6 ml (1.485 mmol)	36 mg (0.083 mmol)	72 µl (3.96 mmol)

### 6.5.7 TiO<sub>2</sub>\_TCPS

The materials were synthesised in a similar way as described in chapter 6.5.2.

**Table 6.7: Ti/COOH/H<sub>2</sub>O ratios used with TiO<sub>2</sub>\_TCPS**

ratio Ti/COOH/H <sub>2</sub> O	Ti(O <sup>i</sup> Pr) <sub>4</sub>	TCPS	H <sub>2</sub> O
1:1:2	0.1 ml (0.33 mmol)	42 mg (0.083 mmol)	12 µl (0.66 mmol)
1:1:4	0.1 ml (0.33 mmol)	42 mg (0.083 mmol)	24 µl (1.32 mmol)
2:1:4	0.2 ml (0.66 mmol)	42 mg (0.083 mmol)	24 µl (1.32 mmol)
2:1:8	0.2 ml (0.66 mmol)	42 mg (0.083 mmol)	48 µl (2.64 mmol)
3:1:6	0.3 ml (0.99 mmol)	42 mg (0.083 mmol)	36 µl (1.98 mmol)
3:1:12	0.3 ml (0.99 mmol)	42 mg (0.083 mmol)	72 µl (3.96 mmol)
4:1:8	0.4 ml (1.32 mmol)	42 mg (0.083 mmol)	48 µl (2.64 mmol)
4:1:16	0.4 ml (1.32 mmol)	42 mg (0.083 mmol)	96 µl (5.28 mmol)

### 6.5.8 TiO<sub>2</sub>\_ATC-4

The materials were synthesised in a similar way as described in chapter 6.5.2. Due to solubility reasons Ti(OEt)<sub>4</sub> was used instead of Ti(O<sup>i</sup>Pr)<sub>4</sub> with ethanol as solvent.

**Table 6.8: Ti/COOH/H<sub>2</sub>O ratios used with TiO<sub>2</sub>\_ATC-4**

ratio Ti/COOH/H <sub>2</sub> O	Ti(OEt) <sub>4</sub>	ATC-4	H <sub>2</sub> O
1:1:2	0.07 ml (0.33 mmol)	26 mg (0.083 mmol)	12 µl (0.66 mmol)
1:1:4	0.07 ml (0.33 mmol)	26 mg (0.083 mmol)	24 µl (1.32 mmol)
2:1:8	0.14 ml (0.66 mmol)	26 mg (0.083 mmol)	48 µl (2.64 mmol)
3:1:12	0.17 ml (0.80 mmol)	21 mg (0.067 mmol)	58 µl (3.20 mmol)

### 6.5.9 TiO<sub>2</sub>\_TAPOA-3

The materials were synthesised in a similar way as described in chapter 6.5.2.

**Table 6.9: Ti/N-OH/H<sub>2</sub>O ratios used with Ti<sub>2</sub>\_TAPOA-3**

ratio Ti/N-OH/H <sub>2</sub> O	Ti(O <sup>i</sup> Pr) <sub>4</sub>	TAPOA-3	H <sub>2</sub> O
1:1:2	0.12 ml (0.396 mmol)	55 mg (0.132 mmol)	14 µl (0.792 mmol)
1:1:4	0.12 ml (0.396 mmol)	55 mg (0.132 mmol)	29 µl (1.584 mmol)
2:1:4	0.24 ml (0.792mmol)	55 mg (0.132 mmol)	29 µl (1.584 mmol)
2:1:8	0.24 ml (0.792mmol)	55 mg (0.132 mmol)	57 µl (3.168 mmol)
3:1:6	0.36 ml (1.188 mmol)	55 mg (0.132 mmol)	43 µl (2.376 mmol)
3:1:12	0.36 ml (1.188 mmol)	55 mg (0.132 mmol)	85 µl (4.752 mmol)
4:1:8	0.48 ml (1.584 mmol)	55 mg (0.132 mmol)	57 µl (3.168 mmol)
4:1:16	0.48 ml (1.584 mmol)	55 mg (0.132 mmol)	114 µl (6.336 mmol)
5:1:10	0.60 ml (1.98 mmol)	55 mg (0.132 mmol)	71 µl (3.96 mmol)
5:1:20	0.60 ml (1.98 mmol)	55 mg (0.132 mmol)	143 µl (7.92 mmol)
6:1:12	0.72 ml (2.376 mmol)	55 mg (0.132 mmol)	85 µl (4.752 mmol)
6:1:24	0.72 ml (2.376 mmol)	55 mg (0.132 mmol)	171 µl (9.504 mmol)

## 6.6 Crystallographic data

	2,3,5,6- tetramethylterephthal- dialdehyde-1,4-dioxime	1,4-bis-[(2-hydroxy- ethylimino)-methyl]-benzene
Empirical formula	C <sub>12</sub> H <sub>16</sub> N <sub>2</sub> O <sub>2</sub>	C <sub>12</sub> H <sub>16</sub> N <sub>2</sub> O <sub>2</sub>
$M_r$	220.27	220.27
crystal system	Triclinic	Monoclinic
space group	$P\bar{1}$	$P2_1/c$
$a$ (pm)	497.83(10)	1320.6(3)
$b$ (pm)	652.68(12)	602.38(12)
$c$ (pm)	913.96(17)	719.41(14)
$\alpha$ (°)	102.123(11)	90
$\beta$ (°)	105.738(12)	96.812(3)
$\gamma$ (°)	98.010(14)	90
$V(\text{pm}^3) \cdot 10^6$	273.31(9)	568.24(19)
$Z$	1	2
$D_x(\text{Mg} \cdot \text{m}^{-3})$	1.338	1.287
$\mu$ (mm <sup>-1</sup> )	0.092	0.089
crystal size (mm)	0.42 x 0.26 x 0.18	0.28 x 0.19 x 0.13
$\theta$ range (°)	2.40 – 30.68	1.55 – 24.99
Reflections coll. / unique	4480 / 1660	2992 / 995
Data / parameters	1660 / 79	995 / 77
GOF on $F^2$	0.647	0.592
$R$ [ $I > 2s(I)$ ]	0.0465	0.0363
wR2	0.1381	0.1178
Largest diff. peak / hole [e $\times$ Å <sup>-3</sup> ]	0.348 / -0.448	0.212 / -0.214

	<b>19</b> · 2CH <sub>2</sub> Cl <sub>2</sub>	<b>21</b>	<b>22</b>
Empirical formula	C <sub>60</sub> H <sub>84</sub> Cl <sub>4</sub> O <sub>16</sub> Ti <sub>4</sub>	C <sub>18</sub> H <sub>36</sub> N <sub>4</sub> O <sub>8</sub> Ti <sub>2</sub>	C <sub>24</sub> H <sub>48</sub> N <sub>4</sub> O <sub>8</sub> Ti <sub>2</sub>
$M_r$	1395.0	532.3	616.6
crystal system	Monoclinic	Monoclinic	Monoclinic
space group	<i>C2/c</i>	<i>P2<sub>1</sub>/c</i>	<i>Cc</i>
<i>a</i> (pm)	2504.90(5)	1548.15(5)	989.40(9)
<i>b</i> (pm)	1509.61(3)	1167.11(4)	3062.1(3)
<i>c</i> (pm)	1776.03(4)	1363.70(5)	1072.13(9)
$\alpha$ (°)	90	90	90
$\beta$ (°)	96.8390(10)	96.862(2)	106.4530(10)
$\gamma$ (°)	90	90	90
$V$ (pm <sup>3</sup> ) · 10 <sup>6</sup>	6668.1(2)	2446.37(15)	3115.2(5)
<i>Z</i>	4	4	4
$D_x$ (Mg · m <sup>-3</sup> )	1.389	1.445	1.314
$\mu$ (mm <sup>-1</sup> )	0.685	0.701	0.560
crystal size (mm)	0.43 x 0.39 x 0.21	0.43 x 0.31 x 0.19	0.40 x 0.40 x 0.20
$\theta$ range (°)	1.58 – 24.50	1.32 – 30.62	1.33 – 24.98
Reflections coll. / unique	25719 / 5546	26049 / 7522	8442 / 4492
Data / parameters	5546 / 387	7522 / 293	4492 / 355
GOF on $F^2$	0.659	0.703	0.712
$R$ [ $I > 2s(I)$ ]	0.0356	0.042	0.045
wR2	0.1418	0.113	0.144
Largest diff. peak / hole [e $\times$ Å <sup>-3</sup> ]	0.763 / -0.724	0.653 / -0.975	0.540 / -0.445



## 7 References

- (1) Schubert, U.; Hüsing, N. *Synthesis of Inorganic Materials*; 2. ed.; Wiley-VCH Verlag GmbH & Co: Weinheim, 2005.
- (2) Brinker, J.; Scherrer, G. W. *Sol-Gel Science: The Physics and Chemistry of Sol-Gel Processing*; Academic Press: London, 1990.
- (3) Livage, J.; Henry, M.; Sanchez, C. *Prog. Solid State Chem.* **1988**, *18*, 259-341.
- (4) Schubert, U. *Acc. Chem. Res.* **2007**, *40*, 730-737.
- (5) Schubert, U. *J. Mater. Chem.* **2005**, *15*, 3701-3715.
- (6) Fric, H.; Schubert, U. *New J. Chem.* **2005**, *29*, 232-236.
- (7) Fric, H.; Puchberger, M.; Schubert, U. *J. Sol-Gel Sci. Technol.* **2006**, *40*, 155-162.
- (8) Fric, H.; Puchberger, M.; Schubert, U. *Eur. J. Inorg. Chem.* **2007**, 376-383.
- (9) Baumann, S. O.; Du, A.; Artner, C.; Maurer, C.; Schubert, U. *Monatsh. Chem.* **2012**, *143*, 1637-1642.
- (10) Rupp, W.; Huesing, N.; Schubert, U. *J. Mater. Chem.* **2002**, *12*, 2594-2596.
- (11) Yamamoto, A.; Kambara, S. *J. Am. Chem. Soc.* **1957**, *79*, 4344-4348.
- (12) Errington, R. J.; Ridland, J.; Clegg, W.; Coxall, R. A.; Sherwood, J. M. *Polyhedron* **1998**, *17*, 659-674.
- (13) Spijksma, G. I.; Bouwmeester, H. J. M.; Blank, D. H. A.; Kessler, V. G. *Chemical Communications* **2004**, 1874-1875.
- (14) Hoebbel, D.; Reinert, T.; Schmidt, H.; Arpac, E. *J. Sol-Gel Sci. Technol.* **1997**, *10*, 115-126.
- (15) Puchberger, M.; Rupp, W.; Bauer, U.; Schubert, U. *New J. Chem.* **2004**, *28*, 1289-1294.
- (16) Seebach, D.; Hungerbühler, E.; Naef, R.; Schnurrenberger, P.; Weidmann, B.; Züger, M. *Synthesis* **1982**, *1982*, 138-141.
- (17) Ivanovici, S.; Puchberger, M.; Fric, H.; Kickelbick, G. *Monatsh. Chem.* **2007**, *138*, 529-539.
- (18) Czakler, M.; Artner, C.; Schubert, U. *Eur. J. Inorg. Chem.* **2012**, 3485-3489.
- (19) Boyle, T. J.; Tyner, R. P.; Alam, T. M.; Scott, B. L.; Ziller, J. W.; Potter, B. G. *J. Am. Chem. Soc.* **1999**, *121*, 12104-12112.
- (20) Barboux-Doeuff, S.; Sanchez, C. *Mater. Res. Bull.* **1994**, *29*, 1-13.
- (21) Perrin, F. X.; Nguyen, V.; Vernet, J. L. *J. Sol-Gel Sci. Technol.* **2003**, *28*, 205-215.
- (22) Doeuff, S.; Henry, M.; Sanchez, C.; Livage, J. *J. Non-Cryst. Solids* **1987**, *89*, 206-16.
- (23) Schubert, U.; Arpac, E.; Glaubitt, W.; Helmerich, A.; Chau, C. *Chem. Mater.* **1992**, *4*, 291-5.
- (24) Bailey, A.; Shang, M.; Fehlner, T. P. *Inorg. Chem.* **2000**, *39*, 4374-6.
- (25) Gbureck, U.; Probst, J.; Thull, R. *J. Sol-Gel Sci. Technol.* **2003**, *27*, 157-162.
- (26) Moraru, B.; Huesing, N.; Kickelbick, G.; Schubert, U.; Fratzl, P.; Peterlik, H. *Chem. Mater.* **2002**, *14*, 2732-2740.

- 
- (27) Schubert, U. *Chem. Mater.* **2001**, *13*, 3487-3494.
- (28) Schubert, U.; Tewinkel, S.; Moeller, F. *Inorg. Chem.* **1995**, *34*, 995-7.
- (29) Schubert, U.; Tewinkel, S.; Lamber, R. *Chem. Mater.* **1996**, *8*, 2047-2055.
- (30) Metelkina, O.; Schubert, U. *Monatsh. Chem.* **2003**, *134*, 1065-1069.
- (31) Urlaub, R.; Posset, U.; Thull, R. *J. Non-Cryst. Solids* **2000**, *265*, 276-284.
- (32) Mehring, M.; Lafond, V.; Mutin, P. H.; Vioux, A. *J. Sol-Gel Sci. Technol.* **2003**, *26*, 99-102.
- (33) Guerrero, G.; Mehring, M.; Mutin, P. H.; Dahan, F.; Vioux, A. *J. Chem. Soc., Dalton Trans.* **1999**, 1537-1538.
- (34) Mehring, M.; Guerrero, G.; Dahan, F.; Mutin, P. H.; Vioux, A. *Inorg. Chem.* **2000**, *39*, 3325-3332.
- (35) Chakraborty, D.; Chandrasekhar, V.; Bhattacharjee, M.; Kraetzner, R.; Roesky, H. W.; Noltemeyer, M.; Schmidt, H.-G. *Inorg. Chem.* **2000**, *39*, 23-26.
- (36) Pevec, A.; Demsar, A.; Pinkas, J.; Necas, M. *Inorg. Chem. Commun.* **2008**, *11*, 5-7.
- (37) Swamy, K. C. K.; Veith, M.; Huch, V.; Mathur, S. *Inorg. Chem.* **2003**, *42*, 5837-5843.
- (38) Puri, D. M.; Mehrotra, R. C. *J. Indian Chem. Soc.* **1962**, *39*, 447-52.
- (39) Bharara, P. C.; Gupta, V. D.; Mehrotra, R. C. *Z. Anorg. Allg. Chem.* **1974**, *403*, 337-46.
- (40) Bharara, P. C.; Gupta, V. D.; Mehrotra, R. C. *J. Indian Chem. Soc.* **1974**, *51*, 859-62.
- (41) Jones, A. C.; Leedham, T. J.; Wright, P. J.; Crosbie, M. J.; Fleeting, K. A.; Otway, D. J.; O'Brien, P.; Pemble, M. E. *J. Mater. Chem.* **1998**, *8*, 1773-1777.
- (42) Johnson, B. F. G.; Klunduk, M. C.; O'Connell, T. J.; McIntosh, C.; Ridland, J. *Journal of the Chemical Society, Dalton Transactions* **2001**, 1553-1555.
- (43) Baumann, S. O.; Bendova, M.; Fric, H.; Puchberger, M.; Visinescu, C.; Schubert, U. *Eur. J. Inorg. Chem.* **2009**, 3333-3340.
- (44) Baumann, S. O.; Bendova, M.; Puchberger, M.; Schubert, U. *Eur. J. Inorg. Chem.* **2011**, 573-580.
- (45) Chaudhary, A.; Dhayal, V.; Nagar, M.; Bohra, R.; Mobin, S. M.; Mathur, P. *Polyhedron* **2011**, *30*, 821-831.
- (46) Buyuktas, B. S.; Aktas, O. *Transition Met. Chem. (Dordrecht, Neth.)* **2006**, *31*, 56-61.
- (47) Baumann, S. O.; Puchberger, M.; Schubert, U. *Dalton Trans.* **2011**, *40*, 1401-1406.
- (48) Aromi, G.; Gamez, P.; Reedijk, J. *Coord. Chem. Rev.* **2008**, *252*, 964-989.
- (49) Vigato, P. A.; Peruzzo, V.; Tamburini, S. *Coord. Chem. Rev.* **2009**, *253*, 1099-1201.
- (50) Clegg Jack, K.; Lindoy Leonard, F.; Moubaraki, B.; Murray Keith, S.; McMurtrie John, C. *Dalton Trans* **2004**, 2417-23.
- (51) Clegg, J. K.; Lindoy, L. F.; McMurtrie, J. C.; Schilter, D. *Dalton Trans.* **2005**, 857-864.
- (52) Clegg, J. K.; Lindoy, L. F.; McMurtrie, J. C.; Schilter, D. *Dalton Trans.* **2006**, 3114-3121.
- (53) Clegg, J. K.; Gloe, K.; Hayter, M. J.; Kataeva, O.; Lindoy, L. F.; Moubaraki, B.; McMurtrie, J. C.; Murray, K. S.; Schilter, D. *Dalton Trans.* **2006**, 3977-3984.
- (54) Bray, D. J.; Clegg, J. K.; Lindoy, L. F.; Schilter, D. *Adv. Inorg. Chem.* **2007**, *59*, 1-37.

- (55) Clegg, J. K.; Bray, D. J.; Gloe, K.; Gloe, K.; Hayter, M. J.; Jolliffe, K. A.; Lawrance, G. A.; Meehan, G. V.; McMurtrie, J. C.; Lindoy, L. F.; Wenzel, M. *Dalton Trans.* **2007**, 1719-1730.
- (56) Saalfrank, R. W.; Dresel, A.; Seitz, V.; Trummer, S.; Hampel, F.; Teichert, M.; Stalke, D.; Stadler, C.; Daub, J.; Schunemann, V.; Trautwein, A. X. *Chem.–Eur. J.* **1997**, *3*, 2058-2062.
- (57) Soldatov, D. V.; Zanina, A. S.; Enright, G. D.; Ratcliffe, C. I.; Ripmeester, J. A. *Cryst. Growth Des.* **2003**, *3*, 1005-1013.
- (58) Bassetti, M.; De Cola, L.; Vallarino, L. M. *Inorg. Chim. Acta* **1985**, *105*, 141-5.
- (59) Pariya, C.; Sparrow, C. R.; Back, C.-K.; Sandi, G.; Fronczek, F. R.; Maverick, A. W. *Angew. Chem., Int. Ed.* **2007**, *46*, 6305-6308.
- (60) Maverick, A. W.; Klavetter, F. L. *Inorg. Chem.* **1984**, *23*, 4129-30.
- (61) Maverick, A. W.; Buckingham, S. C.; Yao, Q.; Bradbury, J. R.; Stanley, G. G. *J. Am. Chem. Soc.* **1986**, *108*, 7430-1.
- (62) Maverick, A. W.; Martone, D. P.; Bradbury, J. R.; Nelson, J. E. *Polyhedron* **1989**, *8*, 1549-56.
- (63) Bonitatebus, P. J., Jr.; Mandal, S. K.; Armstrong, W. H. *Chem. Commun. (Cambridge)* **1998**, 939-940.
- (64) Koiwa, T.; Masuda, Y.; Shono, J.; Kawamoto, Y.; Hoshino, Y.; Hashimoto, T.; Natarajan, K.; Shimizu, K. *Inorg. Chem.* **2004**, *43*, 6215-6223.
- (65) Zhang, Y.; Wang, S.; Enright, G. D.; Breeze, S. R. *J. Am. Chem. Soc.* **1998**, *120*, 9398-9399.
- (66) Fukuda, Y.; Mafune, K. *Chem. Lett.* **1988**, 697-700.
- (67) Labuda, J.; Mafune, K.; Fukuda, Y. *Bull. Chem. Soc. Jpn.* **1990**, *63*, 2610-14.
- (68) Kobayashi, Y.; Nagao, N.; Okeya, S.; Fukuda, Y. *Chem. Lett.* **1996**, 663-664.
- (69) Sato, H.; Furuno, Y.; Fukuda, Y.; Okamoto, K.; Yamagishi, A. *Dalton Trans.* **2008**, 1283-1285.
- (70) Lintvedt, R. L.; Borer, L. L.; Murtha, D. P.; Kuszaj, J. M.; Glick, M. D. *Inorg. Chem.* **1974**, *13*, 18-26.
- (71) Kuszaj, J. M.; Tomlonovic, B.; Murtha, D. P.; Lintvedt, R. L.; Glick, M. D. *Inorg. Chem.* **1973**, *12*, 1297-303.
- (72) Guthrie, J. W.; Lintvedt, R. L.; Glick, M. D. *Inorg. Chem.* **1980**, *19*, 2949-56.
- (73) Andrelczyk, B.; Lintvedt, R. L. *J. Am. Chem. Soc.* **1972**, *94*, 8633-4.
- (74) Lintvedt, R. L.; Schoenfelner, B. A.; Ceccarelli, C.; Glick, M. D. *Inorg. Chem.* **1984**, *23*, 2867-74.
- (75) Lintvedt, R. L.; Ranger, G.; Ceccarelli, C. *Inorg. Chem.* **1985**, *24*, 456-9.
- (76) Ugrinova, V.; Noll, B. C.; Brown, S. N. *Inorg. Chem.* **2006**, *45*, 10309-10320.
- (77) Dulatas, L. T.; Brown, S. N.; Ojomo, E.; Noll, B. C.; Cavo, M. J.; Holt, P. B.; Wopperer, M. M. *Inorg. Chem. (Washington, DC, U. S.)* **2009**, *48*, 10789-10799.

- (78) Grillo, V. A.; Seddon, E. J.; Grant, C. M.; Aromi, G.; Bollinger, J. C.; Folting, K.; Christou, G. *Chem. Commun. (Cambridge)* **1997**, 1561-1562.
- (79) Kluiber, R. W.; Lewis, J. W. *J. Am. Chem. Soc.* **1960**, *82*, 5777-9.
- (80) Saxena, U. B.; Rai, A. K.; Mehrotra, R. C. *Indian J. Chem.* **1967**, *5*, 368-71.
- (81) Saxena, U. B.; Rai, A. K.; Mehrotra, R. C. *Indian J. Chem.* **1971**, *9*, 709-11.
- (82) Saxena, U. B.; Rai, A. K.; Mehrotra, R. C. *J. Prakt. Chem.* **1971**, *313*, 174-8.
- (83) Saxena, U. B.; Rai, A. K.; Mehrotra, R. C. *Z. Naturforsch. B* **1972**, *27*, 1145-8.
- (84) Carraher, C. E., Jr.; Torre, L. P.; Molloy, H. M. *J. Macromol. Sci., Chem.* **1981**, *A15*, 757-71.
- (85) Thewalt, U.; Friedrich, R. *Z. Naturforsch., B: Chem. Sci.* **1991**, *46*, 475-82.
- (86) Singh, M. S.; Narayan, P. *Synth. React. Inorg. Met.-Org. Chem.* **2001**, *31*, 149-156.
- (87) Rose, M. J.; Gray, H. B.; Winkler, J. R. *J. Am. Chem. Soc.* **2012**, *134*, 8310-8313.
- (88) Varhelyi, C.; Kovacs, A.; Gomory, A.; Pokol, G.; Farkas, G.; Sohar, P. *J. Coord. Chem.* **2009**, *62*, 2429-2437.
- (89) Dutta, G.; Kumar, K.; Gupta, B. D. *Organometallics* **2009**, *28*, 3485-3491.
- (90) Kinoshita, S.; Masuda, I. *Polyhedron* **1985**, *4*, 1245-51.
- (91) Nathan, L. C.; Koehne, J. E.; Gilmore, J. M.; Hannibal, K. A.; Dewhirst, W. E.; Mai, T. D. *Polyhedron* **2003**, *22*, 887-894.
- (92) Komiya, N.; Muraoka, T.; Iida, M.; Miyanaga, M.; Takahashi, K.-I.; Naota, T. *J. Am. Chem. Soc.* **2011**, *133*, 16054-16061.
- (93) Maverick, A. W.; Laxman, R. K.; Hawkins, M. A.; Martone, D. P.; Fronczek, F. R. *Dalton Trans.* **2005**, 200-206.
- (94) Nakamura, T.; Niwa, K.; Usugi, S.; Asada, H.; Fujiwara, M.; Matsushita, T. *Polyhedron* **2001**, *20*, 191-201.
- (95) Manassen, J. *Inorg. Chem.* **1970**, *9*, 966-8.
- (96) Hoyt, W. C.; Everett, G. W., Jr. *Inorg. Chem.* **1969**, *8*, 2013-15.
- (97) Kumari, N.; Prajapati, R.; Mishra, L. *Polyhedron* **2007**, *27*, 241-248.
- (98) Tsuchimoto, M. *Bull. Chem. Soc. Jpn.* **2001**, *74*, 2101-2105.
- (99) Choudhary, N. F.; Hitchcock, P. B.; Leigh, G. J. *Inorg. Chim. Acta* **2000**, *306*, 24-29.
- (100) Belokon, Y. N.; Hunt, J.; North, M. *Synlett* **2008**, 2150-2154.
- (101) Kim, I.; Ha, Y. S.; Zhang, D. F.; Ha, C.-S.; Lee, U. *Macromol. Rapid Commun.* **2004**, *25*, 1319-1323.
- (102) Khan, N.-u. H.; Agrawal, S.; Kureshy, R. I.; Abdi, S. H. R.; Mayani, V. J.; Jasra, R. V. *Eur. J. Org. Chem.* **2006**, 3175-3180.
- (103) Quiroz-Guzman, M.; Oliver, A. G.; Loza, A. J.; Brown, S. N. *Dalton Trans.* **2011**, *40*, 11458-11468.
- (104) Balsells, J.; Carroll, P. J.; Walsh, P. J. *Inorg. Chem.* **2001**, *40*, 5568-5574.
- (105) Yeori, A.; Gendler, S.; Groysman, S.; Goldberg, I.; Kol, M. *Inorg. Chem. Commun.* **2004**, *7*, 280-282.

- 
- (106) Tzubery, A.; Tshuva, E. Y. *Inorg. Chem.* **2012**, *51*, 1796-1804.
- (107) Tzubery, A.; Tshuva, E. Y. *Inorg. Chem.* **2011**, *50*, 7946-7948.
- (108) Kim, D.; Song, X.; Yoon, J. H.; Lah, M. S. *Cryst. Growth Des.* **2012**, *12*, 4186-4193.
- (109) Perkins, C. G.; Warren, J. E.; Fateeva, A.; Stylianou, K. C.; McLennan, A.; Jelfs, K.; Bradshaw, D.; Rosseinsky, M. J. *Microporous Mesoporous Mater.* **2012**, *157*, 24-32.
- (110) Reinsch, H.; Krueger, M.; Wack, J.; Senker, J.; Salles, F.; Maurin, G.; Stock, N. *Microporous Mesoporous Mater.* **2012**, *157*, 50-55.
- (111) Gadzikwa, T.; Farha, O. K.; Malliakas, C. D.; Kanatzidis, M. G.; Hupp, J. T.; Nguyen, S. T. *J. Am. Chem. Soc.* **2009**, *131*, 13613-13615.
- (112) Shultz, A. M.; Farha, O. K.; Hupp, J. T.; Nguyen, S. T. *J. Am. Chem. Soc.* **2009**, *131*, 4204-4205.
- (113) Gadzikwa, T.; Farha, O. K.; Mulfort, K. L.; Hupp, J. T.; Nguyen, S. T. *Chem. Commun. (Cambridge, U. K.)* **2009**, 3720-3722.
- (114) Shultz, A. M.; Farha, O. K.; Adhikari, D.; Sarjeant, A. A.; Hupp, J. T.; Nguyen, S. T. *Inorg. Chem. (Washington, DC, U. S.)* **2011**, *50*, 3174-3176.
- (115) Ibarra, I. A.; Bayliss, P. A.; Perez, E.; Yang, S.; Blake, A. J.; Nowell, H.; Allan, D. R.; Poliakoff, M.; Schroeder, M. *Green Chem.* **2012**, *14*, 117-122.
- (116) Davies, R. P.; Less, R.; Lickiss, P. D.; Robertson, K.; White, A. J. P. *Cryst. Growth Des.* **2010**, *10*, 4571-4581.
- (117) Lambert, J. B.; Liu, Z.; Liu, C. *Organometallics* **2008**, *27*, 1464-1469.
- (118) Cavka, J. H.; Jakobsen, S.; Olsbye, U.; Guillou, N.; Lamberti, C.; Bordiga, S.; Lillerud, K. P. *J Am Chem Soc* **2008**, *130*, 13850-1.
- (119) Guillerme, V.; Gross, S.; Serre, C.; Devic, T.; Bauer, M.; Ferey, G. *Chem Commun (Camb)* **2010**, *46*, 767-9.
- (120) Dan-Hardi, M.; Serre, C.; Frot, T.; Rozes, L.; Maurin, G.; Sanchez, C.; Ferey, G. *J. Am. Chem. Soc.* **2009**, *131*, 10857-10859.
- (121) Froeschl, T.; Hoermann, U.; Kubiak, P.; Kucerova, G.; Pfanzelt, M.; Weiss, C. K.; Behm, R. J.; Huesing, N.; Kaiser, U.; Landfester, K.; Wohlfahrt-Mehrens, M. *Chem. Soc. Rev.* **2012**, *41*, 5313-5360.
- (122) Mutin, P. H.; Vioux, A. *Chem. Mater.* **2009**, *21*, 582-596.
- (123) Antonelli, D. M.; Ying, J. Y. *Angew. Chem., Int. Ed. Engl.* **1995**, *34*, 2014-17.
- (124) Yang, P.; Zhao, D.; Margolese, D. I.; Chmelka, B. F.; Stucky, G. D. *Nature (London)* **1998**, *396*, 152-155.
- (125) Yang, P.; Zhao, D.; Margolese, D. I.; Chmelka, B. F.; Stucky, G. D. *Chem. Mater.* **1999**, *11*, 2813-2826.
- (126) Soler-Illia, G. J. d. A. A.; Crepaldi, E. L.; Grosso, D.; Sanchez, C. *Curr. Opin. Colloid Interface Sci.* **2003**, *8*, 109-126.
- (127) Brinker, C. J.; Lu, Y.; Sellinger, A.; Fan, H. *Adv. Mater. (Weinheim, Ger.)* **1999**, *11*, 579-585.

- 
- (128) Alberius, P. C. A.; Frindell, K. L.; Hayward, R. C.; Kramer, E. J.; Stucky, G. D.; Chmelka, B. F. *Chem. Mater.* **2002**, *14*, 3284-3294.
- (129) Kuemmel, M.; Boissiere, C.; Nicole, L.; Laberty-Robert, C.; Sanchez, C.; Grosso, D. *J. Sol-Gel Sci. Technol.* **2008**, *48*, 102-112.
- (130) Bray, D. J.; Antonioli, B.; Clegg, J. K.; Gloe, K.; Gloe, K.; Jolliffe, K. A.; Lindoy, L. F.; Wei, G.; Wenzel, M. *Dalton Trans.* **2008**, 1683-1685.
- (131) Clegg, J. K.; Bray, D. J.; Gloe, K.; Gloe, K.; Jolliffe, K. A.; Lawrance, G. A.; Lindoy, L. F.; Meehan, G. V.; Wenzel, M. *Dalton Trans.* **2008**, 1331-1340.
- (132) Fenton, D. E.; Regan, C. M.; Casellato, U.; Vigato, P. A.; Vidali, M. *Inorg. Chim. Acta* **1982**, *58*, 83-8.
- (133) Steunou, N.; Ribot, F.; Boubekeur, K.; Maquet, J.; Sanchez, C. *New J. Chem.* **1999**, *23*, 1079-1086.
- (134) Lee, S.; Kang, S. K.; Lee, S. J.; Yun, S. S.; Chang, T.-S. *Bull. Korean Chem. Soc.* **2005**, *26*, 1620-1622.
- (135) Glidewell, C.; Turner, G. M.; Ferguson, G. *Acta Crystallogr., Sect. C: Cryst. Struct. Commun.* **1996**, *C52*, 11-14.
- (136) Matilainen, L.; Mutikainen, I.; Leskela, M. *Acta Chem. Scand.* **1996**, *50*, 755-758.
- (137) Dubler, E.; Buschmann, R.; Schmalle, H. W. *J. Inorg. Biochem.* **2003**, *95*, 97-104.
- (138) Erasmus, E.; Conradie, J.; Muller, A.; Swarts, J. C. *Inorg. Chim. Acta* **2007**, *360*, 2277-2283.
- (139) Patil, U.; Winter, M.; Becker, H.-W.; Devi, A. *J. Mater. Chem.* **2003**, *13*, 2177-2184.
- (140) Mendez-Vivar, J.; Bosch, P.; Lara, V. H.; Mendoza-Serna, R. *J. Sol-Gel Sci. Technol.* **2002**, *25*, 249-254.
- (141) Fric, H.; Puchberger, M.; Schubert, U. *Eur. J. Inorg. Chem.* **2008**, 1452-1461.
- (142) Toledano, P.; In, M.; Sanchez, C. *C. R. Acad. Sci., Ser. II* **1991**, *313*, 1247-53.
- (143) Toledano, P.; In, M.; Sanchez, C. *C. R. l'Academie Sci., Ser. II Univers* **1990**, *311*, 1161-6.
- (144) Woisetschlager, O. E.; Geisbauer, A.; Polborn, K.; Beck, W. *Z. Anorg. Allg. Chem.* **2000**, *626*, 766-774.
- (145) Davidson, M. G.; Johnson, A. L.; Jones, M. D.; Lunn, M. D.; Mahon, M. F. *Polyhedron* **2007**, *26*, 975-980.
- (146) Zhao, H.-Y.; Qiu, X.-H.; Xie, Y.-B.; Shen, P.-W. *J. Mol. Struct.* **2004**, *733*, 95-99.
- (147) Chmura, A. J.; Cousins, D. M.; Davidson, M. G.; Jones, M. D.; Lunn, M. D.; Mahon, M. F. *Dalton Trans* **2008**, 1437-43.
- (148) Pandey, A.; Gupta, V. D.; Noth, H. *Eur. J. Inorg. Chem.* **2000**, 1351-1357.
- (149) Rahal, R.; Pigot, T.; Foix, D.; Lacombe, S. *Appl. Catal., B* **2011**, *104*, 361-372.
- (150) Rahal, R.; Daniele, S.; Hubert-Pfalzgraf, L. G.; Guyot-Ferreol, V.; Tranchant, J.-F. *Eur. J. Inorg. Chem.* **2008**, 980-987.
- (151) Severin, K. G.; Ledford, J. S.; Torgerson, B. A.; Berglund, K. A. *Chem. Mater.* **1994**, *6*, 890-8.



- 
- (152) Piszczek, P.; Richert, M.; Grodzicki, A.; Glowiak, T.; Wojtczak, A. *Polyhedron* **2005**, *24*, 663-670.
- (153) Sing, K. S. W.; Everett, D. H.; Haul, R. A. W.; Moscou, L.; Pierotti, R. A.; Rouquerol, J.; Siemieniewska, T. *Pure Appl. Chem.* **1985**, *57*, 603-19.
- (154) Armarego, W. L.; Perrin, D. D. *Purification of Laboratory Chemicals* **1997**, *Fourth Edition*.
- (155) Sheldrick, G. M. *SADABS, Program for Empirical Absorption Correction of Area Detector Data, University of Göttingen, Göttingen (Germany)* **2008**.
- (156) Sheldrick, G. M. *SHELXS/L-97, Programs for Crystal Structure Determination, University of Göttingen, Göttingen (Germany)* **1997**.
- (157) Sheldrick, G. M. *Acta Crystallogr.* **2008**, 112-22.
- (158) Becke, A. D. *J. Chem. Phys.* **1993**, *98*, 5648.
- (159) Lee, C.; Yang, W.; Parr, R. G. *Phys. Rev. B* **1988**, *37*, 785.
- (160) Hamprecht, F. A.; Cohen, A. J.; Tozer, D. J.; Handy, N. C. *J. Chem. Phys.* **1998**, *109*, 6264.
- (161) Staroverov, V. N.; Scuseria, G. E.; Tao, J.; Perdew, J. P. *J. Chem. Phys.* **2003**, *119*, 12129.
- (162) Stephens, P. J.; Devlin, F. J.; Chablowski, C. F.; Frisch, M. J. *J. Chem. Phys.* **1994**, *98*, 11623.
- (163) Frisch, M. J.; Trucks, G. W.; Schlegel, H. B.; Scuseria, G. E.; Robb, M. A.; Cheeseman, J. R.; Montgomery Jr., J. A.; Vreven, T.; Kudin, K. N.; Burant, J. C.; Millam, J. M.; Iyengar, S. S.; Tomasi, J.; Barone, V.; Mennucci, B.; Cossi, M.; Scalmani, G.; Rega, N.; Petersson, G. A.; Nakatsuji, H.; Hada, M.; Ehara, M.; Toyota, K.; Fukuda, R.; Hasegawa, J.; Ishida, M.; Nakajima, T.; Honda, Y.; Kitao, O.; Nakai, H.; Klene, M.; Li, X.; Knox, J. E.; Hratchian, H. P.; Cross, J. B.; Bakken, V.; Adamo, C.; Jaramillo, J.; Gomperts, R.; Stratmann, R. E.; Yazyev, O.; Austin, A. J.; Cammi, R.; Pomelli, C.; Ochterski, J. W.; Ayala, P. Y.; Morokuma, K.; Voth, G. A.; Salvador, P.; Dannenberg, J. J.; Zakrzewski, V. G.; Dapprich, S.; Daniels, A. D.; Strain, M. C.; Farkas, O.; Malick, D. K.; Rabuck, A. D.; Raghavachari, K.; Foresman, J. B.; Ortiz, J. V.; Cui, Q.; Baboul, A. G.; Clifford, S.; Cioslowski, J.; Stefanov, B. B.; Liu, G.; Liashenko, A.; Piskorz, P.; Komaromi, I.; Martin, R. L.; Fox, D. J.; Keith, T.; Al-Laham, M. A.; Peng, C. Y.; Nanayakkara, A.; Challacombe, M.; Gill, P. M. W.; Johnson, B.; Chen, W.; Wong, M. W.; Gonzalez, C.; Pople, J. A. *Gaussian 03, Revision D.01* **2004**.
- (164) Martin, D. F.; Shamma, M.; Ferneliuss, W. C. *J. Am. Chem. Soc.* **1958**, *80*, 4891-5.
- (165) Hampton, G. K.; Light, R. J.; Hauser, C. R. *J. Org. Chem.* **1965**, *30*, 1413-16.
- (166) Bandgar, B. P.; Sadavarte, V. S.; Uppalla, L. S. *Synth. Commun.* **2001**, *31*, 2063-2066.
- (167) Miles, M. L.; Harris, T. M.; Hauser, C. R. *J. Org. Chem.* **1965**, *30*, 1007-11.
- (168) Bousquet, E. W. *Org. Syn.* **1943**, *Coll. Vol. 2*, 313

- (169) Chan, Y.-T.; Li, X.; Soler, M.; Wang, J.-L.; Wesdemiotis, C.; Newkome, G. R. *J. Am. Chem. Soc.* **2009**, *131*, 16395-16397.
- (170) Zhao, Y.; Li, J.; Li, C.; Yin, K.; Ye, D.; Jia, X. *Green Chem.*, *12*, 1370-1372.
- (171) Farha, O. K.; Mulfort, K. L.; Hupp, J. T. *Inorg. Chem. (Washington, DC, U. S.)* **2008**, *47*, 10223-10225.



## 8 Curriculum Vitae

### Personal data

Name	DI Christian Maurer
Address	Obere Amtshausgasse 23-25/7, 1050 Wien
Citizenship	Austrian
Date of Birth	Jul 21 <sup>st</sup> , 1986
Gender	male
Phone	0660/3451736
E-Mail	christian.maurer@dre.at

### Education

Since 02 / 2010	Ph.D. thesis (supervised by Prof. Ulrich Schubert) Institute of Materials Chemistry, Vienna University of Technology
10 / 2005 – 01 / 2010	University Education in Chemistry Master thesis: ‘Synthese modifizierter Polyphosphazene als alternative Bindemittel für Lacke’ (supervised by Prof. Ulrich Schubert) Institute of Materials Chemistry, Vienna University of Technology
08 / 2007	Academic internship, Laboratorium für Anorganische Chemie, ETH Zürich
09 / 1996 – 06 / 2004	Secondary School, BG / BRG St. Pölten Josefstrasse

### Work experience

Since 02 / 2010	Research and Teaching Assistant at the Institute of Materials Chemistry, Vienna University of Technology
10 / 2008 – 12 / 2008	Scientific Assistant at the Institute of Chemical Technologies and Analytics (working group of Prof. Jürgen Fleig), Vienna University of Technology
08 / 2008	Internship (production, extrusion of expandable polystyrene) Sunpor Austria AG
07 / 2007	Internship (production, extrusion of expandable polystyrene) Sunpor Austria AG

07 / 2006 – 08 / 2006	Internship (production, extrusion of expandable polystyrene) Sunpor Austria AG
07 / 2005 – 08 / 2005	Internship (production, extrusion of expandable polystyrene) Sunpor Austria AG

### Military Service

---

09 / 2004 – 04 / 2005	StbK PzB10, St.Pölten-Spratzern
-----------------------	---------------------------------

### Awards

---

2009	Support grand of the Vienna University of Technology
2009	Merit scholarship of the Vienna University of Technology
2007	Merit scholarship of the Vienna University of Technology

### Competences

---

Mother tongues	German
Further language	English: fluent (spoken and written)
Technical competences	good skills in handling chemistry related analysis devices (single crystal XRD, powder XRD, IR, NMR)
IT competences	good skills in MS Office, chemistry related software (ChemOffice, ISIS, XRD refining software, etc)
Driving license	category B

### Further information

---

Hobbies	Ultimate Frisbee, theater, exhibitions
Memberships	Member of the Austrian Chemical Society (GÖCH) Executive committee member of ProGym (Alumni Club of the BG/BRG St.Pölten)

### Publications

---

1. S. O. Baumann, V. A. Du, C. Artner, C. Maurer, U. Schubert: „*Spermine Adducts of Metal Alkoxides*“, *Monatshefte Chemie*, **2012**, *143*, 1637-1642.
2. J. Yang, J. Akbarzadeh, C. Maurer, H. Peterlik, U. Schubert: „*Sol-gel synthesis of ZnTiO<sub>3</sub> using a single-source precursor based on p-carboxybenzaldehyde oxime as a linker*“, *Journal of Materials Chemistry* **2012**, *22*, 24034-24041

3. C. Maurer, E. Pittenauer, Van An DU, G. Allmaier, U. Schubert: "*Cyclic bis( $\beta$ -diketonate)- and bis( $\beta$ -ketoesterate)-bridged titanium and zirconium alkoxide derivatives*"; *Dalton Transactions* **2012**, 41, 2346 - 2353.
4. J. Yang, M. Puchberger, R. Qian, C. Maurer, U. Schubert: "*Zinc(II) Complexes with Dangling Functional Organic Groups*"; *European Journal of Inorganic Chemistry* **2012**, 27, 4294 - 4300.
5. R. Lichtenberger, S. Baumann, M. Bendová, C. Maurer, U. Schubert: "*Modification of yttrium alkoxides:  $\beta$ -Ketoesterate-substituted yttrium alkoxo/hydroxo/oxo clusters*"; *Inorganica Chimica Acta* **2011**, 376, 463 - 469.